Convectively-coupled Kelvin waves over the tropical Atlantic and African regions and their influence on Atlantic tropical cyclogenesis

by

MICHAEL J. VENTRICE

A Dissertation

Submitted to the University at Albany, State University of New York

in Partial Fulfillment of

the Requirements for the Degree of

Doctor of Philosophy

College of Arts & Sciences

Department of Atmospheric and Environmental Sciences

2012

Convectively-coupled Kelvin waves over the tropical Atlantic and African regions and their influence on Atlantic tropical cyclogenesis

by

Michael J. Ventrice

Abstract

High-amplitude convectively coupled atmospheric Kelvin waves (CCKWs) are explored over the tropical Atlantic during the boreal summer. Atlantic tropical cyclogenesis is found to be more frequent during the passage of the convectively active phase of the CCKW, and most frequent two days after its passage. CCKWs impact convection within the mean latitude of the inter-tropical convergence zone over the northern tropical Atlantic. In addition to convection, CCKWs also impact the large scale environment that favors Atlantic tropical cyclogenesis (i.e., deep vertical wind shear, moisture, and low-level relative vorticity).

African easterly waves (AEWs) are known to be the main precursors for Atlantic tropical cyclones. Therefore, the relationship between CCKWs and AEW activity during boreal summer is explored. AEW activity is found to increase over the Guinea Highlands and Darfur Mountains during and after the passage of the convectively active phase of the CCKW. First, CCKWs increase the number of convective triggers for AEW genesis. Secondly, the associated zonal wind structure of the CCKW is found to affect the horizontal shear on the equatorward side of the African easterly jet (AEJ), such that the jet becomes more unstable during and after the passage of the convectively active phase of the CCKW. The more unstable AEJ is assumed to play a role with increased AEW growth. Through the increased number of AEWs propagating over the tropical Atlantic, as well as from the direct impact on convection and the large-scale environment over the tropical Atlantic, CCKWs are recommended to be used as a means for medium-range predictability of Atlantic tropical cyclones.

In addition to modulating tropical cyclone activity over the tropical Atlantic, CCKWs might impact the intensification processes of tropical cyclones. A case study highlighting two August 2010 tropical cyclones (Danielle and Earl) is explored for potential CCKW-tropical cyclone interactions. While predicted to intensify by most model guidance, both Danielle and Earl struggled to do so. It is shown that Danielle and Earl interacted with the convectively suppressed phase of an eastward propagating CCKW during the time they were predicted to intensify. Composite analysis shows that during and after the passage of the convectively suppressed phase of the CCKW over the Atlantic, large-scale vertical wind shear increases as anomalous upper-level westerly winds are collocated with anomalous lower-level easterly winds. Large-scale subsidence associated with the convectively suppressed phase of the CCKW causes the atmosphere to dry. Further, when the upper-level westerly wind anomalies associated with the CCKW are located over the equatorial Atlantic, a tropical upper-tropospheric trough (TUTT) develops over the northern tropical Atlantic. TUTTs are upper-level disturbances known to negatively impact the intensity of tropical cyclones.

CCKWs over the tropical Atlantic tend to occur during preferable locations of the Madden–Julian Oscillation (MJO). Results show that the MJO significantly modulates Atlantic tropical cyclogenesis using real-time multivariate MJO indices. Like CCKWs, AEW activity is found to vary coherently with MJO passages. Furthermore, the MJO also impacts the large-scale environment that favors for Atlantic tropical cyclogenesis. Therefore in addition to CCKWs, the state of the MJO should be used for Atlantic tropical cyclogenesis medium-range predictability.

Acknowledgements

This dissertation is dedicated to my parents, Raymond and Monica Ventrice. My parents have supported me in every aspect of life. I have never felt more loved, cared about, and cherished than what my parents have shown me. My father is the hardest working, most level-headed man that I know and has provided my family a means of living. My mother is a loving, protective woman that possesses all the qualities of an incredible mother. From broken bones, to surgeries, to sore throats, she was there for it all. I also want to acknowledge my brother Chris. Chris is incredibly courageous for his service as a New York City police officer. He is the glue that holds my family together, and was the underlying force that pushed me to strive for excellence. I will forever be in debt to my family, and acknowledge the life that they have provided me with.

I also acknowledge the support of my friends. I have grown close to a group of friends during my studies at the University at Albany. Further, I acknowledge the support from my girlfriend, Mikayla. From all of the memories associated with this group of people, I will never forget my experience at Albany.

Further, I want to thank NASA for the Grant NNX09AD08G and NNX10AU44G that made this work possible.

Contents

1. Introduction

Strong convectively coupled atmospheric Kelvin waves (CCKWs) have been shown to impact rainfall patterns over all tropical regions (Kiladis et al. 2006, and references therein). Further, CCKWs have been shown to impact the timing of the onset of the South China Sea (e.g., Straub et al. 2006), Indian (e.g., Flatau et al. 2003), and West African (e.g., Mounier et al. 2008) summer monsoons. More recently, CCKWs have been shown to have a small, but statistically significant influence on tropical cyclogenesis over the Eastern Hemisphere (Bessafi and Wheeler 2006; Frank and Roundy 2006; Schreck et al. 2011). In spite of the importance of CCKWs, our knowledge of these waves is incomplete. CCKWs are often overlooked in daily tropical weather discussions. This is especially true over the tropical Atlantic with regards to Atlantic tropical cyclogenesis and African weather because tradition has emphasized the easterly wave. Therefore, there is a need to understand the full-impact of CCKWs on convection and circulation over the Atlantic-African zone, as well as the relationship with Atlantic tropical cyclones. This research also explores how CCKWs might influence the dynamics of the West African Monsoon (WAM) system, and African easterly wave (AEW) activity.

AEWs have been regarded as the main precursors to Atlantic tropical cyclones (Carlson 1969a; Zipser and Gautier 1978; Avila and Pasch 1992; Berry and Thorncroft 2005). For the July-September (JAS) months between 1979 and 2001, 85% of all AEWs (603) that propagated over the tropical Atlantic never developed into a tropical cyclone (see Hopsch et al. 2010). This motivates the question, why do only a select number of AEWs develop into tropical cyclones, while the majority of all AEWs do not? This question highlights the importance of determining the factors responsible for development, such as the large-scale environment over the tropical Atlantic, or interactions with African easterly waves.

Frank and Roundy (2006) proposed that tropical cyclogenesis within roughly 20° of the equator might be modulated by the family of zonally-propagating equatorial and near-equatorial waves, and the Madden Julian Oscillation (MJO; Madden and Julian 1972). It is therefore plausible that CCKWs might play a large role over the tropical Atlantic in creating an environment favorable (or unfavorable) for the development of tropical cyclones. In addition to tropical cyclones, CCKWs have been shown to impact mesoscale convective systems (MCSs) over West Africa (Mounier et al. 2007; Laing et al. 2010, 2011). Recent work suggests that the convective triggering of MCSs over African topography might lead to the initiation of AEWs (Berry and Thorncroft 2005; Thorncroft et al. 2008). Therefore, since CCKWs can impact the frequency and duration of MCSs over Africa, they might also impact AEW activity during boreal summer (e.g., Mekonnen et al. 2008).

CCKWs have been shown to interact, and even possibly comprise part of the anatomy of the MJO (Nakazawa 1986; Dunkerton and Crum 1995; Roundy 2012; MacRitchie and Roundy 2012). In a case study during May 1998, Straub et al. (2006) showed that a CCKW propagated over West Africa and later initiated an MJO event over the Indian Ocean. Masunaga (2007) and Roundy (2008) show that numerous CCKWs can compose part of the MJO's convective envelope. These CCKWs often have stronger convective and dynamical signatures when collocated with the convective envelope of the MJO. Further, Straub and Kiladis (2003b) show that CCKW activity over the

Western Hemisphere increases during the decay of the active MJO over the Pacific. Therefore, there is a suggestion that there may be preferable times when CCKWs are more frequent and stronger over the Western Hemisphere with respect to the location of the MJO. This motivates research investigating if the MJO impacts the large-scale environment over the tropical Atlantic.

The major objectives of this dissertation are to understand the direct and indirect impacts of strong boreal summer CCKWs on the large-scale environment over the tropical Atlantic and African regions and their impact on Atlantic tropical cyclogenesis using a combination of observational data and model reanalyses. This dissertation is motivated by the following overarching questions:

i) To what extent do CCKWs impact convection over the tropical Atlantic and African regions? Furthermore, what are the mechanisms in which a CCKW can impact weather variability over these regions?

ii) Which CCKWs are important to consider for tropical cyclogenesis? Is every CCKW important to consider, or those optimally phased with other disturbances that impact the intraseasonal variability of tropical convection such as the MJO?

1.1. Literature Review

1.1.1. The dry-theoretical Kelvin wave

According to Matsuno's (1966) derivation of the shallow-water equations on an equatorial Beta-plane for the Kelvin wave solution, atmospheric Kelvin waves consist of purely zonal flow (Fig.1.1). Zonal velocity is in exact geostrophic balance with the meridional pressure gradient (Holton 2004). These waves exist in the atmosphere as result of the change in sign of the Coriolis parameter at the equator. According to Fig. 1.1., dry atmospheric Kelvin waves have a Gaussian wind structure that is centered about the equator, with a lower-tropospheric ridge in the westerlies and a trough in the easterlies. The upper tropospheric zonal winds associated with the dry-Kelvin wave have a direct out-of-phase relationship with those in the lower-troposphere, such that upper-level zonal divergence is collocated with lower-level zonal convergence. In the lower-stratosphere, dry-Kelvin waves are associated with an average phase speed of 30-60 m s^{-1}. Since the phase speed of a dry-atmospheric Kelvin wave equals that of its group velocity, these modes are non-dispersive. Therefore in theory, dry-Kelvin waves can make multiple transients across the globe.

1.1.2. Observed convectively coupled Kelvin waves

Since satellite observations and global model data have increased in horizontal vertical resolution, more detailed observations of convection in the tropics showed that in addition to westward propagating disturbances, there are also fast and slow eastward propagating disturbances. Nakazawa (1986, 1988) observed short-period eastward propagating synoptic scale active convective cells within the MJO, which are now known to be CCKWs. It is now well known that there are different classes of Kelvin waves, some of which are relatively fast propagating dry modes primarily seen in the stratosphere, while others are slower due to the coupling with convection within the troposphere (Kiladis et al. 2009). Further, there are Kelvin waves that are associated with a "Gill response" to the active convection associated with the MJO (Sobel and Kim 2013). CCKWs often have slow phase speeds (approximately 7-15 m s^{-1}) over the Warm Pool regions (e.g., Yang et al. 2007; Roundy 2012) and when collocated with the convectively active phase of the MJO (e.g., Dunkerton and Crum 1995; Roundy 2008, 2012). CCKWs over the East Pacific (Straub and Kiladis 2002), Atlantic (Wang and Fu 2007), and African regions (Mounier et al. 2007; Nguyen and Duvel 2008; Laing et al. 2008, 2011) have slightly faster phase speeds of approximately 14-20 m s^{-1}.

CCKWs are known to substantially modulate tropical rainfall on synoptic spatial and temporal scales (Gruber 1974; Zangvil 1975; Takayabu 1994; Wheeler and Kiladis 1999; Wheeler et al. 2000; Mekonnen et al. 2008). This modulation of rainfall is found to occur primarily along the latitude of the climatological intertropical convergence zone (ITCZ), which exists between the equator and 15˚N over the central-eastern Pacific and Atlantic basins (Kiladis et al. 2009). Over Africa and South America, the ITCZ varies more substantially with season (Roundy and Frank 2004).

The evolution and spatial structure of boreal summer CCKWs over the tropical Atlantic and African regions from Mekonnen et al. (2008) is shown in Fig. 1.2. Enhanced convection, predominately north of the equator, is collocated with low-level westerly wind anomalies, while suppressed convection is collocated with low-level easterly wind anomalies. Maximum low-level zonal convergence precedes the minimum negative Kelvin filtered brightness temperature anomaly by roughly 15º of longitude, consistent with the observations of Takayabu and Murakami (1994) and Straub and Kiladis (2003a,b). In agreement with Matsuno’s (1966) linear shallow-water Kelvin wave solution, zonal wind anomalies are roughly in phase with geopotential anomalies and are peaked along the equator. A notable difference to Matsuno’s (1966) solution, however, is that CCKWs over the Atlantic have a non-negligible meridional low-level wind component. Dias and Pauluis (2009) performed an idealized modeling study and demonstrated that CCKWs propagating along a narrow precipitation region, such as the boreal summer Atlantic ITCZ, produce a meridional circulation. This meridional circulation modulates both the amount of precipitation and the horizontal extent of the ITCZ, which can affect the phase speed of the CCKW. Further observational evidence of meridional flow composing the dynamical structure of a CCKW is provided over Africa (Mounier et al. 2007), over the Indian Ocean (Roundy 2008), and over the East Pacific (Straub and Kiladis 2003c).

While CCKWs are commonly associated with a lower-level wind structure that is generally opposite to the flow in the upper troposphere, these waves have highly tilted vertical structures in zonal wind, temperature, and humidity (Straub and Kiladis 2002, 2003a; Kiladis et al. 2009). Figure 1.3 is an adaptation to the schematic diagram given in Straub and Kiladis (2003a; their Fig. 6) for the vertical structure of a Kelvin wave coupled with moist convection. While Matsuno’s (1966) solution for the dry Kelvin wave is associated with upper-level divergence collocated with low-level convergence, Fig. 1.3 shows that low-level zonal convergence precedes upper-level zonal divergence. In individual waves, the phase relationship between low-level and upper-level winds will vary with the phase speed and zonal scale of the wave. At lower-levels, high pressure is collocated with the westerly flow and low-pressure is collocated within the easterly flow. For the upper-levels, the opposite is true. Slightly to the east of the deepest convection associated with the convectively active phase of the CCKW (approximately 15º of longitude), shallow-type convection develops where the strongest low-level zonal convergence associated with the CCKW occurs. This shallow-type convection warms the lower-troposphere and its associated circulation vertically advects moisture into the mid-troposphere. Deep convection develops where the upper-level divergence is greatest. The deep convection warms and moistens the mid-to-upper levels of the atmosphere. Slightly to the west of the deepest convection is a stratiform cloud layer. This stratiform cloud layer is associated with a moist signature in the upper-levels and a dry signature at lower-levels, indicating that the low-level westerly flow associated with the CCKW is dry. Stratiform-type precipitation falls through this dry layer and often creates cold pools near the surface.

1.1.3. Convectively coupled Kelvin waves and tropical cyclogenesis

The role of CCKWs on tropical cyclogenesis has only been investigated in a limited number of studies (e.g., Bessafi and Wheeler 2006; Frank and Roundy 2006; Schreck et al. 2011; Schreck and Molinari 2011). Bessafi and Wheeler (2006) examined the role of all equatorial convectively-coupled waves on tropical cyclogenesis over the Indian Ocean. While the relationship is only weakly significant, Indian Ocean tropical cyclogenesis is found to increase when CCKW-convection is located over the eastern Indian Ocean, or just after the passage of its convectively active phase. Frank and Roundy (2006) counted the number of tropical cyclones that developed in a particular phase of all equatorial convectively coupled waves for all basins. A tropical wave was considered when the running mean of its basin wide variance exceeded a threshold. They find that tropical cyclones have a small preference to form within the convectively active phase of CCKWs in all basins, but conclude that CCKWs do not play a significant role in tropical genesis except during isolated events, during Northern Hemisphere spring or southern summer over the southern Indian Ocean. Since then, Roundy has changed this view since the algorithm that was used in Frank and Roundy (2006) was less effective at diagnosing the relationship between CCKWs and tropical cyclogenesis.

Schreck et al. (2011) explored how equatorial convectively coupled waves (using space-time filtered rain rates) modulate tropical cyclogenesis over the West Pacific. Tropical cyclogenesis was attributed to an equatorial wave if the filtered rain rate anomaly exceeded a threshold in a 1º latitude-longitude box containing the genesis location. Tropical-depression type waves were found to be the most common wave-type disturbance associated with tropical cyclogenesis. Using a 3 mm day^{-1} threshold, the MJO had the least number of genesis events, followed by CCKWs. It is important to note that the use of MJO filtered rainfall was misleading, because although tropical cyclone activity increases during the convectively active phase of the MJO, MJO filtered rain rates have a smaller standard deviation than TD-band rain rates. When Schreck et al. (2011) increased the declared threshold to 5 or 6 mm day^{-1}, CCKWs became the second most common wave disturbance associated with tropical cyclogenesis, whereas the most common wave disturbances for all thresholds were tropical depression-type waves.

Schreck and Molinari (2011) investigated the genesis of two West Pacific typhoons, Rammasun and Chataan (in June 2002). They attribute genesis of both tropical cyclones to the generation of potential vorticity (PV) in association with diabatic heating from the passages of a series of CCKWs collocated within the convectively active phase of the MJO (Fig. 1.4). It is important from this analysis to realize that a basic-compositing analysis, where one counts the number of tropical cyclogenesis events in a Kelvin filtered anomaly, would suggest CCKWs are not important for the genesis of these tropical cyclones since there were multiple CCKWs important for this event.

Therefore by averaging in time, the CCKW signal would be washed out. This motivates the current dissertation to investigate the role of CCKWs on Atlantic tropical cyclogenesis using a methodology different to Frank and Roundy (2006) and Schreck et al. (2011). This methodology will be discussed in further detail in Chapter 2.

1.2. Structure of the dissertation

This dissertation contains seven chapters that address the research questions stated in section 1.1. Chapter 2 presents a case study exploring the unexpected genesis of Tropical Storm Debby (2006) and the role of a strong boreal summer CCKW on the genesis of the pre-Debby AEW. An investigation regarding the relationship between Atlantic tropical cyclogenesis and CCKWs is included. The impact of CCKWs on the large-scale environment favorable for Atlantic tropical cyclogenesis (e.g., low-level relative vorticity, moisture, and vertical wind shear) is in Chapter 3. The role of CCKWs on AEW activity is investigated in Chapter 4. An analysis of the impact of a CCKW passage of the intensity of two-mature 2010 Atlantic tropical cyclones (Danielle and Earl) is provided in Chapter 5. Chapter 6 addresses the relative importance of the MJO over the Western Hemisphere during boreal summer. An overview of the key results and potential future work are summarized in Chapter 7.

1.3. Figures

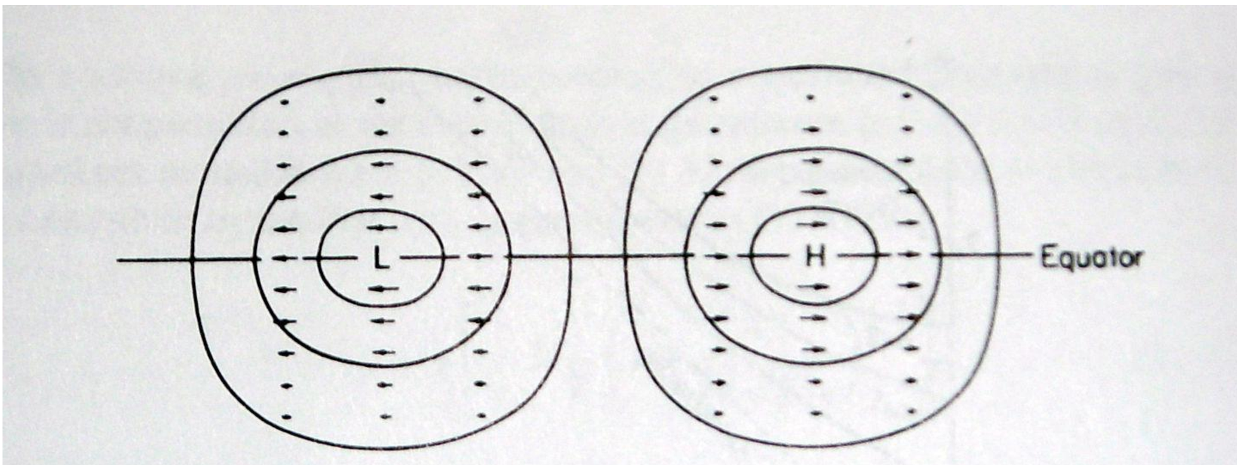

Fig. 1.1. Plan view of horizontal and height perturbations associated with an equatorial Kelvin wave [taken from Holton, An Introduction to Dynamic Meteorology, ed. 4. (2004)].

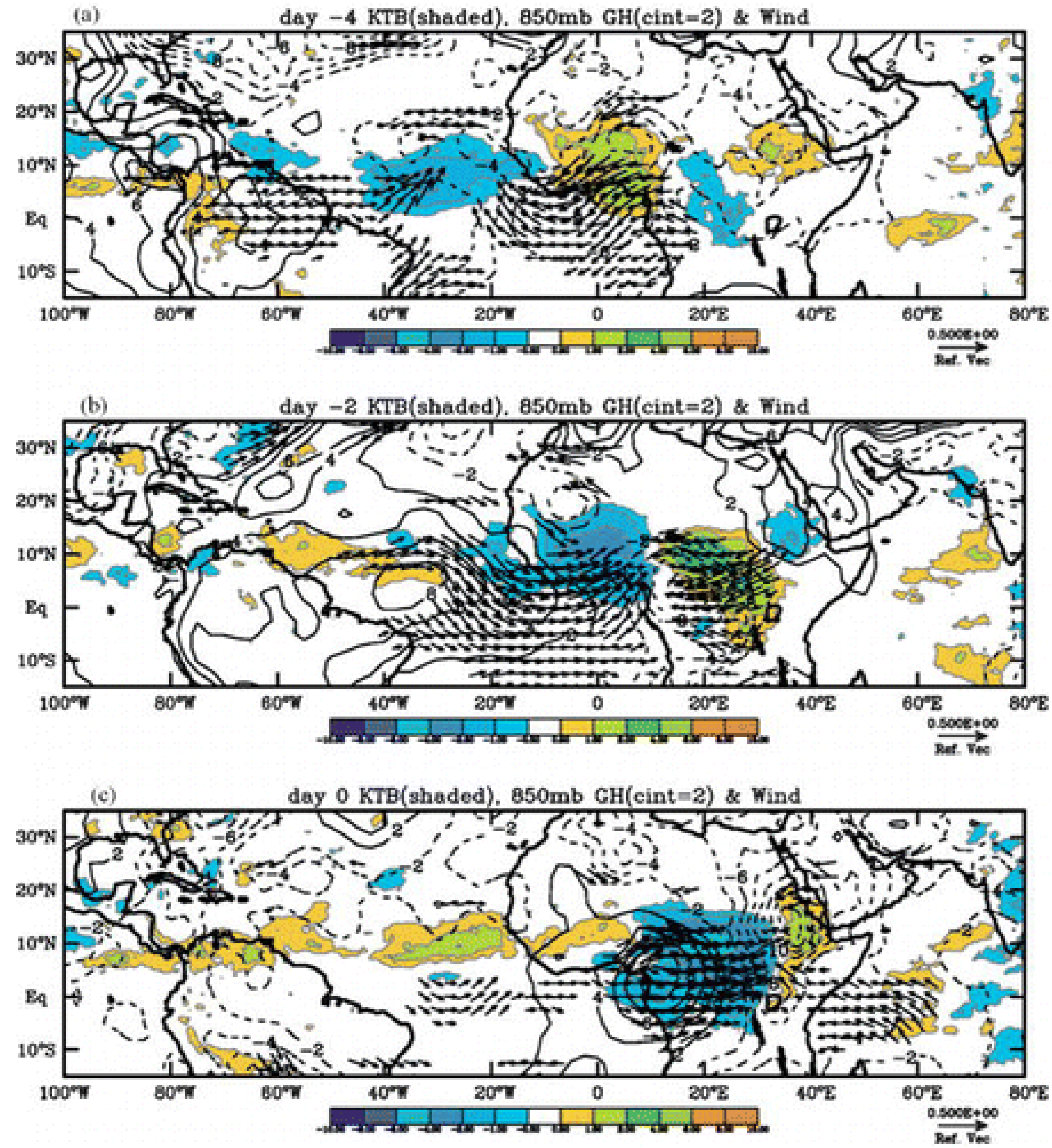

Fig. 1.2. Kelvin regressed brightness temperature (shaded), 850 hPa geopotential heights (contours), and 850 hPa wind vectors. Vectors are drawn if zonal winds are significant at 95% or better (reference wind of 0.5 m s^{-1}). The reference point for regression is 10°N, 20°E [taken from Fig. 3 in Mekonnen et al. (2008)].

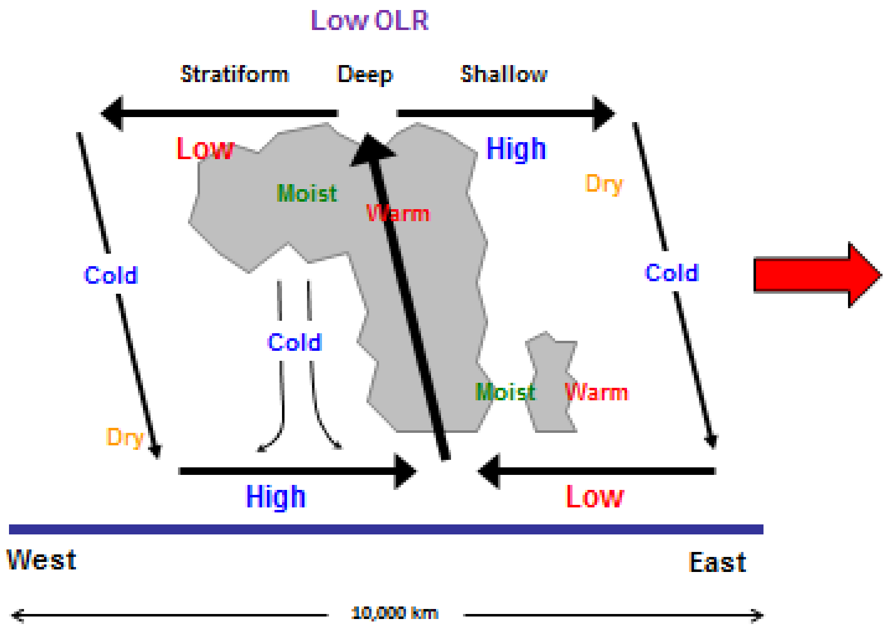

Fig. 1.3. A schematic diagram of the vertical structure of a CCKW. The red arrow points towards the direction of propagation [adapted from Fig. 6 in Straub and Kiladis (2003)].

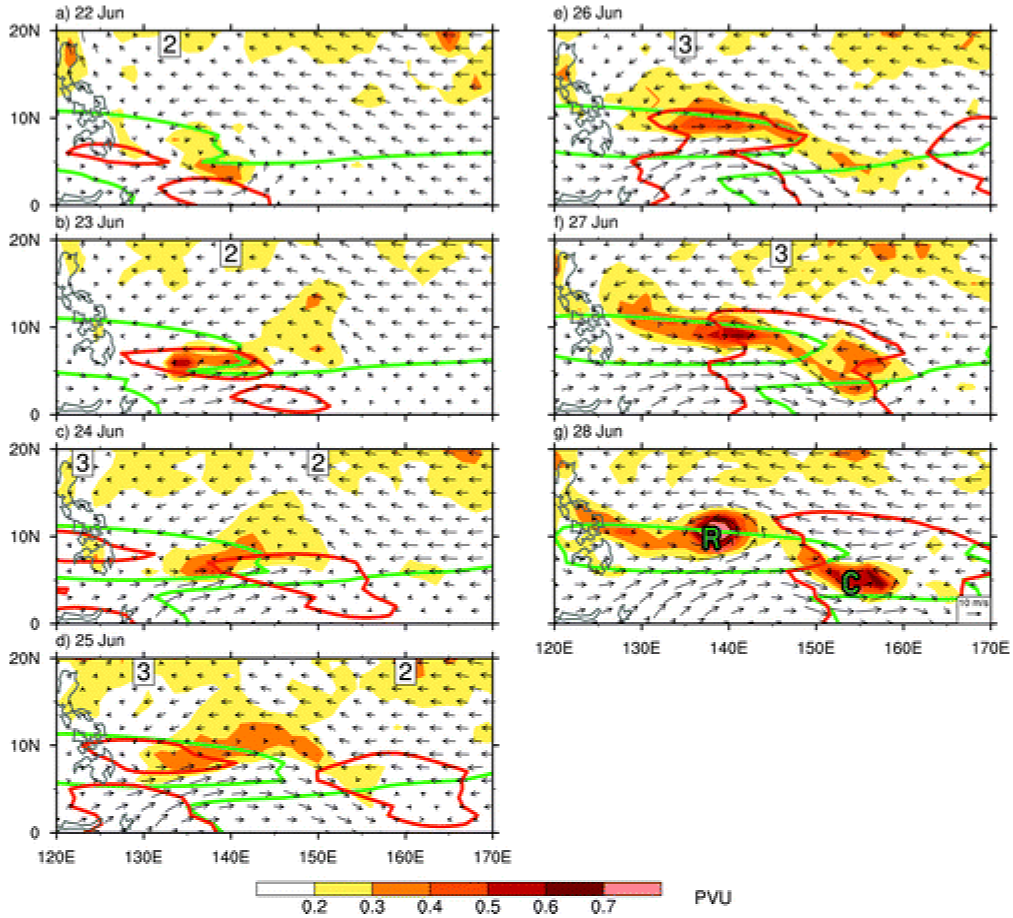

Fig. 1.4. Low-level (850 hPa) PV (shaded) overlaid with MJO-filtered rain rate anomalies (green contours), Kelvin-filtered rain rate anomalies (red contours), and 850 hPa wind vectors. The “R” and “C” represent the time of genesis for typhoons Rammasun and Chataan, respectively [taken from Fig. 6 in Schreck and Molinari (2011)].

2. The role of convectively coupled Kelvin waves on Atlantic tropical cyclogenesis highlighting the genesis of Tropical Storm Debby (2006)

2.1. Introduction

Atlantic tropical cyclones over the MDR are commonly associated with AEWs. For the July-September (JAS) months between 1979 and 2001, 85% of all AEWs (603) that propagated over the tropical Atlantic never developed into a tropical cyclone, highlighting the importance of determining the factors responsible for development (see Hopsch et al. 2010). The genesis of Tropical Storm Debby, associated with the second AEW during the NASA African Monsoon Multidisciplinary Analyses (NAMMA) field campaign (Zawislak and Zipser 2010), was extremely difficult to forecast over the eastern Atlantic. According to the National Hurricane Center's (NHC) post-season tropical cyclone summary, the genesis of Debby occurred more rapidly than anticipated by the Tropical Weather Outlook products. The prediction of a developing tropical cyclone was issued only three hours prior to genesis. The lack of warning is explained by the fact that the pre-Debby AEW was quite weak over Africa just prior to tropical cyclogenesis (e.g., Zawislak and Zipser 2010). This chapter investigates the key processes that contributed to the rapid nature of the tropical cyclogenesis. These processes include an interaction between the AEW and diurnally varying convection at the West African coast and a CCKW over the eastern tropical Atlantic. Our knowledge of CCKWs over the tropical Atlantic during boreal summer remains incomplete. Therefore, a major objective of this chapter is to explore the relationship between boreal summer CCKW passages and Atlantic tropical cyclogenesis

AEWs, the dominant synoptic weather systems observed over Africa and the tropical Atlantic during Northern Hemisphere boreal summer, are westward-propagating tropical waves that grow along the AEJ (e.g., Reed et al. 1977; Thompson et al. 1979; Avila and Pasch 1992; Mekonnen et al. 2006). Before reaching the coast of West Africa, the AEWs that later develop into tropical cyclones have a distinctive cold-core structure below the level of the AEJ, consistent with a positive vorticity maximum at the level of the AEJ (e.g., Reed et al. 1977; Kwon and Mak 1990; Hopsch et al. 2007). They often begin to transform towards more warm-core structures as they move towards the Guinea Highlands (GHs) region [5-13°N, 8-15°W] with regions of deep convection becoming more confined to the trough (Hopsch et al. 2010).

The GHs region was highlighted in Berry and Thorncroft (2005) and Hopsch et al. (2010) as an influential area for the amplification of AEWs, which may increase the likelihood of east Atlantic tropical cyclogenesis. They found that convection triggered over the elevated terrain of the GHs tends to generate low-level potential vorticity (PV), which merges with PV associated with an AEW during the wave passage. This PV merging process might play a critical role in enhancing AEWs propagating over the region. The low-level PV signature is also evident in the appearance of a low-level AEW track at the latitude of the GHs near the coast in addition to a second track over land north of the AEJ (Thorncroft and Hodges 2001).

The GHs region is composed of a series of elevated topographic features located in tropical West Africa, separating a portion of sub-Saharan Africa from the eastern tropical Atlantic. A Tropical Rainfall Measuring Mission (TRMM) 3B42 August daily average rainfall rate greater than 16 mm day^{-1} occurs just downstream of the elevated topography of the GHs region (Fig. 2.1). This exceptional rainfall rate downstream of the GHs region signifies that this area is one of the wettest places on the continent during boreal summer.

Zawislak and Zipser (2010) used infrared (IR) and microwave satellite imagery to observe the convection during the hours prior to classification of Debby. They suggest a “GHs region type” genesis helps to explain the formation of Debby. Chiao and Jenkins (2010) performed a modeling study to explore the processes that influenced the genesis of Tropical Storm Debby. They also concluded that the GHs region played an important role by modulating the low-level westerly flow that deflected northward along the GHs. This deflection enhanced the low-level cyclonic circulation there and transported moist air towards the north, supporting the development of MCSs.

The above studies suggest the importance of understanding the convection generated in the vicinity of the GHs region for downstream tropical cyclogenesis. In this regard, this should include consideration of the role played by the coherent diurnal cycle, known to be dominant in the GHs region (Mekonnen et al. 2006). Past work suggests that convection is generally triggered close to the topography during the late afternoon in the vicinity of the GHs (e.g. Hodges and Thorncroft 1997; Yang and Slingo 2001; Laing et al. 2008). In contrast, an early morning peak in convection is expected over the ocean (e.g., Janowiak et al. 1994). The extent to which interactions between AEWs and the diurnal cycle are important for downstream tropical cyclogenesis is unknown.

Along with the convection generated over the GHs region, this chapter will provide evidence that the pre-Debby AEW formed into a tropical cyclone during the superposition with a CCKW. It is natural to wonder if CCKWs can modulate tropical cyclone activity by enhancing westward propagating AEWs over the tropical Atlantic and/or by influencing the large-scale environment. These ideas will be investigated in this chapter and in Chapters 3 and 4.

The present chapter is structured as follows. Section 2.2 discusses datasets and methodology. Section 2.3 investigates the genesis of Debby focusing on the evolution of the precursor AEW interacting with the diurnally varying convection over the GHs region. Section 2.3 also analyzes the convective influence of CCKWs over the tropical Atlantic and African regions and considers the role of a CCKW on the development of Tropical Storm Debby. Section 2.4 investigates the climatological role of CCKWs on tropical cyclogenesis over the MDR. Finally, section 2.5 includes a discussion and final comments.

2.2. Datasets and Methodology

The European Centre for Medium-Range Weather Forecasts (ECMWF) Re-Analysis (ERA-Interim) dataset was used to investigate the different synoptic evolutions of both the tropical cyclogenesis case study and the composite CCKW analysis (Dee et al. 2010). This dataset covers the period 1989 to present and has a horizontal resolution of 1.5°. The AEW tracking method developed in Berry et al. (2007) was applied on the ERA-Interim data to objectively isolate trough axes of individual AEWs and locate the mean position of the AEJ.

Geostationary Earth Orbit IR data from the Climate Prediction Center (CPC) merged IR dataset was used to view the diurnal cycle of convection over the GHs region and the development of Tropical Storm Debby (Janowiak et al. 2001). This dataset is a composite of all geostationary earth orbiting IR (~11 μm) images from the multifunctional transport satellite [MTSAT; formerly the geostationary meteorological satellite], Geostationary Operational Environmental Satellite (GOES), and Meteosat satellites. Zenith angle corrections are used to match brightness temperatures away from the respective sub-satellite points. This data is made available at 4 km spatial resolution every 30 minutes.

Tropical rainfall information was provided by the TRMM multisatellite precipitation analysis (TMPA; TRMM product 3B42; Huffman et al. 2007). This dataset merges precipitation estimates from passive microwave sensors on a set of low earth orbiting satellites. The precipitation estimates are calibrated using global analyses of monthly rain gauge data. This dataset is made available from 1998-present on 3-hourly 0.25˚ latitude-longitude grids. This data has been averaged to 6-hourly 1˚ latitude-longitude grids to improve computational efficiency. By averaging the data onto a coarser grid, the missing data was interpolated bilinearly in space and linearly in time from the surrounding values (see Schreck et al. 2011 for more details). Less than 6% of the entire original 0.25˚dataset contained a limited number of missing values which was found to be caused by missing geostationary IR coverage over the Indian Ocean before June 1998 (Huffman et al. 2007).

Convection associated with CCKWs is explored using the NOAA's daily averaged interpolated OLR dataset, having a horizontal gridded resolution of 2.5˚ (Liebmann and Smith 1996). To support the analysis of CCKWs, wavenumber-frequency filtering was applied to the daily averaged NOAA interpolated OLR dataset following the methodology of WK99. CCKW filtering was performed with a period range of 2.5-20 days, with eastward wave numbers 1-14. The filter is constrained by the

Kelvin wave dispersion curves for equivalent depths of 8-90 meters. This methodology has been demonstrated similarly in Straub and Kiladis (2002) and Mekonnen et al. (2008). In short, this methodology decomposes a field of data into wavenumber-frequency components for eastward moving wave disturbances. Before the decomposition, the data is detrended and the ends of the time series were tapered to zero to control spectral leakage (see WK99 for additional details).

A time series, henceforth called the CCKW index, was developed based on a selected grid point over the eastern tropical Atlantic (10°N, 15°W). The CCKW index is composed of all days where the minimum negative Kelvin-filtered OLR anomalies were less than -1.5 standard deviations in magnitude during the 1989-2009 JJAS seasons. A total of 142 CCKWs were objectively identified using this methodology. Lags were then used on this time series in order to examine propagating characteristics. For clarification, "Day 0" of the CCKW index is when the minimum Kelvin filtered OLR anomaly moves over the selected base point.

Anomalies for all composited fields were constructed as differences from the long-term mean and the first four harmonics of the seasonal cycle. Bootstrap random resampling tests with one thousand iterations were used to test the statistical significance of the difference of the composite anomalies from zero (e.g., Roundy and Frank 2004). These tests were applied by constructing a number of samples equal in size to the number of events included in the composite, which is obtained by randomly drawing a new set of anomalies with replacement from the original dataset and binning the anomalies for each randomly drawn set.

An analysis of tropical cyclogenesis events during 1979-2009 was performed using the National Climatic Data Center's (NCDC's) IBTrACS v3 dataset (Knapp et al. 2010). The dates of genesis of all tropical cyclones are binned relative to when OLR anomalies associated with the composite convectively active phase of the CCKW reached a level that was negative at the 95% significance level. A bootstrap resampling test was performed for statistical significance. In order to investigate the relationship between CCKWs and tropical cyclogenesis, tropical cyclogenesis is limited to only within the MDR (see section 2.4).

2.3. Case Study: The genesis of Tropical Storm Debby (2006)

2.3.1. The evolution of the African easterly wave associated with Tropical Storm Debby

The evolution of the pre-Debby AEW is highlighted in Figure 2.2. Key diagnostics include the 650 hPa PV, IR brightness temperature, and the mean location of the AEJ and AEW trough axes. The initiation of the pre-Debby AEW occurred after the generation of a strong MCS on 18 August over West Africa (between 10-17°N, 0-5°E; Fig. 2.2b), and is consistent with the triggering hypothesis discussed in Thorncroft et al. (2008). It is difficult to observe the AEW trough axis at this time due to the overall weak characteristics of the AEW. On 19 August, the mid-level circulation began to intensify as the AEW propagated westward over tropical Africa (Fig. 2.2c). Convection was observed on 19 August over Senegal, downstream of the AEW trough axis, consistent with the observations of previous AEW composite studies (e.g., Carlson 1969a,b; Reed et al. 1977; Payne and McGarry 1977; Duvel 1989; Diedhiou et al. 1999; Kiladis et al. 2006).

On 20 August, the AEW trough reached the longitude of the GHs region (Fig. 2.2d). At this time, the peak value of PV associated with the AEW was 0.3 PV units (PVUs). On 21 August, convection was more confined to the AEW trough axis (Fig. 2.2e). This location of convection resulted in an intensification of the mid-level PV, with the PV maximum of 0.6 PVUs located behind the AEW trough axis. Six hours later at 18Z on 21 August, the NHC classified the pre-Debby AEW as a tropical cyclone. On 22 August, the tropical cyclone tracked northwest over the eastern tropical Atlantic; well defined rain bands exist to the east of the tropical cyclone. During the intensification of the pre-Debby AEW, the 850 hPa meridional wind associated with the low-level circulation of the AEW more than doubled from 2.5 ms^{-1} on 00Z August 20 to greater than 5 ms^{-1} on 00Z August 21 after propagating over the GHs region (not shown). As will be shown in the following sub-sections, this development likely had contributions from convection generated downstream of the GHs during the time of the AEW passage (section iii) and the enhancement of convection by a CCKW (section 2.3.5).

2.3.2. Diurnal cycle of convection over the Guinea Highlands region

Figure 2.3 shows the exceedance frequency of pixels less than 233 K for August 1998-2009. This provides an approximate estimation of the coherent diurnal cycle of rainfall (e.g., Duvel 1989; Mounier et al. 2007; Nguyen and Duvel 2008). There are two regions of elevated terrain near the coast of West Africa that compose the “GHs region” (recall Fig. 1). The taller, northern most topographic feature (10-12°N, 10-13°W) is the Fouta Djallon Highlands (FDHs). The FDHs have a climatological daily rainfall rate of 8-12 mm day^{-1}. The southeastern most topographic feature (7-10°N, 7-11°W) is the Nimba

Range. The Nimba Range has a slightly lower climatological daily rainfall rate of 6-10 mm day^{-1}.

The diurnal cycle of convection over these regions is as follows. At 03Z, the strongest convective signals are located in two regions, northwest of the FDHs and just off the coast of West Africa (Fig. 2.3a). A northwest-southeast oriented line of convection is located over the extreme eastern Atlantic next to the coast. During the next three hours (06Z), the continental convection to the northwest of the GHs region weakens (Fig. 2.3b). The northwest-southeast oriented line of oceanic convection is strikingly enhanced at this time. At 09Z, the strongest convective activity continues to move westward over the ocean, slightly increasing in frequency (Fig. 2.3c). The convective signal over the continent continues to weaken.

At 12Z, the convective activity over the continent is at a minimum while convection over the ocean remains pronounced (Fig. 2.3d). The reduction of cloudiness increases daytime solar heating reaching the surface, warming the land and destabilizing the boundary layer. The maximum oceanic convection begins to decrease and shift slightly westward by 15Z. At this time, a new convective signal begins to appear over the coastal terrain downstream of the GHs region (Fig. 2.3e). This convective signal later grows in amplitude and extends across the entire continental-coastal terrain at 18Z (Fig. 2.3f). A 233K exceedance signal greater than 25% occurs over and downstream of the FDHs with a second, more localized area over the Nimba Range. This convective pattern suggests that the elevated topography in this region acts to strongly influence the diurnal cycle of convection there. During the evening hours (21-00Z), the convective signal over the ocean continues to weaken considerably while the convective signal over the continent remains prominent (Fig. 2.3g-h).

In summary, convection most frequently occurs between 00Z-12Z over the eastern tropical Atlantic, in close proximity to the coast of West Africa. This oceanic convective signal is manifested by both *i)* propagating MCSs that were either pre-existing or directly generated over (or downstream) of the GHs topography and *ii)* morning convection generated directly over the ocean. A transition from oceanic dominated convection to continental dominated convection occurs between 15Z and 18Z (Fig. 3e).

2.3.3. The interaction between the convection generated by the Guinea Highlands region and the pre-Debby AEW

Figure 2.4 shows the CPC IR brightness temperature on 03Z August 20 through 00Z August 21 2006, the time of the AEW passage. The AEW trough axis and AEJ location are only plotted every 6 hours due to the time resolution of the ERA-Interim dataset. This figure indicates that the diurnally varying convection generated within the vicinity of the GHs on 20 August was very similar to the coherent evolution described above and that this contributed to the intensification of the pre-Debby AEW leaving the coast of West Africa.

During the early morning hours (03-09Z), convection was generated directly off the coast of West Africa over the eastern tropical Atlantic similar to the coherent diurnal cycle (Fig. 4a-c). Between 09 and 12Z, the convection extended slightly northward over the ocean, but was still very clearly tied to the coast (Fig. 2.4c-d). At 12Z, a clearing along the coastal terrain was observed as the previous day’s convection weakened (c.f. Fig. 2.4d). This clearing occurred ahead and along the AEW trough axis, suggesting that the forcing from the diurnal cycle of convection was greater than that of the AEW. By 15Z, convection began over the land close to the coast directly where the clearing of cloudiness was observed earlier (Fig. 2.4e). At 18Z, deep convection associated with MCSs formed directly downstream of the FDHs (Fig. 4f). These MCSs occurred within the vicinity of the AEW trough axis and through the generation of low-to-mid level PV, the AEW would be expected to strengthen at this time. At 21Z, the convection associated with the MCSs intensified and extended northwestward (Fig. 2.4g). At this time, there are two large-scale convective features. There is a large MCS over the coast of Senegal and second MCS over the eastern tropical Atlantic. The oceanic MCS was linked to the convection generated during the early morning. This MCS differs from the coherent diurnal cycle since it remained prominent during the afternoon which is presumably associated with the forcing from the AEW. The second MCS was linked to the afternoon induced convection over land near the FDHs. This MCS occurred during a time consistent with the generation of new convection in the coherent diurnal cycle. Figure 2.4 suggests that the combined effects of the southerly flow associated with the circulation of the pre-Debby AEW and the topographic influence provided by the FDHs played a critical role in organizing this MCS (e.g., Chiao and Jenkins 2010). Between 00Z and12Z August 21, the convection once initiated over the land merged with the active convection over the ocean, marking the early stages of tropical cyclogenesis.

The initial intensification of the pre-Debby AEW on 20 August occurred after interacting with the diurnally varying convection generated downstream of the GHs region. Convection was observed over the eastern Atlantic during the early morning hours of 20 August, consistent with exceedance frequency composites (c.f., Fig. 2.3a-d).

According to Zawislak and Zipser (2010), the MCS embedded within the oceanic convection just off the coast of West Africa possessed a similar magnitude to the afternoon triggered MCS on 20 August. Recall this MCS over the ocean defied the coherent diurnal cycle of convection by maintaining its structure during a time of day when convection is on average suppressed over the ocean. It is likely that the synoptic forcing by the intensifying AEW influenced the development of both MCSs. This idea is consistent with Gray and Jacobson (1977) who found that the diurnal cycle is more evident within more intense deep convective systems. McGarry and Reed (1978) confirmed this result using the GATE array. However, this was also a time when the convectively active phase of a CCKW was located over the eastern Atlantic and coast of West Africa. The impact of CCKWs on the diurnal cycle of convection over West Africa is unknown and may have aided in the generation of the two strong MCSs that amplified the pre-Debby AEW on August 20.

2.3.4. The convective influence of convectively coupled Kelvin waves over the tropical Atlantic and Africa

Composites of CCKWs over the tropical Atlantic and West Africa are calculated by averaging fields of unfiltered OLR anomalies, Kelvin filtered OLR anomalies, and 200 hPa wind anomalies over the set of dates of the CCKW index (Fig. 2.5). Day 0 is defined to be when the composited minimum Kelvin filtered OLR anomaly is located over the base point (10°N, 15°W), chosen to be close to the West African coast. Consistent with previous studies, this figure clearly highlights eastward progression of negative OLR anomalies within the composited convectively active phase of the CCKW over the tropical Atlantic and Africa.

The convectively suppressed phase of the composited CCKW (black-solid contour) moves eastward ahead of the convectively active phase (black-dashed contour), reducing local convection over the Atlantic ITCZ and tropical African regions. The convectively active phase of the CCKW progresses eastward, locally enhancing convection. A second convectively suppressed phase of the CCKW follows the convectively active phase. This “suppressed-active-suppressed” convective pattern associated with the CCKW travels eastward with an average phase speed of roughly 15 ms^{-1}. This phase speed is consistent with the 7-18 ms^{-1} observed CCKW phase speeds over the Indian Ocean (e.g., Dunkerton and Crum 1995; Roundy 2008; Roundy 2012a,b), the western Pacific (e.g., Wheeler and Kiladis 1999), the eastern Pacific (e.g., Straub and Kiladis 2002), and over West Africa (e.g., Mounier et al. 2007). Kiladis et al. (2009) attributes these slower than theoretical phase speeds to the reduced effective static stability of the atmosphere, which is associated with condensational heating and cooling canceling out most, but not all, of the temperature change linked to vertical motion.

Off-equatorial invigorated convection is collocated with the convectively active phase of the CCKW between Day -2 and Day +1 over the eastern Atlantic and GHs region (Fig 2.5e-g). The enhanced convective signature associated with the CCKW is later located over tropical Africa between Day +1 and Day +4 (Fig. 2.5h-k). The off-equatorial convective signature is consistent with the location of the warmest sea surface temperatures (SSTs) in this region during the boreal summer. Near the equator itself, climatologically cold SSTs within the equatorial Atlantic cold tongue prevent deep convection from occurring there (not shown). This off-equatorial convective signature of the CCKW occurs similarly in the eastern Pacific, where the East Pacific cold tongue is present (Straub and Kiladis 2002).

Along with a coherent eastward moving convective signature, CCKWs also have a coherent wind structure that progresses eastward with the wave. Emphasis will be given to the upper-level wind structure of the CCKW here, but it is acknowledged that CCKWs have a lower-level wind structure that is generally opposite to the flow in the upper troposphere, with low-level convergence preceding upper-level divergence by roughly 15° of longitude (see Mounier et al. 2007; Roundy 2008). The upper-level wind pattern associated with the composited CCKW over the tropical Atlantic is similar to the theoretical dry Kelvin wave solution. Near the equator, upper-level westerly wind anomalies occur ahead of the minimum Kelvin filtered OLR anomaly. These upper-level westerly wind anomalies extend eastward through the leading convectively suppressed phase. Upper-level easterly wind anomalies are observed behind the minimum Kelvin filtered OLR anomaly and extend westward through the second suppressed phase. This anomalous wind pattern highlights large-scale upper-level wind divergence and is consistent with the deep convection associated with the convectively active phase of the CCKW. To the north of the equator, meridional wind anomalies compose a large portion of the upper-level wind structure of the composited CCKW. On Day -2, a broad area of anomalous anticyclonic wind flow is collocated with the convectively active phase of the CCKW over the central Atlantic ITCZ (Fig. 2.5e). These winds are likely a response to the off equatorial heating from convection at this time (e.g., Ferguson et al. 2009; Dias and Pauluis 2009). On Day -1, the anomalous broad upper-level anticyclonic circulation shifts eastward with the convectively active phase of the CCKW (Fig. 2.5f). One day later (Day 0), this anomalous anticyclonic circulation becomes less coherent, but anomalous easterly-northeasterly flow is evident over the entire equatorial Atlantic and anomalous westerly flow is over West Africa (Fig. 2.5f). This anomalous upper-level wind divergence pattern progresses eastward with the convectively active phase of the CCKW during the later lags (Fig. 2.5g-l).

2.3.5. The convectively coupled Kelvin wave associated with the genesis of Tropical Storm Debby

The superposition of a CCKW and the pre-Debby AEW occurred over the eastern tropical Atlantic on 21 August. This exceptional CCKW was associated with a 2σ negative Kelvin filtered OLR anomaly, ranking the wave within the strongest 5% of all JJAS (1979-2009) CCKWs over the selected base point. A time-longitude plot of unfiltered OLR anomalies overlaid with only negative Kelvin filtered OLR anomalies infer that this CCKW was non-dispersive in nature, making at least one circuit around the globe (Fig. 2.6). This CCKW is associated with an eastward progression of negative Kelvin filtered OLR anomalies (dashed contours) beginning over the East Pacific (120˚W) on 14 August and ending over the central Pacific on 6 September (180˚E). For most of this track over the Atlantic and West Africa, unfiltered negative OLR anomalies progress eastward with the Kelvin filtered negative OLR anomalies. The negative Kelvin filtered OLR anomalies associated with the CCKW that influenced the genesis of Debby do not connect to the area of negative Kelvin filtered OLR anomalies back over the eastern Pacific on 16 August. While the negative Kelvin filtered OLR anomalies suggest that the CCKW associated with Debby is different from the upstream CCKW over the central-east Pacific [130-140˚W] during August 14-15, it will be shown that these features are the same and will be illustrated in the upper-level field (see section *2.3.6*). This result suggests that the CCKW associated with the genesis of Debby originated much further west over the Indian Ocean (80˚E) on 3 August. A detailed synoptic view of the interaction between the CCKW and the pre-Debby AEW is now highlighted in Fig. 2.7.

Due to the complexity of this figure, only the convectively active phase of the CCKW is discussed. On 18 August, the convectively active phase of the CCKW was expressed north of the equator over South America (Fig. 2.7a). At this time, the pre-Debby AEW was located roughly near the Greenwich Meridian. The first sign of enhanced convection along the Atlantic ITCZ associated with the CCKW was on 20 August over 5-10˚N, 25-35˚W (Fig. 2.7c). The amplification of negative OLR anomalies over the MDR occurred during the superposition between a pre-existing AEW (pre-Ernesto) and the convectively active phase of the CCKW. Negative OLR anomalies associated with the pre-Ernesto AEW grew in horizontal area, extending over 0-10˚N, 25-60˚W on 21 August (Fig. 2.7d). This AEW later formed into a tropical depression near the Lesser Antilles on 24 August (Fig. 2.7g).

By 21 August, negative OLR anomalies associated with the CCKW were observed over the eastern tropical Atlantic, highlighting the initial interaction between the pre-Debby AEW and the CCKW (Fig. 2.7d). Eighteen hours later, the AEW formed into a tropical cyclone. On 22 August, the tropical cyclone intensified, still within the convectively active phase of the CCKW (Fig. 2.7e). Note that over West Africa, an area of positive OLR anomalies is located within the convectively active phase of the CCKW and is associated with the local suppression forced by a pre-existing westward moving AEW.

Convection associated with Tropical Storm Debby weakened on August 23 after the passage of the convectively active phase of the CCKW (Fig. 2.7f). The suppression of convection over Tropical Storm Debby at this time has been related to its northwestward track into unfavorable conditions associated with a strong Saharan air layer (SAL; see Zipser et al. 2010). This suppression might also be associated with an interaction with the convectively suppressed phase of the CCKW (not shown).

During the subsequent days following the genesis of Debby, the convectively active phase of the CCKW progressed eastward over tropical Africa and provided an environment favorable for deep convection (Fig 2.7f-h). On 25 August, the negative OLR anomalies associated with the CCKW are observed to extend over 30° of longitude over Africa, highlighting the significant role of the CCKW on African convection (Fig. 2.7h).

The focus is now given to the anomalous upper-level wind field associated with the passage of the CCKW. Upper-level westerly wind anomalies were over the equatorial Atlantic, ahead of the convectively active phase of the CCKW on 18 August (Fig. 2.7a). Anomalous upper-level anticyclonic flow developed over the tropical Atlantic (centered over 10˚N, 37˚W) on 21 August during the superposition between the convectively active phase of the CCKW and the pre-Ernesto AEW (Fig. 2.7d). This anomalous anticyclonic circulation was also demonstrated in the CCKW composites suggesting that this is a robust feature of CCKWs (recall Figs. 2.5e,f). Further on 21 August, anomalous equatorial easterly flow was to the west of the minimum Kelvin filtered OLR anomaly, with anomalous equatorial westerly flow to the east (Fig. 2.7e). This anomalous upper-level wind pattern over the eastern tropical Atlantic demonstrates that the CCKW strongly contributed to the increased upper-level divergence over the eastern Atlantic. Further, anomalous northerly winds developed over the eastern tropical Atlantic during the passage of the convectively-active phase of the CCKW. These anomalous northerly winds were most evident during the superposition between the CCKW and the pre-Debby AEW on 21-22 August, and suggests that the CCKW increased both the convection and convective outflow of the pre-Debby AEW. These anomalous northerly winds over the eastern Atlantic are also demonstrated during the passage of the convectively active phase of the composited CCKW (see Fig. 2.5f-g).

The upper-level wind structure of the CCKW was less coherent over tropical Africa. Between the 22nd and 24th August, the upper-level wind anomalies over Africa within the convectively active phase of the CCKW are mostly meridionally oriented (Fig. 2.7e-g). This anomalous wind pattern is inconsistent with the composited CCKW upper-level wind structure and might result from complex interactions occurring over Africa on different spatial and temporal scales that were not associated with the CCKW (e.g., AEWs, equatorial Rossby waves, etc.). In this particular case, the circulation of a pre-existing, very large westward propagating AEW destructively interfered with the upper-level wind structure of the CCKW between 22 August and 24 August. However by 25 August, an anomalous upper-level anticyclonic circulation reestablished within the convectively active phase of the CCKW over eastern Africa (Fig. 2.7h). Anomalous easterly winds extended westward over equatorial Africa and the equatorial Atlantic from the broad anomalous anticyclonic circulation over eastern tropical Africa, suggesting that the CCKW maintained its dynamical structure during the brief period of interference.

A summary of the sequence of events that resulted in the genesis of Tropical Storm Debby now follows. Enhanced, deep convection occurred over the pre-Debby AEW during the passage of the convectively active phase of the CCKW. This convection was found to be associated with two strong MCSs (see Zawislak and Zipser 2010). These MCSs were initially generated downstream of the GHs region on 20 August, in association with the dynamical forcing from the pre-Debby AEW. It has also been demonstrated that these high amplitude MCSs intensified during the superposition between the convectively active phase of the CCKW and the pre-Debby AEW on 21 August. Presumably the influence of deep convection favored within the convectively active phase of the CCKW on the pre-Debby AEW aided the tropical cyclogenesis via increased latent release and PV generation (recall Fig. 2.2e).

2.3.6. The local state of the Madden Julian Oscillation

High amplitude CCKWs are often superimposed with the convectively active phase of the MJO (Dunkerton and Crum 1995). An MJO-phase space type diagram (e.g., WH04), using a new MJO index (see Chapter 7 and Appendix A for further details), indicates that the upper-level divergence associated with the convectively active phase of the MJO was located over the Western Hemisphere (phase 8 with an amplitude greater than 1σ) during the time of Debby's genesis (Ventrice et al. 2011, 2013; see Chapter 6) (Fig. 2.8). Therefore, the CCKW associated with the genesis of Debby may have had contributions from the low-frequency forcing of the MJO over the Western Hemisphere.

Between August 22 and 27, the MJO continued to propagate eastward over the Atlantic and African regions, and later over the Indian Ocean between September 6 and 15.

While MJO-phase space diagrams are useful to identify the phase and amplitude of the MJO, it is difficult to depict the spatial structure of the MJO through such a method. Therefore, Fig. 2.9 shows a time-longitude plot of unfiltered 200 hPa velocity potential (henceforth VP200) anomalies (shaded), with MJO filtered VP200 anomalies (black contours), and Kelvin filtered VP200 anomalies (multi-colored contours). The "D" represents the location and time of genesis of Tropical Storm Debby. MJO activity was strong during the month of July, weakened during early August, and re-strengthened towards the end of August. CCKWs were present during the entire time period. The CCKW associated with the genesis of Debby, which is now identified in the VP200 field, can be traced back to early July, and clearly completed multiple transients around the globe. Recall that the CCKW in the OLR field was less continuous around the globe, and suggests that VP200 might be a more useful field to filter for identifying CCKWs.

Between July 20 and August 5, the convectively suppressed phase of the MJO propagated eastward across the Atlantic. During early August, the MJO signal weakened and the convectively suppressed phase of the CCKW associated with the genesis of Debby became the strongest synoptic feature in the tropics. The convectively suppressed phase of this CCKW propagated eastward over the tropical Atlantic and Africa between August 1 and 19, and later over the Indian Ocean between August 20 and August 25. Once the convectively suppressed CCKW phase propagated over the Indian Ocean, the convectively suppressed phase of the MJO reformed, suggesting a possible relationship between CCKWs and the MJO. Note that positive MJO filtered VP200 anomalies began to develop over the Indian Ocean prior to the passage of the convectively suppressed CCKW phase, and might be a result of a the filtering technique since the positive MJO filtered anomalies start in an area of negative unfiltered VP200 anomalies.

Between July 27 and August 15, weak negative MJO filtered VP200 anomalies propagated eastward across the central Pacific. Thereafter, these negative MJO filtered VP200 anomalies propagated eastward over the East Pacific, at what appears to be too slow of phase speed when compared to the entire eastward progressing envelope of unfiltered negative VP200 anomalies that passed over the Atlantic and African regions between approximately August 16 and September 7. During this time, the space-time filtered VP200 anomalies indicate that the convectively active phases of a pair of CCKWs were the main synoptic features over the Atlantic and African regions. The first of the two CCKWs was the wave associated with the genesis of Debby. As the convectively active phase of the second CCKW propagated over Africa, a new convectively active MJO signal developed there. This "MJO initiation" is questionable since the overall eastward progression of unfiltered negative VP200 anomalies is continuous in time over Africa, and suggests that the filter technique is struggling due to negative VP200 anomalies propagating too fast for MJO-time scale filtering. Nevertheless, there was an apparent phasing between the CCKW associated with the genesis of Debby and the MJO. This idea that CCKWs over the Western Hemisphere might be stronger during preferable MJO states will be addressed later in Chapter 3.

2.4. The climatological relationship between strong convectively coupled atmospheric Kelvin waves and Atlantic tropical cyclogenesis

CCKWs might modulate tropical cyclogenesis over the MDR by *i)* directly amplifying westward propagating AEWs, or *ii)* providing a favorable environment over the tropical Atlantic for genesis. To investigate the general relationship between CCKWs and tropical cyclogenesis, Fig. 2.10 shows a time-longitude composite using the CCKW index of unfiltered OLR anomalies (shaded) and the locations of tropical cyclogenesis events occurring equatorward of 25°N. Generally, there is a low number tropical cyclogenesis events observed between the leading convectively suppressed phase and the convectively active phase of the CCKW. Tropical cyclogenesis is more frequent within the convectively active phase of the CCKW (as is the case of Tropical Storm Debby; larger yellow crossed circle). However, tropical cyclogenesis becomes most frequent just after the passage of the convectively active phase of the CCKW. This increase of tropical cyclogenesis events occurs in the general area after the passage of the convectively active phase and during the initial passage of the second convectively suppressed phase.

To quantify the counts of tropical cyclogenesis events relative to the CCKW in daily intervals, Fig. 2.11 shows the number of tropical cyclogenesis events relative to the local passage of the convectively active phases of CCKWs. The start of Day 0 represents the transition to statistically significant unfiltered negative OLR anomalies associated with the CCKW over the entire MDR (slanted bold black dashed line on Fig. 2.10). One day prior to the convectively active phase of the CCKW (Day -1), a minimum of tropical cyclogenesis is observed. This relatively reduced-period of tropical cyclogenesis activity occurs after the passage of the leading convectively suppressed phase of the CCKW. A large increase in the number of tropical cyclogenesis events is observed between Day -1 and Day +2, the peak in tropical cyclogenesis frequency. This peak is statistically different from the counts of tropical cyclogenesis events in four different lags (Day -3, Day -1, Day 0, and Day +3) at the 95% level. Further, the count of tropical cyclogenesis events on Day +2 is statistically different from the climatology at the 90% level.

This lead-lag relationship between the passage of the convectively active phase of the CCKW and the increased events of tropical cyclogenesis activity may occur due to a lag between convective enhancement over a tropical wave and the actual naming of a tropical cyclone. On the other hand, since the peak of tropical cyclogenesis events does not occur under the convectively active phase of the CCKW (Day +2 occurs between the convectively active phase of the CCKW and the second convectively suppressed phase), the enhancement of tropical cyclogenesis activity might not occur from convective processes alone. We hypothesize that the CCKW may be impacting the large-scale environmental conditions associated with tropical cyclogenesis. This hypothesis will be explored in Chapter 3.

2.5. Discussion and Conclusions

Observations were presented of an initially weak AEW undergoing tropical cyclogenesis after interacting with the convective processes generated downstream of the GHs region, as well as interacting with an eastward propagating CCKW during the 2006 NAMMA field campaign. These observations present a new aspect of tropical weather variability over tropical Africa and tropical cyclogenesis variability over the tropical Atlantic.

CPC IR data indicated that the pre-Debby AEW interacted with the coherent diurnal cycle of convection generated over the GHs region. These daily convective processes enhanced the pre-Debby AEW as it propagated off the coast of West Africa. Early morning oceanic convection was observed prior to the passage of the pre-Debby AEW. This oceanic convection remained active during the afternoon hours, a time when convection is normally suppressed. During the passage of the pre-Debby AEW over the GHs region, deep afternoon convection generated directly northwest of the FDHs and occurred within the vicinity of the AEW trough, enhancing the AEW. On 21 August, the convectively active phase of the CCKW first interacted with the pre-Debby AEW just off the coast of West Africa (Fig. 2.6d). This was the same time that Zawislak and Zipser (2010) observed two of the strongest West African MCSs seen in the JJAS 1998-2007 TRMM climatology. These MCSs were initially generated by the interaction between the diurnal cycle of convection generated by the GHs region and the pre-Debby AEW. On 21 August, the minimum Kelvin filtered OLR value is located roughly 15° west of where the strong MCSs were observed by Zawislak and Zipser (2010). In addition from the forcing of the pre-Debby AEW, it seems likely that these strong MCSs were also influenced by the CCKW.

The genesis of Tropical Storm Debby occurred during the superposition between the convectively active phase of a CCKW and the pre-Debby AEW on 21-22 August. Tropical cyclogenesis occurred during the CCKW passage at 18Z on 21 August. Based on the analysis presented here, it is suggested that the CCKW modulated the wind field over the eastern tropical Atlantic prior to and during the passage of the pre-Debby AEW. The modulation of wind was demonstrated by investigating the upper-level winds, but

CCKWs also influence winds in the lower troposphere. Anomalous low-level westerly wind anomalies are collocated with the convectively active phase of the CCKW, whereas anomalous low-level easterly winds are collocated within the leading convectively suppressed phase (not shown). Therefore, during the superposition of the convectively active phase of the CCKW and the pre-Debby AEW, one might expect an enhancement of the low-level westerly winds near the equator. Vizy and Cook (2010) found that the development of the pre-Debby AEW over the Cape Verde region was associated with a strong low-level westerly jet located just south of the 850-hPa vortex center. The acceleration of low-level westerly flow prior to tropical development has been found to be an influential mechanism in providing the external forcing (e.g., low-level cyclonic vorticity and large-scale vertical ascent) necessary for tropical cyclogenesis (e.g., Gray 1988, 1998; Lee et al. 1989; Briegel and Frank 1997). The acceleration of low-level westerly flow prior to development of Debby may have had a strong contribution from the CCKW.

Vizy and Cook (2010) suggest that the AEW (pre-Ernesto) that preceded the pre-Debby AEW created a surge of low-level westerly flow which provided a favorable environment for the genesis of Debby. An alternative hypothesis is suggested here, highlighting the fact that both AEWs interacted with the same CCKW, a synoptic-scale feature that influenced the MDR roughly during the period 18-24 August. The superposition of the two different AEWs with the convectively active phase of the CCKW occurred over different regions of the MDR. It is possible that Ernesto did not immediately form into a tropical cyclone after interacting with the CCKW on 20 August due to interactions with a strong SAL (Zipser et al. 2010). Ernesto later formed into a tropical cyclone on 24 August, after moving out of the SAL environment. Debby formed immediately into a tropical cyclone over the eastern Atlantic while interacting with the same CCKW but decayed soon after moving northwestward into a strong SAL outbreak (see Zipser et al. 2010). In contrast to this hypothesis, Braun (2010) and Sippel et al. (2011) find that subsidence associated with deep, dry convective mixing over the Sahara created the dry air over the eastern tropical Atlantic, which eventually lead to the decay of Debby.

The local state of the MJO during the time of Debby's genesis consisted of enhanced convection over the Western Hemisphere and suppressed convection over the Indian Ocean and Maritime Continent. The CCKW associated with the genesis of Debby was superimposed with the convectively active phase of the MJO, indicating a possible relationship between the MJO and CCKWs. The nature of the relationship between the MJO and CCKWs is unclear and will be discussed further in Chapter 3.

A coherent relationship between tropical cyclogenesis over the MDR and CCKWs is also revealed from a climatological perspective. Tropical cyclogenesis is found to be significantly lower after the passage of the leading convectively suppressed phase of the CCKW. Tropical cyclogenesis becomes significantly more frequent two days after convection is initially excited by the CCKW. This relationship opposes the past work that suggest relatively minor relationships between tropical cyclogenesis and CCKWs (e.g., Frank and Roundy 2006; Schreck et al. 2011) and is quantified by counting the number of tropical cyclones that form relative to an eastward propagating CCKW.

In order to fully assess the influence of a CCKW passage on tropical cyclogenesis, an analysis of CCKWs within the large-scale environment is needed. Since a two day lag exists between the passage of the leading edge of the convectively active phase of a CCKW and the peak of tropical cyclogenesis frequency, there is a suggestion that CCKWs may alter large-scale environmental conditions over the MDR for a period of time after its passage in addition to enhancing convection. This analysis will be presented in Chapter 3.

2.6. Figures

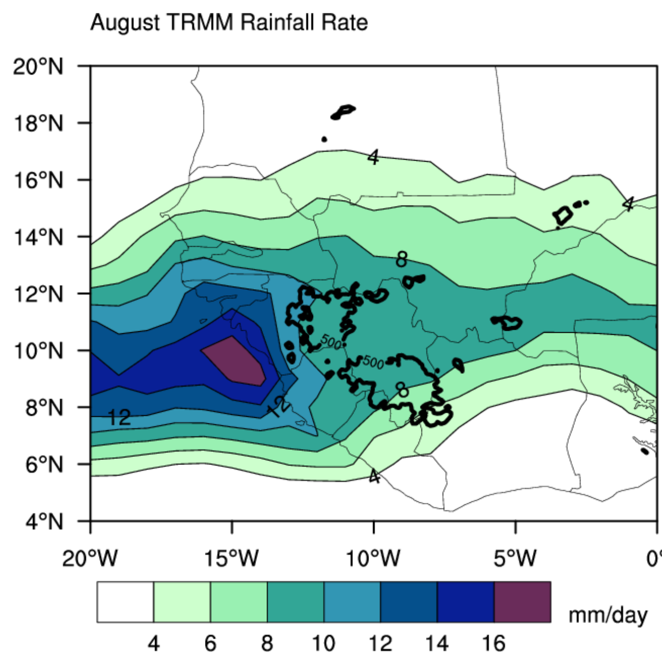

Fig. 2.1. August (1998-2009) averaged TRMM 3B42 rainfall rate (mm day^{-1}) is shaded and elevation (m) is contoured. Shade interval is 2 mm day^{-1}; contour interval is 500 m.

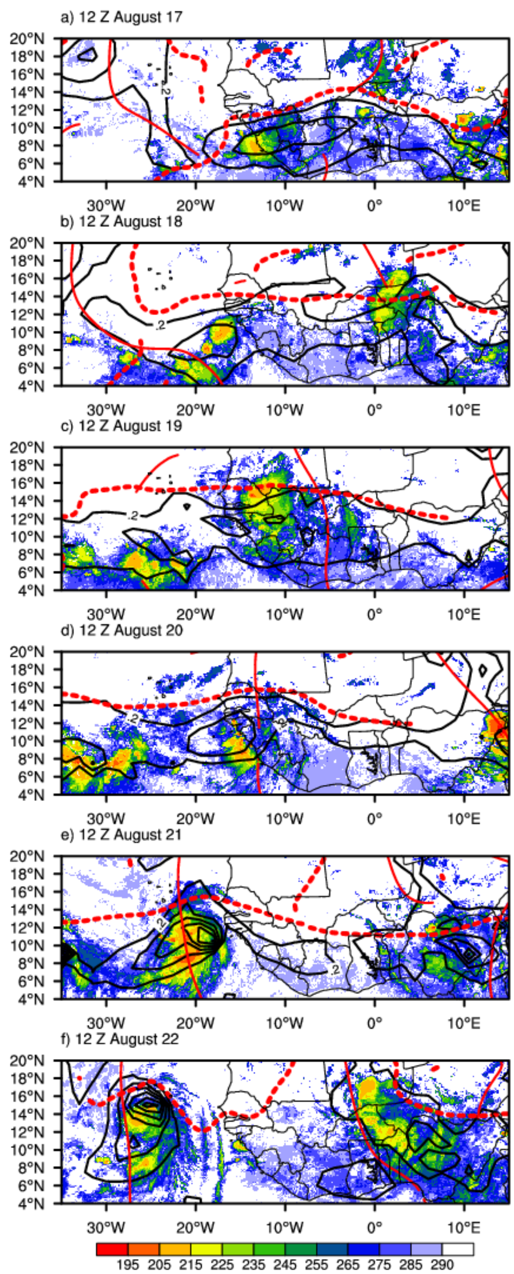

Fig. 2.2. The evolution of the pre-Debby AEW. Brightness temperature is shaded and 650 hPa PV is contoured (black). AEW trough axes are identified as north-south oriented solid lines (red) and the mean position of AEJ is identified by the dashed line (red). Shade interval is 10°K; Contour interval is 0.1 PVUs.

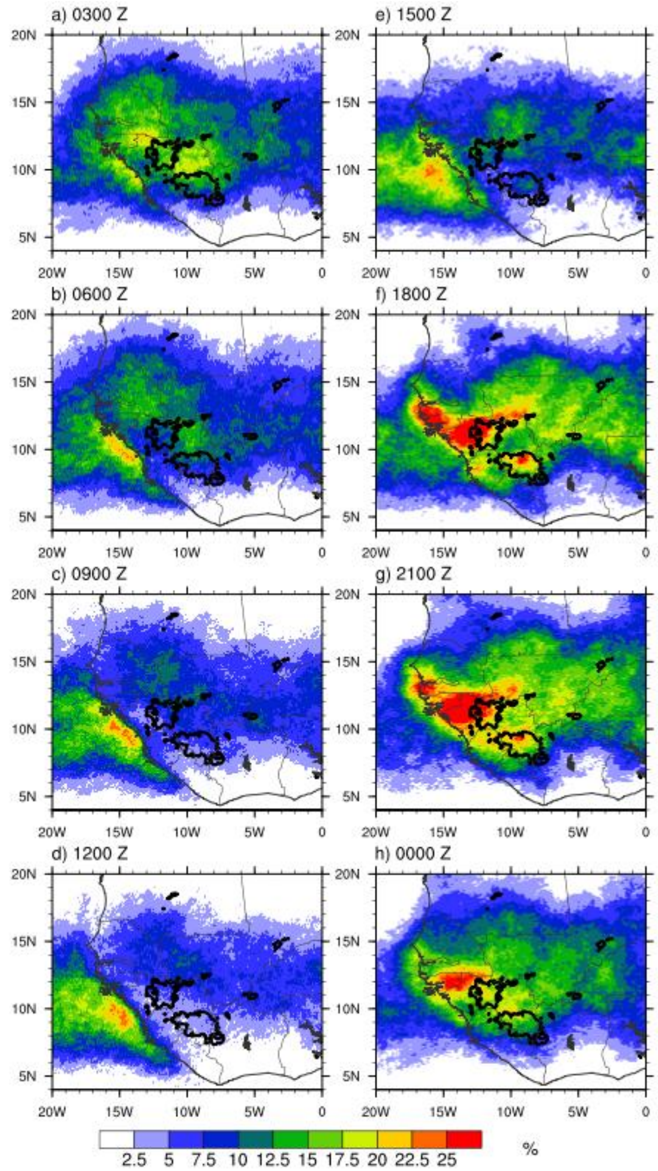

Fig. 2.3. 1989-2009 August hourly averaged 233K exceedance frequency for every 3 hours. Shading represents an estimation of the percentage of time a cloud is precipitating. Shade interval is 0.025.

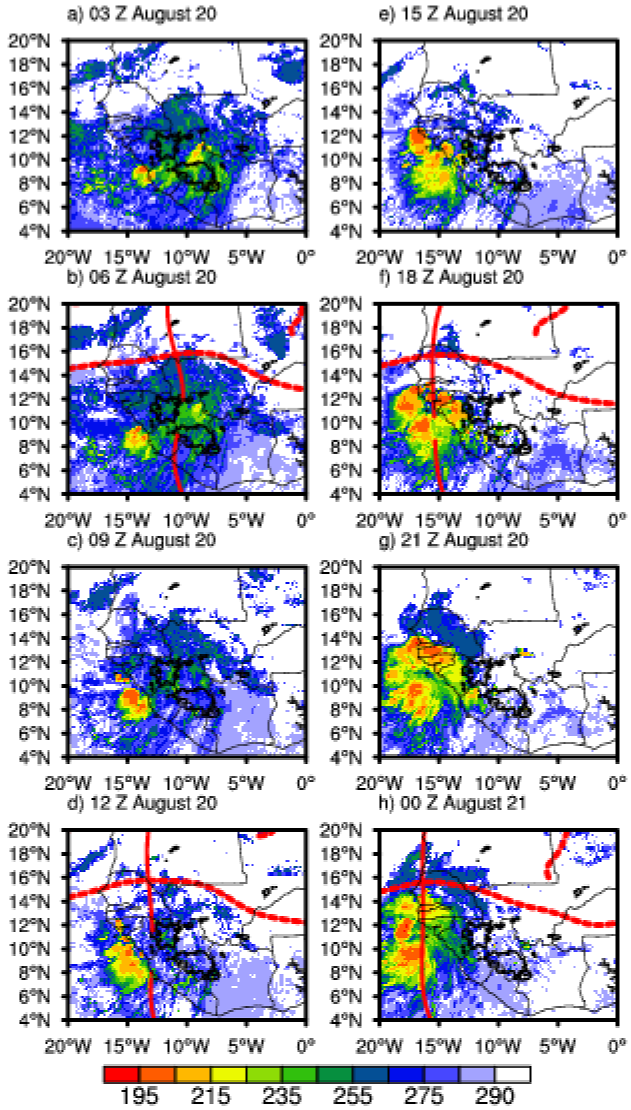

Fig. 2.4. Brightness temperature (shaded) highlighting the interaction between the pre-Debby AEW and the diurnal cycle of convection beginning at 03Z August 20 and ending on 00Z August 21 (2006) for every 3 hours. The AEW trough axis is identified by the north-south oriented line (red) and the AEJ is identified by the zonally oriented dashed line (red). Shade interval is 10°K.

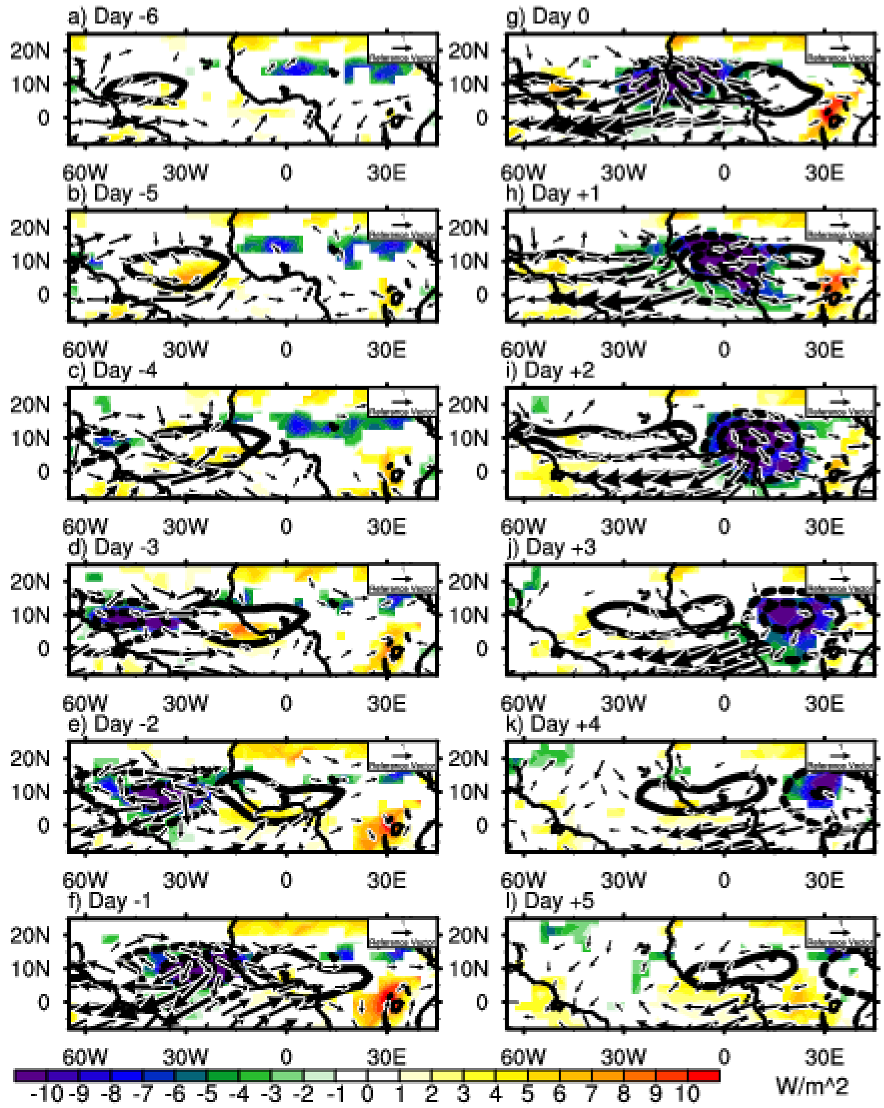

Fig. 2.5. Composite maps of NOAA daily averaged interpolated unfiltered OLR anomalies averaged over each CCKW lag. OLR anomalies statistically different than zero at the 95% level are shaded. Kelvin filtered OLR anomalies are contoured if statistically different than zero at the 95% level. Negative Kelvin filtered OLR anomalies are dashed. Vectors represent 200 hPa wind anomalies only showing magnitudes greater than 0.5 ms^{-1}. Shade interval is 1 Wm^{-2}; contours begin at (+/-) 3 Wm^{-2} and the contour interval is 6 Wm^{-2}; reference wind vector is 1 ms^{-1}.

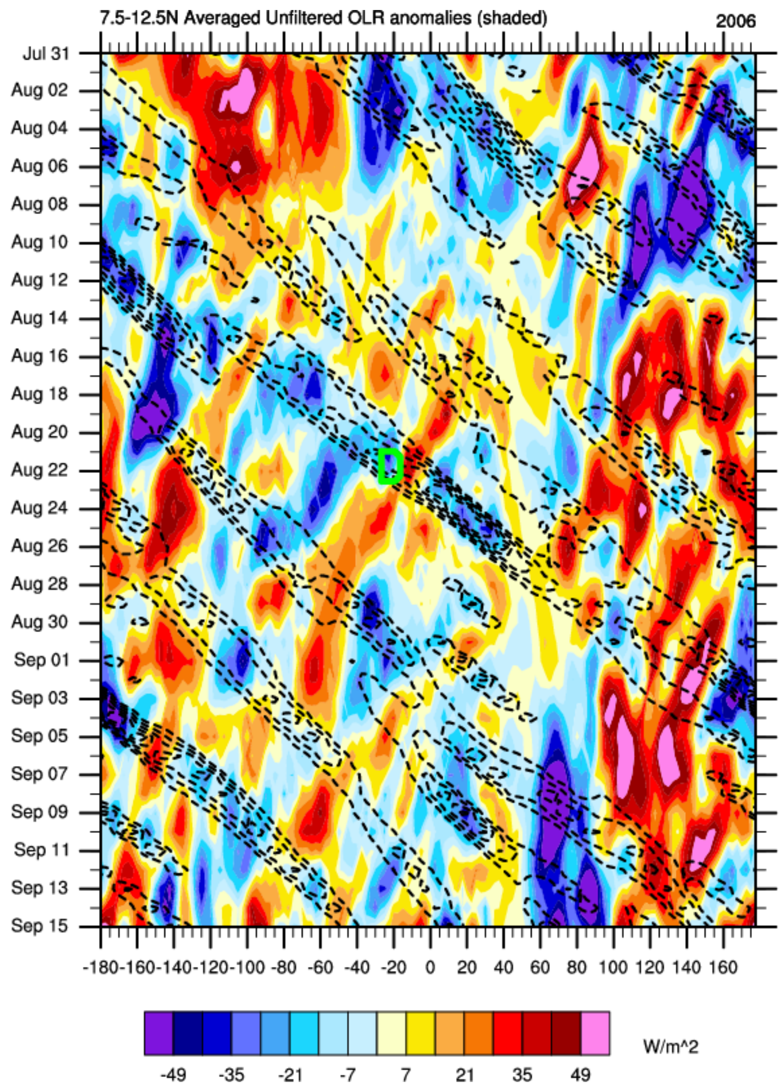

Fig. 2.6. A time-longitude plot averaging unfiltered OLR anomalies (shaded) and only negative Kelvin filtered OLR anomalies (dashed black lines) between the 7.5˚N-12.5˚N latitude band. The “D” represents the location where Debby became a named tropical cyclone. Contours begin at -3 Wm^{-2} and the contour interval is -5 Wm^{-2}.

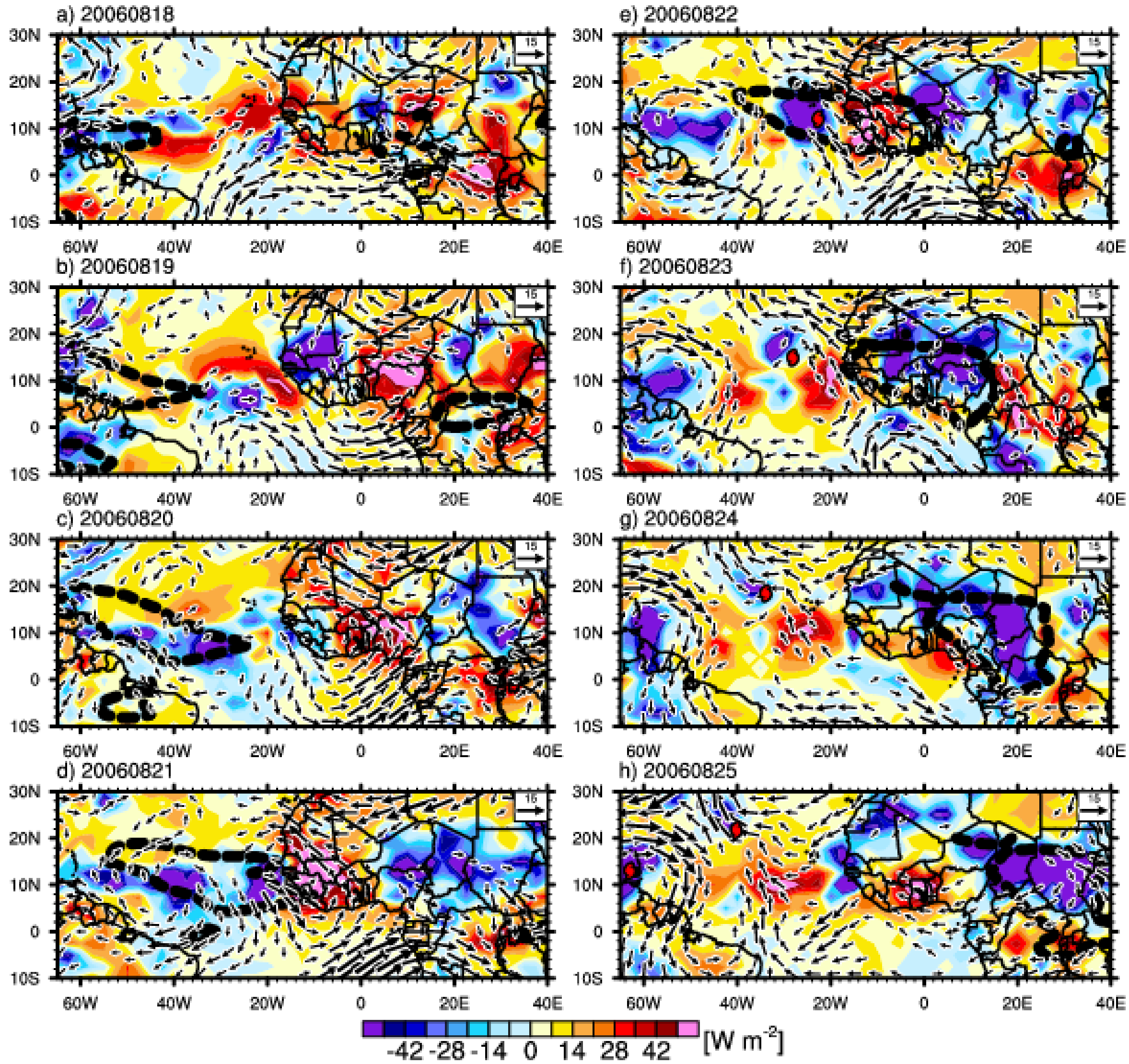

Fig. 2.7. The interaction between the pre-Debby AEW and a CCKW (21-22 August 2006). Shading is unfiltered OLR anomalies. The black dashed contour represents the -10 Wm^{-2} Kelvin filtered OLR anomaly. Vectors represent 200 hPa wind anomalies only showing magnitudes greater than 5 ms^{-1}.

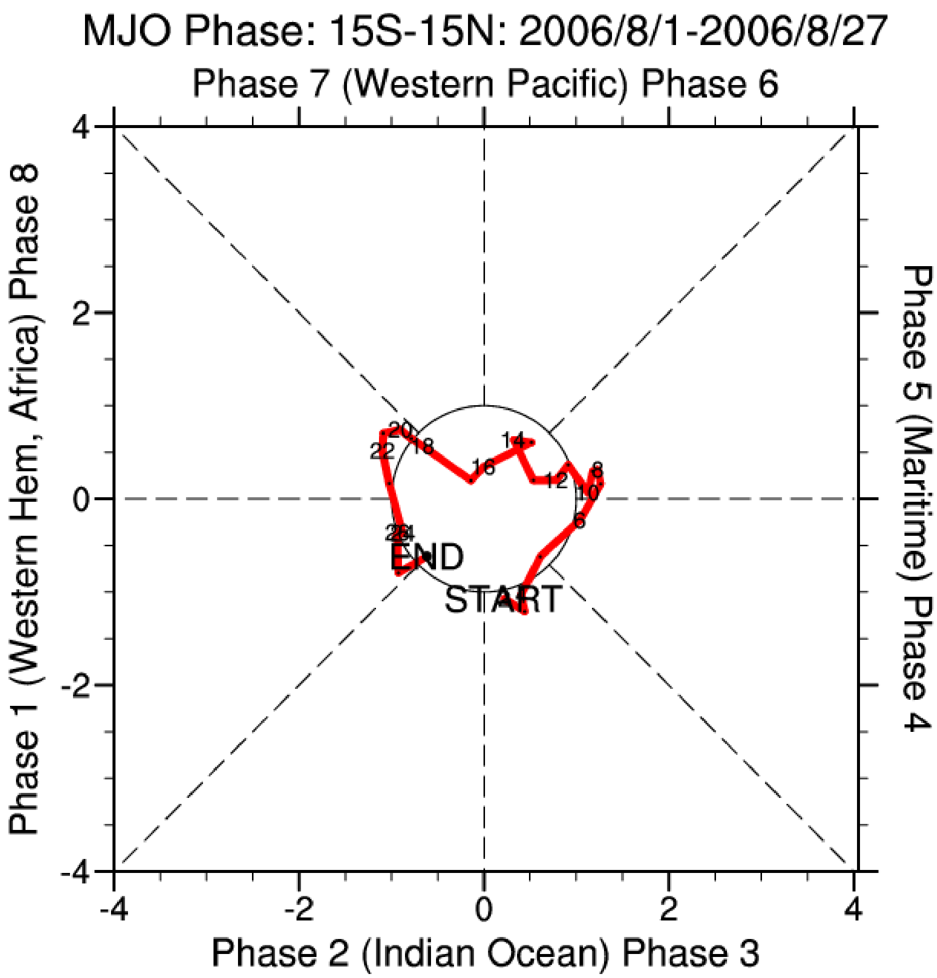

Fig. 2.8. An MJO-type phase space diagram beginning on August 1 and ending on August 27, using a new MJO index derived by a combined EOF analysis using VP200, U850, and U200.

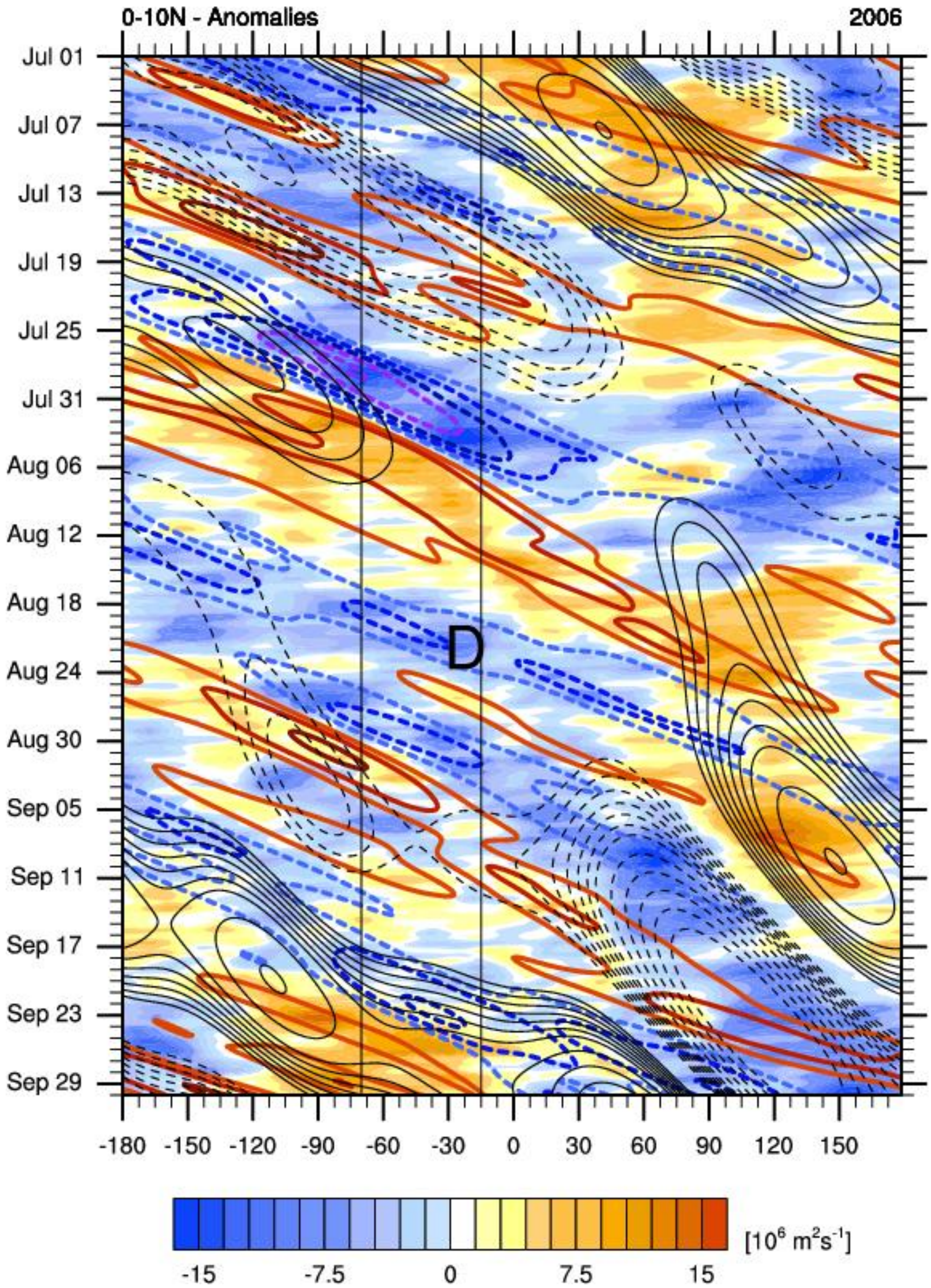

Fig. 2.9. A time longitude plot of unfiltered VP200 anomalies (shaded), MJO filtered VP200 anomalies (black contours; dashed if negative), and Kelvin filtered VP200 anomalies (multi-colored contours; dashed and cold colored if negative) for the dates between July 1 and September 30. The "D" represents the location and time of genesis for Tropical Storm Debby. The two black vertical lines represent the Atlantic's MDR. All fields are averaged over the 0-10ºN latitude band.

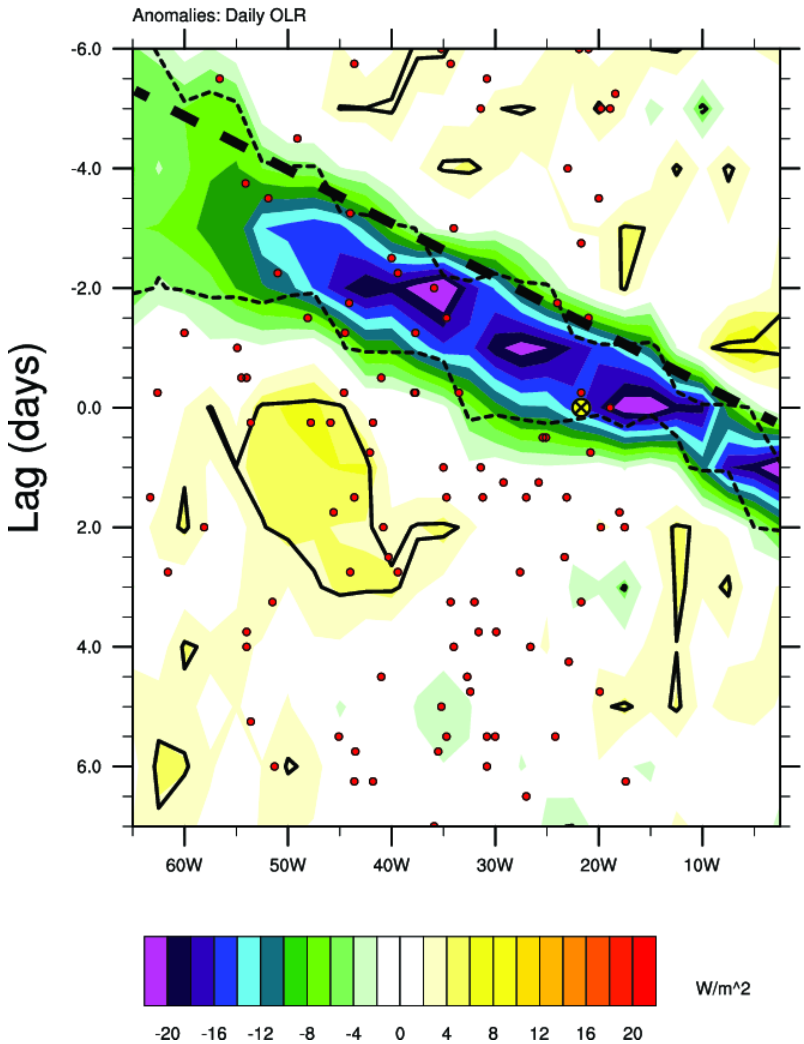

Fig. 2.10. A time-longitude plot of composited OLR anomalies averaged along 10°N during June-September 1979-2009. Composite unfiltered OLR anomalies are shaded. Positive OLR anomalies statistically different than zero at the 95% level are within the solid contour. Negative OLR anomalies statistically different than zero at the 95% level are within dashed contour. The bold, larger dashed black line represents the beginning of "Day 0" in Figure 9. Tropical cyclogenesis within the MDR (5-25°N, 65-15°W) for any given lag is denoted by a red circle. The genesis of Tropical Storm Debby is highlighted by the large yellow crossed circle. Shade interval is 2 Wm^{-2}.

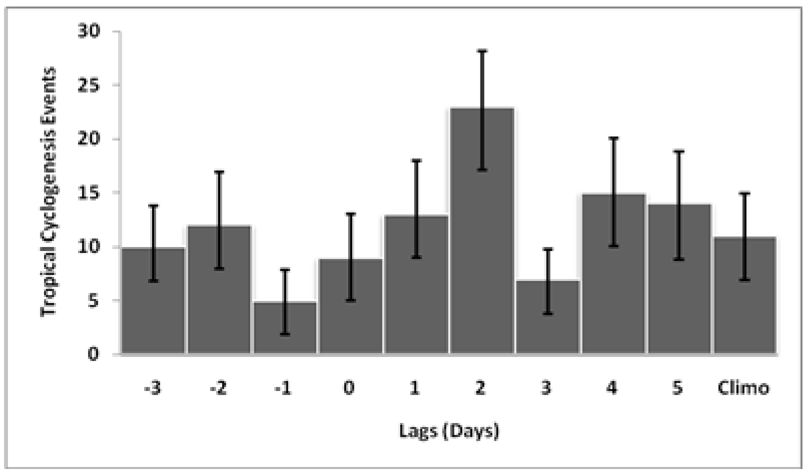

Fig. 2.11. Tropical cyclogenesis events over the MDR (5-25°N, 15-65°W) relative to the CCKW during June-September 1979-2009. "Day 0" highlights the transition to statistically significant negative unfiltered OLR anomalies associated with the CCKW, or the eastern-most side of the convectively active phase. The "Climo" lag represents the climatological number of tropical cyclogenesis events for an average daily lag. Error bars indicate the 90% confidence interval.

3. The impact of convectively coupled Kelvin waves on the large-scale environment over the tropical Atlantic and African regions

3.1. Introduction

Tropical cyclones commonly form when sea surface temperatures are warm and when large-scale environmental conditions (e.g., low-moderate vertical wind shear, increased low-to-mid level moisture, and sufficient low-level cyclonic relative vorticity) are favorable (Gray 1968; 1988; 1998). Such conditions are known to vary on different timescales. At multidecadal timescales, the environment over the Atlantic has been shown to vary with the Atlantic Multidecadal Oscillation (AMO; e.g., Klotzbach and Gray 2008; Aiyyer and Thorncroft 2011). At interannual timescales, the environment is modulated according to the particular phase of the El Niño Southern Oscillation (ENSO; e.g., Gray 1984; Goldenberg and Shapiro 1996). At intraseasonal timescales, the MJO provides periods of favorable or unfavorable conditions over the Atlantic (e.g., Maloney and Shaman 2008; Klotzbach 2010; Ventrice et al. 2011). Additionally, a period of favorable environmental conditions might only last for a few days and still yield a tropical cyclone. These sub-seasonal periods of favorable conditions might be provided by CCKWs.

Chapter 2 discussed the genesis of Tropical Storm Debby (2006). A weak AEW initially strengthened in association with the coherent diurnal cycle of convection found downstream of the Guinea Highlands region. It later formed into a tropical cyclone during the superposition with an eastward propagating CCKW. Further, Chapter 2 also investigated the climatological modulation of Atlantic tropical cyclogenesis by CCKWs. Tropical cyclogenesis was less frequent one-to-two days prior to the passage of the convectively active phase of the CCKW. Tropical cyclogenesis became more frequent during this passage and peaked just after. The relationship between CCKWs and tropical cyclogenesis frequency (see Fig. 2.10 and 2.11) provides motivation to investigate the influences of the CCKW on the large-scale environment for tropical cyclogenesis over the tropical Atlantic.

In addition to the direct enhancement of convection by the CCKW, the lead-lag relationship between CCKWs and Atlantic tropical cyclogenesis suggests that CCKWs may also impact the large-scale environment over the MDR. The purpose of this chapter is to explore the extent to which CCKWs alter this environment. This study will focus on the influence of CCKWs on the large-scale environmental conditions over the tropical Atlantic that is known to impact tropical cyclogenesis (vertical wind shear, moisture, low-level relative vorticity). This aspect differs from previous studies that investigate CCKWs over the tropical Atlantic and West Africa (e.g., Mounier et al. 2007; Wang and Fu 2007; Mekonnen et al. 2008), who investigate the convective influence of CCKWs.

Chapter 3 is structured as follows. Section 3.2 provides datasets and methodologies. Section 3.3 discusses a composite analysis highlighting the role of CCKWs on large-scale environment over the tropical Atlantic and West Africa. A discussion relating the large-scale environment modulation associated with CCKWs and tropical cyclogenesis is provided in Section 3.4. Concluding remarks are given in Section 3.5.

3.2. Datasets and Methodology

The ERA-Interim dataset (Dee et al. 2010) was used to investigate the synoptic evolution of the composited CCKW. This dataset covers the period 1989 to present and has a horizontal resolution of 1.5°. Previous studies (e.g., Kiladis et al. 2009 and references therein) have shown the utility of similar reanalyses for studying the structures of equatorial waves.

Convection associated with CCKWs is explored using NOAA's daily averaged interpolated OLR dataset, with a horizontal gridded resolution of 2.5° (Liebmann and Smith 1996). To support the analysis of CCKWs, wavenumber-frequency filtering was applied on the daily averaged NOAA interpolated OLR dataset following the methodology of Wheeler and Kiladis (1999). Filtering for the Kelvin wave was performed with a period range of 2.5-20 days, with eastward wave numbers 1-14. The filter is constrained by the Kelvin wave dispersion curves for equivalent depths of 8-90 meters.

Following the methodology of Chapter 2, the same CCKW index is used. The CCKW index is composed of all days when the minimum negative Kelvin-filtered OLR anomaly were less than -1.5 standard deviations in magnitude during the 1989-2009 JJAS seasons over the selected grid point (10°N, 15°W).

Anomalies for all composited fields were constructed by subtracting the long-term mean and the first four harmonics of the seasonal cycle. Bootstrap random resampling tests with one thousand iterations were used for statistical significance testing on all anomalies similar to Roundy and Frank (2004). In each of these tests, a new sample equal in size to the original was randomly drawn for the original set of composite dates with replacement. The composite anomalies were considered 90% significant if 900 out of the 1000 random composites had the same sign.

3.3. Composite analysis of convectively-coupled Kelvin waves over the Atlantic

3.3.1. The distribution of June-September Kelvin filtered OLR variance

The geographical distribution of the variance of Kelvin filtered OLR [averaged over 1979-2009 for June-September (JJAS)] is shown in Fig. 3.1. The overall activity is similar to previous studies using Kelvin filtered OLR variance (e.g., Wheeler and Kiladis 1999; Wheeler et al. 2000; Roundy and Frank 2004; Mekonnen et al. 2008; and Kiladis et al. 2009). Peak activity occurs over the equatorial Indian Ocean and northern equatorial west-central Pacific. Kelvin wave activity is also observed generally between 5-10°N over the entire tropical central-to-eastern Pacific and Atlantic Oceans and along 10°N over West Africa. The variance of Kelvin filtered OLR is not symmetric about the equator except for over the Indian Ocean, consistent with the previous analyses of Kelvin wave variance (e.g., Straub and Kiladis 2002; Roundy and Frank 2004; Mekonnen et al. 2008). Over the Atlantic, Kelvin wave OLR variance is observed north of the equator and is characterized by slightly weaker magnitudes compared to the rest of the tropical band.

3.3.2. The vertical structure of the convectively coupled Kelvin wave

The distinctive vertical structure of the CCKW is highlighted in Fig. 3.2 using the ERA-Interim reanalysis data. This figure is sampled when the composite minimum Kelvin filtered OLR anomaly is located over 15°W. The cross-section is averaged over the latitudinal band 5°S-10°N to maximize the signature of the CCKW within the selected fields. It is important to note that the scales represented in the composite CCKW represent those of the average CCKW, but individual CCKWs may have different spatial and temporal scales. Nevertheless, the resulting vertical structure compares remarkably well with the time-height composites of Straub and Kiladis (2003c) and Kiladis et al.

(2009), who used 12 hourly radiosonde data over the Pacific island of Majuro (7.1°N, 171.4°E).

The zonal wind-height cross-section composite illustrates a strong westward tilt with height of weak zonal wind anomalies through the lower-troposphere and an eastward tilt with height of higher amplitude zonal wind anomalies in the upper-troposphere and lower-stratosphere (Fig. 3.2a). In agreement with Straub and Kiladis (2003a,c), low-level (850 hPa) zonal wind convergence is observed to precede upper-level (250 hPa) divergence by roughly 15° of longitude. The most dominant wind signature is located in the upper-troposphere, highlighted by strong westerly anomalies between 15°W-15°E and strong easterly wind anomalies between 30-60°W. These easterly wind anomalies over 30°W-60°W are observed throughout the 100-300 hPa layer and extend westward through 120°W. Therefore, a deep layer of anomalous upper-level easterly flow exists over the tropical Atlantic after the passage of the CCKW. This anomalous upper-level easterly flow extends well over 90° of longitude (15°W-120°W) and exists over a deep layer (700-400 hPa) of anomalous westerly flow.

The temperature (Fig. 3.2b) and specific humidity (Fig. 3.2c) cross sections display vertical structures similar to the observations of Kiladis et al. (2009). Lower-tropospheric moistening begins over 30°E and extends back westward with height, becoming vertical in nature over 15°W. Simultaneously, a warming of the lower troposphere occurs represented by the positive temperature anomaly beginning in the lower troposphere over Africa, extending back westward with height to 300 hPa over 10°W. Over the longitudes of 15°W-0°E, the lower troposphere begins to dry and cool, while the mid-upper troposphere remains moist and warm in association with deeper convection. The broad cold anomaly extending from 850-500 hPa at 15°W is associated with adiabatic cooling due to vertical ascent. In contrast to observations of Straub and Kiladis (2003c) and Kiladis et al. (2009), no cold pool exists near the surface over 15°W, which is attributed to a lack of convective cold down drafts reaching the surface. This result might arise from the location of the composite, sampling the moist Atlantic ITCZ, or it could represent a shortcoming of the model-derived reanalysis. The vertically stacked oriented lines of negative and positive temperature anomalies that tilt eastward with height between the 200-50 hPa layer over 15°W highlights the upward propagation of wave energy, which is consistent with an eastward moving upper tropospheric heat source (Lindzen 1967; Lindzen and Matsuno 1968; Andrews et al. 1987) and with the observations of Straub and Kiladis (2003c) and Kiladis et al. (2009).

The temperature and moisture evolution is also linked to the morphology of cloudiness highlighted in Straub and Kiladis (2002). This morphology begins with shallow convection over 10°E, progressing to deep convection over 15°W, and finally stratiform cloudiness which is associated with a moist upper troposphere and dry lower-troposphere over 30°W. The area of cold anomalies below 850 hPa over 15-30°W highlights the evaporation of stratiform precipitation in the low-level drier air.

3.3.3. The role of the convectively coupled Kelvin wave on the environmental conditions favorable for Atlantic tropical cyclogenesis

i) Vertical wind shear

The vertical wind structure of the observed CCKW over the tropical Atlantic is characterized by upper-tropospheric winds opposite to those in the lower-troposphere (recall Fig. 3.2a). Therefore, CCKWs are expected to impact the vertical wind shear patterns over the MDR. The JJAS climatological 925-200 hPa vertical wind shear pattern over the tropical Atlantic, including portions of South America and West Africa is shown in Fig. 3.3. The direction of shear represents the vector difference between 925 hPa and 200 hPa. Consistent with results of Aiyyer and Thorncroft (2011), this figure shows that the tropical Atlantic is characterized by two different background vertical wind shear states. The western subtropical Atlantic is characterized by westerly vertical wind shear associated with the subtropical westerly jet, whereas a large portion of the eastern tropical Atlantic is characterized by easterly vertical wind shear associated with the tropical easterly jet.

To investigate the influence of CCKWs on synoptic-scale vertical wind shear patterns over the tropical Atlantic, Fig. 3.4 shows composites of 925-200 hPa vertical wind shear magnitude anomalies (shaded) and vector anomalies (vectors) averaged over each lag of the CCKW index. As in Fig. 3.3, the direction of shear represents the vector difference between 925 hPa and 200 hPa. At Day -6, westerly shear vector anomalies occur within and to the east of the convectively suppressed phase of the composited CCKW over the western tropical Atlantic (Fig. 3.4a). These westerly shear vector anomalies shift eastward with time over the tropical Atlantic between the leading convectively suppressed and convectively active phase of the CCKW (Fig. 3.4a-e). At Day -2, an anomalous anticyclonic shear signature develops within the convectively active phase of the CCKW and highlights the atmospheric response to diabatic heating associated with deep convection (e.g., Ferguson et al. 2009; Dias and Pauluis 2009). This anomalous anticyclonic signature is consistent with the composite upper-level wind structure of the CCKW over the Atlantic at this particular time (see Fig. 2.5). At Day -1, the anomalous anticyclonic shear signature is now located just west of the minimum Kelvin filtered OLR anomaly, resembling a Gill-Matsuno-type response to deep convection (Gill 1980). Further at this time, northeasterly shear vector anomalies are to the west of the convectively active phase of the CCKW and extend westward over South America (Fig. 3.4f). Thereafter, easterly shear vector anomalies are observed to progress eastward behind the convectively active phase of the CCKW, consistent with dynamical structure of the CCKW (recall Fig. 3.2b).

It is important to realize that a particular phase of a CCKW affects the magnitude of vertical wind shear differently depending on the direction of the environmental background wind shear. To illustrate this point, we focus on the westerly vertical wind shear phase of the CCKW over the western tropical Atlantic at Day -4 (Fig. 3.4c). The background westerly shear over South America (Fig. 3.3) significantly increases within the westerly shear phase ahead of the convectively active phase of the CCKW. Vertical wind shear also significantly increases over the entire tropical north Atlantic poleward of 10°N. Figure 3.3 shows that these are regions where the climatological vertical wind shear is westerly. Therefore the westerly vertical wind shear phase of the CCKW is acting to increase the background westerly shear over these regions. In contrast to the impact of the CCKW on vertical wind shear over the western tropical Atlantic, over the eastern tropical Atlantic where the climatological shear is easterly (Fig. 3.3), significantly reduced vertical wind shear is observed equatorward of 10°N within the westerly shear phase of the CCKW (Fig. 3.4c). The westerly vertical wind shear phase of the CCKW opposes the climatological easterly shear and reduces the background vertical wind shear there. While on Day 0, vertical wind shear reduces over South America and over the western tropical Atlantic as the easterly shear phase of the CCKW reduces the climatological westerly shear there (Fig. 3.4g). Vertical wind shear is also reduced over Africa and poleward of 10°N over the tropical Atlantic for the same reason. Between 0-10°N over the eastern tropical Atlantic, vertical wind shear increases as the easterly shear phase of the CCKW increases the climatological easterly shear there. Throughout the subsequent lags (Day +1 through Day +5), vertical wind shear increases over equatorial Africa as the easterly shear phase of the CCKW increases the climatological easterly there (Fig. 3.4h-l).

To elaborate on the influence of the CCKW on the vertical wind shear magnitude anomaly over the tropical Atlantic, Fig. 3.5 shows a time longitude plot of 925-200 hPa vertical wind shear magnitude anomalies averaged within the 0-25°N band over each lag of the CCKW index. Day 0 now represents the time when the minimum composited Kelvin-filtered OLR anomaly passes over a grid point located in the central MDR (10°N, 45°W). A quadrupole signature is apparent within the vertical wind shear magnitude anomaly field. Where the climatological background shear is westerly over the MDR (30-65°W), four days prior to the passage of the convectively suppressed phase of the CCKW, vertical wind shear begins to increase. Wind shear magnitude anomalies continue to amplify just before the passage of the minimum Kelvin filtered OLR anomaly. But directly after the passage of the minimum Kelvin filtered OLR anomaly, shear is reduced. These negative wind shear magnitude anomalies are smaller in amplitude than the positive wind shear magnitude anomalies observed prior to the passage of the minimum Kelvin filtered OLR anomaly, but they remain weakly negative up to four days after the passage of minimum Kelvin filtered OLR anomaly.

Where the climatological background shear is easterly over the MDR, including West Africa (30°W-0°E), the opposite vertical wind shear evolution is observed. Roughly 3-4 days before the passage of the convectively active phase of the composited CCKW, vertical wind shear magnitude anomalies become negative. Wind shear magnitude anomalies over this region remain negative until the passage of the minimum Kelvin filtered OLR anomaly. Tropical Storm Debby (2006) formed within the convectively active phase of a CCKW over the eastern Atlantic (Chapter 2). Vizy and Cook (2009) found that the pre-Debby AEW experienced 40% less vertical wind shear over the coast of West Africa when compared to the preceding AEW (pre-Ernesto). This reduction of vertical wind shear over the pre-Debby AEW over the coast of West Africa corresponds well to where the vertical wind shear is expected to be reduced by the CCKW. After the passage of the convectively active phase of the composited CCKW over the eastern MDR, vertical wind shear magnitude anomalies become positive and remain anomalously strong up to four days and beyond.

ii) Atmospheric moisture

The relationship between atmospheric moisture and CCKWs is now investigated. Roundy and Frank (2004) found that total column water vapor (TCWV) does not project strongly onto the Kelvin band. However, their type of wavenumber–frequency analysis only examined signals that propagate eastward at typical Kelvin wave phase speeds. Therefore, this analysis excludes any westward moving features that might be forced by the CCKW. In contrast, the composites in Fig. 3.6 are able to capture the evolution of both eastward and westward propagating structures within the water vapor anomaly field. Figure 3.6 shows unfiltered TCWV anomalies (shaded) averaged over each CCKW lag.

Significant negative TCWV anomalies are observed within the convectively suppressed phase of the CCKW and significant positive TCWV anomalies are collocated within the convectively active phase of the CCKW throughout all lags. In addition to this anomalous TCWV pattern, significant TCWV anomalies are found to occur outside of the Kelvin filtered OLR anomalies and are observed to progress westward with time.

An area of significant negative TCWV anomalies is observed over West Africa on Day -6 (Fig. 3.6a). Later on Day -1, this area of significant negative TCWV anomalies is located farther west over 10-25°N, 40-50°W (Fig. 3.6b-f). This westward moving dry signature is hypothesized to be associated with a Saharan air layer (SAL) outbreak in some cases, and provides evidence that CCKWs may influence such events. An alternative hypothesis could be that CCKWs commonly phase with or modulate westward propagating waves (e.g., AEWs). These westward propagating waves could then act to initiate the SAL outbreak. A SAL preceded the CCKW that influenced the genesis of Debby (Zawislak and Zipser 2010; Zipser et al. 2010). The negative TCWV anomalies associated with the westward moving envelope of dry air seem to interfere with the positive TCWV anomalies associated with the convectively active phase of the CCKW on Day -2 (Fig. 3.6e). This interference results in negative TCWV anomalies occurring within the poleward half of the convectively active phase of the CCKW. One day later (Day -1), significant positive TCWV anomalies progress eastward over the eastern MDR collocated with the convectively active phase of the CCKW, while negative TCWV anomalies associated with the possible SAL outbreak continue to move westward (Fig 3.6f).

By Day 0, no significant TCWV anomalies are observed within the eastern side of the convectively active phase of the CCKW (Fig. 3.6g). The lack of significant TCWV anomalies within the eastern side of the convectively active phase of the CCKW appears to occur from the superposition between the positive TCWV anomalies that are associated with the eastward propagating CCKW and negative TCWV anomalies that are associated with a westward propagating disturbance. By Day +1, positive TCWV anomalies return to the eastern side of the convectively active phase of the CCKW, while no significant anomalies are observed within the western side. The western side of the convectively active phase of the CCKW is still superposed with the anomalously dry signature associated with the westward propagating disturbance and therefore the anomalies are reduced to zero.

After the passage of the convectively active phase of the CCKW over the tropical Atlantic, areas of significant anomalous moisture progress back towards the west (Fig 3.6g-l). Therefore, TCWV increases over the tropical Atlantic during and after the passage of the convectively active phase of the CCKW. This increased moisture signature is a composed from a combination of both eastward and westward moving signatures.

iii) Low-level (925 hPa) relative vorticity

Finally, low-level (925 hPa) relative vorticity is plotted in Fig. 3.7 for each CCKW lag. Between Day -6 and Day -1, scattered areas of anomalous anticyclonic relative vorticity progress eastward with the leading suppressed phase of the CCKW (Fig. 3.7a-f). Over the west-northwestern MDR on Day -6, a large area of anomalous anticyclonic relative vorticity is poleward of the convectively suppressed phase of the

CCKW (Fig. 3.7a). On Day -5, a preexisting area of anticyclonic relative vorticity over the eastern Atlantic increases in magnitude during the superposition with the convectively suppressed phase of the CCKW (Fig. 3.7b). This anticyclonic relative vorticity anomaly then progresses back towards the west throughout the subsequent lags (Fig. 3.7a-h). When compared to the composite TCWV anomalies, this westward moving area of anomalous anticyclonic relative vorticity slightly leads the westward moving area of anomalously dry air associated with the possible SAL outbreak discussed earlier (c.f., Fig 3.6a-h).

On Day-3, the convectively active phase of the CCKW is located over the MDR and a zonally-oriented strip of cyclonic relative vorticity anomalies forms over the tropical Atlantic (5-10°N, 30-55°W; Fig. 3.7d). One day later (Day -2), these positive relative vorticity anomalies amplify within the convectively active phase of the CCKW (Fig. 3.7e). On Day -1, the cyclonic relative vorticity anomalies reduce in magnitude and remain quasi-stationary (Fig. 3.7f). Anticyclonic relative vorticity anomalies that were generated over West Africa on Day -3 during the passage of the suppressed phase of the CCKW (see Fig. 3.7d) have progressed westward and interfere with the eastward progression of cyclonic relative vorticity anomalies (Fig. 3.7d-f). During the following lags, this couplet of anomalous cyclonic and anticyclonic relative vorticity moves westward together across the MDR (Fig. 3.7g-j).

On Day -1, an area of significant anomalous cyclonic relative vorticity forms in between the leading convectively suppressed phase and the convectively active phase of the CCKW (Fig. 3.7f). This location is consistent with where the strongest low-level zonal wind convergence occurs (recall Fig. 3.2a). Under the superposition of the convectively active phase of the CCKW on Day 0, this area of anomalous cyclonic relative vorticity intensifies (Fig. 3.7g). This anomalous cyclonic relative vorticity did not exist on Day -2, and is suggestive that it was generated by CCKW interacting with the topography of the Guinea Highlands region. Between Day +1 and Day +5, the convectively active phase of the CCKW propagates eastward over Africa, generating anomalous low-level cyclonic relative vorticity, which then later moves back towards the west (Fig. 3.7h-l).

On Day +1, a complicated pattern develops over the MDR (Fig. 3.7h). A wave-like pattern is expressed within the low-level relative vorticity field and consists of two separate areas of anomalous anticyclonic relative vorticity (located over 15-20°N, 60-65°W and 5-15°N, 40-50°W, respectively), with an area of anomalous cyclonic relative vorticity (10-15°N, 50-60°W) in between. Further, an additional but weaker area of anomalous cyclonic relative vorticity is located over 10-13°N, 30-35°W. This wave-like pattern within the relative vorticity field moves westward with time and potentially represents a westward propagating train of easterly waves. To build perspective, Fig. 3.8 shows anomalies of Kelvin filtered OLR (shaded) and 925 hPa stream function (contoured) averaged over the dates of the CCKW index. Day -2 through Day +2 are only shown to focus on the westward propagating structures over the tropical Atlantic. Negative stream function anomalies (dashed contours) progress eastward with the convectively active phase of the CCKW. On Day -2, a large couplet of negative and positive stream function anomalies is observed over the tropical Atlantic and West Africa (Fig. 3.8a). The minimum negative stream function anomaly is collocated with the minimum negative Kelvin filtered OLR anomaly. The maximum positive stream function anomaly is located within the convectively suppressed phase of the Kelvin wave, however is located slightly to the northwest of the maximum positive Kelvin filtered OLR anomaly.

By Day -1, the large couplet of negative and positive stream function anomalies is located slightly more westward than on Day -2 (Fig. 3.8b). This westward shift of stream function anomalies highlights an interference pattern between a westward propagating signature and the eastward propagating CCKW signature. Positive stream function anomalies are located within the convectively active phase of the CCKW because of the interference. By Day 0, the anomalous stream function couplet is located farther westward, but reduces in horizontal extent (Fig. 3.8c). During this time, negative stream function anomalies are once again collocated with the convectively active phase of the CCKW. The anomalous stream function couplet over the tropical Atlantic is located further west on Day +1 (Fig. 3.8d). By Day +2, a new area of anomalous negative stream function develops east of the couplet over 40°W, confirming the train of westward propagating disturbances observed in Fig. 3.7.

A vertical cross-section of meridional wind anomalies through 10°N on Day +2 is used to investigate the vertical structure of the westward propagating wave train over 30-60°W (Fig. 3.9). Over West Africa, a large upper-level anti-cyclonic circulation is observed over a low-level cyclonic circulation. The low-level cyclonic circulation is centered over ~5°E, whereas the upper-level anti-cyclonic circulation is centered slightly westward over ~0°E. Recall that the minimum negative Kelvin filtered OLR anomaly is located over 10°E on Day +2 (c.f., Fig. 3.4i), therefore these results suggest that the large circulations over Africa are a response to the CCKW passage. Over the tropical Atlantic, vertically stacked anomalies of meridional wind stretch from the surface to 250 hPa. The southerly meridional wind anomalies peak near 600 hPa, while the northerly meridional wind anomalies peak near 500 hPa, consistent with past observations of AEWs over the Atlantic (see Fig. 6 in Kiladis et al. 2006).

An alternative interpretation of the wave-like disturbances that develop over the Atlantic after the passage of the CCKW is that of a possible breakdown of the Atlantic ITCZ into individual vortices. A similar scenario occurred during the observations of Nieto Ferreira and Schubert (1997) over the Pacific. Their Fig. 1 shows an East Pacific ITCZ breakdown that resulted in five tropical depressions. Further examination of this event revealed that this ITCZ breakdown occurred during the passage of the convectively active phase of a CCKW (not shown). More recently, Schreck and Molinari (2011) discussed a similar PV strip over the Western Pacific that broke into two separate vortices and eventually spawned Typhoons Rammasun and Chataan. This breakdown occurred just after the passage of a series of CCKWs during an active MJO phase. The organization of deep cumulus convection within the ITCZ during a CCKW passage increases latent heat release and produces a low-level cyclonic PV anomaly, which then occasionally breaks down into individual vortices.

3.3.4. Where do strong Atlantic CCKWs originate from?

CCKWs are commonly thought to be triggered by preexisting tropical convection, however extra-tropical Rossby wave trains perturbing deep into the tropical wave guide have also been shown to initiate CCKWs (Straub and Kiladis 2003a). CCKWs that form in association with Rossby wave trains are frequently found over the western Pacific. CCKWs over the tropical Atlantic have been linked to pressure surges that propagate equatorward along the lee of the Andes (Liebmann et al. 2009). Similar to CCKWs found over the western Pacific, these pressure surges are associated with extra-tropical Rossby wave trains interacting with the Andes. When a strong mid-latitude trough propagates across the Andes, cold air is funneled down the lee of the Andes and deep into the tropics. This cold air intruding the tropics triggers an elongated band of deep convection ahead of it. The remnants of this organized convection propagate towards the equator where it sets up favorable conditions for the initiation of a Kelvin wave.

In addition to CCKWs that are generated by pressure surges over South America, the strongest CCKWs that propagate over the tropical Atlantic are linked with the location of active convection associated with the MJO. Fig. 3.10 shows a time-longitude composite of unfiltered VP200 anomalies overlaid with Kelvin filtered OLR anomalies (black contours) and MJO filtered OLR anomalies (orange contours) averaged over the set of dates identified using the CCKW index. Each variable is averaged over the 5-10°N latitude band to maximize the convective signatures of CCKWs and the MJO during boreal summer. The MJO filtering is performed following the methodology of Kiladis et al. (2005), using a period of 30-96 days, with eastward wavenumbers 0-9 (Kiladis et al. 2005). Recall Day 0 represents the time when the minimum composite negative Kelvin filtered OLR anomaly is located over 10°N, 15°W.

According to Fig. 3.10, the eastward progression of negative VP200 anomalies occurs in tandem with the convectively active phase of the composited CCKW (black dashed contour). An eastward progression of negative VP200 anomalies within the convectively active phase of the CCKW was also demonstrated by Mekonnen et al (2008). At lag -6 over 90°W, the convectively active phase of the composited CCKW first appears over the Pacific Basin. The convective signature of the CCKW occurs where the active convection associated with MJO (orange dashed contour) weaken. This result does not necessarily mean that the CCKW was generated by the active convection associated with MJO, however it does suggests a common phasing between the two features. Further, it appears that the low frequency active convection associated with the MJO propagates eastward across the Western Hemisphere with the composited CCKW convective signature. This result suggests that the strongest CCKWs observed over the tropical Atlantic region are commonly associated with the decay of the active convective signal of the MJO over the Pacific and eastward progression over the Western Hemisphere. This result is consistent with the scenario preceding the genesis of Debby (recall Fig. 2.8), as well as the results of Straub and Kiladis (2003b) and Mekonnen et al. (2008), who find CCKWs over the eastern Pacific and Africa are commonly associated the demise of the MJO convective signature over the Pacific.

At lag +6, the convectively active phase of the composited CCKW is located over the Indian Ocean. After the passage of the composited CCKW, a new MJO convective signal forms and later propagates eastward throughout the later lags. This result suggests that CCKWs might be an important feature in the genesis of the MJO. This result is consistent with the findings of Straub et al. (2006). Furthermore, this result implies CCKWs that are associated with the decay of the convectively active phase of the MJO over the Pacific might occasionally be involved with the generation of a new MJO convective signature over the Indian Ocean roughly two weeks later.

3.4. Discussion and Conclusions

Chapter 2 showed that over the entire tropical Atlantic, just prior to the passage of the convectively active phase of the CCKW, there is reduced tropical cyclogenesis frequency. After the passage, there is more frequent genesis. We have highlighted here how the passage of CCKWs impact vertical wind shear, moisture, and low-level relative vorticity. These factors are now summarized in turn to explain the tropical cyclogenesis frequency variations noted by in Chapter 2.

Vertical Wind Shear

Over the western tropical Atlantic, genesis is infrequent prior to the passage of the minimum Kelvin filtered OLR anomaly when the climatological westerly shear is increased by the Kelvin wave induced westerly shear. But after the passage of the minimum Kelvin filtered OLR anomaly over the western tropical Atlantic, Kelvin wave induced easterly shear reduces the climatological westerly shear consistent with the observation of more frequent genesis events there. Over the eastern Atlantic, genesis is less frequent just prior to the passage of the minimum Kelvin filtered OLR anomaly as Kelvin wave induced westerly shear reduces the climatological easterly shear. After the passage of the minimum Kelvin filtered OLR anomaly, more frequent genesis events are observed as Kelvin wave induced easterly shear over the eastern MDR increases the climatological easterly shear. In a comparison study between non-developing and developing AEWs, Hopsch et al. (2010) found that AEWs that develop over the tropical Atlantic occur when there is increased 850-200 hPa vertical wind shear over the southern MDR. Our results are consistent with Hopsch et al. (2010), such that 925-200 hPa vertical wind shear increases over the southern MDR after the passage of the CCKW during a time of frequent Atlantic tropical cyclogenesis.

The fact that, in contrast to the western tropical Atlantic, tropical cyclogenesis over the eastern tropical Atlantic is found to be favored when the CCKW enhances the local shear deserves comment. Tuleya and Kurihara (1981) performed a modeling study showing that mean easterly shear is more favorable for tropical cyclogenesis than westerly shear with respect to a westward moving wave in the Northern Hemisphere. They find that the easterly shear value most favorable for the early development of the tropical cyclone was 15 ms^{-1}. This result is consistent with Figs. 3.3 and 3.4, highlighting an 11-18 ms^{-1} mean easterly shear value over the eastern Atlantic after the passage of the minimum Kelvin filtered OLR anomaly. Nolan and McGauley (2011) find discrepancies between their idealized simulations and statistical favorability of easterly wind shear for genesis and suggest that the strong correlation between easterly shear and other favorable factors, such as increased thermodynamic favorability, or with geographical areas that have stronger initiating disturbances could be responsible for the relationship. Further,

easterly shear zones also tend to consist of enhanced low to mid-level moisture, low level westerly winds, and off equatorial low-level cyclonic vorticity. Therefore, it is possible that much of the association between easterly shear and tropical cyclones is caused by these other favorable factors that occur along with easterly shear, while some of the easterly shear might be unfavorable.

It is possible that the anomalous easterly shear phase of the CCKW seen here, west of the anomalous CCKW convection, is associated with a region of enhanced AEW activity (c.f. Mekonnen et al. 2008; Leroux et al. 2010). This increased AEW activity may be more important for tropical cyclogenesis frequency there than the shear. This aspect will be explored in Chapter 4.

Moisture

Two-to-three days before the passage of the convectively active phase of a CCKW, anomalously dry air is advected westward from West Africa over the MDR. One possible source of the dry air is from the Sahara; but mid-latitude influences may also be playing a role (Braun 2010). It is hypothesized that the low-level dynamical structure of the CCKW influences SAL outbreaks due to enhancement of lower-tropospheric easterly flow within the convectively suppressed phase of the CCKW. The anomalously dry air also likely contributes in suppressing deep convection over the MDR prior to the passage of the convectively active phase of the CCKW, which would tend to reduce the frequency of genesis.

Moisture significantly increases over the tropical Atlantic during the passage of the convectively active phase of the CCKW. This moist signature progresses eastward with the convectively active phase of the CCKW. After the passage of the convectively active phase of the CCKW over the tropical Atlantic, areas of significant moist anomalies progress back towards the west. Through the combination of eastward and westward moisture signatures over the tropical Atlantic, moisture is increased over the tropical Atlantic over an eight-to-nine day period.

Agudelo et al. (2010) suggested that the likelihood of a developing AEW increases when the wave enters an environment characterized by pre-existing moist convection. Consistent with that, Hopsch et al. (2010) conclude that the presence of dry mid-to-upper level air just ahead of the non-developing AEW composite was a major limitation for that wave to undergo tropical cyclogenesis. Mid-to-upper level dry air is less likely to be located over the tropical Atlantic during the passage of the convectively active phase of a CCKW. Therefore, any AEWs propagating off the coast of West Africa during a time when the convectively active phase of a CCKW is located over the tropical Atlantic will soon enter an environment where moist convection is present. Following the arguments presented by Hopsch et al. (2010) and Agudelo et al. (2010), theses AEWs will be more likely to develop thereafter.

Low-Level Relative Vorticity

Anomalous anticyclonic relative vorticity is generated within the leading suppressed phase of the CCKW and is assumed to contribute to the anomalously low genesis activity then. Further, a broad area of anomalous anticyclonic relative vorticity is observed to progress westward across the tropical Atlantic prior to the passage of the convectively active phase of the CCKW over the eastern tropical Atlantic. This area of anomalous anticyclonic relative vorticity slightly leads the anomalous dry SAL air that progresses westward discussed above.

During the passage of the convectively-active phase of the CCKW, a zonally oriented strip of low-level cyclonic relative vorticity develops over the tropical Atlantic. This strip of cyclonic relative vorticity later becomes part of a wave-like pattern that develops over the tropical Atlantic after the passage of the convectively active phase of the CCKW. This wave-like pattern progresses westward throughout subsequent lags and is associated with a train of westward propagating easterly waves. Kiladis et al. (2009) discusses the amplification of WIG waves during the passage of a CCKW, but these westward propagating disturbances have a wavelength of ~2500 km and a westward phase speed of ~7-8 m s^{-1}, implying that they are more similar to easterly waves (c.f., Fig. 14 in Mekonnen et al. 2008). The increased low-level cyclonic flow and increased easterly wave activity over the tropical Atlantic during and after the passage of the CCKW occurs during a time when genesis is most frequent.

Summary

The overall low tropical cyclogenesis activity that occurs just ahead of the convectively active phase of the CCKW arises from unfavorable large-scale environmental conditions (including enhanced westerly vertical wind shear and reduced easterly vertical wind shear, reduced atmospheric moisture, and anomalous anticyclonic low-level relative vorticity), along with the influence of the westward moving SAL or mid-latitude dry air outbreak (see Dunion and Velden 2004). The increasing trend of tropical cyclogenesis events observed between Day 0 and Day +2 in Fig. 2.10 and 2.11 occurs from the combination of the direct enhancement of convection associated with the convectively active phase of a CCKW, as well as more favorable large-scale environmental conditions (reduced westerly vertical wind shear and enhanced easterly vertical wind shear, increased atmospheric moisture, and anomalous cyclonic low-level relative vorticity) for tropical cyclogenesis.

This chapter provides information pertaining to the role of CCKWs on weather variability over the tropical Atlantic. From an operational forecasting perspective, in addition to extreme precipitation events over tropical regions such as Africa (e.g., Mekonnen et al. 2008), we recommend that CCKWs be monitored daily for their potential influence on tropical cyclogenesis over the MDR (Chapter 2; Ventrice et al.

2012a). Our results suggest a common phasing with the active convection associated with the MJO. By assessing the particular phase of the real-time multivariate MJO (RMM) phase space (e.g. Wheeler and Hendon 2004), and the location of active convection associated with a CCKW, the possibility exists to make useful medium-range predictions of anomalously active or suppressed Atlantic tropical cyclogenesis activity.

3.6. Figures

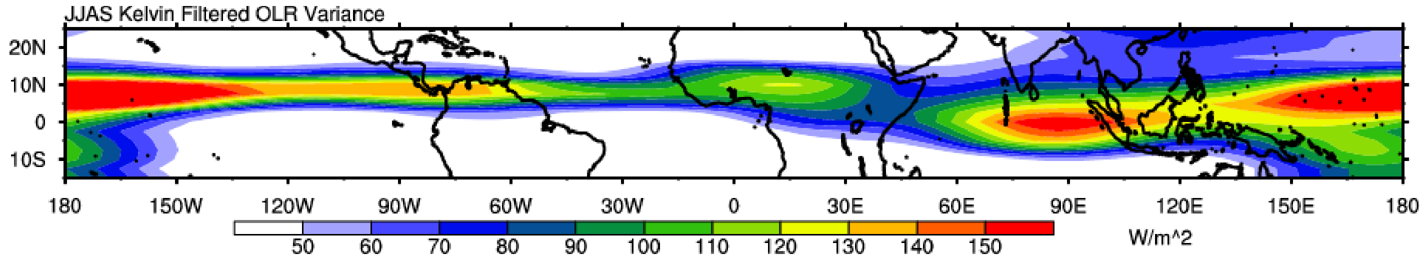

Fig. 3.1. Distribution of June-September mean variance of NOAA interpolated OLR filtered for the Kelvin band. Kelvin wave activity is determined by filtering OLR in the period of 2.5-20 days with eastward wavenumbers 1-14. The filter is constrained by the Kelvin wave dispersion curves for equivalent depths of 8-90 meters.

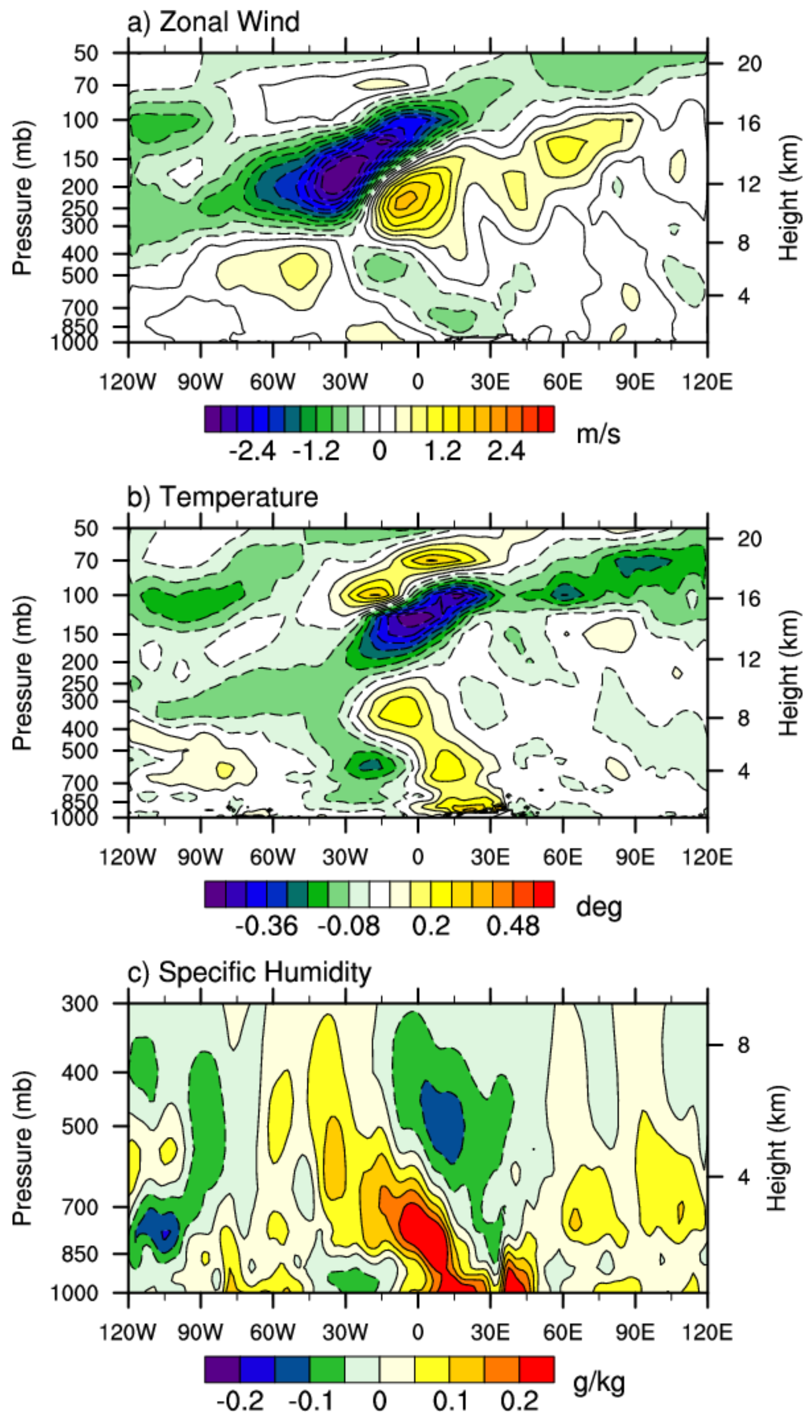

Fig 3.2. Height-longitude cross section composites averaged over the 5˚S-10˚N latitude band for anomalies of (a) zonal wind, (b) temperature, and (c) specific humidity. The minimum Kelvin filtered OLR anomaly is located at the longitude of 15˚W.

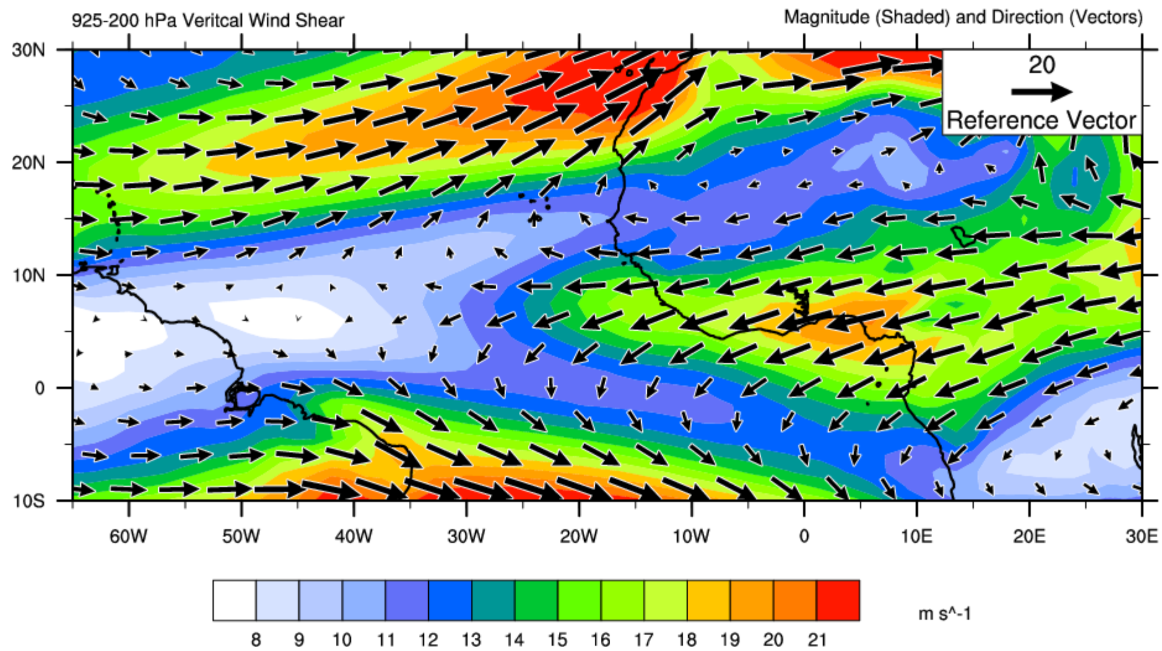

Fig. 3.3. The June-September climatological 925-200 hPa vertical wind shear vectors and magnitudes (shaded). The direction of shear represents the vector difference between 925 hPa and 200 hPa.

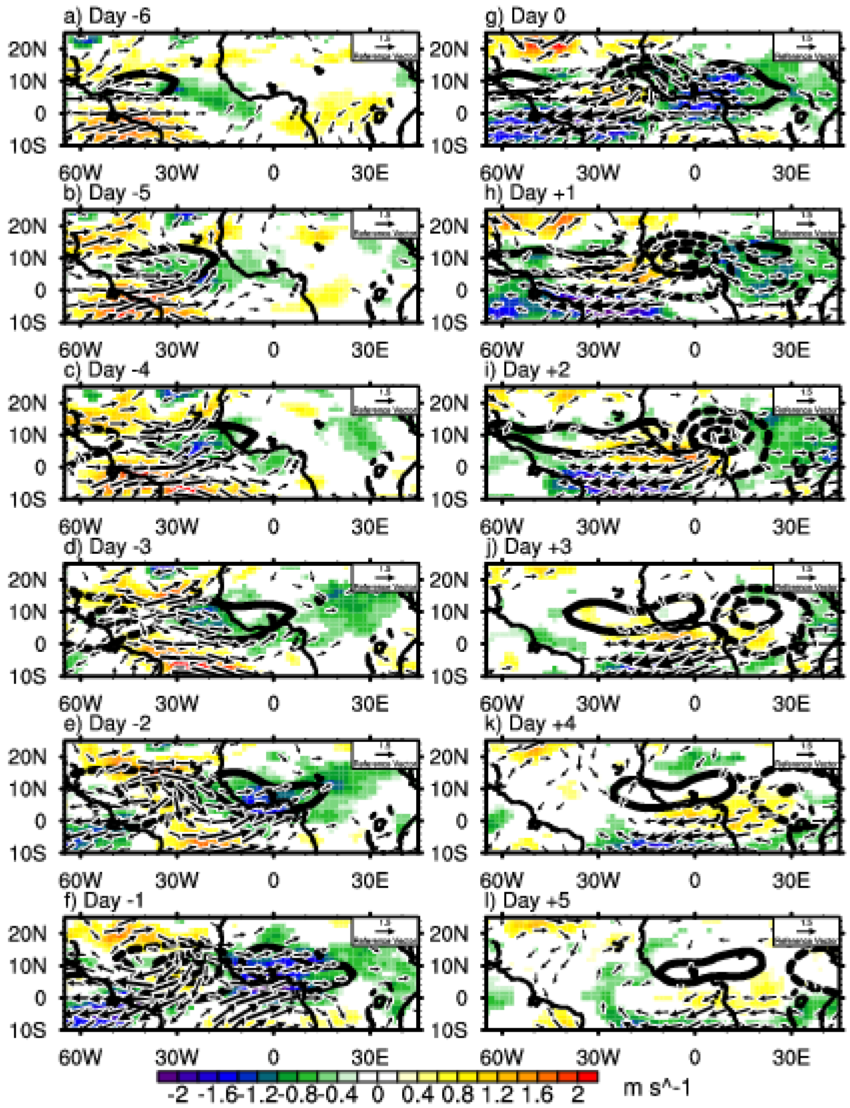

Fig. 3.4. The 925-200 hPa vertical wind shear vector and magnitude (shaded) anomaly composite averaged over each CCKW lag. Wind shear magnitude anomalies statistically different than zero at the 95% level are shaded. The direction of shear represents the vector difference between 925 hPa and 200 hPa. Vectors are not drawn if less than 0.75 ms^{-1}. Kelvin filtered OLR anomalies are contoured if statistically different than zero at the 95% level. Negative Kelvin filtered OLR anomalies are dashed. Shade interval is 0.2 ms^{-1}; contours begin at +/-3 Wm^{-2}; contour interval is 6 Wm^{-2}; reference vector is 1.5 ms^{-1}.

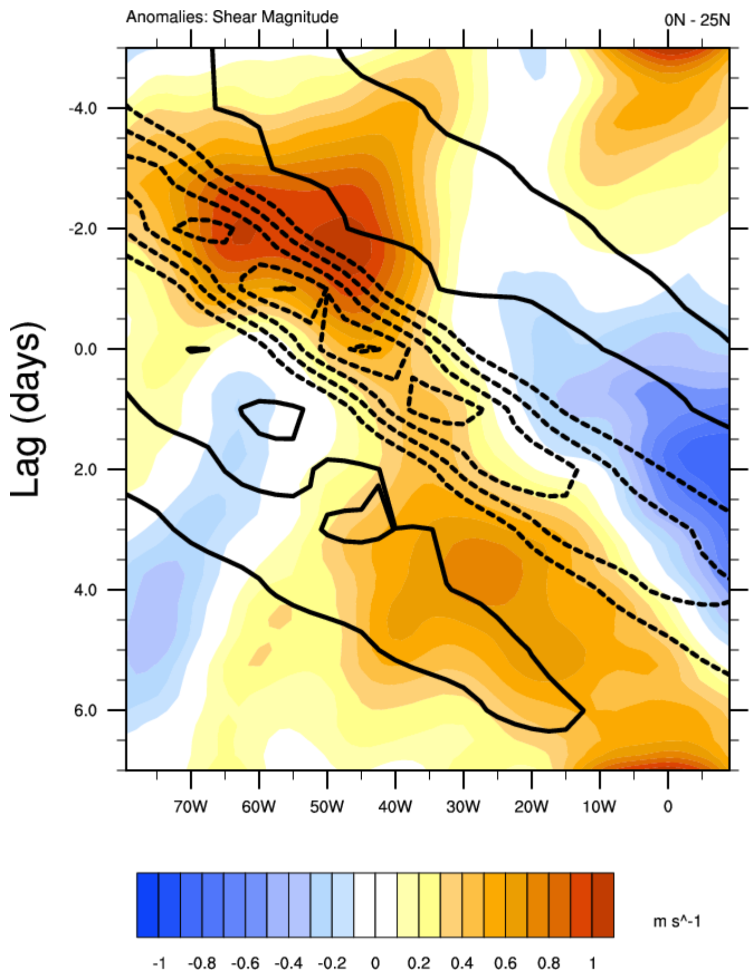

Fig. 3.5. A time-longitude composite of mean absolute value of anomalous 925-200 hPa vertical wind shear of the total wind averaged over each CCKW lag and the 0-25˚N latitude band. A five day running average was applied to temporally smooth the data. Kelvin filtered OLR anomalies are contoured if statistically different than zero at the 95% level. Negative Kelvin filtered OLR anomalies are dashed. Kelvin filtered OLR anomalies are averaged over the 5-10˚N latitude band. "Day 0" is when the minimum Kelvin filtered OLR anomaly moves over 10°N, 45°W. Shade interval is 0.1 ms^{-1}; contour interval is 3 Wm^{-2}.

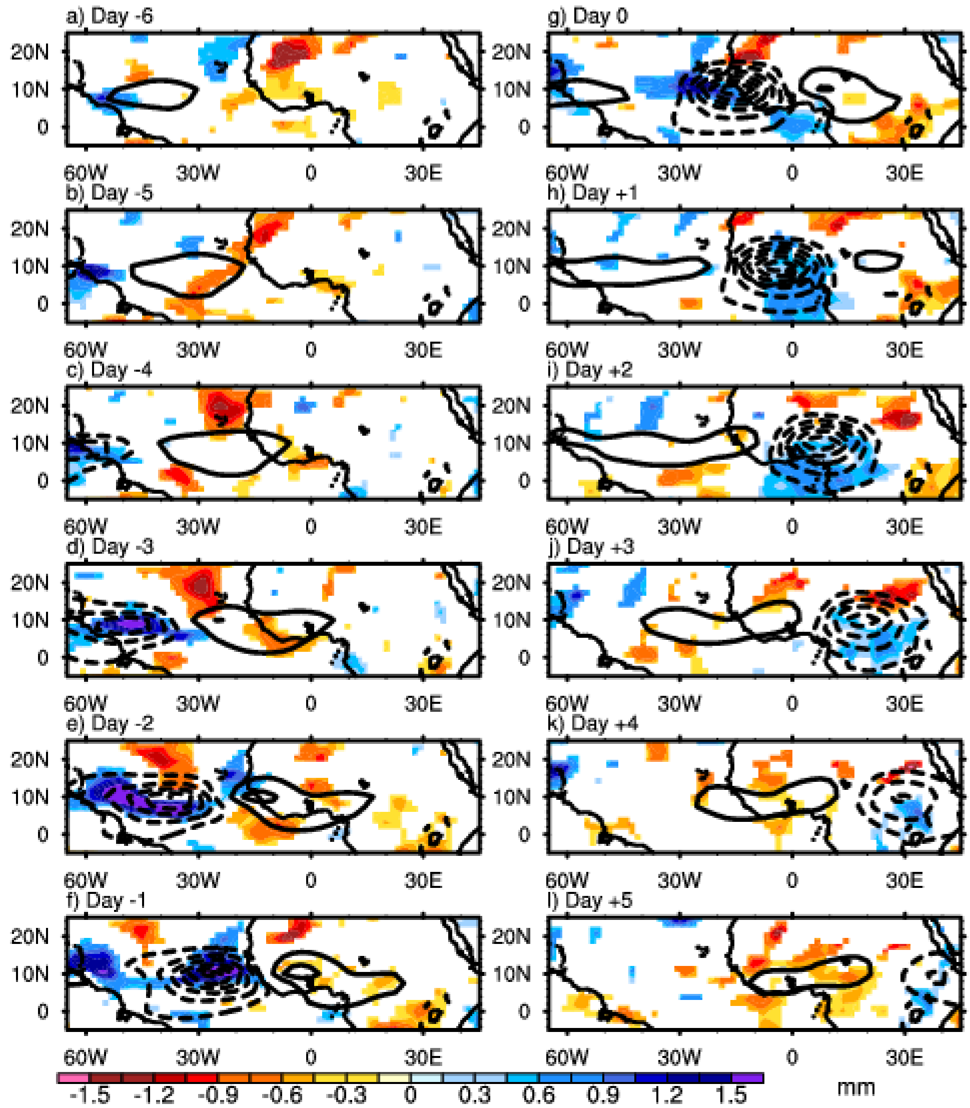

Fig. 3.6. Total column water vapor anomaly composite averaged over each CCKW lag. Anomalies statistically different than zero at the 95% level are shaded. Kelvin filtered OLR anomalies are contoured if statistically different than zero at the 95% level. Negative Kelvin filtered OLR anomalies are dashed. Shade interval is 0.15 mm; contour interval is 3 Wm^{-2}.

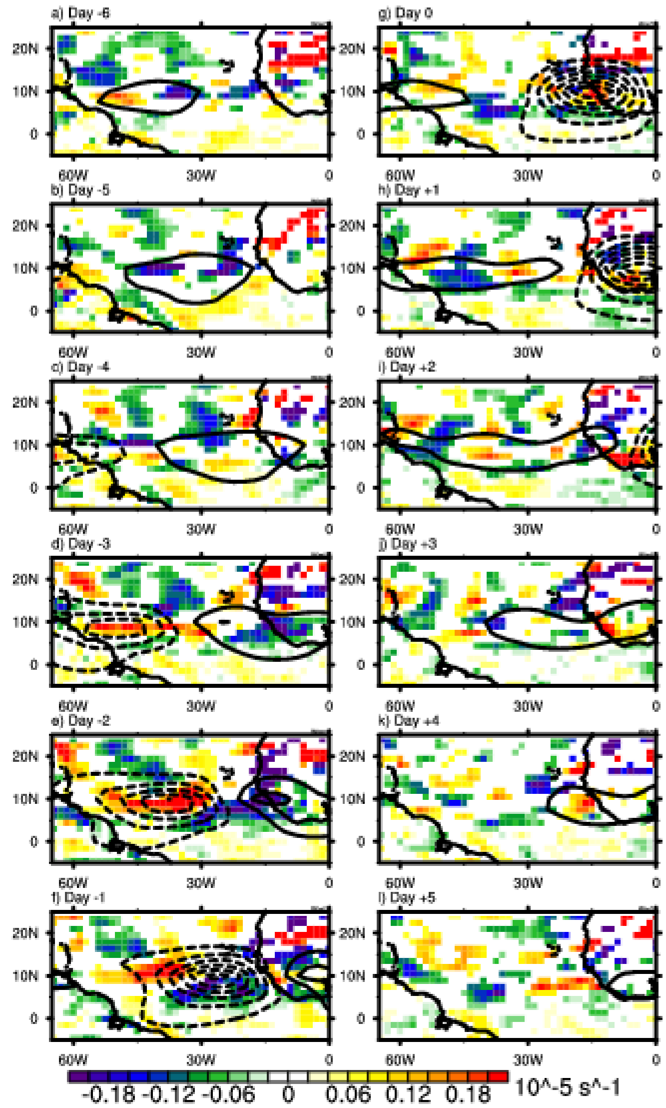

Fig. 3.7. 925 hPa relative vorticity anomaly composite averaged over each CCKW lag. Anomalies statistically different than zero at the 90% level are shaded. Kelvin filtered OLR anomalies are contoured if statistically different than zero at the 95% level. Negative Kelvin filtered OLR anomalies are dashed. Shade interval is 0.02 x 10^{-5} s^{-1}; contour interval is 3 Wm^{-2}.

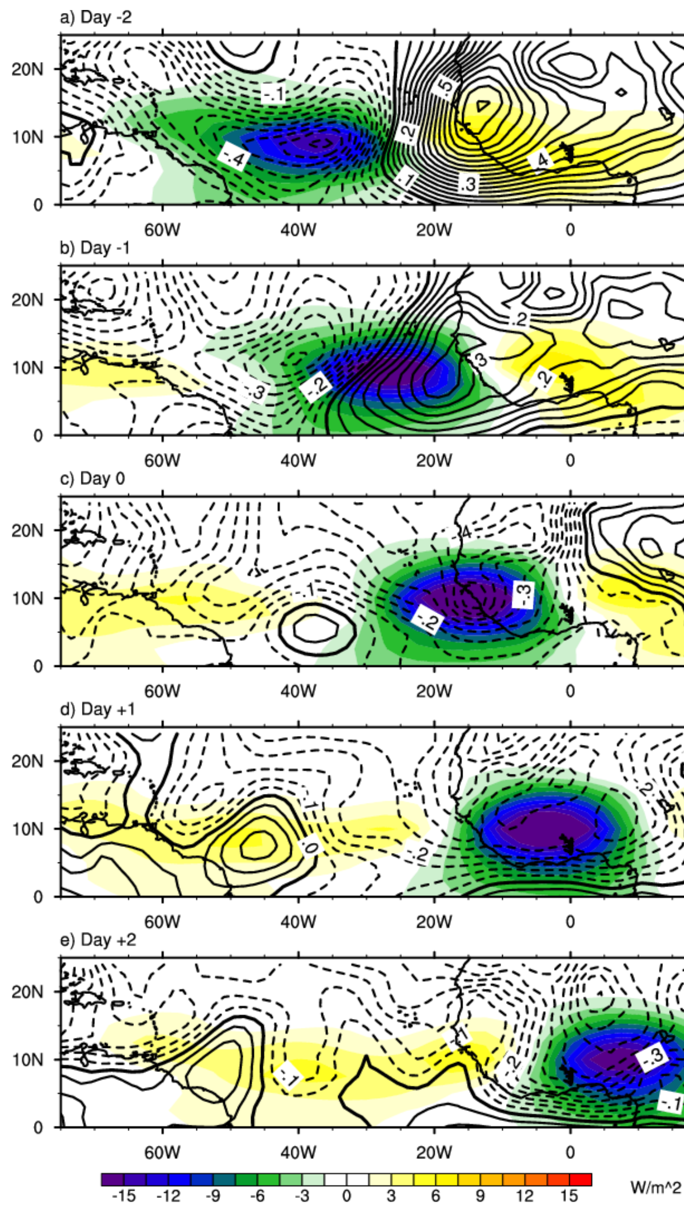

Fig. 3.8. 925 hPa stream function anomaly composite averaged over particular lags of the CCKW index. Kelvin filtered OLR anomalies are shaded. Stream function anomalies are contoured. Negative stream function anomalies are dashed. Shade interval is 1.5 Wm^{-2}; contour interval is 0.1 x 10^6 m^2s^{-1}.

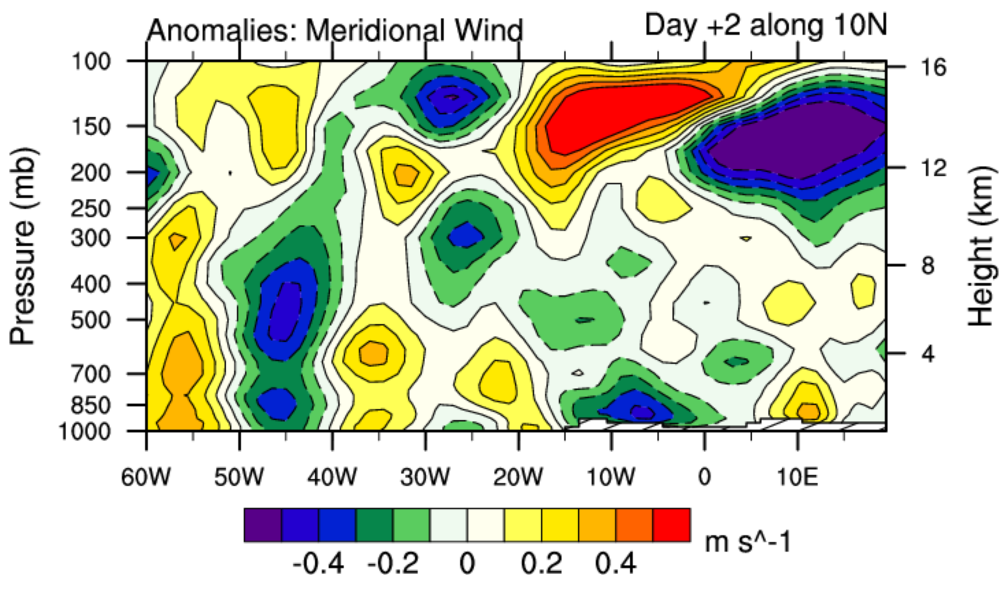

Fig. 3.9. A cross-section of meridional wind anomalies along 10 ˚N on Day +2. Counter interval is 0.1 ms^{-1}.

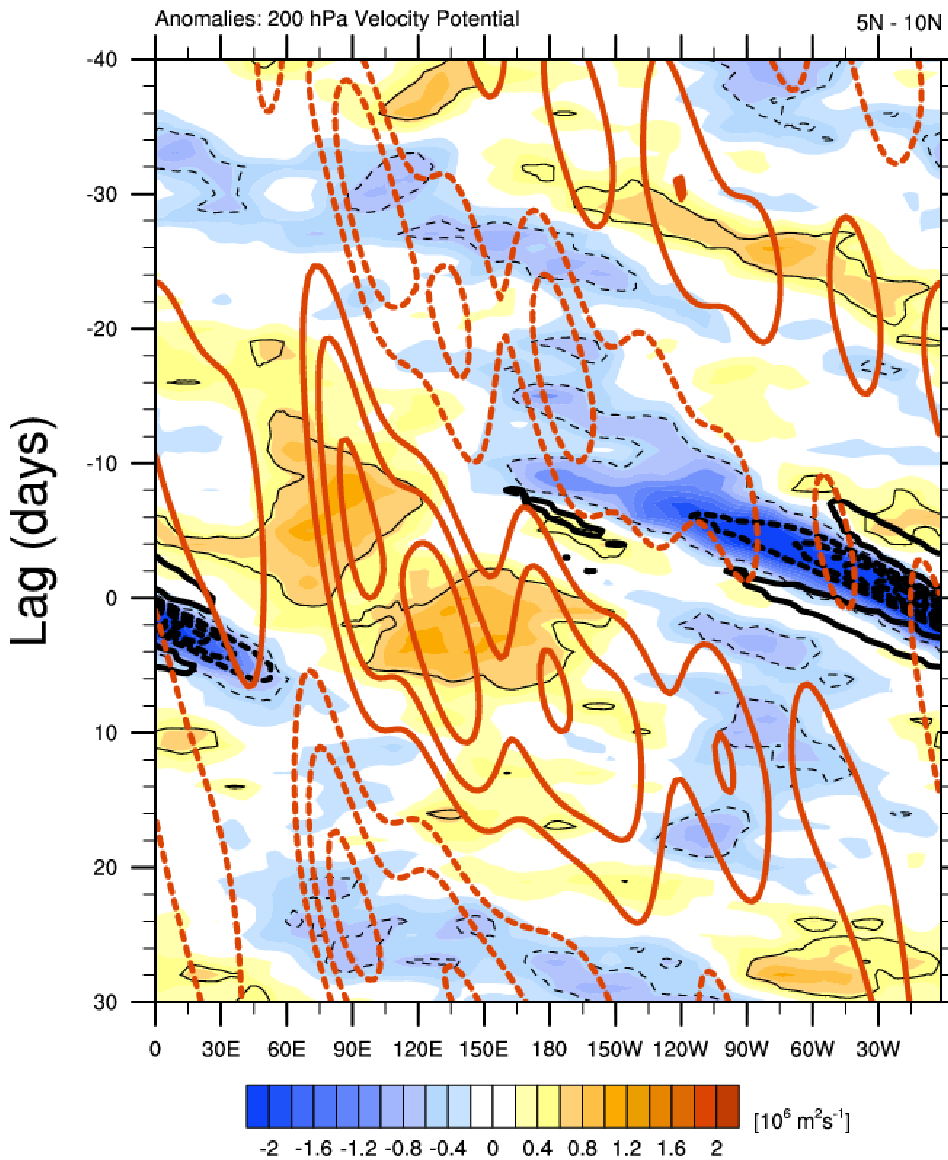

Fig. 3.10. A time-longitude composite of daily averaged unfiltered 200 hPa velocity potential anomalies. Unfiltered 200 hPa velocity potential anomalies statistically different than zero at the 90% level are within the black lines (dashed-black lines if negative). Day 0 is when the minimum negative Kelvin filtered OLR anomaly is located over 10˚N, 15˚W. Kelvin filtered OLR anomalies are represented by the bold, black contours and are drawn every 3 Wm^{-1}. MJO filtered OLR anomalies are represented by the orange contours and are drawn every 0.5 Wm^{-2}. Negative filtered OLR anomalies are dashed. All variables were averaged over the 5-10˚N latitude band.

4. The role of convectively coupled Kelvin waves on African easterly wave activity

4.1. Introduction

This chapter discusses the role of CCKW passages on the initiation and intensification of AEWs. Given the large body of work on AEWs, it is perhaps surprising that there is still a lack of understanding of when and how these waves originate. Recent work (e.g., Mekonnen et al. 2006; Hall et al. 2006; Thorncroft et al. 2008) have proposed that AEWs are triggered by convection in the entrance region of the AEJ. Thorncroft et al. (2008) suggest that AEWs rely on the presence of intense upstream convective triggers linked to African topography. It is argued here that CCKWs can provide such triggers over African topography by providing a favorable environment for convection and wave growth. This notion provides new insight on a concept that is not yet fully understood and could be used to support the prediction of AEW activity at weekly timescales.

Synoptic case study work of Carlson (1969a) and, more recently, Berry and Thorncroft (2005) highlighted the role of orographic convection in triggering AEWs. Berry and Thorncroft (2005) suggested that the strong AEW that developed into Hurricane Alberto (2000) was triggered by strong convection over the Darfur Mountains (~25ºE) on July 30-31, 2000. In a climatological study of AEW activity, Mekonnen et al. (2006) also noted the importance of the eastern African highlands on AEW genesis. In agreement with Berry and Thorncroft (2005), they found that the Darfur Mountains and the Ethiopian Highlands (~35°E) are both preferable regions for AEW genesis. This triggering hypothesis was also supported by idealized modeling of Thorncroft et al (2008). While the model they used had a flat lower-boundary, the atmospheric response to imposed upstream heating in the Darfur region (close to the entrance of the African easterly jet) was a developing train of AEWs that propagated westward with time, providing strong evidence in support of the triggering hypothesis. It will be shown here that the increased convection linked to the genesis of the pre-Alberto AEW over the Darfur Mountains occurred during the passage of the convectively active phase of a strong eastward propagating CCKW.

While this part of this chapter focuses on the triggering of AEWs by convection associated with the convectively active phase of the CCKW, it should be recognized that convection can also impact the presence and amplitude of AEW-activity through, at least, two other mechanisms. Schubert et al. (1991) highlighted the role played by inter-tropical convergence zone (ITCZ) heating in the creation of a zonally symmetric PV strip that is barotropically unstable for AEW growth (see also Hsieh and Cook 2005). Numerous studies have also shown that convection and associated heating coupled with the AEW itself can intensify pre-existing AEWs (e.g. Thorncroft and Hoskins 1994, Hsieh and Cook 2008). Unraveling the relative roles played by convection on the genesis and growth or maintenance of AEWs is difficult and likely requires a modeling study that is beyond the scope of this chapter.

Observational studies using high resolution rainfall and brightness temperature datasets (e.g., GOES-9, CLAUS, TRMM 3B42, etc.) reveal that most of the organized rainfall within the convective envelope of the CCKW is composed of smaller scale cloud clusters that move westward (e.g., Straub and Kiladis 2002; Mounier et al. 2007; Mekonnen et al. 2008; Kiladis et al. 2009; Schreck and Molinari 2011; Laing et al. 2011; Tulich and Kiladis 2012). Mounier et al. (2007) observed an increase of MCS activity within the convective envelope of a CCKW over Africa during early July 1984. Their results show that CCKWs are able to modulate convective activity over the whole ITCZ domain by impacting the frequency and intensity of MCSs, with an emphasis over the Cameroon Highlands and central Africa. Nugyen and Duvel (2008) and Laing et al. (2011) also find that MCSs are more frequent, larger, and more intense within the convective envelope of CCKWs.

Mekonnen et al. (2008) observed an increase in AEW activity immediately after the passage of the convectively active phase of a CCKW over Africa during the boreal summer of 1987. However, Mekonnen et al. (2008) suggests that this case was a rare event, stating that on average only three AEWs initiate per year over Africa during the passage a CCKW. In support of CCKWs modulating AEW activity, Leroux et al. (2010) suggested that intraseasonal variability of AEW activity can vary with eastward propagating modes such as CCKWs and the MJO. These eastward propagating disturbances are suggested to impact convection and the characteristics of the AEJ over Africa, which thereafter would impact AEW activity. Using Wheeler and Hendon’s (2004) real-time multivariate MJO indices, Chapter 6 explores the role of the MJO on AEW activity through its impact on upstream convection and the AEJ.

Matthews (2004) showed that African convection strongly varies at intraseasonal timescales and attributed the dominant mode of variability to the superposition between a dry westward propagating equatorial Rossby wave response and a dry eastward propagating Kelvin wave response over Africa. Both the dry Rossby and Kelvin wave responses originated from active convection associated with the MJO over the West Pacific warm pool, which then propagated around the globe and intersected over Africa

20 days later. The dry-Kelvin wave response destabilized the atmosphere, increased the surface monsoon flow and moisture supply into West Africa up to 20%, and increased the cyclonic shear on the equatorward flank of the AEJ. The increased cyclonic shear on the equatorward flank of the AEJ enhanced the instability of the jet and was attributed by the author to cause a period of enhanced AEW and transient convective activity.

The intraseasonal variability of boreal summer rainfall over West Africa was first documented by Janicot and Sultan (2001) and Sultan et al. (2003). Two major periodicities where identified in convective activity. The first periodicity lies in the 10-25 day range, with a distinct peak at 15 days, while the other covers the 25-60 day range. The latter of the two periodicities is believed to be associated with the MJO (e.g., Matthews 2004; Maloney and Shaman 2008; Janicot et al. 2009; Pohl et al. 2009; Ventrice et al. 2011).

The 10-25 day range periodicity has been attributed to the “quasi-biweekly zonal dipole” (QBZD; Mounier et al. 2008). Mounier et al. (2008) found that both the QBZD and Kelvin filtered signals peak in June, with much of the QBZD spatial structure consisting of an eastward progression of convection. However, they claim that the even though the QBZD is dependent on CCKW activity, they are separate entities. The stationary component of the QBZD appears to be over exaggerated in Fig. 3 of Mounier et al. (2008) due to their erratic choice of time lags. As a result, the eastward propagating signature that has been attributed to CCKWs is obscure and deemed less important than the stationary component. It is likely that the eastward propagating convective signatures associated with the QZBD are driven primarily by CCKWs, whereas the stationary component of the QBZD is the local response to the passage of the CCKW. This hypothesis would suggest that CCKWs might be the main source of intraseasonal variability in the WAM system on the 10-25 day temporal scale.

This chapter is motivated by the hypothesis of Mekonnen et al. (2008) that CCKWs could act as convective triggers for AEWs. This idea is different from Matthews (2004), since we investigate the impact of a moist Kelvin wave on the large scale environment that favors AEW activity. Enhanced convection triggered by the CCKW may be important for the initiation of AEWs over Africa. This chapter will extend upon Mekonnen et al. (2008) and provide further detail on how CCKWs might affect AEW genesis and growth.

This chapter is structured as follows. Section 4.2 discusses the datasets and methodology used. The influence of CCKW passages on AEW activity is presented in Section 4.3.. A discussion and conclusion is in Section 4.5.

4.2. Datasets and Methodology

The ERA-Interim dataset (Dee et al. 2011) was used to investigate the impact of a CCKW passage on the synoptic environment over tropical Africa. The 1.5° gridded horizontal resolution version covering the period from 1989 to 2009 is used.

Tropical rainfall information associated with the pre-Alberto AEW case study is provided by the TRMM 3B42 product. Geostationary Earth IR data from the CPC merged IR dataset was used to investigate the convective burst over Darfur that has been attributed to as the initiation of the pre-Alberto AEW (Berry and Thorncroft 2005).

Following Leroux et al. (2010), AEW activity was diagnosed by calculating the eddy kinetic energy (EKE) based on ECMWF-Interim wind data that were filtered in a 2-

10 day band (u' and v'). The EKE, defined as:

$$EKE = \frac{1}{2}(u'^2 + v'^2)$$

and was calculated at the level of the AEJ (700 hPa).

The CCKWs used in the composite analysis were identified by filtering NOAA's daily averaged interpolated OLR dataset (e.g., Liebmann and Smith 1996) in wavenumber and frequency within the Kelvin band (a period of 2.5-20 days, with eastward wave numbers 1-14, constrained by the Kelvin wave dispersion curves for equivalent depths of 8-90 meters).

Following the methodology of Chapters 2 and 3, the same CCKW index is used and is composed of all JJAS dates between 1989 and 2009 when the minimum negative Kelvin filtered OLR anomaly (less than -1.5 standard deviations in magnitude) was over the selected grid point (10°N, 15°W).

Anomalies for all composited fields were constructed by subtracting the long-term mean and the first four harmonics of the seasonal cycle. Bootstrap random resampling tests with one thousand iterations were used for statistical significance testing on all anomalies similar to Roundy and Frank (2004). In each of these tests, a new sample equal in size to the original was randomly drawn for the original set of composite dates with replacement. The composite anomalies were considered 95% significant if 950 out of the 1000 random composites had the same sign.

4.3. Convectively Coupled Kelvin waves and African easterly wave activity

Focus is now given to the impact of CCKWs on AEW activity during boreal summer. First, the role of the convectively active phase of a CCKW on the initiation of the pre-Alberto AEW (2000) is investigated for motivation. This is followed by a composite analysis that examines the relative importance of CCKWs on the large-scale environment that favors the initiation and growth of AEWs.

4.3.1. Case Study: The initiation of the pre-Alberto African easterly wave in July 2000

According to the NHC's post season discussion, the precursor to Hurricane Alberto (2000) was attributed to a well-defined AEW that can be traced back to central tropical Africa. The initiation of this particular AEW has been investigated in previous literature (e.g., Berry and Thorncroft 2005; Lin et al. 2006). Berry and Thorncroft (2005) suggest that convection triggered over the Darfur Mountains led to the genesis of the pre-Alberto AEW. This case will be used to illustrate that in addition to the initial convective burst that has been attributed to the genesis of Alberto, several other MCSs over different locations in tropical Africa, were initiated during the passage of the convectively active phase of a CCKW.

A time-longitude plot of unfiltered TRMM 3B42 rain rate anomalies and Kelvin filtered TRMM rain rate anomalies is used to highlight the role of CCKWs on the pre-Alberto AEW (Fig. 4.1). Only the +/- 2 mm day^{-1} Kelvin filtered TRMM rain rate anomaly contour is shown to reference the location of CCKWs. ERA-Interim southerly winds at the level of the AEJ (700 hPa) are contoured black if greater than 2 ms^{-1} to indicate southerly flow associated with the circulation of AEWs. All variables were averaged over the 5-15°N latitude band. The letter "A" represents the time and location of the July 30th convective burst over the Darfur Mountains [20-30ºE] that has been attributed to the genesis of the pre-Alberto AEW (Berry and Thorncroft 2005). The circulation associated with the pre-Alberto AEW began one day after this convective burst (July 31). While the dynamical signature associated with the pre-Alberto AEW shows gradual intensification during its westward propagation over tropical Africa, consistent with the observations of Berry and Thorncroft (2005), its rain-rate signature reveals distinct periods of strengthening and weakening. The strengthening and weakening of the pre-Alberto AEW rain rate signature has not been discussed in previous studies and appears to be related to the passage of the convectively active and suppressed phases of consecutive eastward propagating CCKWs.

Between July 27 and August 9, two CCKWs propagated eastward across tropical Africa. The high resolution TRMM 3B42 product shows that the higher amplitude rain rate anomalies that occur within the convective envelopes of both CCKWs are associated with westward propagating convective disturbances. In contrast to the convectively active phase, the convectively suppressed phases of both CCKWs (dashed black contours) are associated with reduced rain rate anomalies. Therefore during the analysis period, a suppressed-enhanced-suppressed-enhanced-suppressed sequence of unfiltered anomalous rain rates is clearly visible within the westward propagating MCSs over Africa. It is evident from Fig. 4.5 that rainfall patterns during this period over Africa were highly influenced by CCKW activity.

The anomalous rain rate signature associated with the MCS that is linked to the genesis of the pre-Alberto AEW originates on July 30 over the Darfur Mountains (~25°E), consistent with the observations of Berry and Thorncroft (2005). The initiation of this MCS occurred roughly 15º of longitude to the east of the maximum Kelvin filtered TRMM rain rate anomaly. Past research has shown that the maximum low-level zonal wind convergence associated with CCKWs is located about 15º of longitude to the east of the center of the convective envelope (Takayabu and Murakami 1994; Straub and Kiladis 2003a,b). Therefore, this MCS developed in a region relative to the CCKW that was associated with increased low-level zonal wind convergence and vertical ascent (not shown). One day later (July 31), 700 hPa southerly winds associated with the pre-Alberto AEW circulation developed during the passage of the CCKW, indicating when the dynamical signature associated with the AEW had begun.

Between July 30 and 31, the pre-Alberto AEW was still superimposed with the convective envelope of the first CCKW. During this time, the pre-Alberto AEW had an anomalous rain rate signature greater than 40 mm day^{-1}. By August 1, the pre-Alberto AEW was collocated with the convectively suppressed phase of the CCKW. During the superposition, the anomalous rain rate signature associated with the pre-Alberto AEW weakened. Note that this convectively suppressed CCKW phase reduced rain rate anomalies to zero for other pre-existing westward moving MCSs over Africa.

The superposition between the pre-Alberto AEW and the convectively active phase of the following CCKW occurred between August 1 and 2 around 10°W-0°E. During this time, the anomalous rain rate signature associated with the pre-Alberto AEW increased to values greater than 40 mm day^{-1} again. At this time, Berry and Thorncroft (2005) note the merging between low-level PV generated over the Guinea Highlands region [5-13ºN, 8-15ºW] with the pre-Alberto AEW. The low-level PV generated over the Guinea Highlands region was presumed to be generated with a coherent diurnal cycle there. Berry and Thorncroft (2005) deemed this as the final stage of an AEW life cycle and called it the “west coast development” stage. While AEWs may intensify over western tropical Africa from local processes, these results suggest that the intensification of the pre-Alberto AEW over western Africa was also in association with the superposition of the convectively active phase of an eastward propagating CCKW.

In order to investigate the initiation of the pre-Alberto AEW in greater detail, maps of CPC-merged IR (shaded) overlaid with Kelvin filtered TRMM anomalies (black contours) and ERA-interim 850 hPa wind anomalies (vectors) are constructed every six hours for the period beginning at 00Z July 30 and ending 06Z July 31 (Fig. 4.2). The domain of Fig. 4.2 is focused over eastern Africa, where the northeastern extent of the Gulf of Guinea is located in the lower left corner. At 00Z July 30, the convectively active phase of the leading CCKW is located between 0-15°E, while its convectively-suppressed phase is located between 25-30°E. Note that scattered MCSs were present across eastern Africa at this time, consistent with a time of day when convection is most frequent there (Yang and Slingo 2001; Laing et al. 2008, 2011). By 06Z July 30, a small MCS developed over 11°N, 24°E, with a brightness temperature value that was less than 200K, in between the convectively suppressed and active phases of the CCKW. Consistent with Fig. 4.1, this MCS formed roughly 15° of longitude to the east of the maximum positive Kelvin filtered TRMM rain rate anomaly. The MCS formed during a time of day (00-06Z) when convection is on average suppressed, suggesting that forcing from the CCKW was able to overcome the forcing associated with the coherent diurnal cycle of convection. This MCS is found to be the leading convective disturbance associated with the pre-Alberto AEW (recall Fig. 4.1).

By 12Z July 30, the small MCS grew in horizontal extent and magnitude during the superposition with the eastward most edge of the convectively active phase of the CCKW (Fig. 4.2c). Note that the scattered pre-existing MCSs over 30-40°E weakened while superimposed with the convectively suppressed phase of the CCKW. These MCSs weakened during a time of day when convection is on average most frequent and remain in a suppressed state while superimposed with the convectively suppressed phase of the CCKW through 18Z July 30 (Fig. 4.2d). By 18Z July 30, the pre-Alberto MCS is now centered about 20°E and is observed to further amplify and grow in horizontal extent while superimposed with the convectively active phase of the CCKW. At this time, easterly wind anomalies [over 5-15ºN, 25-35ºE] are observed to the east of the convectively active phase of the CCKW, whereas westerly wind anomalies [over 5-10ºN, 0-5ºE] are observed to its west. This low-level wind signature is consistent with the low-level wind structure of the CCKW over Africa (Mounier et al. 2007). However, northerly wind anomalies are also evident within the maximum positive Kelvin filtered TRMM rain rate anomaly. These northerly wind anomalies are attributed to the formation of the low-level wind signature of the pre-Alberto AEW, not the CCKW. Further, at this time, the deepest convection is collocated with the northerly flow, consistent with the observed structure of an AEW over Africa (e.g. Carlson 1969a,b; Reed et al. 1977; Duvel 1990; Diedhiou et al. 1999; Payne and McGarry 1977; Fink and Reiner 2003; Kiladis et al. 2006).

By 00Z July 31, the pre-Alberto AEW has shifted slightly westward while still superimposed with western half of the convectively active phase of the CCKW (Fig 4.2e). By 06Z July 31, deep convection associated with the AEW remained prominent while superimposed with the convectively active phase of the CCKW (Fig. 4.2f). This deep convection remained active during a time of day when convection is on average suppressed, suggesting that the combined forcing from the CCKW and the newly spawned AEW is greater than that of the forcing from the coherent diurnal cycle of convection over Africa.

Depending on the phase of the CCKW, rainfall is either increased or reduced over tropical Africa (e.g., Mounier et al 2007; Mekonnen et al. 2008; Laing et al. 2011). The convectively active phase of the CCKW is associated with increases in the amplitude and frequency of westward moving MCSs, whereas its convectively suppressed phase is associated with a reduction of both. In the pre-Alberto AEW case, the convectively suppressed phase of the leading CCKW may have contributed to the decay of the MCS on July 29 that Hill and Lin (2003) argue was important for the pre-Alberto AEW genesis over the Ethiopia Highlands (recall Fig. 4.1). The initiation of the MCS that Berry and Thorncroft (2005) argue later developed into the pre-Alberto AEW has been shown to occur during the passage of the convectively active phase of an eastward propagating CCKW. This MCS amplified within the convectively active phase of the CCKW during a time of day when convection is expected to be active. However, this MCS also remained prominent while superimposed with the convectively active phase of the CCKW through 06Z, a time of day where convection is on average suppressed over Darfur. A study comparing CCKWs and the diurnal cycle of convection within the tropics is needed to fully understand the role of the CCKW and diurnally varying convection but is beyond the scope of this study. Motivated by the results above, we now explore the climatological influence of CCKWs over tropical Africa in order to better understand the physical reasons of why the pre-Alberto AEW initiated during the passage of the CCKW.

4.3.2. The climatological role of convectively coupled Kelvin waves on the synoptic environment over Africa

The zonal wind anomaly structure of a composite CCKW has strong westward tilts in the lower troposphere, with upper-tropospheric winds generally opposite to those in the lower-troposphere (e.g., Straub and Kiladis 2002; Kiladis et al. 2009; Ventrice et al. 2012b; see Fig. 3.2). Because of this vertical wind structure, CCKWs must influence the background low-level easterly vertical wind shear over tropical Africa during boreal summer. For example, the amplification of low-level easterly vertical wind shear over Africa could provide a favorable environment for the development of organized convection (e.g., Rotunno et al. 1988; Lafore and Moncrieff 1989). This organization of convection is comprised of MCSs, westward intergio gravity waves, and "squall lines" (Tulich and Kiladis 2012). Further, since CCKWs strongly impact the zonal wind in the lower troposphere, we expect CCKWs to alter the nature of the mid-level AEJ. These parameters are now explored in turn to investigate the role of CCKWs on the synoptic environment important for convection and AEW growth over Africa.

i) 925-700 hPa Vertical Wind Shear

The organization of ordinary convection into propagating MCSs is favored under moderate vertical wind shear of the horizontal wind (e.g., Rotunno et al. 1988; Lafore and Moncrieff 1989). Over Africa, Laing et al. (2008, 2011) found that frequent deep convection is associated with maxima in the 925-600 hPa easterly shear over northern tropical Africa during May to August. This low-level vertical wind shear varies day-to-day and is composed by the low-level monsoon westerlies and the mid-level AEJ. Since CCKW wind anomalies are characterized by strong westward vertical tilts with height, both the 925 hPa and 700 hPa zonal wind fields are strongly influenced by CCKW passages. Therefore, these waves must affect the low-level vertical wind shear over Africa.

Anomalies of 925-700 hPa vertical wind shear magnitude (shaded) and direction (vectors) are averaged over each lag of the CCKW index to investigate the influence of the CCKW on low-level shear over Africa (Fig. 4.3). The direction of shear represents the vector difference between 925 hPa and 700 hPa. On Day -1, the convectively suppressed phase of the CCKW is located over western tropical Africa, while its convectively active phase is located over the eastern tropical Atlantic (Fig. 4.3a). Anomalous easterly shear extends from the western half of the convectively suppressed phase of the CCKW through the convectively active phase, covering over 30° of longitude. This anomalous easterly shear adds 0.5-1 ms^{-1} to the background easterly shear over Africa. Northeast of the convectively suppressed phase of the CCKW is a small area of anomalous westerly shear. The anomalous westerly shear is created by anomalous low-level (850 hPa and below) easterly flow associated with the convectively suppressed phase of the CCKW, where easterly anomalies weaken above 850 hPa. This anomalous westerly shear is collocated with the convectively suppressed phase of the CCKW and reduces the background low-level easterly vertical wind shear over Africa during the next two days (Fig. 4.3b,c).

By Day 0, the convectively active phase of the CCKW is located over the coast of West Africa (Fig. 4.3b). Anomalous easterly vertical wind shear is collocated with the convectively active phase of the CCKW, which increases the background easterly vertical wind shear there. In addition to occurring within the convectively active phase of the

CCKW, significant anomalous easterly shear extends eastward to the maximum positive Kelvin filtered OLR anomaly. Note that in addition to the convective envelope of the CCKW, the area in between the leading suppressed phase and the convectively active phase of the CCKW is also an environment that favors for the development of organized convection due to the enhancement of background low-level easterly shear there (e.g., Laing et al. 2008, 2011).

A vertical cross section of anomalous zonal wind on Day 0 over the longitude at 8.5ºN shows that the increased easterly vertical wind shear in between the leading convectively suppressed phase and the active phase of the CCKW (0º-10ºW) is primarily driven by anomalous easterly winds extending back towards the west with height (Fig. 4.4). The anomalous easterly shear within the convectively active phase of the CCKW (0º-25ºW) is from the combination of mid-tropospheric easterly flow undercut by anomalous westerly flow.

Between Day +1 and Day +4, anomalous easterly vertical wind shear progresses eastward with the convectively active phase of the CCKW (Fig. 4.3c-f). Following this convectively active phase of the CCKW is its suppressed phase, which is associated with anomalous westerly vertical wind shear. Between Day +1 and Day +4, this anomalous westerly vertical wind shear reduces the background easterly vertical wind shear over the equatorial Atlantic and Africa by roughly 0.5 ms^{-1} (Fig. 4.3c-f).

By increasing the background low-level easterly vertical wind shear over Africa, the CCKW provides an environment known to be favorable for the organization of ordinary convection into propagating MCSs (e.g., Rotunno et al. 1988; Lafore and Moncrieff 1989; Laing et al. 2008, 2011). The more frequent, stronger MCSs within the convective envelope of the CCKW also increase the likelihood of initiating or intensifying a pre-existing AEW (e.g., Thorncroft et al. 2008). This increased vertical wind occurs within the convectively active phase of the CCKW, but increased vertical wind shear also occurs just ahead of it. Recall that the MCS that later developed into the pre-Alberto AEW formed in between the leading convectively suppressed phase and convectively active phase of a CCKW, indicative that it formed in a region relative to the CCKW where low-level vertical wind shear is enhanced (Fig. 4.2c). This MCS grew during the passage of the convectively active phase of the CCKW, consistent with the region relative to CCKW where increased low-level easterly vertical low-level wind shear is present.

ii) The impact of convectively coupled Kelvin waves on the horizontal structure of the African easterly jet

Fields of total 700 hPa easterly winds (dashed contours), anomalies of 700 hPa zonal wind (shaded), and Kelvin filtered OLR anomalies (bold contours) are averaged over each lag of the CCKW index to investigate the impact of the CCKW passage on the horizontal structure of the AEJ (Fig. 4.5). Easterly 700 hPa wind anomalies generally occur within the convectively suppressed phase of the CCKW. These easterly anomalies also extend westward through the eastward most edge of the convectively active phase, consistent with the westward vertical tilted structure of the CCKW. Anomalous westerly winds follow the minimum negative Kelvin filtered OLR anomaly of the CCKW (Fig. 4.5d-l). These anomalous westerly winds extend westward through the following convectively suppressed phase of the CCKW (Fig. 4.5h-i), again consistent with the westward vertical tilted structure of the CCKW. It is important to comment on the anomalous easterly wind signature over the Atlantic between Day -4 and Day -2 (Fig. 4.5c-e). During this time, there are easterly anomalies collocated within the convectively active phase of the CCKW. This signature is not representative of the expected structure of the CCKW and is associated with an interference pattern caused by a westward moving signature that has been attributed to a SAL outbreak across the tropical Atlantic between Day -6 and Day 0 (Ventrice et al. 2012b; see Fig. 3.6).

The AEJ can be modulated by the CCKW in two main ways. The first is associated with the equatorial wind structure of the CCKW, which can modulate the horizontal shear of the AEJ on the equatorward side (e.g., Matthews 2004). The second process is associated with convection generated by the CCKW over Africa. Following the argument of Thorncroft and Blackburn (1999), increased convection on the equatorward side of the jet generates PV near the level of the jet, acting to strengthen the jet. On Day -6, the highest amplitude easterly winds associated with the AEJ are located over West Africa and centered over the coast of West Africa, indicated by the -9 ms^{-1} isotach (Fig. 4.5a). Between Day -5 and Day -2, the -9 ms^{-1} isotach extends westward over the central tropical Atlantic (to ~40°W), highlighting a westward extension of the AEJ (Fig. 4.5b-e). This westward extension of the jet over the tropical Atlantic separates moist monsoonal air equatorward of the jet, and a dry SAL poleward of it. Consistent with these observations, Fig. 3.6 showed an area of anomalously dry air progressed westward across the northern tropical Atlantic during the passage of the convectively active phase of a CCKW.

Over Africa, the 700 hPa easterly wind anomalies associated with the convectively suppressed phase of the CCKW increase the total magnitude of the AEJ between Day -4 and Day +1 (Fig. 4.5c-h). Between Day -1 and Day +1, Kelvin wave induced easterly anomalies accelerate the upstream half of the AEJ, extending the jet entrance region eastward over the Darfur Mountains. Previous literature that has focused on the intraseasonal variability of AEW activity (e.g., Leroux et al. 2010; Ventrice et al. 2011; Alaka and Maloney 2012) have shown that an eastward extension of the AEJ entrance region over the Darfur Mountains precedes a period of increased AEW activity. We hypothesize that the eastward extension of the AEJ entrance region will increase barotropic and baroclinic energy conversions for AEW growth over the Darfur Mountains and Ethiopian Highlands. Therefore, the convectively suppressed phase of the CCKW may reinforce the upstream half of the AEJ to pre-condition, or "load" the jet for a future period of increased AEW activity. These easterly wind anomalies are present for about four days and so whether these exist long enough to influence the subsequent AEW activity is an open question that should be investigated in future work.

For all days in Fig. 4.5, the maximum zonal wind anomaly is generally peaked equatorward of the AEJ. This signature suggests that the CCKW is affecting the horizontal shear across the AEJ, which modifies the vorticity sign-reversal in the jet core. A tighter horizontal gradient of easterly zonal wind is indicative of a more unstable AEJ, and vice versa. In order to verify that the CCKW's impact on the horizontal shear of the AEJ is significant enough to affect the meridional gradient of vorticity over Africa, Fig. 4.6 shows the raw negative gradient of absolute vorticity (henceforth NGAV; shaded) averaged over each CCKW lag between Day -1 and Day +5. Areas where the NGAV is anomalously more negative, such that it is statistically different than zero at the 95% level, are represented by the blue-dashed contour. To clarify, the collocation of significant NGAV anomalies and the raw NGAV strip can be interpreted as the AEJ becoming significantly more unstable. On Day -1, the AEJ is more unstable over western tropical Africa between 20ºW-0ºW during the passage of the convectively active phase of the CCKW (consistent with anomalous westerlies on the equatorward side of the AEJ), and over eastern Africa between 16-22ºE during the passage of the its suppressed phase (consistent with an eastward extension of the AEJ there as seen in fig. 4.5f). Over western Africa, the AEJ is anomalously unstable through Day +2, or two days after the passage of the convectively active phase of the CCKW (Fig. 4.6b-d).

By Day +2, the AEJ is more unstable over central tropical Africa [5ºE -18ºE] during the passage of the convectively active phase of the CCKW. The AEJ over central Africa remains anomalously unstable up to two days after the passage of the convectively active phase of the CCKW (until Day +4; Fig. 4.6d-f). Between Day +3 and Day +5, significant NGAV anomalies are collocated with the raw NGAV strip over eastern tropical Africa [20-30ºE] during, and just after the passage of the convectively active phase of the CCKW. This result suggests that the AEJ is more unstable over the “trigger region” during this time (Fig. 4.6e-g).

The combined effect of enhanced convection and anomalous 700 hPa westerly winds associated with the convectively active phase of the CCKW increases the instability of the AEJ during and up to two days after its passage. While the AEJ becomes more unstable during the passage of the convectively active phase of the CCKW, moist convection triggered by the CCKW is assumed to play a prominent role with regards to modulating AEW activity over Africa.

iii) 2-10 day filtered Eddy Kinetic Energy

The passage of the convectively active phase of the CCKW might increase AEW activity over Africa by increasing the number of strong and long lasting MCSs over Africa that can serve as convective triggers (e.g., Mounier et al. 2007; Nguyen and Duvel 2008; Laing et al. 2011). These MCSs thrive in an environment characterized by increased low-level easterly shear, which then propagate back toward the west within a more unstable AEJ.

A time-longitude composite of 2-10 day filtered daily averaged EKE anomalies composited over each lag of the CCKW index shows the relationship between CCKWs and AEW activity (Fig. 4.7). Recall that Day 0 is when the minimum Kelvin filtered OLR anomaly is located over the base point (10°N, 15°W). Between Day -5 and Day +2, no significant positive EKE anomalies develop over the tropical Atlantic during the passage of the convectively active phase of the CCKW. Positive EKE anomalies first develop over West Africa (15°W-0°E) after the passage of the convectively active phase of the CCKW over the coast of West Africa. This result suggests that the convectively active phase of the CCKW is insufficient alone to modulate AEW activity over the tropical Atlantic. Positive EKE anomalies are generated directly after the passage of the convectively active phase of the CCKW over western tropical Africa [between 20°W and 0°E]. Thereafter, this large area of positive EKE anomalies over West Africa progresses westward over the Atlantic with an average phase speed of 9.0 m s^{-1}, consistent with the phase speed of an AEW (e.g., Kiladis et al. 2006, and references therein). It is likely that this anomalous EKE signature is composed of many instances where pre-existing AEWs are becoming stronger after the passage of the convectively active phase of the CCKW, similar to the pre-Alberto case in 2000 and the pre-Debby AEW case in 2006 (see Chapter 2).

Positive EKE anomalies also develop over the Darfur Mountains (25°E) and over and downstream of the Ethiopian Highlands (30-35°E) during the passage of the eastern most edge of the convectively active phase of the CCKW between Day +2 and Day +3. Recall that the wind signature associated with the pre-Alberto AEW formed within the convectively active phase of the CCKW over the Darfur Mountains (Fig. 4.2). The positive EKE anomalies generated over the Darfur Mountains amplify within the convectively active phase of the CCKW and progress westward on time scales consistent with AEWs directly after the passage. This area of positive EKE anomalies progresses westward across tropical Africa between Day +6 and Day +10 and over the tropical Atlantic thereafter.

Interestingly on Day -1, significant positive EKE anomalies are generated over 20-30°E prior to and during the passage of the convectively suppressed phase of the CCKW. Recall that this is when the entrance region of the AEJ extends eastward over eastern highlands of Africa (Fig. 4.5f). Therefore, any diurnally driven MCSs generated over the Darfur Mountains and Ethiopian Highlands prior to the passage of the convectively suppressed phase of the CCKW over might be sufficient enough to trigger an AEW due to the increased barotropic and baroclinic energy conversions associated with the eastward shifted jet. Further work is needed on the role of CCKWs and the eastward shifted AEJ over the eastern African highlands and their combined impact on AEW activity.

4.4. Discussion and Conclusions

Composite analysis shows that boreal summer CCKWs modulate the frequency of occurrence of AEWs, consistent with the hypothesis of Mekonnen et al. (2008). This relationship was illustrated using the case of the pre-Alberto (2000) AEW initiation. A TRMM 3B42 rain-rate anomaly time-longitude plot showed that the initiation of the pre-Alberto AEW occurred during the passage of a CCKW (Fig. 4.1). The convection attributed to the genesis of the pre-Alberto AEW described by Berry and Thorncroft (2005) was likely triggered by the passage of an eastward propagating CCKW. It has been shown that a series of consecutive CCKWs strongly influenced the pre-Alberto AEW over Africa. We have also shown that the initiation and west coast developing stages (e.g., Berry and Thorncroft 2005) of the pre-Alberto AEW were times when the pre-Alberto AEW was superposed with a convectively active phase of a CCKW.

The convectively active phase of CCKWs modulates the synoptic environment over tropical Africa through convective and dynamical processes that provides a favorable environment for increasing AEW activity. Figure 4.8 shows two schematic diagrams characterizing the evolution of the environment over Africa during the passage of a CCKW over West Africa at arbitrary times t = 0 (when the active phase of the CCKW is over the Guinea Highlands) and t = t + 3 days (when the active phase of the CCKW is over the eastern African highlands). Beginning with time t = 0 (c.f., Day 0 in the composite analysis), the convectively active phase of the CCKW is located over the Guinea Highlands region in West Africa (Fig. 4.8a). Enhanced low-level easterly shear (purple arrow) extends from the convective envelope of the CCKW eastward to the center of its convectively suppressed phase, with anomalous low-level westerly shear ahead of this convectively suppressed phase. Since the low-level shear is climatologically easterly over Africa and is attributed to the combination of the mid-level AEJ and low-level monsoon westerlies, the Kelvin-induced low-level westerly shear that occurs just the east of the leading suppressed phase of the CCKW reduces the background low-level easterly vertical wind shear. In contrast, the Kelvin-induced low-level easterly shear that occurs within and immediately to the east of the convectively active phase of the CCKW increases the background low-level easterly shear over Africa. The increased anomalous easterly shear generated by the CCKW is a known condition that is beneficial for strong and long-lasting MCS development (e.g., Mounier et al. 2007; Nguyen and Duvel 2008; Laing et al. 2011). By increasing the frequency of strong, long-lasting MCSs, the CCKW increases the number of convective triggers over Africa that is suggested to be important for AEW initiation over the eastern African highlands (e.g., Thorncroft et al. 2008).

The AEJ (red dashed line) becomes more unstable (thick dark-red dashed line) over western Africa during the passage of the convectively active phase of the CCKW. It is important to note that there are two ways to explain the impact of the CCKW on the instability of the AEJ. The first is the direct impact from enhanced convection by the CCKW, which generates a strip of PV (i.e., Schreck and Molinari 2011; MacRitchie and Roundy 2012) that provides a favorable environment for wave formation (Schubert et al. 1991; Hsieh and Cook 2005). The second being the CCKW enhances horizontal shear against the equatorward side of the AEJ (i.e., Matthews 2004). For this schematic, we only show the latter. CCKW induced anomalous westerly flow at the level of the AEJ increases horizontal shear on the equatorward side of the AEJ, indicative of a more unstable jet. The more unstable jet is consistent with the time when convection is enhanced over Africa by the CCKW. Since the CCKW provides an environment associated with a more unstable AEJ and intense moist convection, a westward propagating AEW response (orange slanted line) develops just after the passage of the convectively active phase of the CCKW over the Guinea Highlands region.

Roughly three days later (c.f., Day +3 in the composite analysis), the convective envelope associated with the CCKW is located over the Darfur Mountains (Fig. 4.8b). Enhanced low-level easterly shear propagates eastward with the CCKW, now providing a favorable environment for organized convection over the eastern African highlands. Westerly wind anomalies at the level of the AEJ extend westward from the convectively active phase of the CCKW, increasing the horizontal shear on the equatorward side of the AEJ over the Congo region. Consistent with an environment favorable for AEW initiation and growth, a new AEW response develops over the eastern African highlands during the passage of the convectively active phase of the CCKW. The AEW response to the CCKW passage over the Guinea Highlands region at time t = 0 has propagated back towards the west over the tropical Atlantic and becomes important to consider for Atlantic tropical cyclogenesis (e.g., Chapters 2 and 3).

4.5. Figures

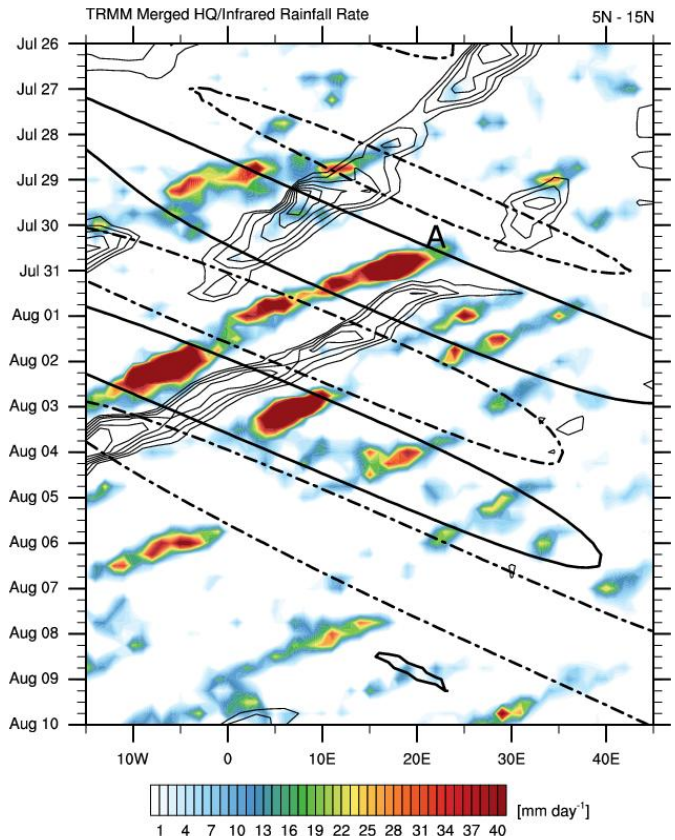

Fig. 4.1. A time-longitude plot of unfiltered rain-rate anomalies (positive anomalies shaded only) overlaid with Kelvin filtered rain-rate (contoured) averaged between the 5-15°N band for the period of July 26-August 10, 2000. The initiation of the MCS linked to the genesis of the pre-Alberto AEW is denoted as the letter "A". The +/- 2 mm day^{-1} Kelvin filtered rain-rate anomaly is only contoured to indicate each phase of the CCKW. Positive values of total meridional wind is contoured (black); contouring begins at 2 ms^{-1}; contour interval is 1 ms^{-1}.

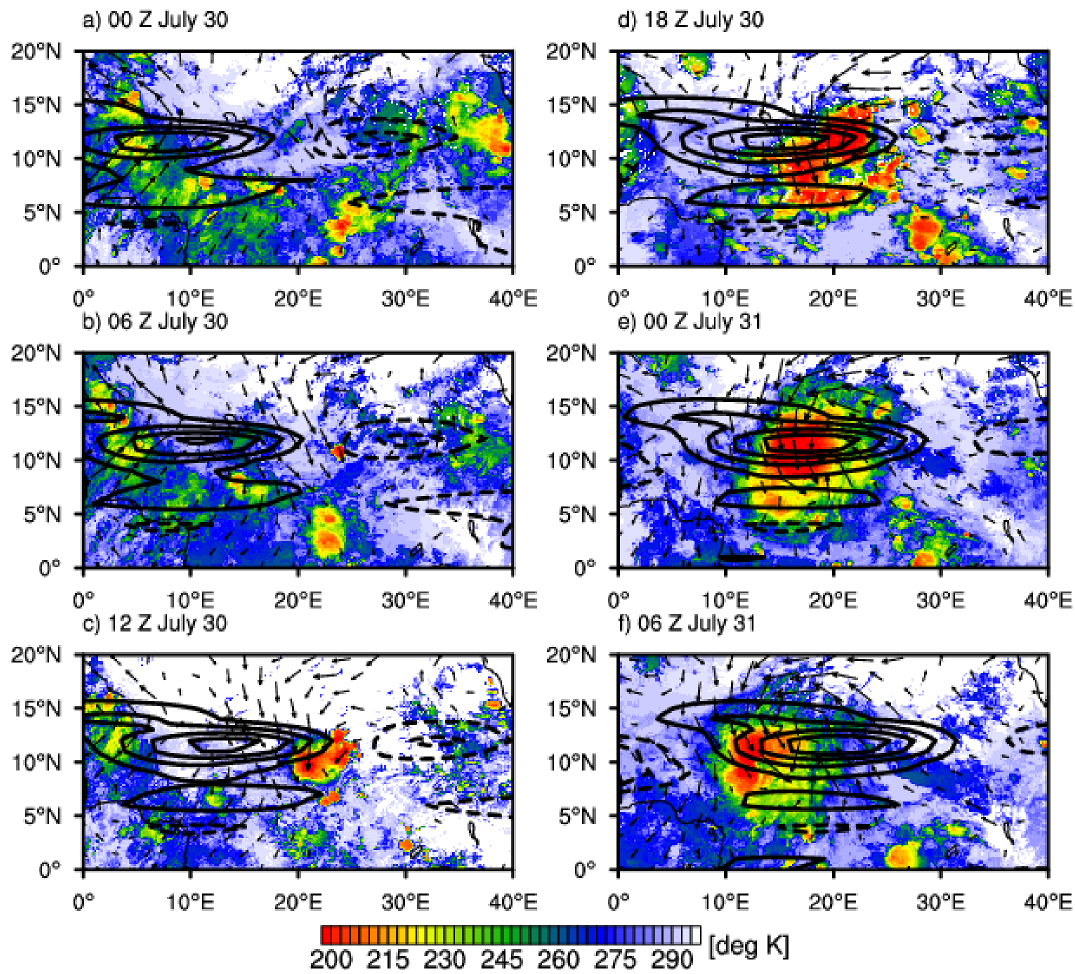

Fig. 4.2. Infrared radiation (shaded) overlaid with Kelvin filtered rain rate anomalies (black contours) and 850 hPa wind anomalies (vectors) for the period beginning at 00Z July 30, 2000 and ending 06Z July 31, 2000. Shade interval is 2.5 $^{\circ}$K; contours interval is 3 mm day^{-1}; reference vector is 10 ms^{-1}.

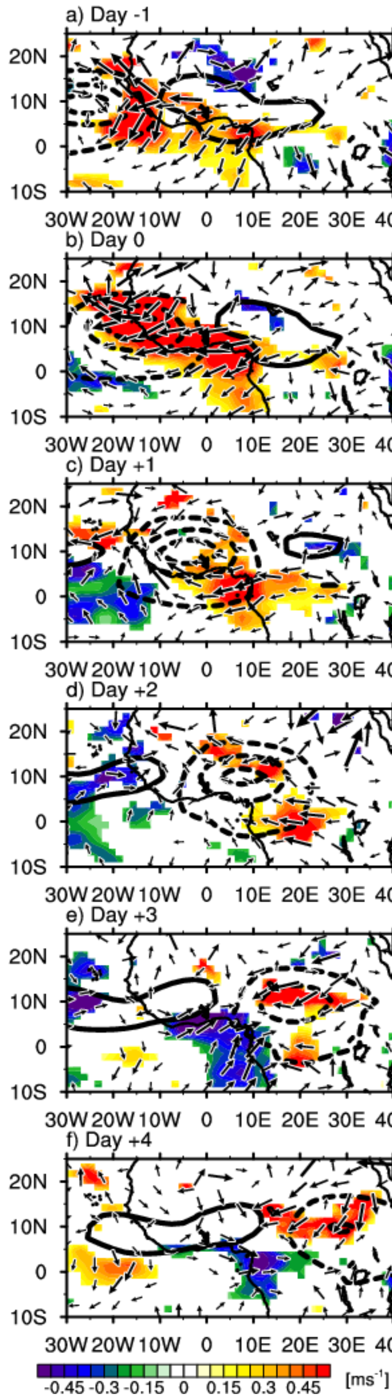

Fig. 4.3. The 925-700 hPa vertical wind shear vector and magnitude (shaded) anomaly composite averaged over each CCKW lag. Wind shear magnitude anomalies statistically different than zero at the 90% level are shaded. Vectors represent the vector difference between 925 hPa and 700 hPa. Kelvin filtered OLR anomalies are contoured if statistically different than zero at the 95% level. Negative Kelvin filtered OLR anomalies are dashed. Shade interval is 0.1 ms^{-1}; contour interval is 3 Wm^{-2}; reference shear vector is 0.5 ms^{-1}.

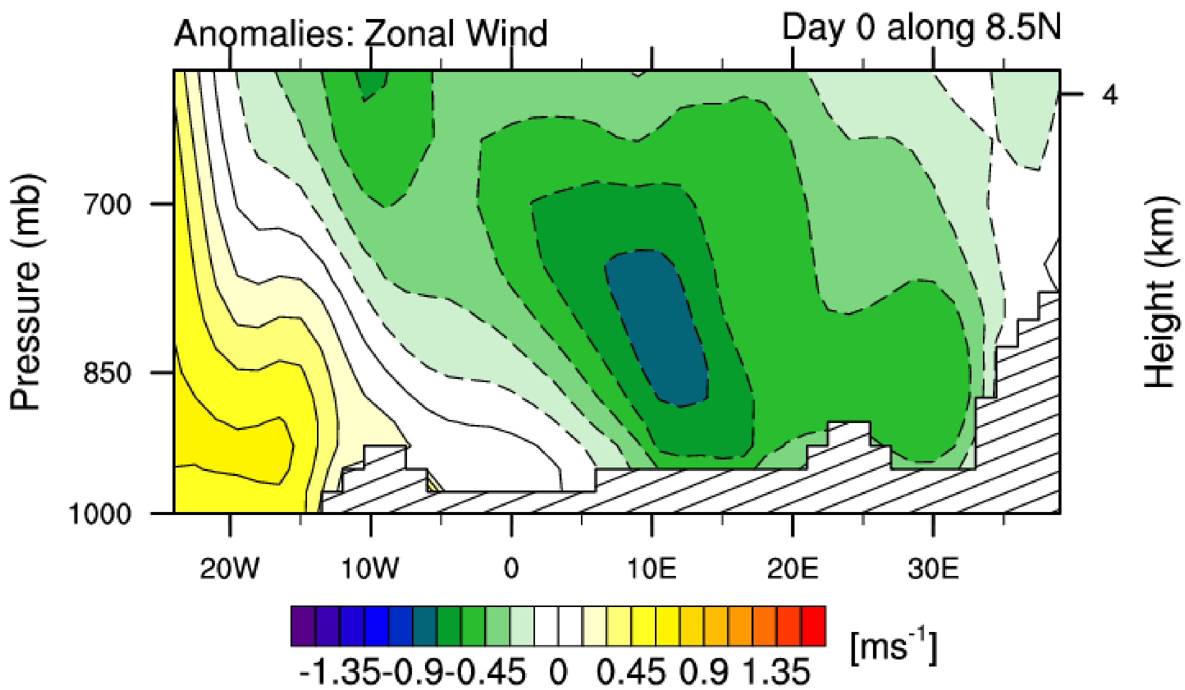

Fig. 4.4. A height-longitude composite of zonal wind anomalies along 8°N on Day 0 of the CCKW index. The slanted black line-on-white fill represents the topography of West Africa.

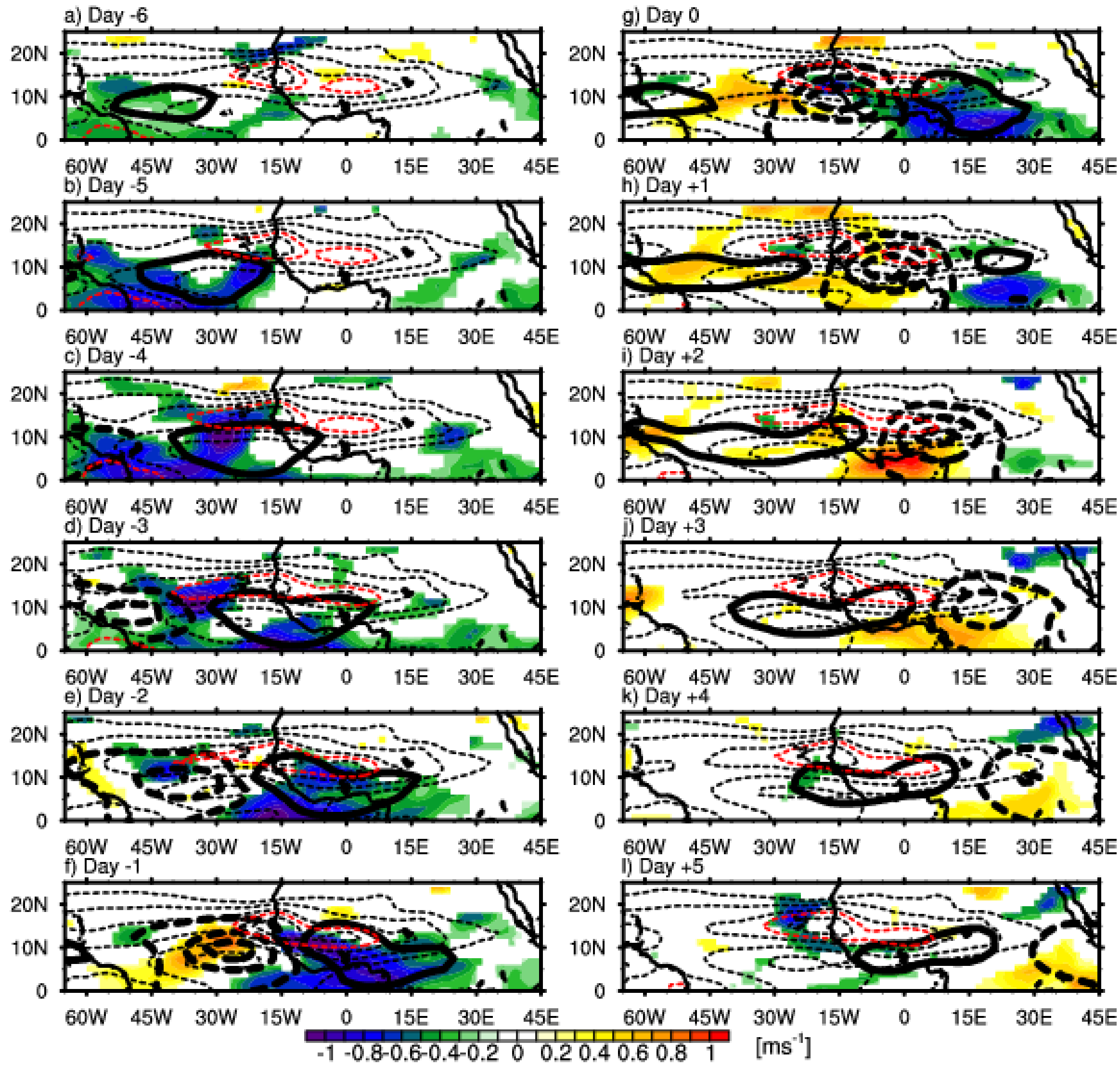

Fig. 4.5. 700 hPa zonal wind anomalies averaged over each CCKW lag. Anomalies statistically significantly different than zero at the 95% level are shaded. Total raw easterly zonal wind is composited for each CCKW lag and contoured. Kelvin filtered OLR anomalies are contoured (bold). Negative Kelvin filtered OLR anomalies are dashed. Shade interval is 0.2 ms^{-1}; Kelvin filtered OLR contour interval is 3 Wm^{-2}; easterly 700 hPa winds contour range is from -10 to -4 ms^{-1}; wind contour interval is 2 ms^{-1}. The red dashed contour highlights the -9 ms^{-1} contour.

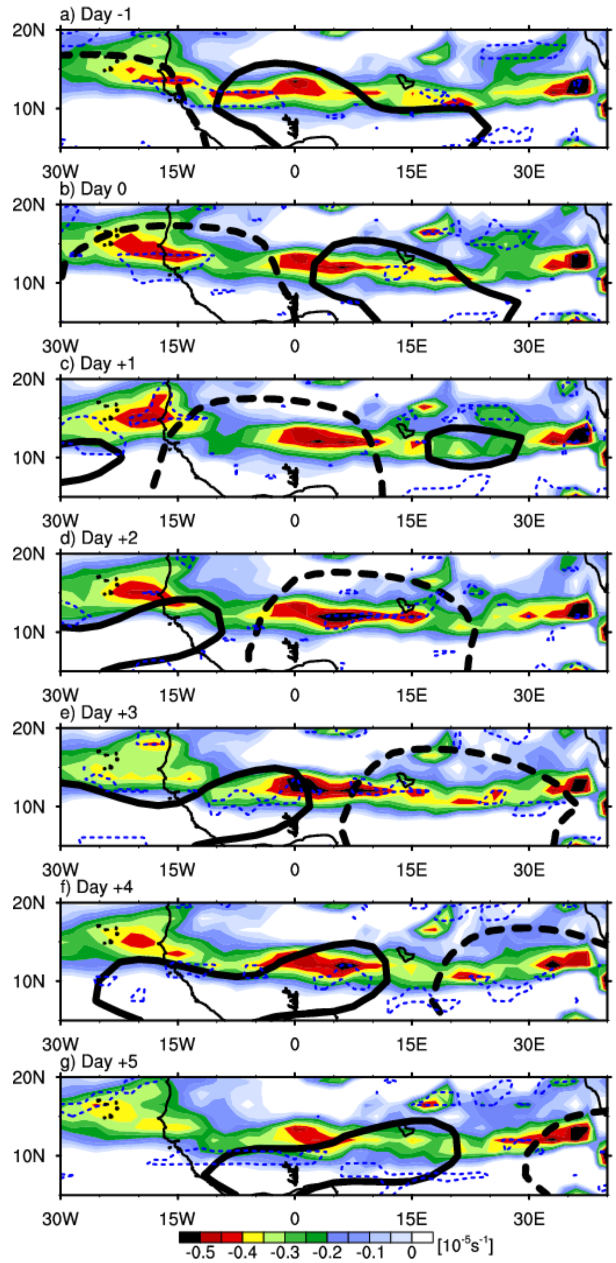

Fig. 4.6. The raw negative meridional gradient of absolute vorticity (shaded) averaged over each CCKW lag. Negative anomalies of the meridional gradient of absolute vorticity that are statistically different than zero at the 95% level are represented by the blue-dashed contours. Kelvin filtered OLR anomalies are contoured black (dashed if negative). Shade interval is 0.05 $10^{-5}s^{-1}$; the +/- 3 Wm^{-2} Kelvin filtered OLR anomalies is only drawn.

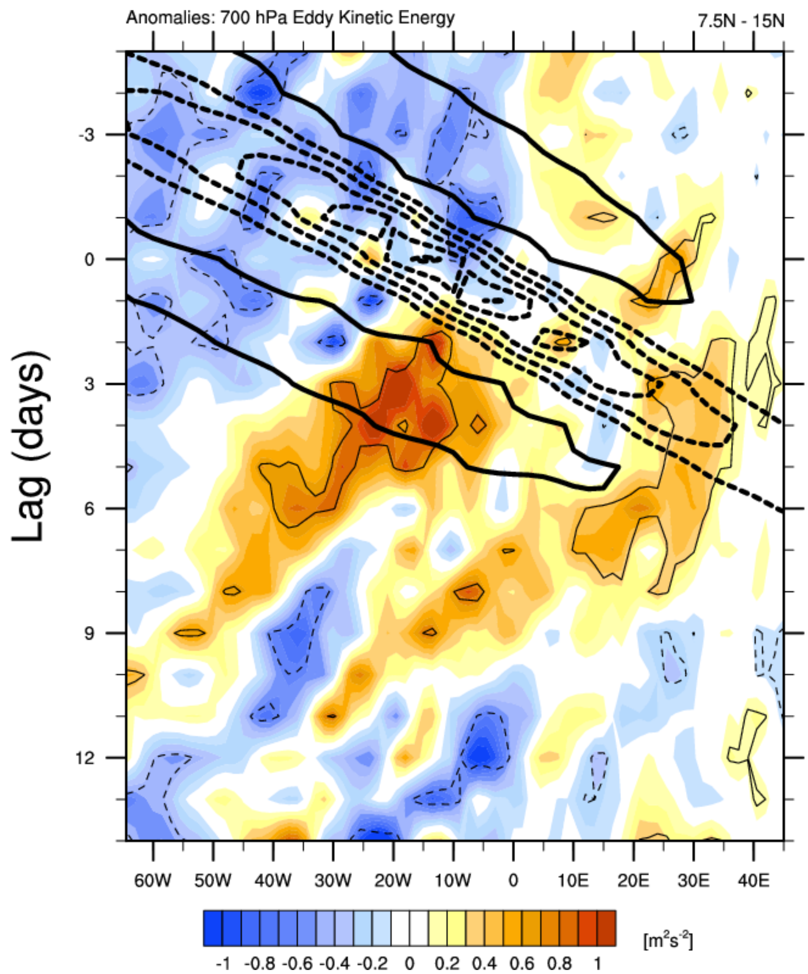

Fig. 4.7. A time-longitude composite of daily averaged 700 hPa eddy kinetic energy of 2-10 day filtered 700 hPa winds (shaded) averaged and over each lag of the CCKW index between the 7.5-15°N band. Positive (Negative) eddy kinetic energy anomalies statistically different than zero at the 90% level are within the solid (dashed) contour. Kelvin filtered OLR anomalies are averaged over the 5-10°N latitude band and are contoured with bold lines. Negative Kelvin filtered OLR anomalies are dashed. Shade interval is 0.1 m^2s^{-2}; contour interval is 3 Wm^{-2}.

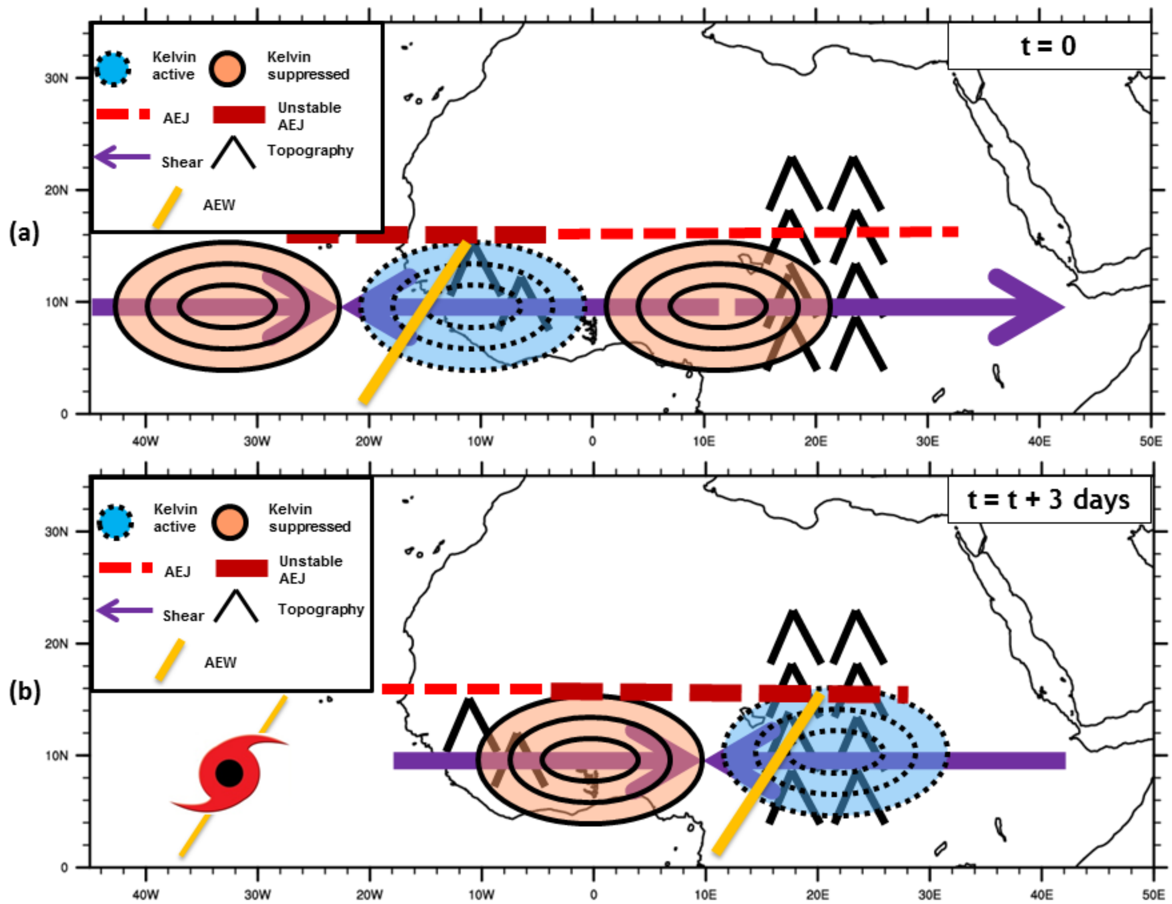

Fig. 4.8. A schematic diagram representing the modulation of the African environment and AEW activity by the passage of a CCKW when the convective envelope of the CCKW is over (a) the Guinea Highlands and (b) approximately three days later when it is over the eastern African highlands.

5. The role of the convectively-suppressed phase of a Kelvin wave on the intensity of two mature tropical cyclones

5.1. Introduction

The impact of the convectively suppressed phase of CCKWs on the intensity of tropical cyclones is unknown. This chapter explores the passage of the convectively suppressed phase of a CCKW on two tropical cyclones in 2010, Hurricane Danielle and Tropical Storm Earl. Hurricane Danielle was forecasted by all numerical and statistical guidance to continuously intensify through 06Z August 25 with exception of GFNI (Fig. 5.1). However, this forecast did not verify and it will be shown that Danielle's intensification process was interrupted at 9Z August 24 (forecast hour 27 in Fig. 5.1) by an unexpected brief weakening that lasted until 00Z August 25. This sudden weakening of the tropical cyclone caused a two-day delay in its intensification, as it finally reached Category 3 status by early August 27. Similar intensity forecast issues were also associated with the subsequent tropical cyclone over the eastern tropical Atlantic, Tropical Storm Earl. These intensity forecast issues occurred during the passage of the convectively suppressed phase of a CCKW over the tropical Atlantic. While CCKWs have been generally thought as equatorially trapped waves (e.g., Matsuno 1966), it has been shown in Chapters 2 and 3 that CCKWs can impact the large-scale synoptic environment over the northern tropical Atlantic during boreal summer. It is therefore reasonable to hypothesize that CCKWs may also affect the intensity of tropical cyclones by directly modulating their surrounding environment. The purpose of this work is to provide preliminary evidence that suggests CCKWs might impact tropical cyclone intensity and to motivate future exploration.

Yanase et al. (2010) suggested that CCKWs might modulate tropical cyclone intensity over the West Pacific. In a modeling study, they showed that Typhoon Durian developed and underwent rapid intensification over the West Pacific while superimposed with the convectively active phase of an eastward propagating CCKW. Such results indicate a possible relationship between CCKWs and tropical cyclone intensity and motivate this study of similar scenarios over the Atlantic. In contrast to the convectively active phase of a CCKW intensifying a mature tropical cyclone, its convectively suppressed phase might delay, or even weaken the intensification of a pre-existing tropical cyclone. This chapter explores the potential impact of the strong convectively suppressed phase of a CCKW on Hurricane Danielle and Tropical Storm Earl (2010).

The present chapter is structured as follows. Section 5.2 discusses datasets and methodology used. Section 5.3 investigates the impact of the convectively suppressed phase of a CCKW passage on Hurricanes Danielle and Earl. A composite analysis of CCKWs is given in Section 5.4 for physical interpretation of how CCKWs impact the large-scale environment over the tropical Atlantic that might affect the intensity of a tropical cyclone. Discussion and final comments are presented in section 5.5.

5.2. Datasets and Methodology

The ERA-Interim reanalysis is used to investigate the synoptic evolution of both the tropical cyclone case studies and the composite CCKW analysis (Dee et al. 2010). Geostationary Earth Orbit IR data from the CPC merged IR dataset was used to view the convective signatures of Danielle and Earl (Janowiak et al. 2001).

The Observing System Research and Predictability Experiment (THORPEX) Interactive Grand Global Ensemble (TIGGE) database is used to analyze how operational numerical weather prediction models represented the CCKW that interacted with Danielle and Earl. TIGGE began during a workshop at the ECMWF in 2005 (Richardson et al. 2005) to enhance collaborations in the development of ensemble prediction systems between operational centers and universities by increasing the availability of data for research. Upper and lower tropospheric winds, and mean sea level pressure (MSLP) from the ECMWF (0.28º horizontal resolution) and National Centers for Environmental Prediction (NCEP; 1º horizontal resolution) model control forecasts are compared.

Information regarding the intensity of Hurricanes Danielle and Earl is taken from NHC's best track data. Tropical cyclogenesis points and tracks were from the National Climatic Data Center's (NCDC's) IBTrACS v4 dataset (Knapp et al. 2010).

i) Kelvin waves in upper-level velocity potential

CCKWs are identified by filtering ERA-Interim's 200 hPa velocity potential (henceforth VP200) in wavenumber and frequency following the methodology of Wheeler and Kiladis (1999). CCKW filtering was performed with a period range of 2.5-20 days, with eastward wavenumbers 1-14, and equivalent depths of 8-90 meters. Figure 5.2 shows Kelvin-filtered VP200 variance for June-September. The strongest equatorial Kelvin filtered VP200 variance is located over the East Pacific extending eastward over the Atlantic and western Africa. The weakest equatorial Kelvin-filtered VP200 variance is located over the eastern Indian Ocean, Maritime Continent, and northern Australian regions. Higher Kelvin filtered VP200 variance is located approximately along 20ºS - 40ºS over the Southern Indian extending eastward across the central southern Pacific, highlighting the Southern Hemisphere extra-tropical cyclone track. It is important to note that the Kelvin filtered JJAS VP200 variance signature is spatially different than Kelvin filtered JJAS OLR variance (recall Fig. 3.1). This notion suggests that it might be more appropriate to filter an upper-level wind field for boreal summer CCKWs over the Western Hemisphere instead of OLR or rainfall. Further, VP200 is a new diagnostic to identify CCKWs and more work is needed to understand differences with the OLR diagnostics.

For the composite analysis, all dates are selected when the maximum positive Kelvin filtered VP200 anomaly (greater than 1.5σ during JJAS 1989-2009), or its convectively suppressed phase, was located over the equatorial Atlantic (5°S-5°N, 45°W). A total of 85 CCKWs were objectively identified using this methodology. Anomalies for all CCKW composites are constructed as differences from the seasonal cycle. The annual cycles for all fields are constructed by using the seasonal cycle and its first four harmonics. Bootstrap random resampling tests with one thousand iterations are used for statistical significance testing on all anomalies (e.g. Roundy and Frank 2004).

5.3. The interaction between a Kelvin wave and two Atlantic tropical cyclones

5.3.1. Hurricane Danielle Overview

The track and intensity for Hurricanes Danielle and Earl during the period between August 20 and August 30 is shown in Fig. 5.3. It will be shown that this period is also consistent with a time when the convectively suppressed phase of a CCKW passed over the tropical Atlantic. The genesis of Danielle occurred late on August 21 over the eastern tropical Atlantic. Danielle quickly intensified into a strong Category 1 hurricane between 12Z August 23 and 06Z August 24. At 09Z August 24, the National Hurricane Center (NHC) forecasted Danielle to become a Category 3 hurricane by the afternoon of August 25 (Fig. 5.4a). However, an unexpected weakening of Danielle occurred around

12Z on August 24, which resulted in a 15 knot maximum wind speed decrease in just 12 hours. This unexpected decay resulted in the NHC's (9Z August 24) forecast to have a 30 knot error in just 12 hours (Fig. 5.4b). According to the NHC's post season tropical cyclone report, Danielle's sudden weakening was attributed to a southwestward propagating shortwave-subtropical trough that was located approximately over 25ºN, 46°W on August 24. It is important to note that Danielle was located over 28-29ºC water when the tropical cyclone weakened, indicating that the ocean was in a favorable state for tropical cyclone intensification and therefore, not responsible for any intensity changes with Danielle (not shown). After the tropical cyclone's brief weakening, it slowly intensified and later became the season's first major hurricane on August 27.

5.3.2. Hurricane Earl Overview

Three days after Danielle became a named tropical cyclone (August 24), tropical storm Earl formed over the eastern Atlantic (recall Fig. 5.3). The NHC's post summary report states that Earl developed from a strong AEW. While the intensity of Earl was better predicted by the NHC when compared to Danielle, it was still forecasted to reach hurricane strength too quickly (Fig. 5.5a). The NHC forecasted Earl to become a hurricane three days after becoming a depression (on August 27), but like Danielle, its intensification was delayed. Earl did not reach hurricane strength until August 29, two days after the NHC's 21Z August 25 forecast. The delayed intensification of Earl resulted in 15-25 knot wind errors during the 24-to-48 hour forecast time frame (Fig 5.5b).

5.3.3. The role of the convectively suppressed phase of a strong convectively coupled Kelvin wave on Hurricane Danielle and Earl

While it might be coincidental that the intensifications of both Danielle and Earl were delayed, Fig. 5.6 shows that both tropical cyclones interacted with the convectively suppressed phase of a CCKW during the time when they were expected to intensify. In this figure, negative VP200 anomalies represent large-scale mass divergence, while positive VP200 anomalies represent convergence. CCKW waves are indicated by black contours, such that negative Kelvin filtered VP200 anomalies are dashed and represent the convectively active phase of the CCKW, and vice versa. The initial genesis locations and tracks of Hurricane Danielle and Earl are shown. Both Danielle and Earl developed within a broad region of negative unfiltered VP200 anomalies over the eastern Atlantic. Between August 20 and September 1, positive VP200 anomalies, associated with the convectively suppressed phase of a CCKW, propagated eastward across the Atlantic. Both Danielle and Earl intensified to a Category 1 Hurricane and Tropical Storm, respectively, on the leading edge of the convectively suppressed phase of the CCKW. It wasn't until the passage of the maximum positive VP200 Kelvin filtered anomaly when Danielle unexpectedly weakened, and Earl begun to struggle to intensify.

According Fig. 5.6, Danielle appears to have intensified just after the passage of the maximum Kelvin filtered VP200 anomaly. During this time, Danielle was tracking poleward, away from the deep tropics and cannot be represented in this analysis (recall Fig. 5.3). Therefore, Fig. 5.7 shows maps of CPC-merged IR (shaded), and Kelvin filtered 200VP anomalies (contours) beginning at 12Z August 22 and ending at 12Z August 29. At 12Z August 22, Danielle was a tropical storm and located over the eastern

Atlantic [12.4ºN, 33.4ºW] (Fig. 5.7a). The convectively active phase of an eastward propagating CCKW (blacked dashed contours) was located over West Africa [centered about 10ºN, 5ºE], while it's following convectively suppressed phase was located at the longitude of South America. Chapter 2 showed that Atlantic tropical cyclogenesis is most frequent two days after the passage of the convectively active phase of a CCKW. Therefore, it is suggested that the convectively active phase of the CCKW over West Africa impacted the geneses of both Danielle (August 21) and Earl (August 24).

Recall that Danielle intensified between August 22 and August 23. By 12Z August 24, Danielle's maximum sustained winds suddenly weakened by 10 kt. At this time, the suppressed phase of a CCKW was located equatorward of Danielle [over 0ºN, 50ºW] (Fig. 5.7c). Between August 24 and August 25, Danielle recurved northward away from, presumably, an unfavorable environment associated with the convectively suppressed phase of the CCKW (Fig. 5.7c-d). When Danielle began to track more northward, the tropical cyclone intensified into a major hurricane (Fig. 5.7d-f).

On August 24, Earl became a tropical depression over the eastern tropical Atlantic (Fig. 5.7c). Between August 25 and August 28, Earl was superimposed with the strong suppressed phase of the CCKW, and remained a tropical storm (Fig. 5.7d-g). The minimum surface pressure of Earl only dropped 8 hPa during this time, indicative of very little intensification. Due to Earl's westward track, the tropical cyclone remained superimposed with the convectively suppressed phase of the CCKW for a longer period of time than Danielle. By August 29, Earl was no longer superimposed with the convectively suppressed phase of the CCKW (Fig. 5.7h). At this time, Earl rapidly intensified into a major hurricane during the transition into the convectively active phase of the CCKW.

Both Fig. 5.6 and Fig. 5.7 show that the convectively suppressed phase of a CCKW was superimposed with Hurricane Danielle and Tropical Storm Earl when they were forecasted to intensify. Both tropical cyclones were predicted to intensify into hurricanes too fast by the NHC. While only an association has been shown between the convectively suppressed phase of the CCKW and the delayed intensification of Danielle and Earl, it provides some preliminary evidence that CCKWs may play a role in affecting the intensity of tropical cyclones.

5.3.4. The large-scale environment over the tropical Atlantic

It is difficult to know precisely how a CCKW can affect a mature tropical cyclone. High resolution model runs are needed to investigate if tropical cyclone inner-core dynamics respond to CCKW passages. It is possible, however, to investigate how the large-scale environment over the tropical Atlantic reacted to the passage of the strong convectively suppressed CCKW phase. Figure 5.8 shows box chart plots of Kelvin filtered VP200 anomalies, TCWV anomalies, and 1000-600 hPa vertical wind shear magnitude anomalies averaged over the tropical Atlantic [0-20ºN, 25-55ºW] between August 15 and September 11, 2010.

Weak negative Kelvin filtered VP200 anomalies were present over the tropical Atlantic between August 15 and August 21, suggestive of the passage of the convectively active phase of a CCKW. Note that the magnitude of these negative Kelvin filtered VP200 anomalies are three times stronger when using daily averaged filtered data instead of 6-hourly filtered data, indicating a caveat of the space-time filtering technique (not shown). Between August 16 and August 21, the tropical Atlantic was characterized by increased moisture and reduced 1000-600 hPa vertical wind shear. Between August 22 and August 31, negative Kelvin filtered VP200 anomalies swap to positive, highlighting the passage of the CCKW's convectively suppressed phase. It was this convectively suppressed CCKW phase that interacted with both Danielle and Earl. During its passage, the large-scale environment over the tropical Atlantic was characterized by reduced TCWV and increased vertical wind shear, suggestive of a more hostile environment for tropical cyclone intensification. Recall that during this time, Hurricane Danielle and Earl both struggled to intensify. It wasn't until after the passage of the subsequent convectively active phase of the CCKW when synoptic scale moisture increased and 1000-600 hPa vertical wind shear reduced over the tropical Atlantic.

During the passage of the convectively suppressed phase of the CCKW, the large-scale environment over the Atlantic became less favorable for tropical cyclone intensification. This unfavorable environment is assumed to be associated with the passage of the convectively suppressed phase of the CCKW. In order to explore this hypothesis, a CCKW composite analysis is presented in section 5.4.

5.3.5. Operational Numerical Weather Prediction Models

Operational forecasters rely heavily on model guidance for tropical cyclone intensity changes. Therefore, given the poor forecasts, it is important to consider whether operational numerical weather prediction (NWP) models accurately identified the convectively suppressed phase of the CCKW during mid-August. Unfiltered VP200 anomalies from the 00 UTC August 17 forecast from the widely used ECWMF and NCEP control runs are investigated (Fig. 5.9). The reanalysis from ERA-Interim is shown for verification. Between August 20 and 27, the ERA-Interim reanalysis shows a coherent eastward propagating envelope of positive VP200 anomalies over the Atlantic, highlighting the convectively suppressed phase of the CCKW. The ECWMF forecast does capture an eastward propagation of positive VP200 anomalies across the tropical Atlantic between August 21 and August 27. However during this time, the ECWMF forecast also shows a slower, stronger eastward propagating positive VP200 anomaly over the East Pacific. The NCEP forecast does not show an eastward propagating envelope of positive VP200 anomalies over the tropical Atlantic. Instead, the forecast shows a weak stationary positive VP200 anomaly signature at the longitude of South America (70ºW) and a strong, slow westward propagation of negative VP200 anomalies from 20ºW on August 20 to 40ºW on August 27. This result indicates that the NCEP forecast was not accurately representing the CCKW.

Maps of MSLP, initialized at 00Z August 17, are shown for both ECMWF and NCEP to investigate the MSLP field over the tropical Atlantic (Fig. 5.10 and 5.11, respectively). Figure 5.10 shows the 90-to-198 hour forecasts with 12 hour increments from the 00UTC August 17 forecast from the ECWMF control run. It is important to note that the horizontal resolution of the operational NWP models is unable to accurately resolve the actual MSLP of mature tropical cyclones. In the ECMWF forecast, a tropical cyclone (Danielle) tracks westward across the tropical Atlantic between ECWMF forecast hour (ECfH) 90 and 198, with a slight northward recurvature. By August 25 at 06Z, the ECWMF forecast (ECfH 198) suggested that Danielle would be located at 17ºN, 56ºW. This forecast was slightly too fast, since Danielle was located at 18ºN, 50ºW by 06Z August 25.

Figure 5.11 shows the 90-198 hour forecast from the NCEP control run. The NCEP forecast does not suggest the development of a tropical cyclone until NCEP forecast hour (NfH) 138. Spatially, Danielle's pressure field is much larger in the NCEP forecast than in the ECMWF forecast. Further, Danielle is slightly more intense in the NCEP forecast, and tracks Danielle to the west at a slower pace than does the ECWMF forecast. This result might be the result of NCEP having a lower spatial resolution than ECWMF, but recall that NCEP did not correctly represent the CCKW as well. At 06Z August 25, the NCEP forecast (NfH 198) suggested that Danielle would be located at 14ºN, 43ºW, which was too slow. The location discrepancy between both models might be related to the fact that the ECWMF better represented the convectively suppressed phase of the CCKW, whereas the NCEP forecast did not. The convectively suppressed phase of the CCKW is associated with enhanced trades near the surface (e.g., Straub and Kiladis 2002; Mounier et al. 2007; Mekonnen et al. 2008; Kiladis et al. 2009). Therefore, these enhanced trades create a background state characterized by increased westward flow that could increase the westward movement of Danielle and may help to explain the location discrepancy between the two models.

In order to understand how the convectively suppressed phase of a CCKW modulates the large-scale environment over the tropical Atlantic, the role of the convectively suppressed phase of the CCKW on the large-scale environment is explored below.

5.4. Composite analysis: The role of the convectively suppressed phase of strong convectively coupled Kelvin waves on the tropical Atlantic's large-scale environment

To investigate the climatological role of strong convectively suppressed CCKW phases over the tropical Atlantic, composites are constructed using all June-September dates when the maximum positive Kelvin filtered VP200 anomaly greater than 1.5σ in magnitude was located at the longitude of 45ºW (Day 0). The longitude base point is chosen to be centered over the MDR. Anomalous low-level zonal winds, 1000-600 hPa vertical wind shear, and TCWV, are investigated in turn. Further, anomalous 200 hPa geopotential height (200Z) and winds are investigated for tropical-extratropical interactions.

5.4.1. Low-level (850 hPa) zonal winds

Figure 5.12 is a time-longitude composite of unfiltered 850 hPa zonal wind anomalies (shaded) and Kelvin filtered VP200 (contours) averaged over the latitudes between 0-20ºN. The solid black contours represent positive Kelvin filtered VP200 anomalies, or the convectively suppressed phase of the CCKW. Easterly wind anomalies are generally observed to be collocated within the convectively suppressed phase of the CCKW and remain over the tropical Atlantic up to three days after its passage. Westerly winds are located slightly ahead of the convectively suppressed phase of the CCKW, indicating large-scale divergence of the zonal wind. Therefore, low-level trades are reduced prior to the passage of the convectively suppressed phase of the CCKW, and enhanced during and after. The enhancement of low-level trades by the convectively suppressed phase of the CCKW might affect the intensity of a mature tropical cyclone by increasing low-to-mid level vertical wind shear over the tropical cyclone. Further, since the vertical zonal wind structure of a CCKW is tilted back towards the west with height (see Fig. 3.2a), initially, low-level easterlies will be strongest near the surface. These enhanced surface easterlies might cause the vertical alignment of the tropical cyclone to tilt to the east with height, where the low-level vortex is advected to the west faster than its mid-level vortex and result in a decoupling with convection. These principles would need to be tested more extensively in both observational and modeling studies.

Recall that the ECWMF forecast better represented the convectively suppressed phase of the CCKW that interacted with Danielle and Earl with respect to the NCEP forecast. The ECWMF forecast had a faster westward track speed of Danielle than did NCEP, suggestive that the ECWMF forecast had stronger trades than the NCEP forecast. Figure 5.13 supports this hypothesis, where the 00Z August 17 ECWMF forecast of 850 hPa zonal wind anomalies showed a coherent eastward propagation of low-level easterly wind anomalies that were preceded by an area of eastward progressing low-level westerly wind anomalies (low-level zonal divergence) during the passage of the convectively suppressed phase of the CCKW. In marked contrast, the NCEP forecast showed only a strong westward propagating signature, with a prominent low-level westerly wind component that can be attributed to Danielle itself.

5.4.2. Vertical Wind Shear

Vertical wind shear magnitude anomalies, defined as the vector difference between 1000 and 600 hPa levels, is averaged over the set of dates used in the composite analysis between 0-20ºN (Fig. 5.14). Vertical wind shear is generally reduced to the east of the maximum positive Kelvin filtered VP200 anomaly, and is strengthened to the west.

This agrees with Fig. 5.12, where low-level westerly wind anomalies occur to the east of the convectively suppressed phase of the CCKW, and easterly wind anomalies within and to the west. Recall that both Danielle and Earl intensified just prior to the passage of the maximum positive Kelvin filtered VP200 anomaly, or in a location relative to the Kelvin wave where vertical wind shear is reduced. Both tropical cyclones stopped intensifying after the passage of the maximum positive Kelvin filtered VP200 anomaly, or in a location relative to the Kelvin wave where vertical wind shear is stronger.

5.4.3. Total Column Water Vapor

The weakening of tropical cyclones is often attributed to dry air. Figure 5.15 is a time-longitude composite of TCWV anomalies averaged over 0-20ºN. Anomalously dry air is observed to progress eastward with the convectively suppressed phase of the CCKW. Since TCWV is integrated over the entire depth of the atmosphere, the dry signature associated with the convectively suppressed phase of the CCKW could exist over multiple pressure levels. Therefore, it is inconclusive to state at which level the dry air is most prominent, however it is likely a representation of moisture in the mid to lower troposphere. Over the eastern Atlantic, the eastward progression of anomalous dry associated with the convectively suppressed phase of the CCKW is interrupted by a westward propagating disturbance. This interaction causes positive TCWV anomalies to be collocated within the convectively suppressed phase of the CCKW there. This westward propagating disturbance is presumably associated with a westward propagating AEW that develops within the leading convectively active phase of the CCKW (recall Chapter 4).

5.4.4. Upper-level (200 hPa) Geopotential Height

The strongest signature of CCKWs over the Western Hemisphere is their upper-level zonal wind signature. The upper-level dynamical structure of the CCKW has zonal winds generally peaked near the equator, with upper-level westerlies ahead of the convectively active phase of the CCKW, and upper-level easterlies to its east (recall Fig. 3.2a). Therefore, the opposite should be true for the convectively suppressed phase of the CCKW. It is plausible that the upper-level westerly wind anomalies associated with the CCKW might favor the intrusion of extra-tropical waves into the tropics (e.g., Ambrizzi et al. 1995).

Figure 5.16 shows daily lagged composites of 200Z anomalies (shaded), 200 hPa wind anomalies (vectors), and Kelvin filtered VP200 anomalies (contours). For all lags, negative 200Z anomalies are to the east of the maximum positive Kelvin filtered VP200 anomaly, with positive 200Z to its west. These 200Z anomalies extend from 10ºS to 10ºN and are peaked in magnitude near the equator. After the passage of the convectively suppressed phase of the CCKW, upper-level westerly wind anomalies straddle the equator, indicative of westerly-wind duct. At Day +2, negative 200Z anomalies develop over the central Atlantic, poleward of the enhanced 200 hPa westerly flow at the equator (Fig. 5.16e). These negative 200Z anomalies remain quasi-stationary through Day +5 and are indicative of a tropical upper-tropospheric trough (TUTT). An anomalous cyclonic upper-level wind circulation is collocated with the TUTT over the area 15ºN-35ºN, 40ºW-60ºW. The upper-level westerly wind anomalies on the equatorward side of the TUTT increases vertical wind shear there, a feature not favorable for the intensification of tropical cyclones. Recall that NHC suggested that the brief weakening of Hurricane Danielle on August 14 was due to increased vertical wind shear from an interaction with a TUTT. It is therefore suggested that TUTTs commonly intrude the tropics after the passage of the convectively suppressed phase of the CCKW.

5.4.5. Summary

The convectively suppressed phase of the CCKW is associated with changes in various atmospheric fields over the northern tropical Atlantic that are known to impact tropical cyclone intensity. The tropical Atlantic experiences large-scale subsidence and reduced atmospheric moisture during the passage of the convectively suppressed phase of the CCKW. Further, vertical wind shear increases after its passage. This vertical wind shear adjustment also includes the intrusion of a TUTT over the central Atlantic that occurs after the passage of the convectively suppressed phase of the CCKW.

5.5. Conclusions

The intensification of Hurricane and Danielle and Tropical Storm Earl was interrupted during the passage of the convectively suppressed phase of a CCKW over the tropical Atlantic. During the passage of the convectively suppressed phase of the CCKW, the large-scale atmosphere over the tropical Atlantic dried and vertical wind shear increased. Once both tropical cyclones tracked away from the convectively suppressed phase of the CCKW, they intensified into the first two major hurricanes of the season.

Forecasts from the ECMWF and NCEP control runs were investigated to see whether NWP models were capable of representing the convectively suppressed phase of the CCKW. While the ECWMF forecast showed an eastward progression of positive VP200 anomalies associated with the convectively suppressed phase of the CCKW, it had a second area of positive VP200 anomalies over the East Pacific that propagated eastward too slowly and were too strong. In the NCEP forecast, there was no eastward progression of positive VP200 anomalies. Instead, the most dominant feature in the NCEP forecast was a westward propagating area of negative VP200 anomalies associated with the Danielle. With respect to the forecasted track of Danielle, ECWMF tracked Danielle to the west too fast, whereas the NCEP forecast was too slow. This result may be due to the ECWMF forecast having anomalous low-level easterlies over the MDR where the NCEP forecast had anomalous westerlies (Fig. 5.13).

The climatological role of the convectively suppressed phase of CCKWs on the large-scale environment over the tropical Atlantic was investigated through composite analysis. An environment characterized by large-scale subsidence, reduced moisture, and increased vertical wind shear occurs during and after the passage of the convectively suppressed phase of the CCKW. Further, a TUTT develops over the central Atlantic after the passage of the convectively suppressed phase of the CCKW. This TUTT develops when anomalous upper-level westerly winds, associated with the convectively suppressed phase of the CCKW, are over the equatorial Atlantic. It is assumed that the TUTT increases vertical wind shear over the Atlantic for a period after the passage of the convectively suppressed phase of the CCKW.

The results from this analysis suggest that the convectively suppressed phase of CCKWs might negatively impact the intensity of tropical cyclones. A quantitative analysis of all CCKW passages during the presence of an Atlantic tropical cyclone is needed. It is recommended that CCKWs are identified in the VP200 field for this analysis. This is due to CCKWs having a stronger upper-level wind signature than convective signature over the tropical Atlantic during boreal summer. Further, more work on how NWP models handle eastward propagating CCKWs is needed. If model forecasts are unable to correctly represent CCKWs, the model will have problems with forecasting tropical rainfall, tropical cyclones, and other large-scale atmospheric features within and outside of the tropics.

5.7. Figures

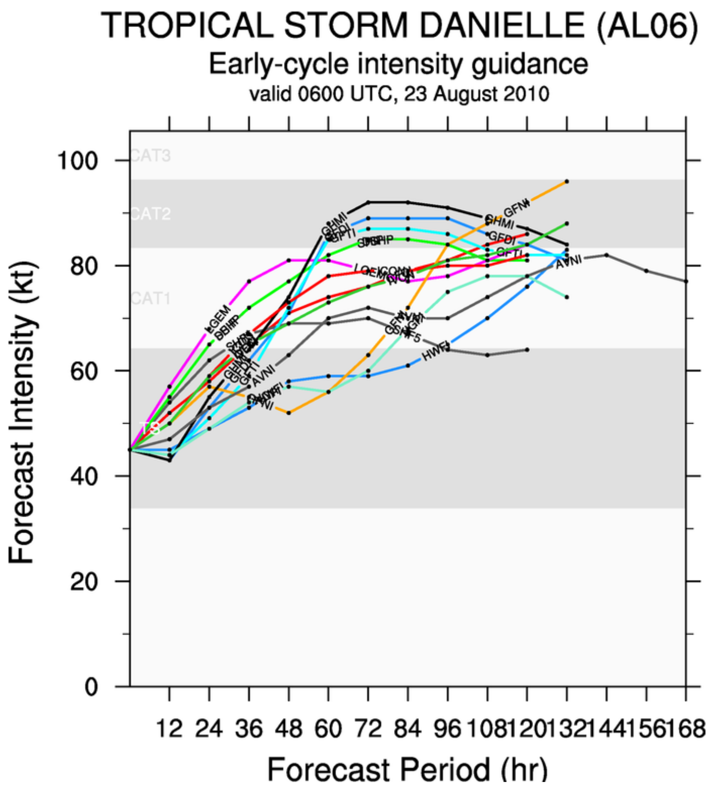

Fig. 5.1. The 0600 UTC August 23, 2010 model guidance intensity forecast for Hurricane Danielle.

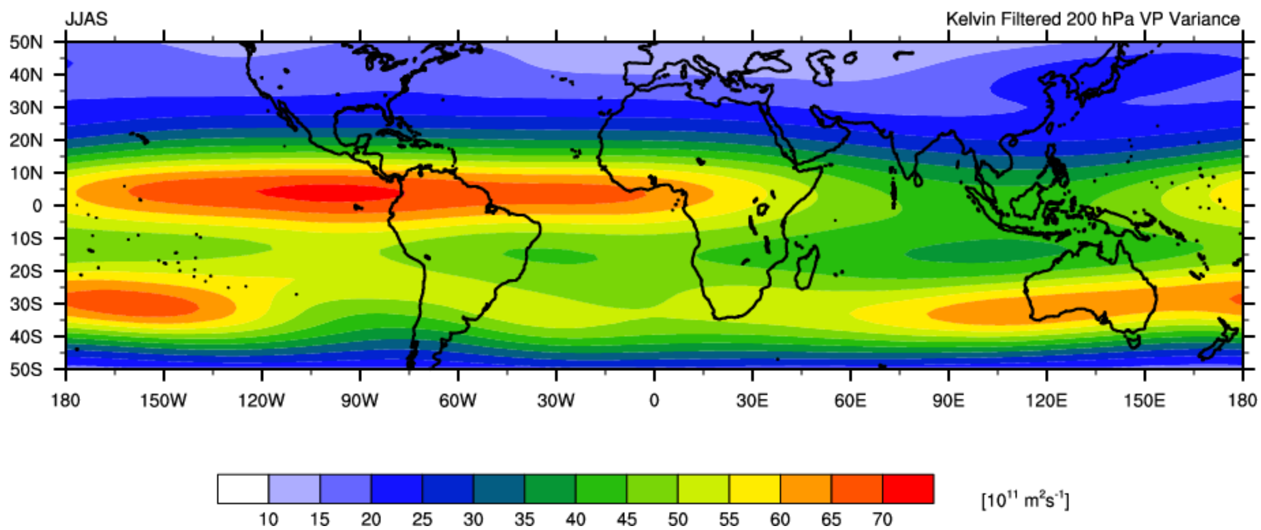

Fig. 5.2. June-September Kelvin filtered VP200 Variance for all years between 1990-2009.

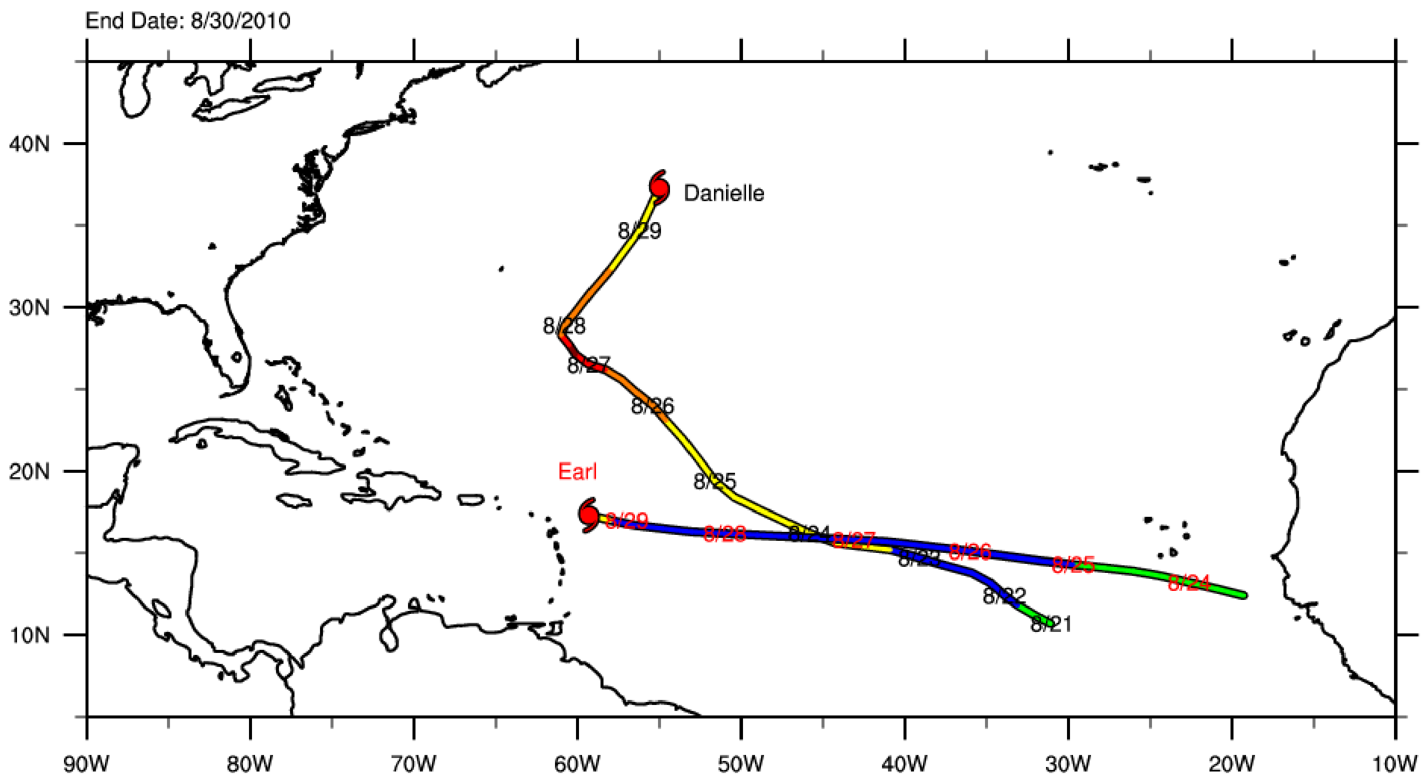

Fig. 5.3. Tracks and intensities for Hurricanes Danielle (black) and Earl (red) for the period ending on August 30, 2010. Tropical cyclone track line intensities: Green = Depression; Blue = Tropical Storm; Yellow = Cat. 1; Orange = Cat. 2; Red = Cat. 3; Brown = Cat. 4. Date string for each day is at 12Z.

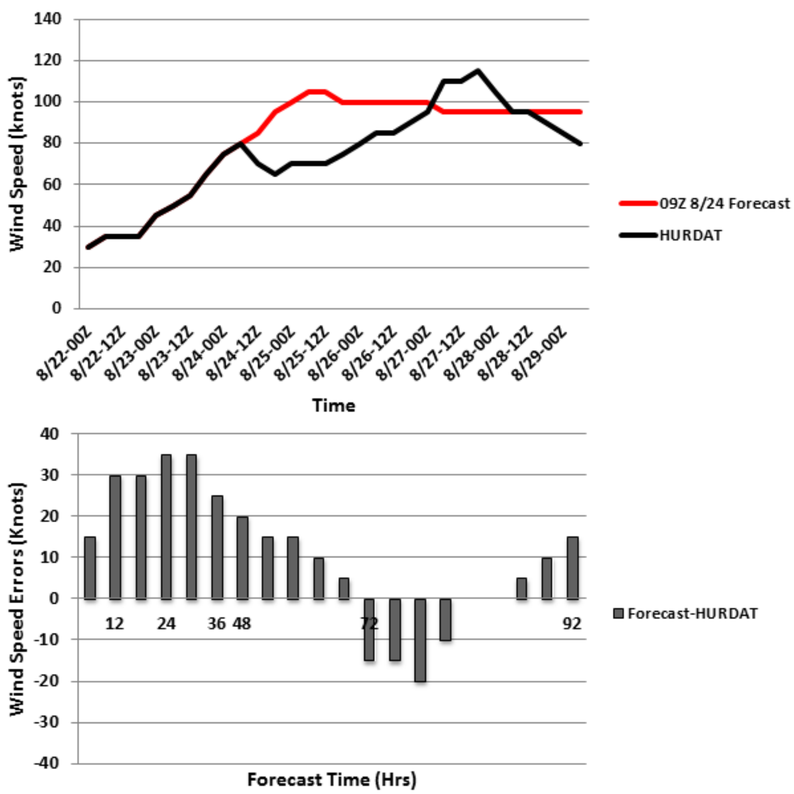

Fig. 5.4. (Top) Time series of Danielle's maximum wind speed from HURDAT (black line) and the 09Z August 24 NHC official forecast (red line). (Bottom) The NHC official forecast – HURDAT to represent the maximum wind speed errors (in knots).

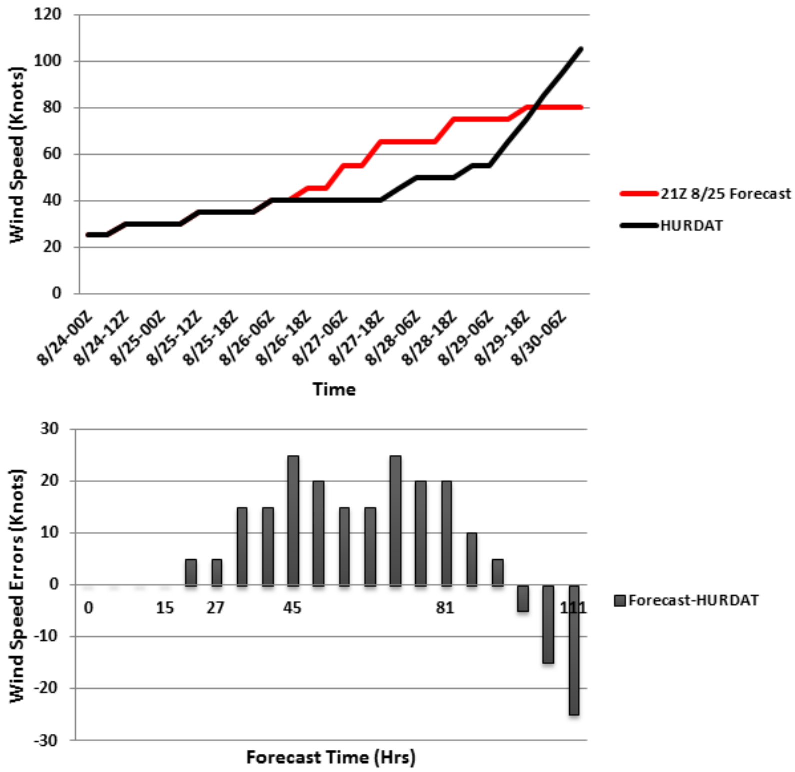

Fig. 5.5. Same as Fig. 5.4, but for Earl. The 21Z August 25 NHC official forecast is illustrated by the red line.

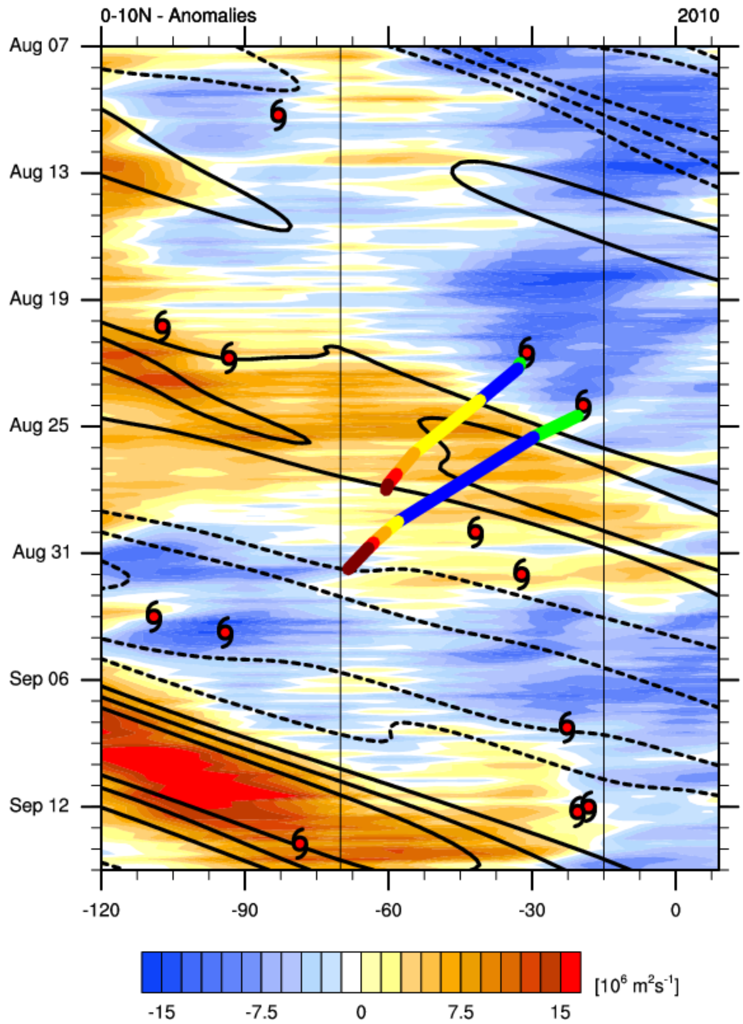

Fig. 5.6. A time-longitude plot of unfiltered VP200 anomalies (shaded) and Kelvin filtered VP200 anomalies (black contours; dashed if negative) for the period from August 7 to September 15, 2010. Tropical cyclone track line intensities: Green = Depression; Blue = Tropical Storm; Yellow = Cat. 1; Orange = Cat. 2; Red = Cat. 3; Brown = Cat. 4.

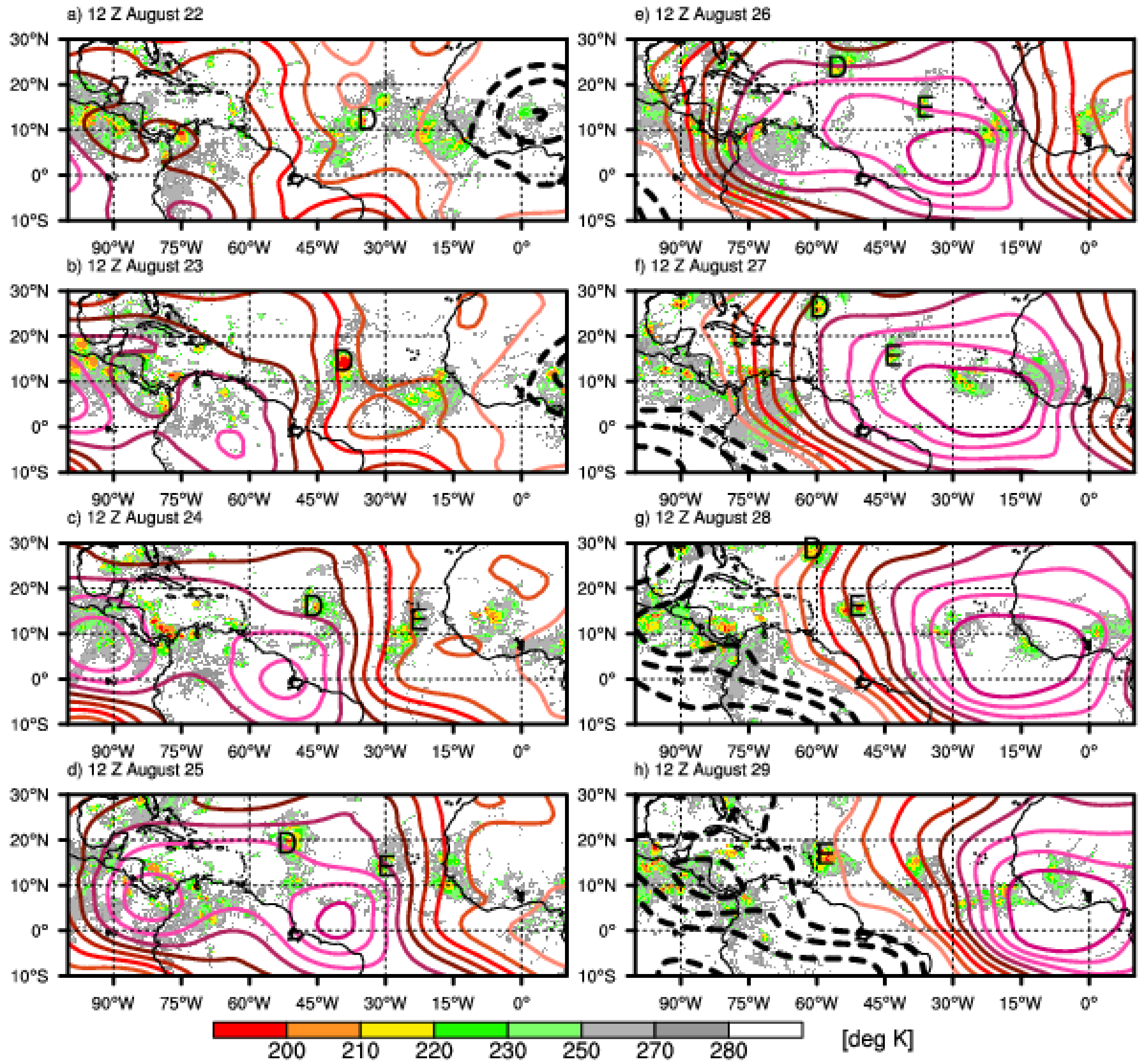

Fig. 5.7. Maps of CPC-merged IR (shaded), and Kelvin filtered VP200 anomalies (contours; black and dashed if negative, warm-colored and solid if positive) beginning at 12Z August 22 and ending at 12Z August 29. The locations of Danielle and Earl are denoted as the letters "D" and "E", respectively.

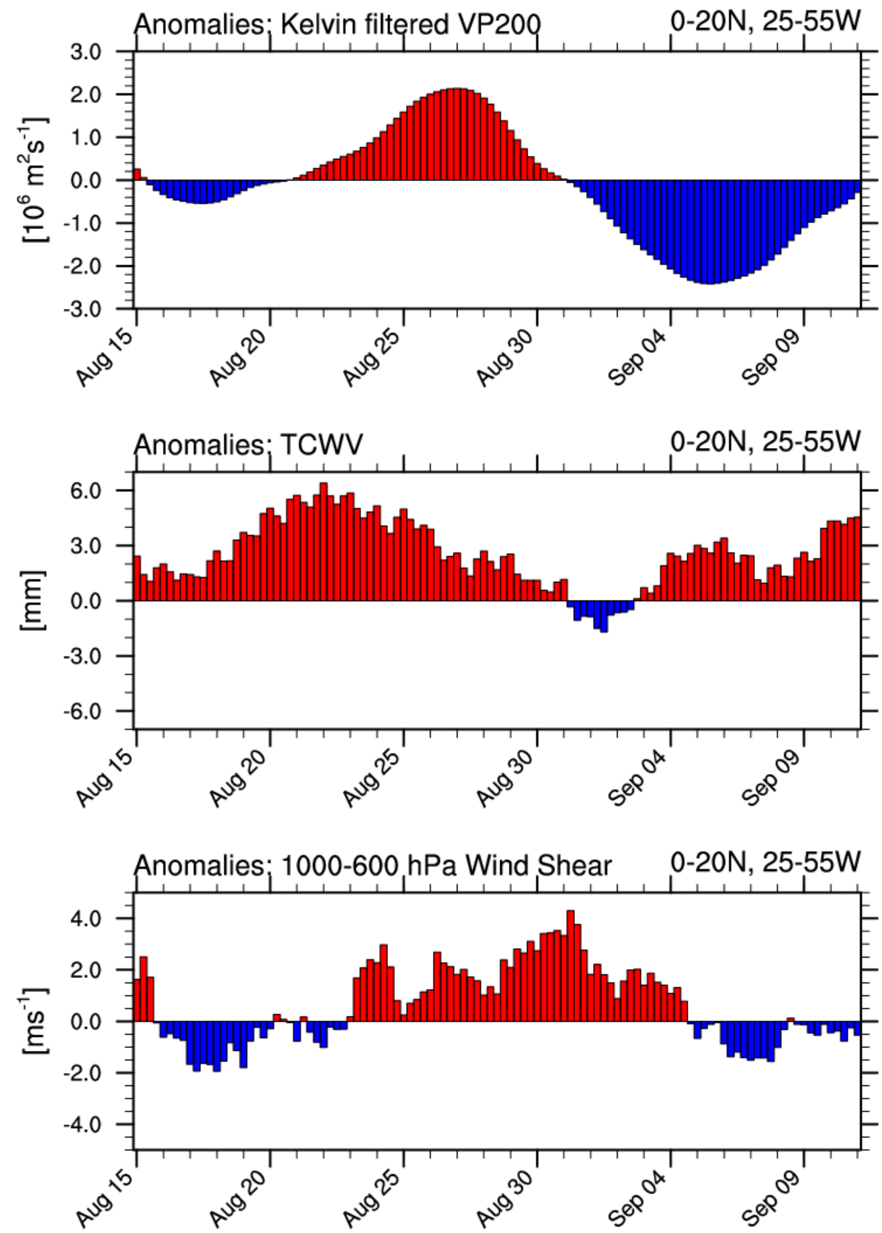

Fig. 5.8. Box charts highlighting the large-scale environment over the tropical Atlantic [averaged over 0-20ºN, 25-55ºW] between August 15 and September 11, 2010. (Top) Kelvin filtered VP200 anomalies; (Middle) Total column water vapor anomalies; (Bottom) 1000-600 hPa vertical wind shear magnitude anomalies.

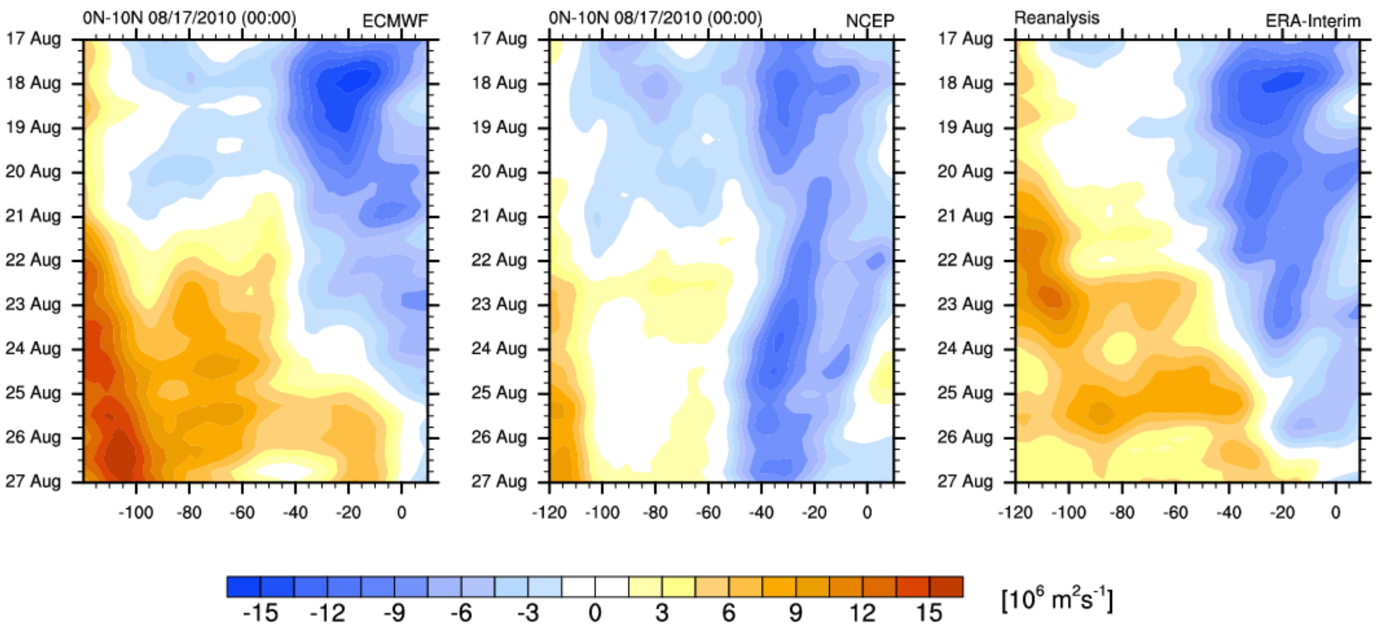

Fig. 5.9. Time-longitude plots of unfiltered 200VP anomalies averaged over the 0-10ºN latitude band for August 17 – August 27. (Left) ECWMF control run forecast for the 00Z August 17 run; (Center) NCEP control run forecast for the 00Z August 17 run; (Right) ERA-Interim reanalysis.

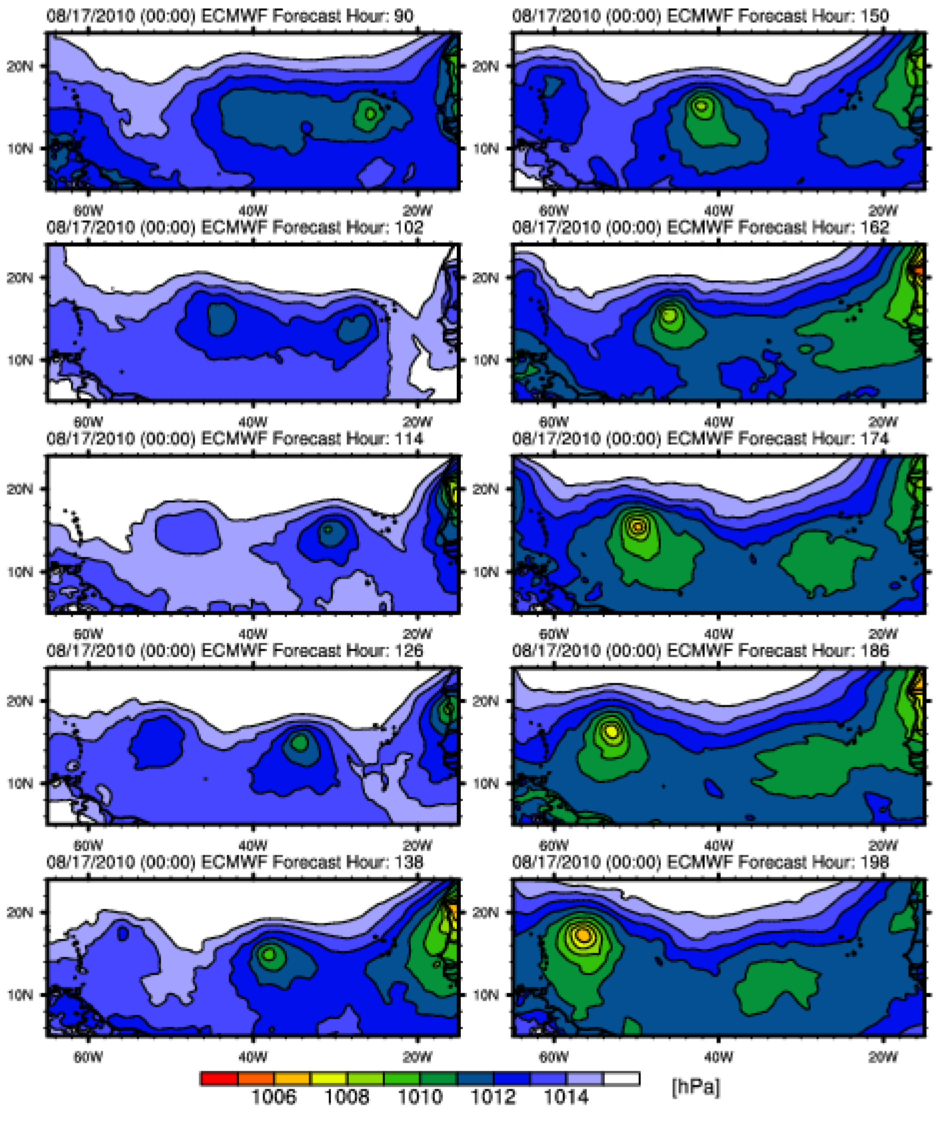

Fig. 5.10. Mean sea level pressure (shaded) for the ECWMF 00Z August 17 control run forecast beginning at forecast hour 90 and ending at forecast hour 198.

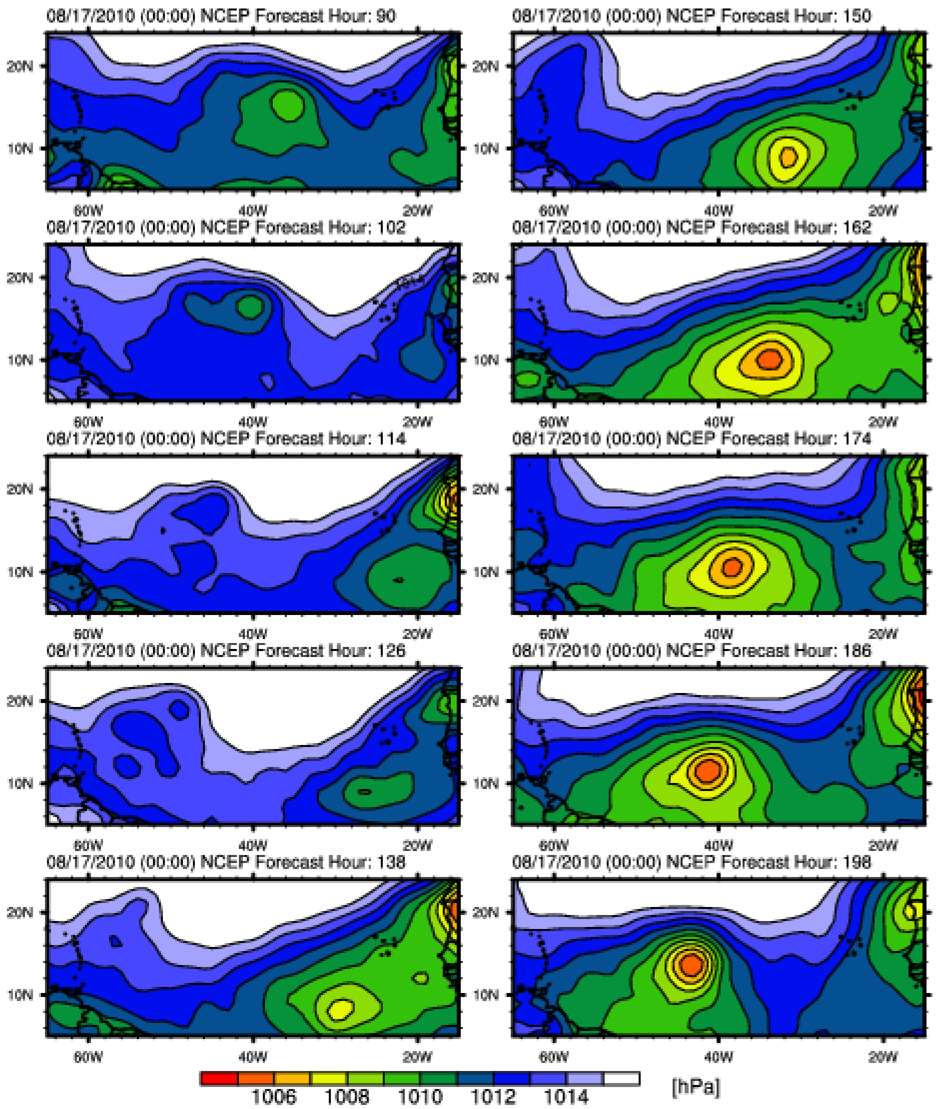

Fig. 5.11. Same as Fig. 5.10, but for the NCEP control run.

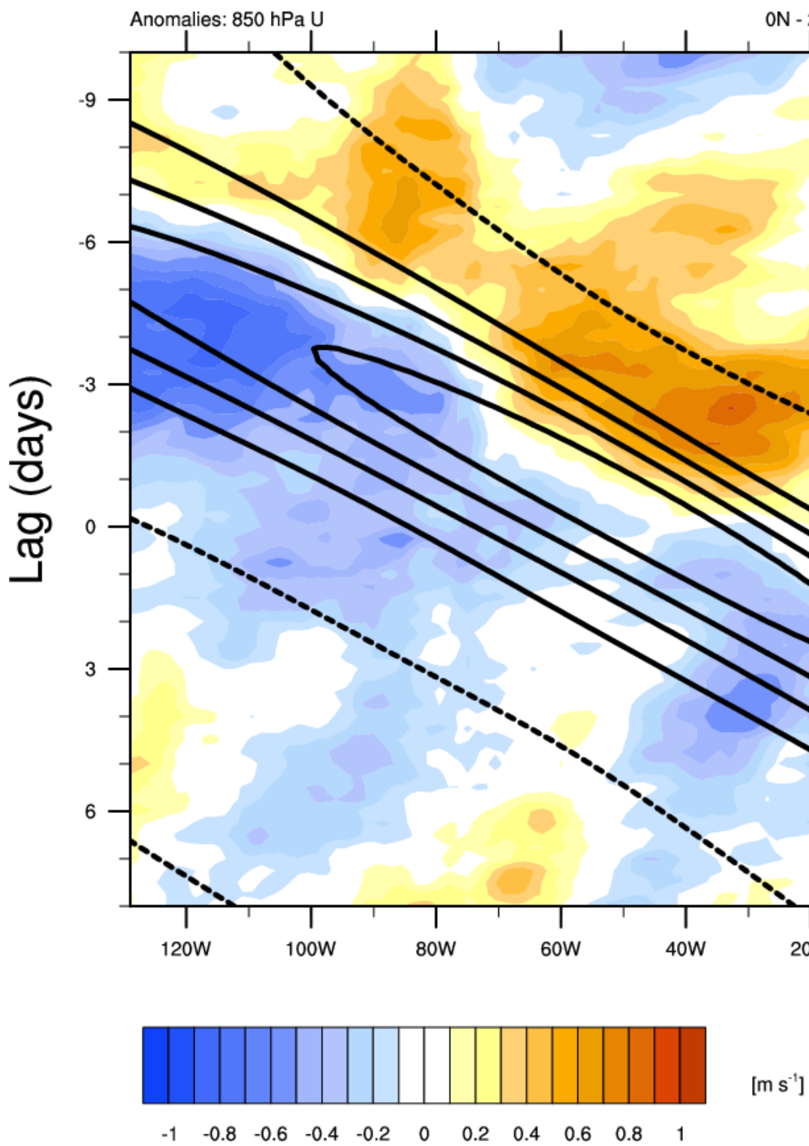

Fig. 5.12. A time-longitude composite of unfiltered 850 hPa zonal wind anomalies (shaded) and Kelvin filtered VP200 anomalies (contours; dashed if negative) averaged over the 0-20ºN latitude band. Day 0 represent the time when the maximum Kelvin filtered VP200 anomaly is located at the longitude of 45ºW.

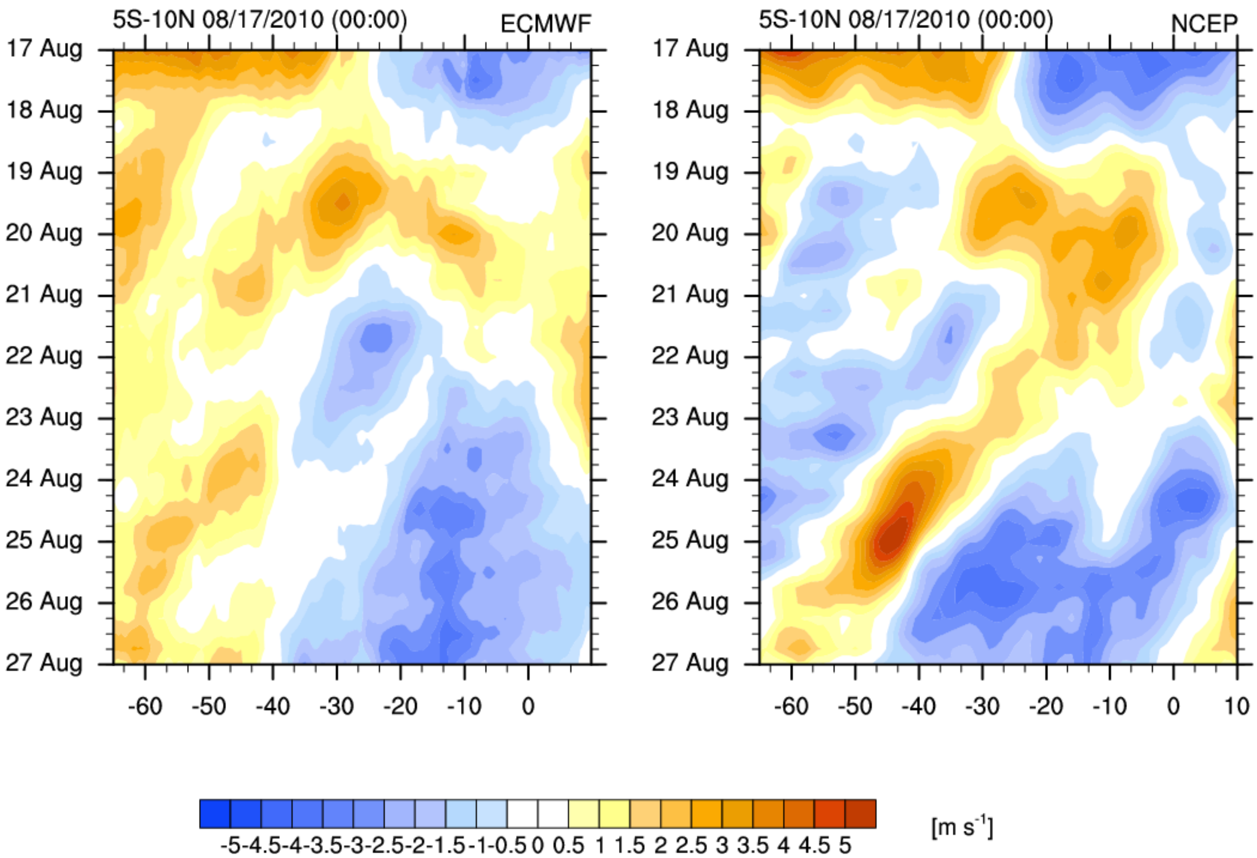

Fig. 5.13. Time-longitude plots of unfiltered 850 hPa zonal wind anomalies averaged over the 5°S-10ºN latitude band for August 17 – August 27. (Left) ECWMF control run forecast for the 00Z August 17 run; (Right) NCEP control run forecast for the 00Z August 17 run.

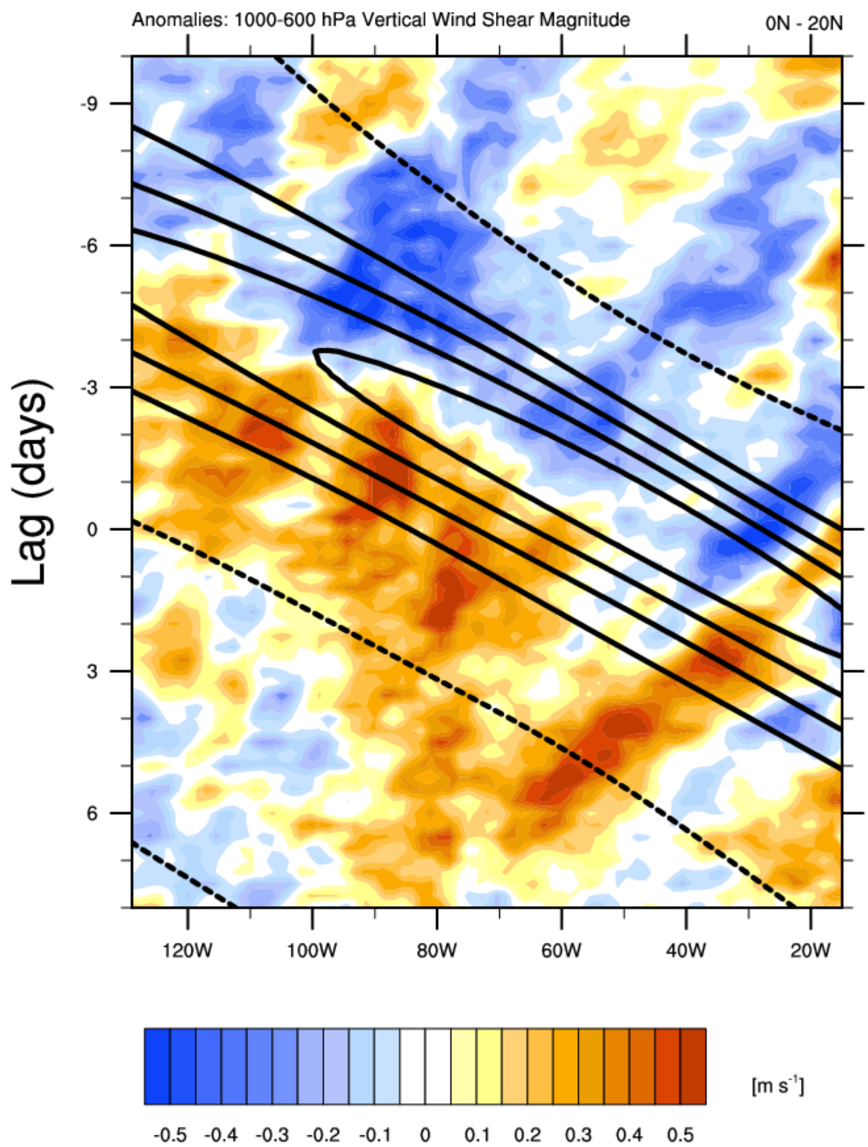

Fig. 5.14. Same as Fig. 5.12, but for 1000-600 hPa vertical wind shear magnitude anomalies.

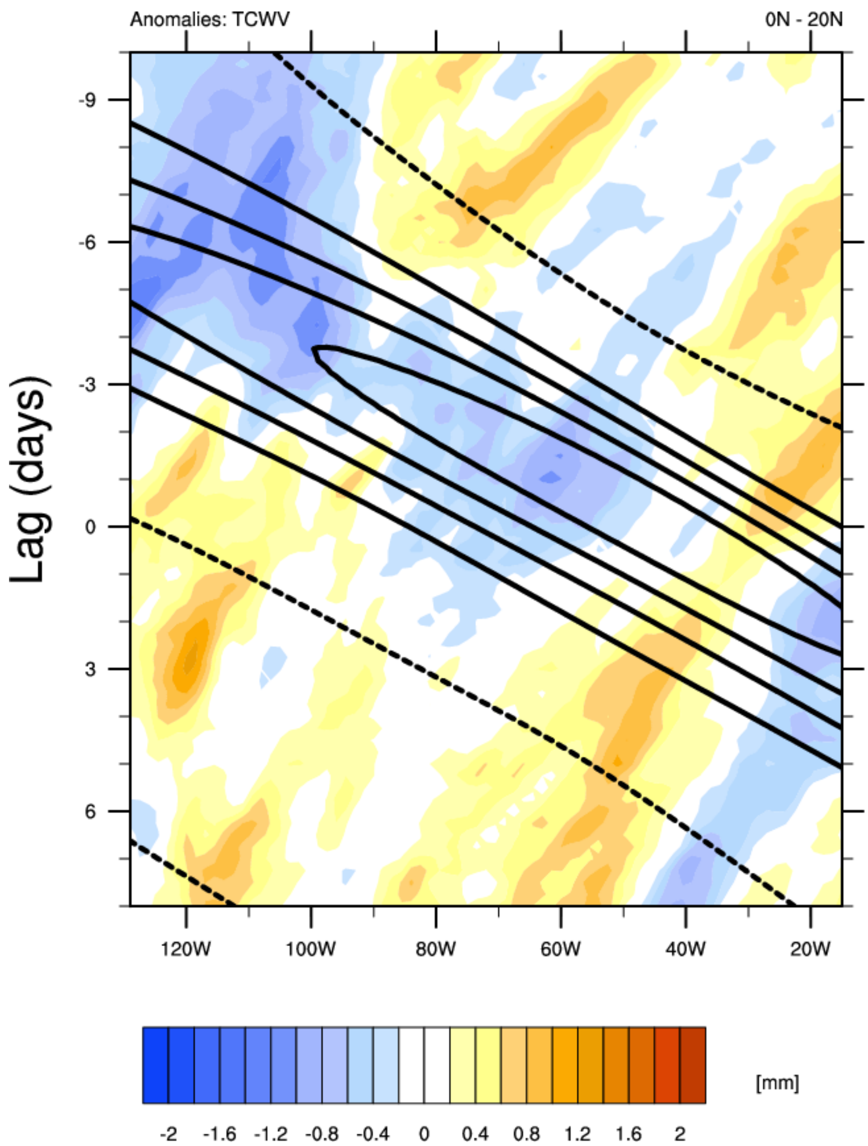

Fig. 5.15. Same as Fig. 5.12, but for total column water vapor anomalies.

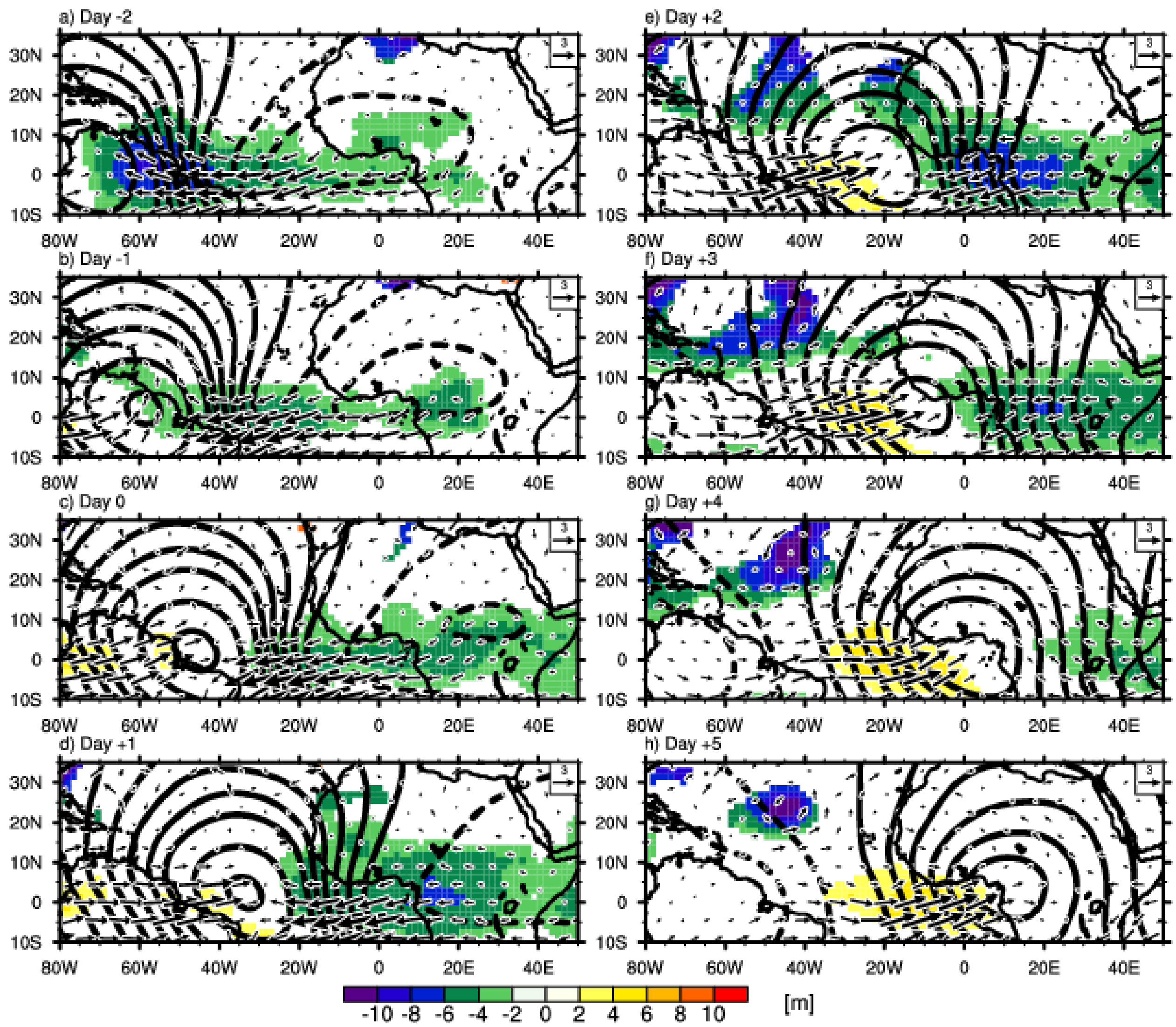

Fig. 5.16. Composite maps of 200 hPa geopotential height anomalies (shaded), 200 hPa wind anomalies (vectors), and Kelvin filtered VP200 anomalies (contoured; dashed if negative).

6. The Madden Julian Oscillation over the Western Hemisphere during boreal summer

6.1. Introduction

Over the tropical Atlantic and Africa, the fluctuations associated with the MJO are less well documented than for other tropical regions and our understanding of the MJO over the Western Hemisphere remains incomplete. Several studies have suggested that the influence of the MJO on sub-Saharan Africa is weak (e.g., Knutson and Weickmann 1987; Annamalai and Slingo 2001; Wheeler and Weickmann 2001; Roundy and Frank 2004) and others suggest no influence at all (e.g., Knutson et al. 1986; Murakami et al. 1986). These conclusions are sensitive to the variables analyzed, as well as the choice of diagnostic for the MJO. More knowledge about the MJO and its relative impacts on Western Hemisphere weather variability is needed.

The focus of this chapter is on the influence of the MJO on Western Hemisphere convection and circulation. Wheeler and Hendon's (2004) real-time multivariate MJO (RMM) PCs is used to identify the location and amplitude of the MJO. Further, the relationship between the MJO and Atlantic tropical cyclones is investigated. This section if focused on answering the following two questions: 1) How does AEW activity over Africa and the tropical Atlantic Ocean evolve with the MJO, 2) How is the MJO associated with the frequency and distribution of tropical cyclogenesis events over the tropical Atlantic Ocean? We might expect these questions to be related, such that increasing the frequency of AEW will result in more precursors for Atlantic tropical cyclones.

6.2. Datasets and Methodology

6.2.1. Wheeler and Hendon's Real-time Multivariate MJO indices

To identify the location and amplitude of the MJO, WH04's RMM indices are utilized. The indices are the PC time series of the two leading Empirical Orthogonal Functions (EOFs) of combined daily mean tropical (averaged 15°N-15°S) 850 and 250 hPa zonal wind and OLR anomalies. The seasonal cycle and a portion of the low-frequency variability associated with El Niño Southern Oscillation (ENSO) are removed before calculating the EOF. The indices, RMM1 and RMM2, were constructed to observe MJO events independent of seasonality constraints. RMM1 and RMM2 are approximately in quadrature and describe the average large-scale, eastward propagating convective and circulation anomalies associated with the MJO. The evolution of the MJO is visualized in a two-dimensional phase-space diagram, with RMM1 as the horizontal and RMM2 as the vertical Cartesian axes. The RMM indices are expressed as a selection of eight phases with each phase corresponding to a rough geographical location of the active convective phase of the MJO. RMM phase 1 consists of convection associated with the MJO over the western equatorial Indian Ocean, whereas RMM phase 8 represents the eastward propagation of the MJO signal over the Western Hemisphere.

6.2.2. Composite Analysis

Composites are constructed by averaging fields of data over each one of the eight RMM phases during JJASO (for 1989 – 2008). Data were averaged over the set of all dates for a particular phase when amplitudes were greater than one standard deviation. Anomalies for all composited fields were constructed as differences from the seasonal cycle. The seasonal cycles for all fields were constructed by using the annual cycle and its first four harmonics. Statistical significance testing was performed on all anomalies by bootstrap random resampling tests. These tests were applied by constructing a number of samples equal in size to the anomaly dataset, which is obtained by randomly drawing a new set of anomalies with replacement from the original dataset and binning the anomalies for each randomly drawn set. One thousand iterations were used for each test. We chose the year range to be consistent with the ECMWF-Interim analysis described below. Forty-two MJO events are subjectively analyzed in the RMM Indices. For clarification, the average time spent in each RMM phase is about 4-8 days.

Consistent with many previous studies, the convective signal of the MJO is highlighted by using the NOAA's daily averaged interpolated OLR dataset at 2.5˚ horizontal resolution from 1989 – 2008 (Liebmann and Smith 1996). Variations in the large-scale environment and AEW activity are explored using the ECMWF-Interim dataset at 1.5° horizontal resolution. Following Chapter 4, AEW activity is diagnosed by calculating the EKE based on 700 hPa ECMWF-Interim wind data that were filtered in a 2-10 day band. ECMWF-interim wind data were also used to calculate low-level vorticity and shear. TCWV data was used from the dataset to estimate atmospheric moisture.

An analysis of tropical cyclogenesis events was performed by binning the number of tropical cyclones that formed during each RMM phase (from 1974 – 2009, excluding 1978). We define a genesis event as a tropical cyclone that was at least classified as a tropical depression in the NCDC's IBTrACS v2 dataset (Knapp et al. 2010). We analyzed tropical cyclone development in a region similar to that of Maloney and Shaman (2008), concentrating on the east Atlantic ITCZ region between 60°W and the

Africa coast. This area received relatively little emphasis in the investigations of Mo (2000) and Maloney and Hartmann (2000), but it is a region that we expect to be strongly impacted by AEW variability (c.f. Hopsch et al. 2010).

6.3. The Influence of the MJO on the large-scale environment over West Africa

6.3.1. The MJO's convective signature

Figure 6.1 shows composites of OLR anomalies (shaded) and 200 hPa wind anomalies (vectors) for each of the eight RMM phases. Focus is first given to the convective nature of the MJO. While the strongest convective signatures associated with the MJO are observed over the Warm Pool regions, convection also appears to be modulated over the Western Hemisphere within the mean ITCZ during particular RMM phases. The convective signal associated with the MJO first appears over the western Atlantic in RMM phase 7. During this time, the convection in the position of the mean ITCZ is enhanced over the western Caribbean and the tropical western Atlantic. During RMM phase 8, negative OLR anomalies first develop over Africa and persist into phase 2. The strongest convective signal over tropical Africa occurs in phase 1, a time when convection begins to form over the equatorial Indian Ocean. Negative OLR anomalies extend further to the west over Africa during phase 2 and over the eastern tropical Atlantic during phase 3. A reduction of negative OLR anomalies is observed locally over western-central tropical African during phase 3. Therefore, Phases 8, 1, and 2 clearly represent the convectively active phase of the MJO over West Africa.

Focusing on the MJO's upper level circulation, a wavenumber one signature of upper-level divergence and convergence propagates eastward across the entire globe between RMM phase 1 and 8. Convection is enhanced locally with regards to where the upper-level flow is divergent and is suppressed where the upper-level flow is convergent for each RMM phase. Since convection and circulation varies coherently over Africa with respect to RMM phase, it is important to investigate how AEW activity varies over Africa and the tropical Atlantic Ocean. If AEW activity does coherently vary with the MJO, more frequent seedlings for tropical cyclones may also indirectly produce a relationship between Atlantic tropical cyclogenesis and the MJO. These principles are discussed further below.

6.3.2. The impact of the MJO on African easterly activity

Figure 6.2 shows composites of 700 hPa EKE anomalies for each RMM phases. EKE anomalies vary coherently through the different phases of the MJO, suggesting that the MJO modulates AEW activity. Phases 1-3 have large prominent regions of enhanced EKE with longitudinal extents greater than 30°. Positive EKE anomalies occur during phase 1 over interior tropical Africa (Fig. 6.2a). These positive EKE anomalies increase in magnitude and extend slightly to the west during phase 2 (Fig. 6.2b). During this phase, the strongest positive anomalies are located over sub-Saharan Africa. During phase 3, the strongest positive EKE anomalies shift poleward and extend westward over western tropical Africa (Fig. 6.2c). By RMM phase 4, the strongest positive EKE anomalies are only located over the eastern tropical Atlantic (Fig. 6.2d). During this time, negative EKE anomalies develop over eastern and central Africa, indicating a reduction of AEW activity. The transition from positive to negative EKE anomalies over West Africa continues through RMM phase 5 (Fig. 6.2e). Phases 6 and 7 have the most prominent regions of negative EKE anomalies over tropical Africa. Phase 8 consists of significant negative EKE anomalies over the coast of West Africa extending westward over the MDR. Therefore, positive EKE anomalies shift westward over Africa and the eastern tropical Atlantic during RMM phases 1-4, and negative EKE anomalies shift westward over Africa during RMM phases 6-8. It is interesting to note how these patterns compare to the two EOFs of EKE seen by Leroux et al. (2010). Their EOF1 is characterized by single-signed anomalies over West Africa and the tropical Atlantic somewhat similar to what we observe in Figure 6.2. This provides further evidence that the variability explored by Leroux et al. (2010) was likely dominated by the MJO.

Negative EKE anomalies occur together with the first convectively active phase of the MJO over West Africa (RMM phase 8). Positive EKE anomalies develop over tropical Africa one phase later (RMM phase 1). These positive EKE anomalies remain over West Africa through RMM phase 3. Convection first becomes more locally suppressed over Africa during RMM phase 3 yet positive EKE anomalies remain over West Africa. The EKE anomalies then swap to negative anomalies over tropical Africa one RMM phase later (RMM phase 4).

The MJO can excite AEW activity by two mechanisms (i) more intense convection which provides increased convective triggers and/or latent heat release for AEW growth and (ii) a more unstable AEJ (Leroux and Hall 2009). It was discussed that convective triggers lead periods of enhanced AEW activity in the previous paragraph. Leroux et al. (2010) also found a strong lead-lag asymmetry between convection and AEW activity. The convective signal was strongest two to five days prior to a period of enhanced AEW activity. This result is similar to the present study, in that enhanced convection leads enhanced AEW activity by one RMM phase. Leroux et al. (2010) also observed a westward moving OLR signal, a result which they suggest may arise from intraseasonal wave modes that have Rossby-wave structures or the westward propagation of clusters of AEWs. Furthermore, Leroux et al. (2010) explore the AEJ in relation to AEW activity and emphasized an acceleration of the AEJ entrance region prior to a period of enhanced AEW activity. The MJO – AEJ relationship is now explored using the RMM indices below.

6.3.3. The impact of the MJO on the African easterly jet

In order to explore the variation of the AEJ between the different RMM phases, we consider the zonal wind at 700 hPa (Fig. 6.3). Focus is first given to the evolution of the dynamical signal of the MJO in the 700 hPa wind field.

During RMM phase 1, significant westerly wind anomalies are observed equatorward of the AEJ core over West Africa and the eastern tropical Atlantic (Fig. 6.2a). These anomalous equatorward westerly winds are associated with the low-level westerly wind phase of the MJO. As convection over the Indian Ocean grows northward and eastward during RMM phase 2, the anomalous equatorial westerly winds shift eastward and grow in magnitude over equatorial Africa, consistent with the eastward progression of the MJO (Fig. 6.3b). These anomalous equatorial westerly winds continue to grow in magnitude and shift eastward during RMM phases 3 and 4 (Fig. 6.2c and 6.2d, respectively). Anomalous easterly wind anomalies form over the eastern tropical Atlantic during RMM phase 5 (Fig. 6.3e). These anomalous winds are associated with the low-level easterly wind phase of the MJO. The equatorial easterly wind anomalies grow in magnitude and extend eastward through RMM phase 8, consistent with the eastward progression of the MJO (Fig. 6.3f-h). In summary, a coherent eastward-progressing equatorial wind pattern is expressed, such that anomalous equatorial westerly winds occur over tropical Africa during RMM phases 1-5, followed by anomalous equatorial easterly winds during RMM phases 6-8.

Focus is now given to how the MJO could impact the AEJ. The modulation of the AEJ involves two contributions, with the first being the low-level equatorial wind structure of the MJO. This equatorial wind pattern will act to influence the horizontal shear of the jet on the equatorward side. The other contributor is local convection associated with the MJO over Africa. Anomalous convection equatorward of the jet generates PV near the level of the jet, which would act to strengthen the jet following the argument of Thorncroft and Blackburn (1999). Keeping these principles in mind, we begin our analysis when convection associated with the MJO is first observed over Africa during RMM phase 8.

During RMM phase 8, enhanced convection over Africa is observed along roughly 13°N (recall Fig. 6.1h). During this time, anomalous easterly winds are generally peaked equatorward of the AEJ and is suggestive of a southward shifted jet (Fig. 6.3h). Further during RMM phase 8, the AEJ is strongest in magnitude when compared to all RMM phases, highlighted by the large area of -9 ms^{-1} winds over West Africa, with the largest area of -10 ms^{-1} winds centered over 0°E. While the magnitude of the AEJ is strong, it does not necessarily mean that it is unstable for AEW growth. The equatorial easterly wind phase of the MJO, which has the greatest expression over Africa during RMM phase 8, reduces the meridional gradient of zonal wind there. This suggests that the AEJ is less unstable, which is consistent with low AEW activity (recall Fig. 6.2f-h). In support of this, the sign reversal in the meridional gradient of absolute vorticity is less negative than any other RMM phase (Fig. 6.4h). Therefore, even though phase 8 is associated with a stronger AEJ, which is generally expected to be more unstable, the impact of the low-level dynamical structure of the MJO supersedes this by weakening the horizontal shear.

During RMM phases 1 and 2, negative OLR anomalies are observed over Africa, north of 15°N (Fig. 6.1a, b). In addition, easterly wind anomalies are poleward of the AEJ core during these phases, indicating a northward shift of the AEJ. Further during RMM phase 2, easterly wind anomalies are observed within the vicinity of the AEJ entrance region, highlighting an eastward extension of the AEJ. To provide perspective, the -8 ms^{-1} wind contour extends to 18°E, roughly 5° further east than for any other RMM phase. This eastward extension of the AEJ occurs when easterly wind anomalies migrate northward from the Indian Ocean to over India, consistent with the observations of Leroux et al. (2010) (not shown). Equatorial westerly winds associated with the MJO form over Africa during RMM phase 1 and extend eastward during phase 2. This causes a tightening of the zonal wind gradient, and indicates a more unstable jet, expected to enhance AEW growth. Further, the sign reversal in absolute vorticity becomes more negative during RMM phase 1, and most negative during phase 2, indicating the jet is indeed more unstable at these times (Fig. 6.4a,b). Recall that during RMM phases 1 and 2, there are positive EKE anomalies over West Africa, indicating a period of increased AEW activity.

Recall that convection reduces over tropical West Africa during RMM phase 3 and is suppressed during RMM phases 4-7 (Fig. 6.1c). Westerly wind anomalies remain prominent equatorward of the AEJ during RMM phases 4 and 5, consistent with a more unstable AEJ (Fig. 6.4d, e). Yet during this time, AEW activity is anomalously low over much of tropical Africa and implies that an unstable jet, without the presence of convection, is not sufficient for a period of anomalous AEW activity (recall Fig. 6.2).

In summary, consistent with the convectively active phases of the MJO, the AEJ is enhanced during RMM phases 8, 1, and 2. The jet is strongest during RMM phase 8, however it less unstable and is located further south than RMM phases 1 and 2. RMM phase 8 is also consistent with anomalously low AEW activity over tropical Africa and especially over the MDR. The AEJ becomes more unstable during RMM phase 1, and most unstable during RMM phase 2. Further the AEJ is unstable during RMM phases 4 and 5, but convection is suppressed and AEW activity is anomalous low over Africa during this time. The enhancement of jet instability is related to increased horizontal shear by the low-level equatorial westerly wind phase of the MJO. Also during RMM phases 1 and 2, the AEJ is observed to shift northward when AEW activity is anomalously high. These results are consistent with Alaka and Maloney (2012), who find similar relationships between MJO phase and variability of the AEJ and AEW activity during boreal summer.

The results from this section suggest that sub-seasonal variability of AEW activity arises due to the MJO directly influencing convection over tropical Africa, as well as the characteristics of the AEJ. Our results are similar to Leroux et al. (2010) and confirm that most of their results are related to the MJO. We now explore the extent to which the variability in AEW activity has an influence on downstream tropical cyclone activity.

6.4. Tropical Cyclogenesis Analysis

Given that most Atlantic tropical cyclones form in association with AEWs over the tropical Atlantic we expect that the variability in AEW activity, highlighted in the previous section, will impact tropical cyclogenesis frequency. To evaluate this, we now explore and interpret the extent to which there is a coherent relationship between the RMM indices and tropical cyclogenesis inside the MDR. We define the MDR as the area between 5-25°N and 15-60°W. This analysis extends previous work on the same topic (e.g., Maloney and Shaman 2008; Klotzbach 2010) since in addition to considering variations in the large scale environment, we emphasize here the role of the AEW variability on tropical cyclogenesis over the MDR. We suggest that the MJO might modulate tropical cyclone activity via “weather-related impacts” through variability in AEWs (e.g., Hopsch et al. 2010) and an “environmental impact” through variability in large-scale parameters known to impact the probability of tropical cyclogenesis such as vertical shear and moisture (e.g., Roundy and Frank 2004; Aiyyer and Thorncroft 2010; Klotzbach 2010). We perform a simple count of the number of tropical cyclones that formed during each phase of the MJO to highlight which RMM phases favor tropical cyclone development (Fig. 6.5a). Confidence intervals for the total number of tropical cyclones for each RMM phase are assessed by bootstrap random resampling tests.

The distribution of tropical cyclogenesis events inside the MDR for each RMM phase when amplitudes are greater than 1σ is shown in Figure 6.5a. The result shows that tropical cyclone development inside the MDR occurs most during RMM phases 1, 2, and 5. The peak of tropical cyclone events in these RMM phases is statistically significantly different from the counts in RMM phases 7 and 8 at the 95% level. These results are somewhat consistent with Klotzbach (2010), who found RMM phases 1 and 2 were the most favorable RMM phases for tropical cyclone activity over the entire Atlantic Basin. He found when averaging RMM phases 1 and 2, large-scale atmospheric conditions were more favorable for developing tropical cyclones, e.g. reduced vertical wind shear and higher atmospheric moisture. However, he did not consider other individual RMM phases in his analysis.

A gradual downward trend of tropical cyclogenesis events occur during RMM phases 1-4. Intriguingly a second peak of tropical cyclogenesis events is revealed during RMM phase 5 with a more rapid decline in tropical cyclogenesis events during RMM phases 6-8. To assess if the tropical cyclogenesis counts are real and not manifested due to the varying number of dates that compose each composite, we divide the number of tropical cyclogenesis events by the number of MJO days (greater than 1σ) for each RMM phase (Fig. 6.5b). The results reveal that during RMM Phases 1, 2, and 5 a tropical cyclone is twice as likely to spawn inside the MDR when compared to RMM phase 8. However during RMM phase 3, a tropical cyclone is three times more likely to spawn inside the MDR when compared to RMM phase 8. Therefore the peaks in RMM phases 1, 2, and 5 are largely reduced due to the number of sampling days. An analysis of the large-scale environmental conditions is further needed to interpret the tropical cyclogenesis variability within the RMM indices which is provided below.

6.4.1. The influence of the MJO on the large-scale environment over the tropical Atlantic

To relate the tropical cyclone peaks to the well-known favorable parameters of tropical cyclogenesis, we first show 200-925 hPa vertical wind shear magnitude anomalies of the zonal wind over the MDR (Fig. 6.6). We interpret the reduction of vertical wind shear over the MDR by the location of strongest convection associated with the MJO.

During RMM phases 1-4, enhanced convection associated with the MJO progresses eastward and northward over the Indian Ocean. Upstream (to the west) of the deep convection over the Indian Ocean, anomalous upper level easterly winds form due to convective outflow, as well as a "Gill" like response (recall Fig. 6.1). This anomalous upper level convective outflow acts to reduce vertical wind shear over the MDR and increase vertical wind shear over the extreme eastern tropical Atlantic and Africa (Fig. 6.6a-d). Recall that the 925-200 hPa vertical wind shear is climatologically westerly over the western and central MDR, and is easterly over the extreme eastern tropical Atlantic and Africa (see Fig. 3.3). The opposite is true for RMM phases 5-8, showing significant positive vertical wind shear magnitude anomalies over the western and central MDR, with negative vertical wind shear magnitude anomalies over the extreme eastern tropical Atlantic and Africa (Fig. 6.6e-h). This vertical wind shear pattern occurs when deep convection associated with the MJO is located over the eastern Pacific. This location of MJO convection consists of dynamics similar to El Niño, and produces upper level westerly convective outflow over the MDR. These conditions are consistent with an enhancement of vertical wind shear over the western and central MDR. Therefore, the MJO modulates vertical wind shear over the MDR on intraseasonal timescales. A significant reduction of vertical wind shear over the western and central MDR is observed during RMM phases 1-4, with a significant enhancement during RMM phases 5-8.

Next, composites of TCWV anomalies are shown in Fig. 6.7 for each RMM phase. Significant positive TCWV anomalies, or an anomalously moist troposphere, develop over the MDR during RMM phase 1 (Fig. 6.7a). Positive TCWV anomalies over the MDR become more positive during phase 2, and are most positive in phase 3 (Fig. 6.7b-c). Positive TCWV anomalies during RMM phases 1-3 are all roughly north of 10°N over the MDR. A transition from positive to negative TCWV anomalies occurs during RMM phases 4 and 5. Significant negative TCWV anomalies then form over the MDR during RMM phase 6, become most negative in phase 7, and remain negative through phase 8 (Fig. 6.7f-h). Positive TCWV anomalies during RMM phases 5-8 are observed mostly south of 10°N, possibly hinting at a southward shift of the Atlantic ITCZ. Recall that there is low-AEW activity over Africa and the tropical Atlantic during these RMM phases (recall Fig. 6.3e-h). Therefore, the reduced moisture signal over the MDR could be also due to the reduced number of AEWs propagating off West Africa during this time.

Finally, low-level (925 hPa) relative vorticity is shown in Fig. 6.8 for each RMM phase. The low-level relative vorticity field is modulated by two contributions. The first contribution is the low-level wind structure of the MJO and the second being the location and intensity of local convection. During RMM phases 1-4, large regions of enhanced relative vorticity are observed over the MDR. This pattern is consistent observations of the MJO's convective and low-level westerly wind phase over the Warm Pool region (e.g., Schreck and Molinari 2011; MacRitchie and Roundy 2012). During RMM phase 1, scattered regions of significant positive relative vorticity anomalies are observed over the north-central MDR (Fig. 6.8a). Negative relative vorticity anomalies are equatorward of this. This pattern is more coherent during RMM phase 2 with stronger positive anomalies over the entire MDR (Fig. 6.8b). During RMM phase 3, the positive relative vorticity anomalies are oriented in a narrow-latitudinal band which seems to curve northward over the MDR (Fig. 6.8c). We hypothesize the anomalous low-level cyclonic relative vorticity is diabatically generated from enhanced convection over the MDR, which follows a similar pattern in structure (recall Fig. 6.1c). A narrow band of positive relative vorticity anomalies is later observed over the north-central MDR during RMM phase 4 with negative relative vorticity anomalies equatorward of it (Fig. 6.8d).

During the subsequent RMM phases 5-8, the low-level easterly wind phase of the MJO is located over the MDR. These phases are consistent with large areas of suppressed convection over the MDR. Mostly negative relative vorticity anomalies are observed over the MDR during this time with positive relative vorticity anomalies equatorward, indicative of a southward shifted AEW track (Fig. 6.8e-h). Therefore, the low-level vorticity field over the MDR varies coherently between the different RMM phases. This result is consistent with the low-level dynamical signal of the MJO and in situ convection over the MDR.

6.5. Conclusions

The MJO has been shown to modulate convection and the large-scale environment over tropical Africa and the Atlantic during boreal summer. The results presented in this chapter suggest that the MJO directly influences AEW activity. The MJO influences AEW activity by enhancing or suppressing convection locally over Africa, as well as altering the characteristics of the AEJ. This change in AEW activity, along with MJO induced modulations of large-scale environmental parameters including vertical wind shear, low-level relative vorticity, and moisture, is consistent with coherent variability in tropical cyclogenesis activity over the MDR.

Figure 6.9 represents a conceptual schematic of the Wheeler and Hendon RMM phase space separating RMM phases associated with the enhancement of the AEJ, the convectively active RMM phases, RMM phases associated with enhanced AEW activity, and RMM phases associated with enhanced MDR tropical cyclone activity. Convection associated with the MJO develops over tropical Africa during a time when the AEJ is strongest in magnitude, yet less unstable. Enhanced AEW activity over Africa tends to develop locally after a period of enhanced convection. Enhanced MDR tropical cyclogenesis activity occurs during a time when AEW activity is high over tropical West Africa.

The convective signal of the MJO over Africa is not as large as the signal over the Indian and Pacific Oceans. Distinct phases of the MJO are associated with either enhanced or suppressed convection over Africa. Convection first becomes active over Africa during RMM phase 8, and becomes most enhanced during RMM phases 1 and 2. During RMM phase 3, convection becomes suppressed over tropical Africa, yet is enhanced over the tropical Atlantic. A westward movement of enhanced convection is observed over West Africa during RMM phases 1-3. The following RMM phases 4-7 consist of suppressed convection over sub-Saharan and equatorial Africa.

AEW activity over West Africa is enhanced during RMM phases 1-3. Positive EKE anomalies move westward over Africa and the tropical Atlantic during RMM phases 1-4. The period of anomalously high AEW activity during RMM phase 1, and especially during RMM phase 2, is associated with a more unstable and northward shifted AEJ. Further, during RMM phase 2 the AEJ extends further eastward than in any other RMM phase. During RMM phase 4, convection and AEW activity over tropical Africa becomes locally suppressed. These negative EKE anomalies extend westward and amplify during the subsequent RMM phases 5-8. While RMM phases 4 and 5 are associated with a more unstable jet, AEW activity is anomalously low due to convection being locally suppressed by the MJO.

Tropical cyclones develop more frequently during certain RMM phases when compared to others. Klotzbach (2010) found RMM phases 1 and 2 to contain the highest frequency of tropical cyclogenesis over the Atlantic. He also found that these phases contained statistically significant differences (to RMM phases 6 and 7) in the large-scale environment, in reference to significant reductions in vertical wind shear, anomalously high moisture, and enhanced low-level cyclonic relative vorticity. Our results are consistent with the observations of Klotzbach (2010), however in addition we find that enhanced tropical cyclogenesis activity during RMM phase 3. In addition, RMM phases 1-3 are associated with a period of anomalously high AEW activity (recall Fig. 6.2a-c). Therefore, this period of enhanced tropical cyclone activity in the MDR entails a period of enhanced AEW activity, or more frequent/stronger seedlings.

We hypothesize that the suppressed tropical cyclone activity during phases 7 and 8 results in part from reduced AEW activity over tropical West Africa and the eastern tropical Atlantic. AEWs that are either less frequent and/or weaker might reduce the frequency of tropical cyclogenesis. Furthermore over the MDR, these phases contain enhanced vertical wind shear, significant areas of negative low-level vorticity anomalies, and very dry atmospheric conditions, all of which are unfavorable conditions for tropical cyclogenesis.

The distribution of tropical cyclogenesis events during RMM phases 1-3 and phases 7-8 evolves together with AEW activity over Africa. When EKE values are anomalously high over both West Africa and the MDR (RMM phases 1-3), tropical cyclogenesis events are high inside the MDR. The opposite is true during RMM phases 7-8. This relationship highlights the potential influence of the MJO on upstream AEW activity and the development of tropical cyclones inside the MDR.

Accurately positioning a true MJO signal would likely lead to much needed, better quality forecasts on longer timescales for African weather. Better understanding of the association between the MJO and AEWs will help African forecasters to more precisely predict periods of wetness or dryness over Africa on weekly timescales. For instance, Matthews (2004) suggests that the JET2000 field experiment (Thorncroft et al. 2003) failed to observe “strong” AEWs probably because it was scheduled during an anomalously strong convectively suppressed RMM phase over Africa (Phase 5, amplitude greater than 2σ). The results shown in this chapter suggest that if this field experiment had occurred during RMM phases 1-3 rather than RMM phases 5-6, there would have been a higher likelihood to observe strong AEWs over Africa.

6.6. Figures

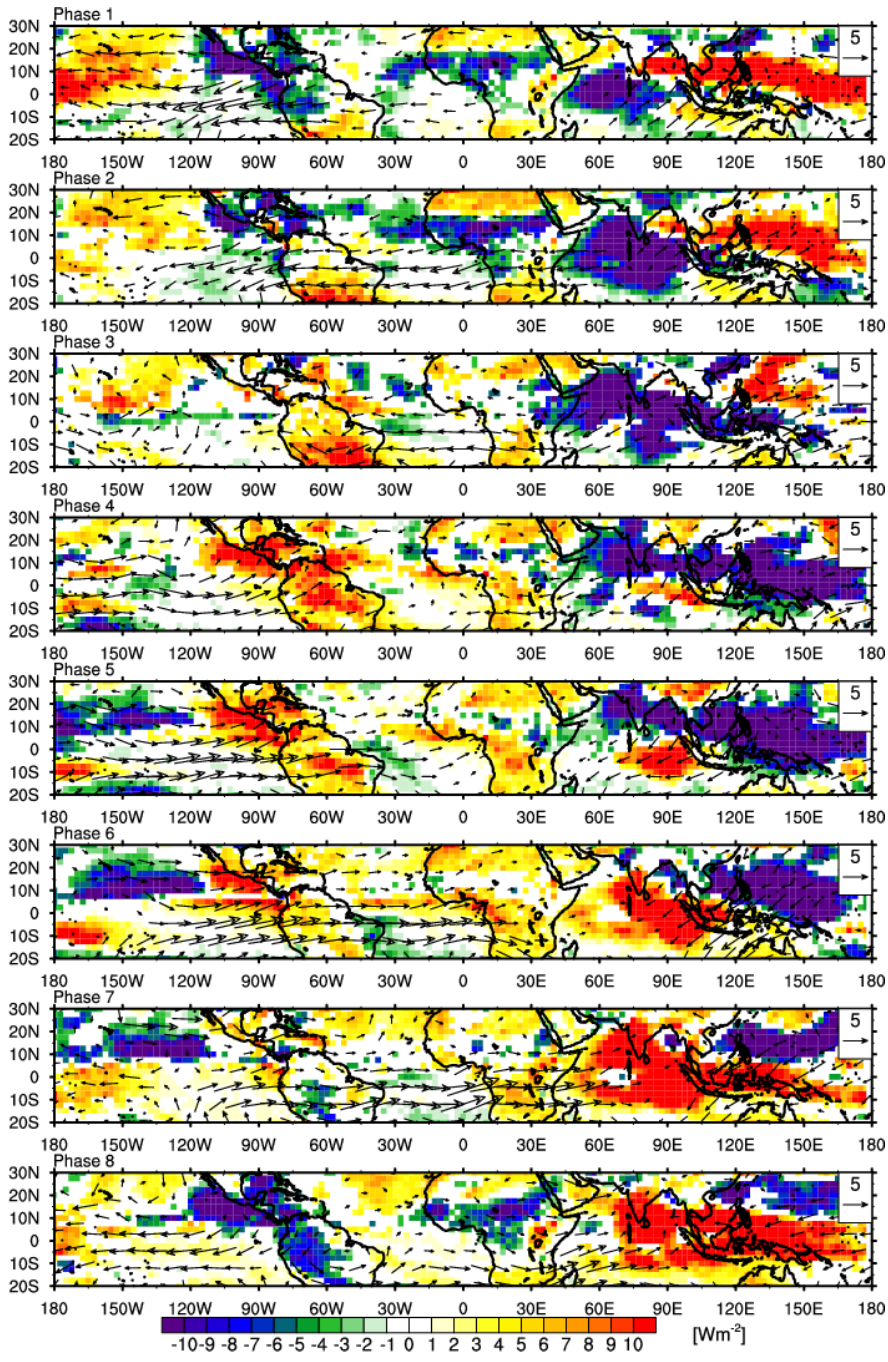

Fig. 6.1. NOAA daily averaged interpolated OLR anomalies for the Northern Hemisphere summer months (June-September) from 1989-2009 for each real-time multivariate MJO phase. Anomalies statistically significantly different than zero at the 95% level are only shaded. 200 hPa wind anomalies are represented as vectors.

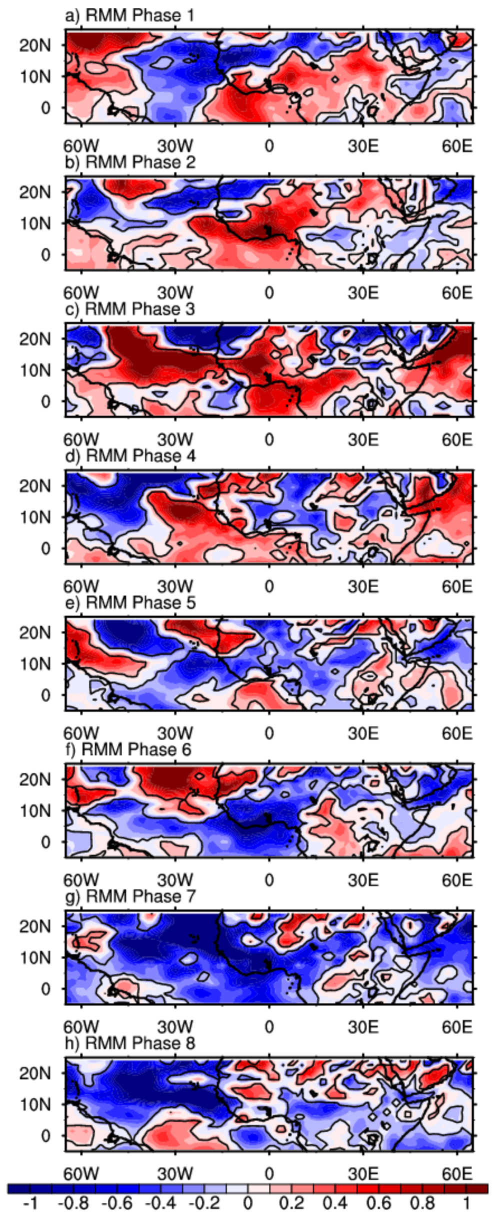

Fig. 6.2. 2-10 day filtered EKE analysis at 700 hPa for each RMM phase. Anomalies statistically significantly different than zero at the 95% level are within the solid black contour. Red shading represents increased AEW activity, where blue shading represents reduced AEW activity. Shaded units are in m^2s^{-2}; shade interval is 0.1 m^2s^{-2}.

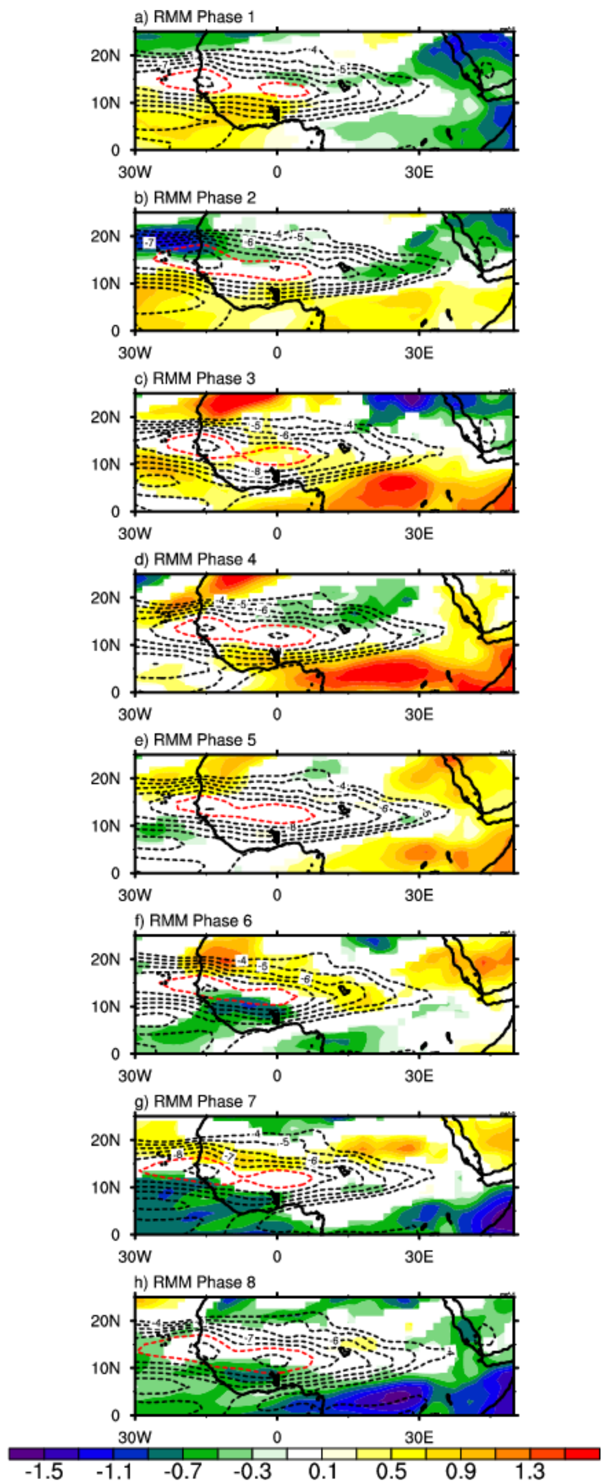

Fig. 6.3. 700 hPa zonal wind anomalies for each RMM phase. Anomalies statistically significantly different than zero at the 95% level are shaded. Shaded units are in ms^{-1}; shade interval is 0.2 ms^{-1}. Total raw easterly zonal wind is composited for each RMM phase and contoured. Contour units are in ms^{-1}; contour range is from -10 to -4 ms^{-1}; contour interval is 1 ms^{-1}. Negative contours are dashed. Red dashed contour highlights the -9 ms^{-1}contour.

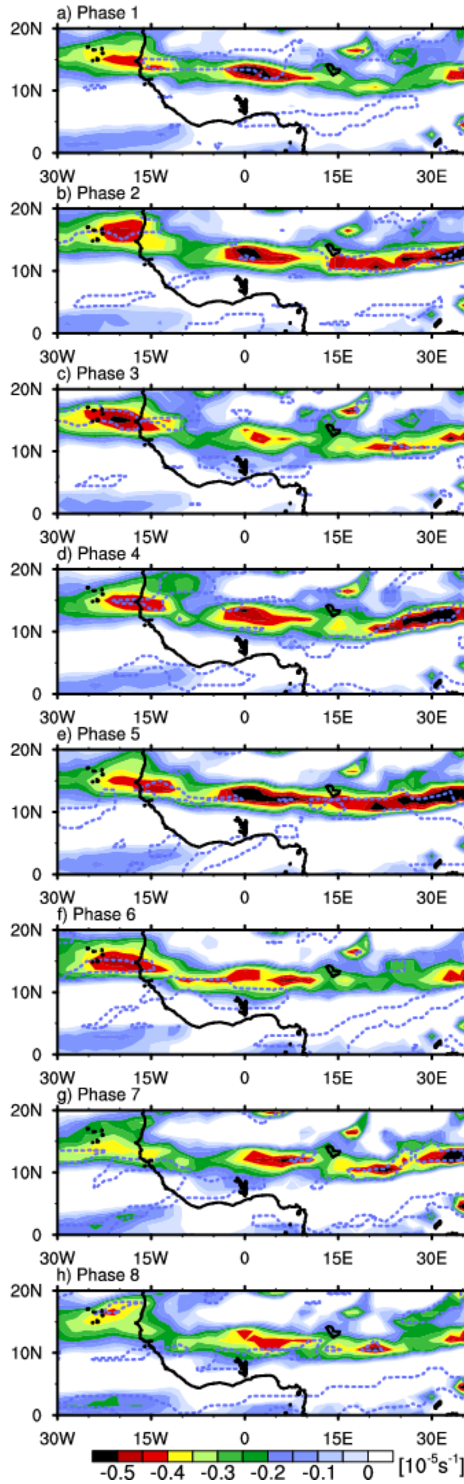

Fig. 6.4. The raw negative meridional gradient of absolute vorticity (shaded) averaged over each RMM phase. Negative anomalies of the meridional gradient of absolute vorticity that are statistically different than zero at the 95% level are represented by the blue-dashed contours. Shade interval is 0.05 $10^{-5}s^{-1}$.

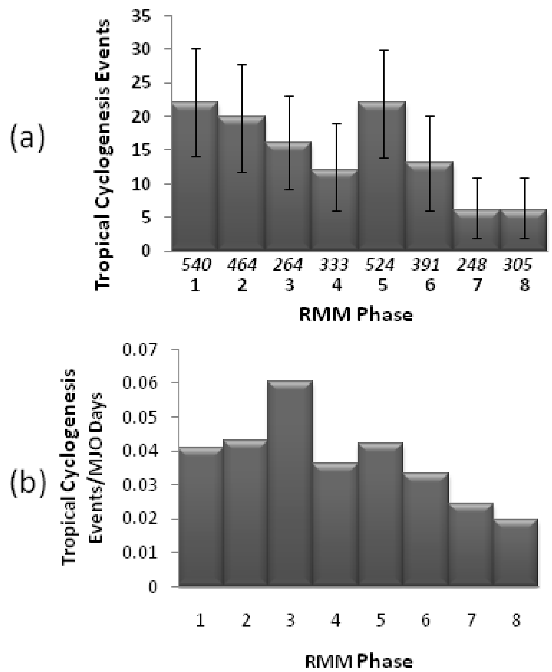

Fig. 6.5. (a) Tropical cyclogenesis JJASO climatology (1974-2009) for each RMM phase for tropical cyclones formed only within the MDR. The number of MJO days for each composite is placed above each RMM phase number. Error bars indicate the 95% confidence interval. (b) Same as (a) however normalized by the number of MJO days for each RMM phase.

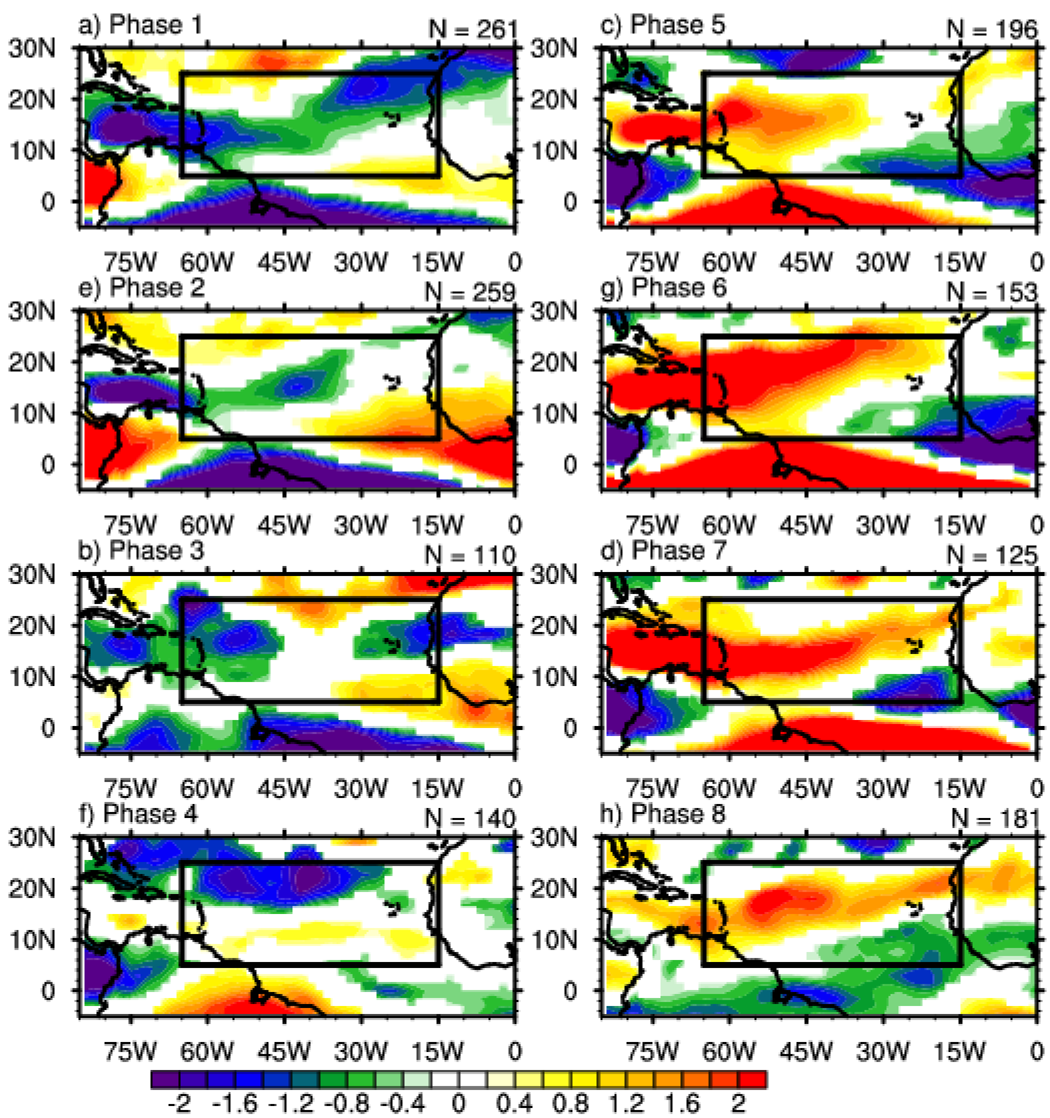

Fig. 6.6. Mean absolute value 200-925 hPa zonal vertical wind shear anomalies for each RMM phase. Anomalies statistically significantly different than zero at the 90% are only shaded. The black box represents the MDR. Shaded units are in ms^{-1}; shade interval is $0.5\ ms^{-1}$.

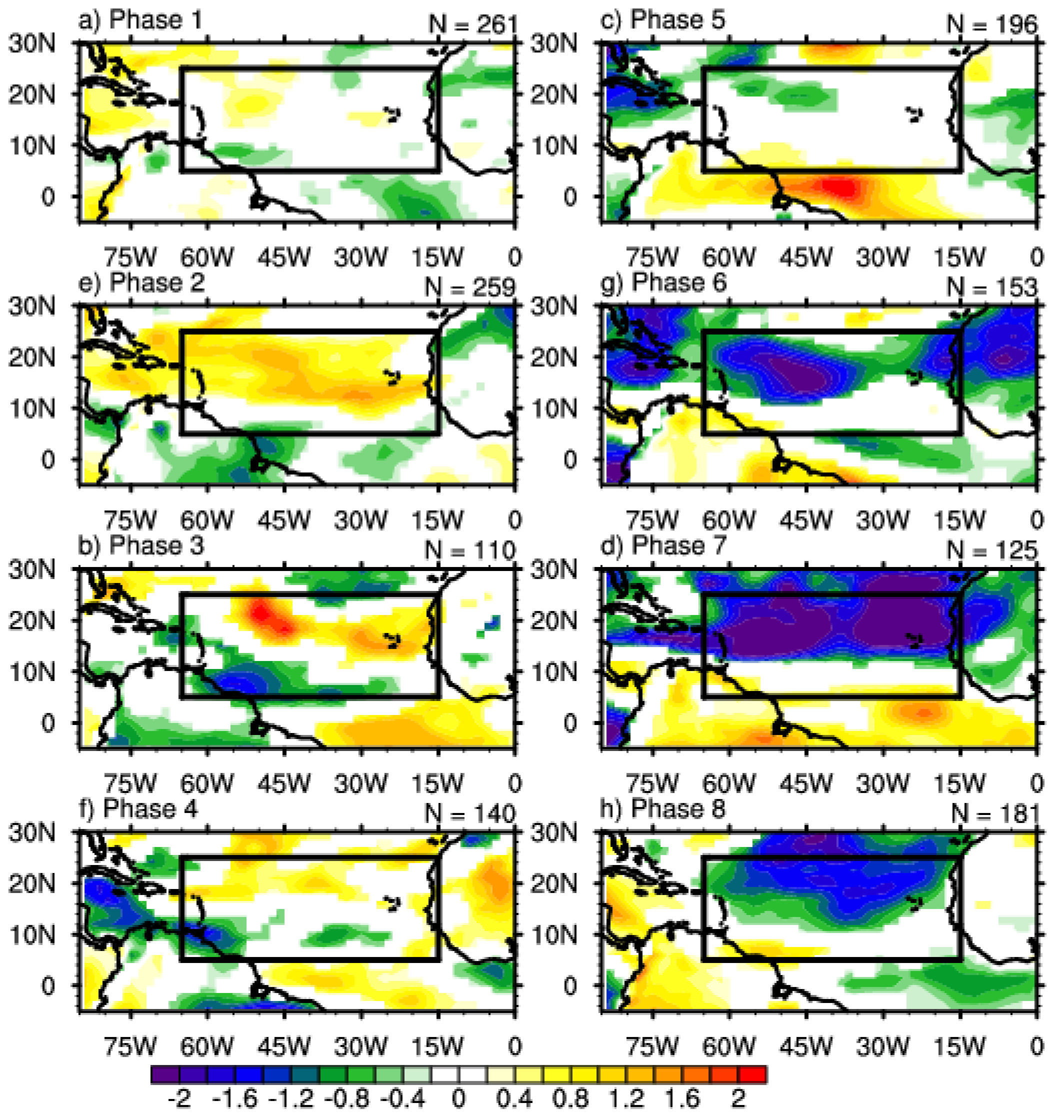

Fig. 6.7. Total column water vapor anomalies for each RMM phase. Anomalies statistically significantly different than zero at the 90% level are only shaded. The black box represents the MDR. Shaded units are in mm; shade interval is 0.2 mm.

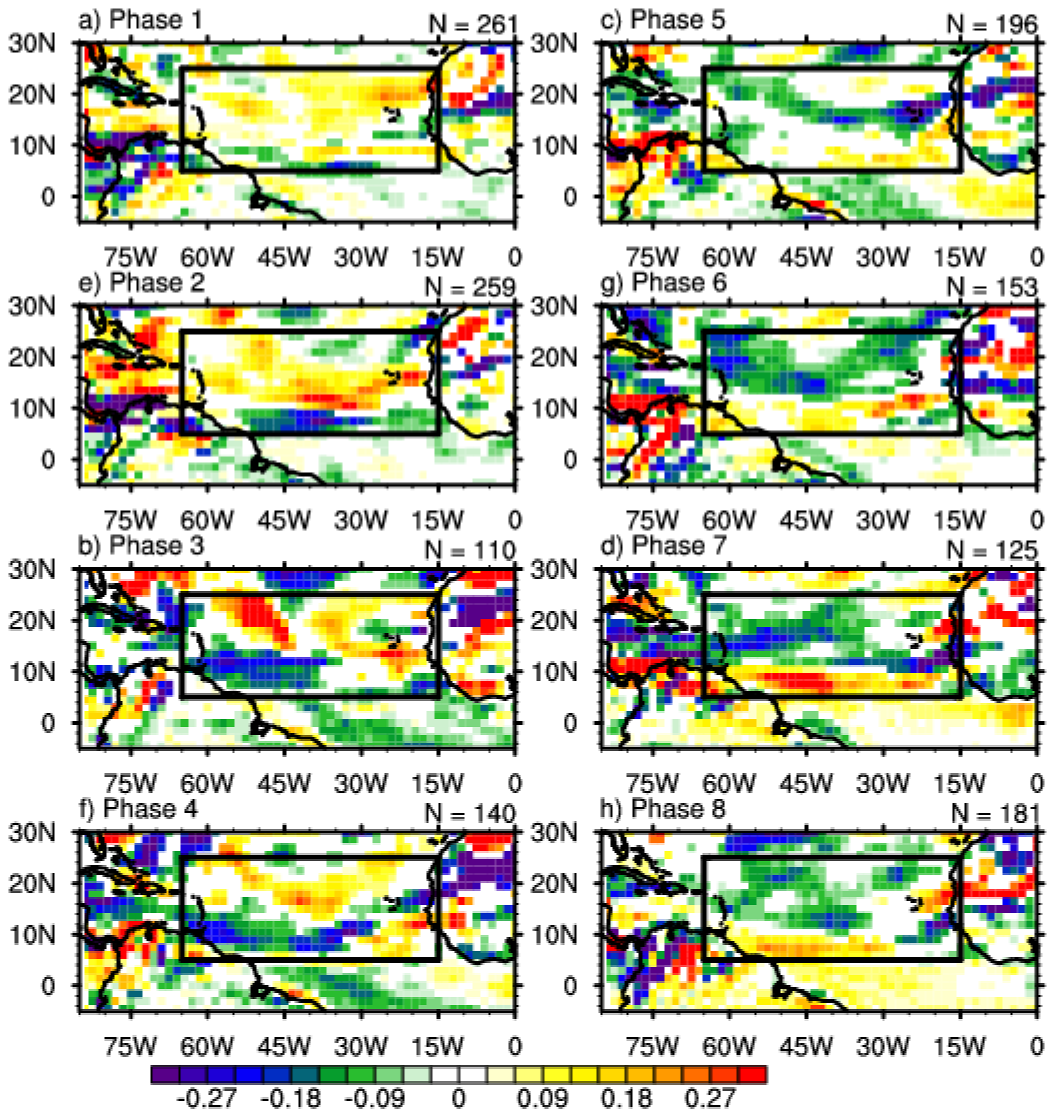

Fig. 6.8. 925 hPa relative vorticity anomalies for each RMM phase. Anomalies statistically significantly different than zero at the 90% level are only shaded. The black box represents the MDR. Shaded units are in 10^{-5} s^{-1}; shade interval is 0.03 x 10^{-5} s^{-1}.

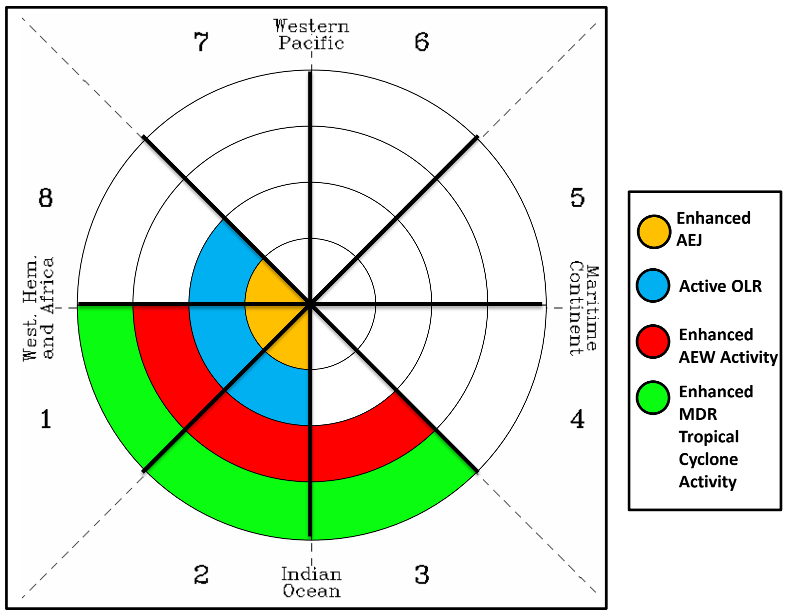

Fig. 6.9. A schematic RMM phase diagram. The orange shading represents an acceleration of the AEJ. The blue shading represents the convectively active RMM phases over Africa. The red shading represents the RMM phases associated with enhanced AEW activity over Africa. The green shading represents the RMM phases that are associated with enhanced tropical cyclone activity over the MDR. *Note: there are no MJO amplitude implications with this figure.*

7. Conclusions and Prospective Research

This dissertation has addressed the impact of CCKWs on Western Hemisphere tropical weather variability and Atlantic tropical cyclogenesis frequency. Strong boreal summer CCKWs have been shown to affect the large-scale environment over the northern tropical Atlantic that favors tropical cyclogenesis. The strongest CCKWs are found to be collocated with the convectively active phase of the MJO. This CCKW-MJO relationship highlights potential for medium-to-long range predictability of Atlantic tropical cyclone activity.

7.1. Convectively coupled Kelvin waves and their role in Atlantic tropical cyclogenesis

Convection over the northern tropical Atlantic is influenced by CCKW passages during boreal summer. On average, CCKWs propagate eastward across the tropical Atlantic with a mean phase speed of approximately 15 ms^{-1}. The convectively active phase of the CCKW enhances convection north of the equator, within the mean latitude of the ITCZ. In contrast to the shallow-derived Kelvin wave (Matsuno 1966), observed CCKWs over the tropical Atlantic have non-negligible meridional wind component, consistent with the observations of CCKWs over the East Pacific (e.g., Straub 2002). More specifically, composite analysis shows that when the convectively active phase of the CCKW is located over the tropical Atlantic, an upper-level anticyclonic circulation is collocated with it and can be interpreted as a response to increased diabatic heating.

The relationship between CCKW passages and Atlantic tropical cyclogenesis is as follows. Tropical cyclogenesis is found less frequent just prior to the passage of the convectively active phase of the CCKW, within the leading convectively suppressed phase. Genesis becomes more frequent during the passage of the convectively active phase of the CCKW, but is most frequent two days after its passage. CCKWs can influence the development of a tropical cyclone over the Atlantic via two ways. The first and most common way is by directly enhancing westward propagating AEWs over the tropical Atlantic. When superimposed with the convectively active phase of the CCKW, the AEW is in an environment that favors deep convection and wave growth. The case study of the genesis of Tropical Storm Debby (2006) was shown to illustrate the direct enhancement of a weak AEW at the coast of West Africa by the convectively active phase of a CCKW. Tropical Storm Debby quickly developed into a tropical cyclone while superimposed with the convectively active phase of the CCKW over the eastern tropical Atlantic.

CCKWs can also influence Atlantic tropical cyclogenesis without the presence of a precursor westward propagating AEW. The convectively active phase of the CCKW initiates convection and generates low-level cyclonic relative vorticity (at the latitude of the mean ITCZ). Griffin (2012) showed the precursor to Hurricane Karl (2010) was not related to an incipient AEW. He found that the precursor to Karl developed during the passage of the convectively active phase of a CCKW over the western tropical Atlantic. This type of CCKW-related tropical cyclogenesis is also discussed by Schreck and Molinari (2010) over the West Pacific.

i. Future Work

An important aspect about Kelvin filtering that was not addressed in this dissertation is the choice of wavenumbers, period, and equivalent depths. While the results from this dissertation were based on a CCKW-index following the Kelvin filtering methodology of Wheeler and Kiladis (1999), it by no means is a perfect fit for CCKWs. CCKWs over the Eastern Hemisphere will have different propagation speeds, periods, and equivalent depths to those over the Western Hemisphere. Therefore when filtering data for CCKWs, it might be more appropriate to select a different set of wavenumbers, period, and equivalent depth depending on the geographical area of interest (see Roundy 2012a,b). In addition, OLR or rainfall might not be the best field to filter for CCKWs over the Western Hemisphere. Since boreal summer CCKWs over the Atlantic have a strong upper-level wind signature, filtering upper-level winds or velocity potential might isolate CCKWs better than a convection-related field. This concept should be explored in future work and compared to the results presented in this dissertation.

Future research into how NWP models represent CCKWs is also needed. Models that rely on convective parameterization often struggle with accurately representing eastward propagating convectively coupled disturbances such as CCKWs. Therefore, there are times where models might predict periods of increased or reduced Atlantic tropical cyclone activity as a result of not propagating a particular phase of a CCKW eastward. These might be times when model forecast skill drops. By not accurately representing eastward propagating convective disturbances in the tropics, downstream extra-tropical pattern forecasts might also be less accurate and deserves consideration.

7.2. The impact of convectively coupled Kelvin waves on the large-scale environment over the tropical Atlantic

In addition to the direct enhancement of convection over the tropical Atlantic, CCKWs can also impact the large-scale environment that favors tropical cyclogenesis. To illustrate this, composites of 850-200 hPa vertical wind shear, TCWV, and low-level

(925 hpa) relative vorticity were shown. In order to understand how CCKWs modulate deep-layer vertical wind shear over the Atlantic, it is important to understand the climatological vertical wind shear state over the Atlantic during boreal summer. Climatologically, westerly vertical wind shear exists over the western tropical Atlantic and easterly vertical wind shear exists over the eastern tropical Atlantic. The easterly vertical wind shear is composed from the overturning circulation of the WAM. Therefore, the deep-layer vertical wind shear over the western tropical Atlantic will be affected oppositely to that over the eastern tropical Atlantic during the passage of CCKWs. Kelvin-induced westerly shear exists to the east of the convectively active phase of the CCKW, and easterly shear to its west. Therefore, Kelvin-induced westerly shear increases the background westerly shear over the western tropical Atlantic, and reduces the background easterly shear over the eastern Atlantic. The opposite is true for the Kelvin-induced easterly sheared phase.

CCKWs can also impact large-scale moisture and low-level vorticity fields over the tropical Atlantic. Composite analysis showed that positive TCWV anomalies are collocated with the convectively active phase of the CCKW and progress eastward with it. Further, low-level cyclonic relative vorticity develops over the tropical north Atlantic during the passage of the convectively active phase of the CCKW. This cyclonic relative vorticity then progresses back to the west and is a component of a train of AEWs that develops after the passage of the convectively active phase of the CCKW.

i. Future Work

A westward progressing area of anomalous dry air was shown in the CCKW-TCWV anomaly composite (recall Fig. 3.6). This signature was assumed to be associated with a Saharan air layer outbreak and suggests that these events could be predicted at intraseasonal time scales knowing the particular location of a CCKW. However, it is unclear why a SAL outbreak is related to a CCKW passing over the tropical Atlantic. This concept needs to be explored in greater detail in future work. Hypotheses of why SAL outbreaks are linked to CCKW passages are as follows. When the convectively active phase of the CCKW is located over the tropical Atlantic, it's convectively suppressed phase is located at the coast of West Africa. Enhanced low-level trades are associated with the convectively suppressed phase of the CCKW and might encourage the transport of dusty dry air from the Sahara. Another hypothesis and preliminary work not shown suggests that there could be complex interactions occurring between the CCKW, extra-tropical circulation, and the Saharan heat low. Intraseasonal variability of the Saharan heat low has been documented by Chauvin et al. (2010) and can highly influence agriculture in parts of West Africa. Therefore, knowing whether a CCKW passage could affect the heat low is extremely important for those residing in West Africa.

7.3. Convectively Coupled Kelvin waves and African easterly wave activity

CCKWs may "trigger" AEWs as follows. Near elevated topography in West Africa, convection first initiates in an environment characterized by increased low-level easterly vertical wind shear generated by the CCKW. The region relative to the CCKW that is favorable for "triggering" convection is where the low-level zonal wind convergence is greatest, or in between the leading convectively suppressed phase and active phase of the CCKW. Further, large-scale, slow upward motion associated with the CCKW is coincident with easterly winds at nearly all heights, implying that shallow convection can be initiated well to the east of the convergent region in the low-level easterlies. As this shallow convection deepens to congestus stages, it moistens the environment, setting the stage for deeper convection. This convection then propagates back towards the west and grows within the convectively active phase of the CCKW. In addition to generating vertical wind shear, the convectively active phase of the CCKW is associated with westerly wind anomalies at the level of AEJ. These westerly wind anomalies are peaked near the equator, therefore increasing the horizontal wind shear on the equatorward side of the AEJ. Through the combined affect from the increased horizontal shear and increased convection, the AEJ becomes more unstable.

Climatologically, AEW activity is found to increase after the passage of the convectively active phase of the CCKW over the Guinea Highlands region and during its passage over the Darfur and Ethiopian Highlands. Due to the increased frequency of AEWs after the passage of the convectively active phase of the CCKW, there will be more frequent seedlings for downstream tropical cyclogenesis. This relationship might partially explain why tropical cyclogenesis is most favorable after, not during the passage of the convectively active phase of the CCKW.

i. Future Work

An issue that needs to be addressed in future work relates to the eastward extension of the AEJ over the eastern African highlands, which occurs during the passage of the convectively suppressed phase of the CCKW. Could this eastward extension be sufficient enough for AEW genesis even though there is local suppression forced by the

CCKW? A second, more general question regarding the impact of CCKWs on the AEJ is could the sub-weekly period that the AEJ becomes more unstable in association with the passage of the convectively active phase of the CCKW be long enough to aid in an extended period of enhanced AEW activity? Or does the common phasing with a lower frequency mode, such as the MJO become important to consider (e.g., Ventrice et al. 2011, 2012b)? Such questions should be further studied using observations and models to better understand the variability of AEWs in support of operational forecasting at daily to intraseasonal timescales.

7.4. Convectively coupled Kelvin waves and tropical cyclone intensity

Preliminary evidence shown in this dissertation suggests that the convectively suppressed phase of CCKWs might negatively affect the intensity of tropical cyclones. The convectively suppressed phase of a CCKW, identified in the VP200 field, was shown to superimpose with Hurricane Danielle and Tropical Storm Earl (2010) during times when both tropical cyclones were predicted to intensify. During this superposition, Danielle weakened and Earl remained a tropical storm. It wasn't until Danielle recurved poleward north of 20ºN, and when Earl propagated westward enough to no longer be superimposed with the convectively suppressed phase of the CCKW, that both tropical cyclones intensified. During the passage of the convectively suppressed phase of the CCKW, the large-scale environment dried and 1000-600 hPa vertical wind shear increased.

A climatology of the convectively suppressed phase of all CCKWs identified within the VP200 field was used to show the large-scale impact over the tropical Atlantic. The convectively suppressed phase of the CCKW is associated with enhanced low-level easterly flow, anomalously dry air, and large-scale subsidence. Further, 1000-600 hPa vertical wind shear increases after its passage. This increased vertical wind shear is consistent with the development of a TUTT, which forms during the passage of the upper-level westerly wind phase of the CCKW. The TUTT signature is indicative of the relative importance of CCKWs on the extratropical circulation, or vice versa.

i. Future Work

A climatological analysis of all CCKWs passages during the time when Atlantic tropical cyclones were present in the 5°N-25°N latitude band is needed. For this analysis, it is recommended to identify CCKWs in VP200 and not OLR. This is due to CCKWs having a stronger VP200 signature over the Atlantic with respect to OLR. Further, VP200 is an extremely smoothed field due to its inverse Laplacian operator. Therefore, it is plausible that tropical cyclones will project less onto VP200 than OLR. These ideas deserve further insight and the results will be useful for identifying CCKW-tropical cyclone relationships.

Preliminary work (not shown) suggests a relatively minimal relationship between the timing of rapid intensification of Atlantic tropical cyclones and a particular phase of CCKWs. Therefore, the relationship might exist in the context of the lack of intensification, or even brief weakening of the tropical cyclone within the vicinity of the convectively suppressed phase of the CCKW. The lack of intensification of a mature tropical cyclone during the passage of the convectively suppressed phase of a CCKW is difficult to prove quantitatively. Testing a Kelvin filtered VP200 index in SHIPS might provide additional information for tropical cyclone intensity forecasts. Since CCKWs propagate towards the east, knowing that a particular phase of a CCKW is located over the East Pacific at a particular time could provide as a predictor for tropical cyclone intensity change at a later time.

A TUTT was shown to develop during the passage of the upper-level westerly wind phase of the CCKW. Composites of total 200 hPa zonal winds show there is a swap from mean equatorial easterly winds to mean equatorial westerly winds after the passage of the convectively suppressed phase of the CCKW (not shown). Is this TUTT a result of the formation of a westerly wind duct in the equatorial Atlantic? More generally, are CCKWs synoptic disturbances that could manifest a westerly wind duct near the equator? Or is the TUTT a result from extra-tropical wave-breaking that commonly occurs during CCKW passages over the East Pacific and or Atlantic? Further, does the CCKW-TUTT relationship change depending on the season and or location? The answers to these questions could help bridge tropical extra-tropical interactions with regards to CCKWs and extra-tropical circulation.

7.5. The Madden Julian Oscillation over the Western Hemisphere

Using WH04's RMM PCs, the impact of the MJO on Western Hemisphere tropical weather variability was shown. Convection first develops over West Africa during RMM phases 8, 1, and 2. This is a time when convection associated with the MJO develops and propagates northward over the Indian Ocean. Convection becomes suppressed over West Africa during RMM phase 4, and remains suppressed through RMM phase 7.

In addition to convection, AEW activity was shown to vary coherently with the MJO. AEW activity is anomalously active over West Africa during RMM phases 1-3, and is suppressed during RMM phases 5-8. Therefore, increased African convection, associated with the convectively active phase of the MJO, precedes a period of increased AEW activity by roughly one RMM phase, consistent with the idea of convective triggering of AEWs proposed by Thorncroft et al. (2008). The AEJ was also found to vary coherently with the phase of the MJO. The AEJ was found to be more unstable during RMM phases 1-5, and less unstable during RMM phases 6-8. RMM phases 1-5 consists of a one-to-two week period when 700 hPa equatorial westerly wind anomalies associated with the MJO are located over West Africa and increases horizontal shear on the equatorward side of the AEJ. In contrast, RMM phases 6-8 are consistent with 700 hPa equatorial easterly wind anomalies associated with the MJO are located over West Africa and reduces the horizontal shear on the equatorward side of the AEJ.

Since AEW activity varies coherently with the MJO, it was proposed that tropical cyclone activity over the MDR may also have a similar relationship as a result of more seedlings for tropical cyclones. The results showed that tropical cyclogenesis frequency does vary coherently with the MJO, such that tropical cyclones over the MDR becomes more frequent during RMM phases 1-3, and less frequent during RMM phases 6-8. Therefore, a period of increased tropical cyclogenesis activity over the MDR occurs during a time when AEW activity becomes anomalous active over West Africa. Furthermore, the large-scale environment over the tropical Atlantic was shown to be more favorable (i.e., reduced vertical wind shear, increased moisture, and anomalous cyclonic low-level relative vorticity) for tropical cyclogenesis during RMM phases 1-3.

The strongest CCKWs are often phased with the convectively active phase of the MJO. Therefore, and in addition to CCKWs, the impact of the MJO over the Western

Hemisphere is non-negligible and should be considered for medium-to-long range prediction of AEWs and subsequent tropical cyclones over the tropical Atlantic.

i. Future Work

Future work on the MJO over the Western Hemisphere is also needed. While the combined EOF approach of WH04 is effective over the Warm Pool regions, it struggles at times over the Western Hemisphere, as well during particular RMM phases. No perfect indicators of the MJO exist for real-time applications. Occasionally, the Wheeler and Hendon RMM indices do not diagnose a coherent MJO signal even when other indicators suggest it is present. This problem can be attributed to the indices being susceptible to contamination from convectively-coupled equatorial Rossby waves and CCKWs (Wheeler and Hendon 2004; Roundy et al. 2010). Such interference by equatorial wave modes might cause the RMM principle components to suggest there is an MJO signal when there really isn't one. For example, the 'artificial' MJO signal may be composed of a series of strong equatorial CCKWs over the equatorial Indian Ocean. These conditions might result in a fast counterclockwise propagation of RMM indices in phases 1, 2 and 3 followed by dampening of the RMM amplitude once the active convection associated with the CCKW weaken. Such interference by ERWs can also yield a clockwise rotation of the RMM indices, suggesting westward propagation.

On the other hand, some such equatorial wave signals might comprise part of the anatomy of the MJO. Further work might even indicate that not retaining these different wave modes may allow for a stronger or weaker relationship between Atlantic tropical cyclone activity and the RMM indices. Further, the initiation of the MJO is poorly understood. It is possible that the birth of a new MJO event arises from CCKWs (recall

Fig. 2.9 and Fig. 3.10). Therefore, filtering out these waves might cause us to ignore information relevant to the MJO signal itself. This suggests the need for future work to interpret different RMM indices from which the equatorial wave modes signals have been removed, such as those applied by Roundy et al. (2010). The relationship between Atlantic tropical cyclone activity and the MJO may change with the removal of the equatorial wave modes.

Although the RMM Indices derived by WH04 has proven to be effective at times, this sort of MJO index, where by EOFs are calculated of equatorially averaged fields, is by no means the only approach worth pursuing. There may be alternative MJO indices that will have different sensitivities to the features of the MJO and that these different indices may be more suitable for specific applications. To this end, alternative indices should be explored in order to promote a better understanding of the MJO and its global impacts. This idea is promoted by Ventrice et al. (in submission), and preliminary work is shown in Appendix A.

7.6. Real-time monitoring of convectively coupled Kelvin waves

This dissertation has shown the numerous impacts of CCKWs on tropical Atlantic and African weather variability. Therefore, there is a need to monitor these waves in real-time. Monitoring CCKWs over the Western Hemisphere during boreal summer can be achieved through analysis of time-longitude plots of unfiltered or space-time filtered fields. It is not recommended to use looping maps of OLR, IR, or rainfall to identify CCKWs because it is extremely difficult to the human eye to see eastward propagating disturbances in an environment characterized by westward propagating waves and MCSs that are superimposed with a diurnal cycle of convection. Furthermore, trying to observe

CCKWs in time-longitude plots of unfiltered OLR, IR, and rainfall is also difficult over the Western Hemisphere since CCKW only excite convection within the mean ITCZ. Therefore, it is necessary to pick the particular latitude that is consistent with the mean location of the ITCZ.

Unfiltered fields of 200U and 200VP are useful to identify CCKWs over the Western Hemisphere. Figures 7.1 and 7.2 are 90-day time-longitude plots of anomalous 200 hPa zonal winds and velocity potential, respectively, taken from the 0.5º GFS and are averaged about the equator (5ºS-5ºN). For both figures, there are westward propagating signatures associated with Rossby-waves and or extra-tropical cutoff lows, stationary signatures associated with interannual signals, and eastward propagating signatures highlighting individual CCKWs and MJO events. Both figures clearly show a CCKW moving over the East Pacific (~120ºW) during the current analysis date (Oct. 17, 2012).

Only a limited number of methods have been attempted to observe and forecast CCKWs in real-time using space-time filtering techniques. Wheeler and Weickmann (2001) investigated forecasting convectively-coupled tropical wave modes by using their real-time filtering approach. This filtering approach is achieved by filtering OLR anomaly data with zero-padding applied to all future times, and then made predictions through simple extrapolation. This methodology successfully captures CCKWs in real-time analysis, but in forecast mode, it tends to dampen higher frequency wave modes such as CCKWs too fast and sometimes limits the usefulness of the forecast. Figure 7.3 is an example of the space-time zero padded technique, where Kelvin filtered VP200 (contours) are overlaid on unfiltered VP200 anomalies for the same time period as Fig.

7.2. In all cases, the Kelvin filtered VP200 anomalies (contours) should be used as a compliment to the unfiltered VP200 counterpart.

Another approach to identify CCKWs in real-time was developed by Roundy and Schreck (2009) that was later modified in Roundy (2012c) and is based off a statistical approach to real-time filter convectively-coupled tropical waves by using an algorithm which combines filtering in the wavenumber frequency domain with time extended empirical orthogonal functions. This methodology avoids the distortion at the end of the dataset observed in data filtered in the wavenumber frequency domain without the addition of zero-padding future times and acts to statistically predict future CCKWs reasonably well.

A new approach to identify CCKWs in real-time that could be considered for future work is by performing an EOF analysis using space-time Kelvin filtered VP200 anomalies, where the first two EOFs are only used. This methodology is similar to Wheeler and Hendon's (2004) Real-time Multivariate MJO indices, however this index would be used to identify CCKWs. The EOFs would be constructed by only using Kelvin filtered VP200, therefore it would be not be based on combined EOFs like those in Wheeler and Hendon (2004). Figure 7.4 shows the first two EOFs of the new CCKW-VP200 index. A wavenumber two pattern is evident in both EOF1 and EOF2, where both EOFs equally explain 19.7% of the variance of the original Kelvin filtered VP200 field. A composite of unfiltered VP200 anomalies and winds using all July-September dates when the CCKW-VP200 index was greater than 1σ in amplitude is shown (Fig. 7.5). Like the EOFs, a wavenumber two signature is expressed in the VP200 anomalies, however higher amplitude anomalies are focused over the Western Hemisphere when compared to those over the Eastern Hemisphere for all eight (arbitrary) phases. The higher amplitude VP200 anomalies over the Western Hemisphere suggest the index's potential use for identifying CCKWs over the East Pacific and Atlantic during boreal summer. Like Wheeler and Hendon's (2004) MJO phase diagram, the CCKW-VP200 index can also be expressed in such a manner (Fig. 7.6). The CCKW-VP200 phase space diagram suggests that at the most current date (October 17, 2012), a CCKW was located over the East Pacific and or Indian Ocean, consistent with Figures 7.1, 7.2, and 7.3.

It is recommended the use of these approaches to identify CCKWs in real-time as compliments to numerical weather prediction forecasts given the well-known problems that dynamical models have with the representation of convectively coupled waves in the tropics (Lin et al. 2006). We should continue developing ways to identify CCKWs in real-time so we can begin to implement CCKWs in daily weather forecast discussions.

This dissertation has explored the various impacts of CCKW passages over the tropical Atlantic and Africa during boreal summer. It was shown that the strongest CCKWs are often phased with the convectively active phase of the MJO. Since both CCKWs and the MJO are disturbances that impact Atlantic tropical cyclogenesis activity, it is possible to predict Atlantic tropical cyclogenesis activity at 2-4 week lead times.

Boreal summer CCKWs impact convection within the mean latitude of the ITCZ and provide an environment over the tropical Atlantic and Africa favorable for the genesis of tropical cyclones and AEWs, respectively. The strongest CCKWs are often superimposed with the convectively active phase of the MJO, and therefore the state of the MJO should also be considered. However, CCKWs can still impact the large-scale environment over the tropical Atlantic and Africa in the absence of a coherent MJO event. Therefore, CCKWs are extremely important tropical waves that impact weather variability for all seasons over the Atlantic and African continent and should no longer be disregarded.

7.2. Figures

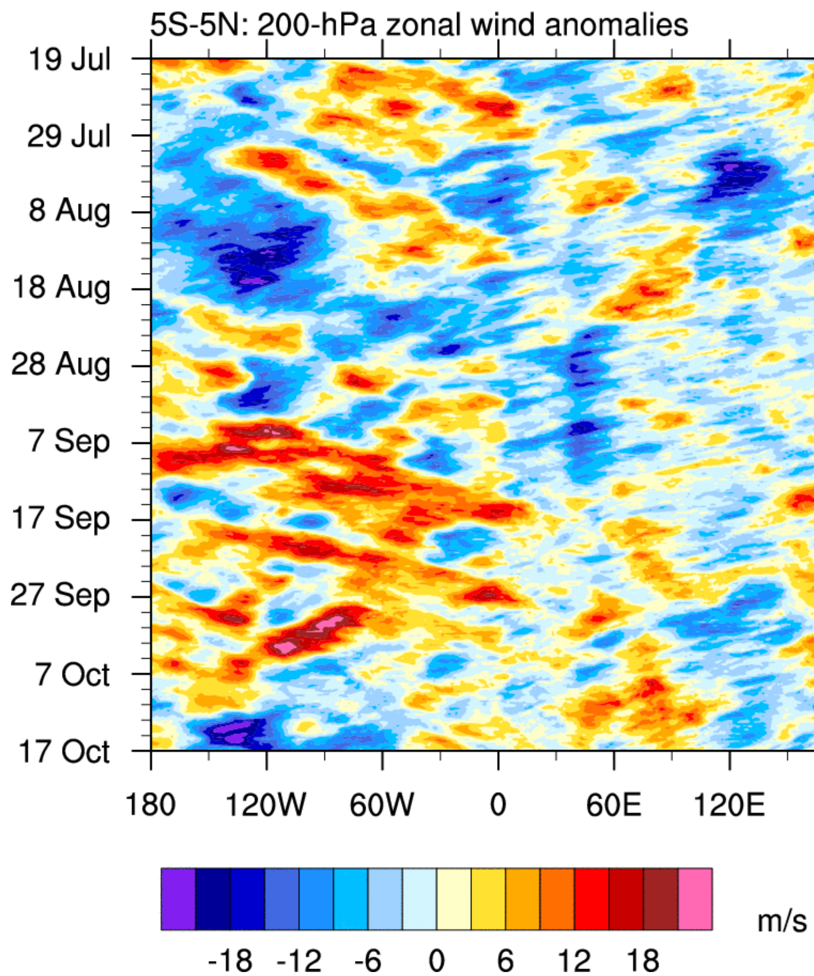

Fig. 7.1. Time-longitude plot of 200 hPa zonal wind anomalies averaged about 5ºS-5ºN for the period July 19 – October 17, 2012. The most current date of this analysis was Oct. 17, the date when the plot was generated.

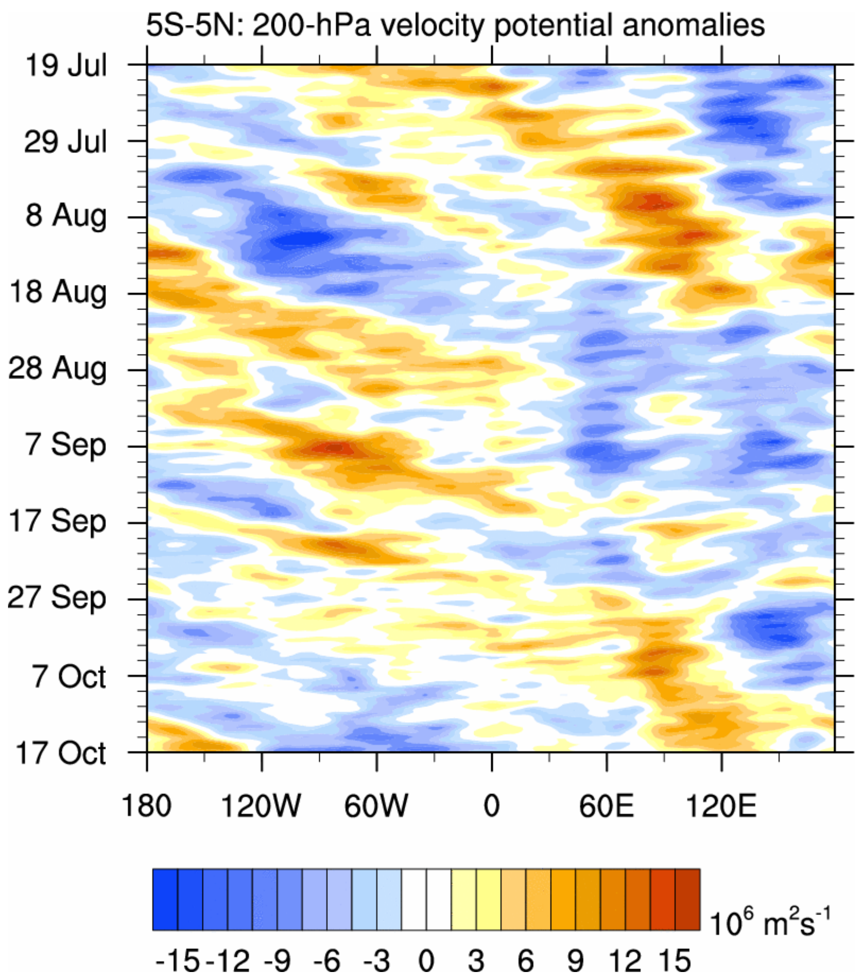

Fig. 7.2. Same as Fig. 7.1, but for 200VP.

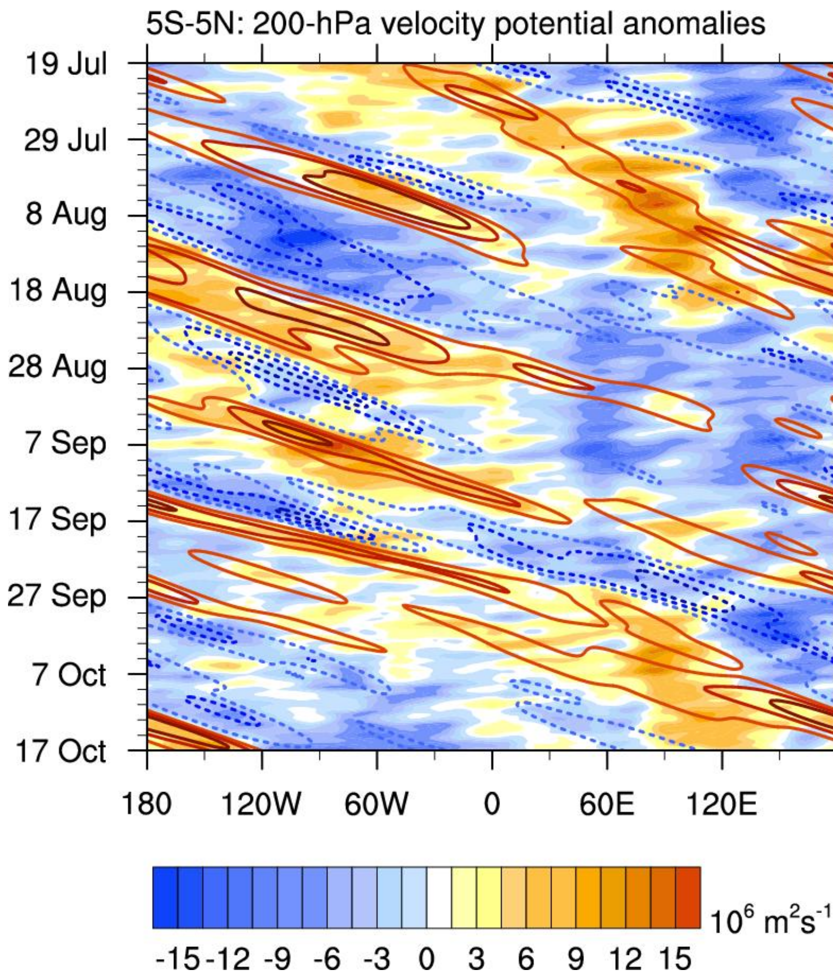

Fig. 7.3. Same as Fig. 7.2, but with Kelvin filtered VP200 in contours. Negative Kelvin filtered VP200 anomalies are represented by blue-dashed contours. Positive Kelvin Filtered VP200 anomalies are represented by warm-colored contours.

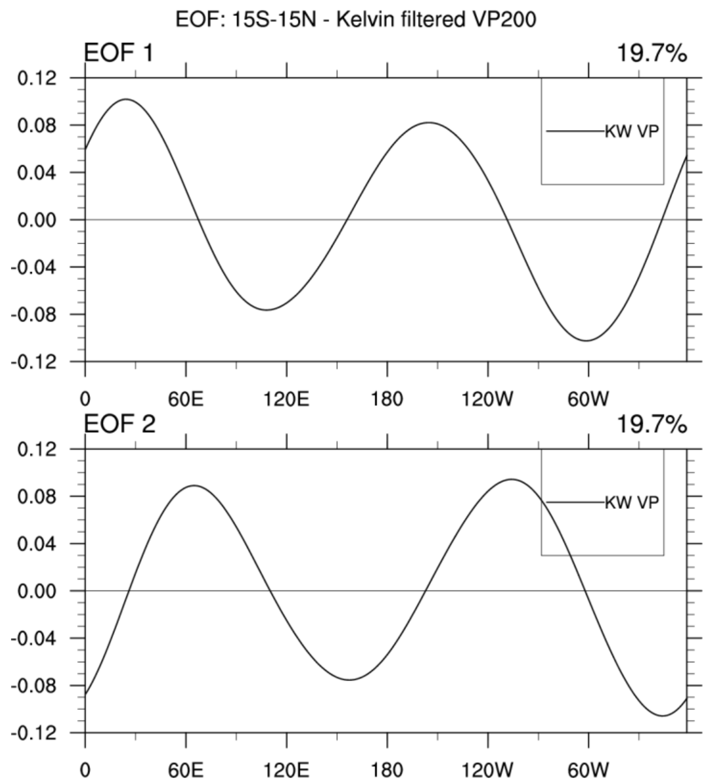

Fig. 7.4. The first two EOFs from the CCKW-VP200 index. Kelvin filtered VP200 is averaged from 15ºS-15ºN prior to the EOF calculation.

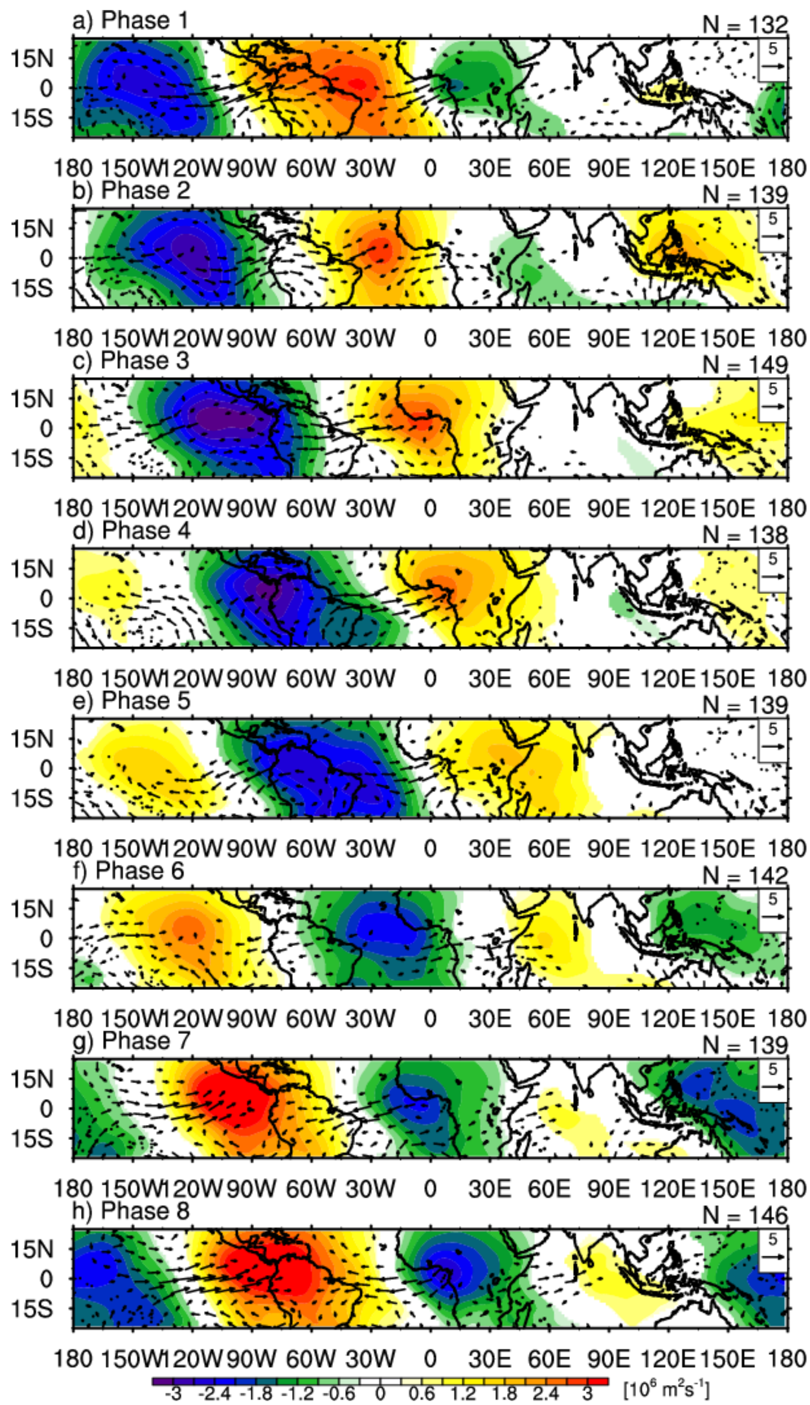

Fig. 7.5. Composites of unfiltered VP200 (shaded) and 200 hPa wind anomalies (vector) for all July-September dates when the CCKW-VP200 index amplitude were greater than 1σ.

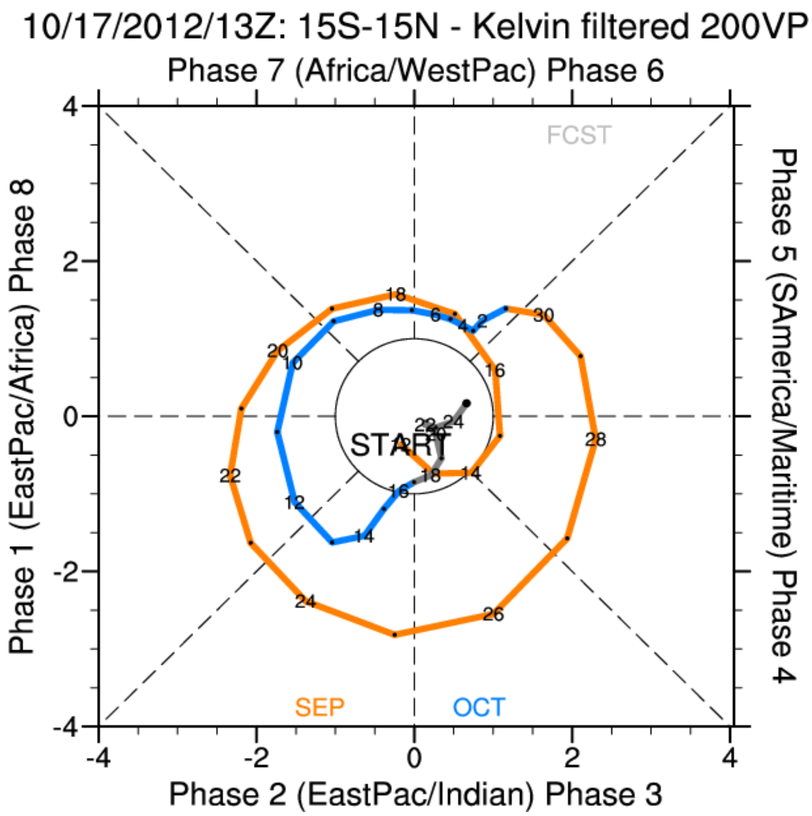

Fig. 7.6. The CCKW-VP200 phase space diagram for all dates between September 12 and October 17, 2012 (most current date). The grey line (forecast) is constructed by simple extrapolation of the Kelvin filtered VP200 signal.

Appendix A. A Modified Multivariate Madden Julian Oscillation Index using Velocity Potential

Similar to the methodology of WH04 with respect to their combined EOF analysis, comparable or slightly stronger relationships with Western Hemisphere convection (Fig. A), 2-10d filtered EKE over Africa (Fig. B), and Atlantic tropical cyclones (Fig. C) are found when exchanging OLR with VP200 and are called the velocity potential MJO (VPM) indices. Additional details can be found in Ventrice et al. (2013).

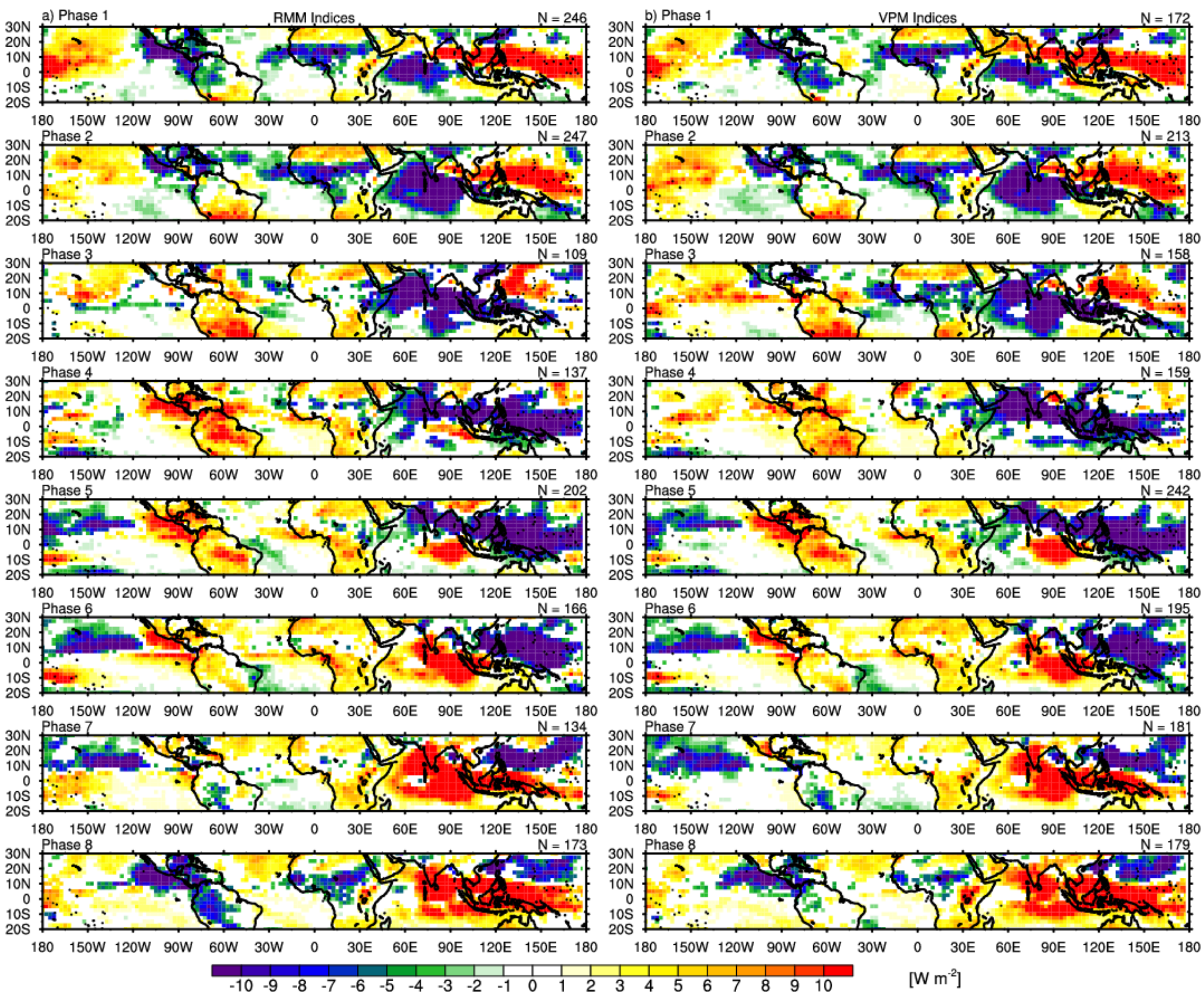

Fig. A. JJAS composite of anomalous OLR (shaded) for each MJO phase using (a) the RMM PCs (b) the VPM PCs using VP200 instead of OLR. Anomalies statistically different than zero at the 90% level are shaded.

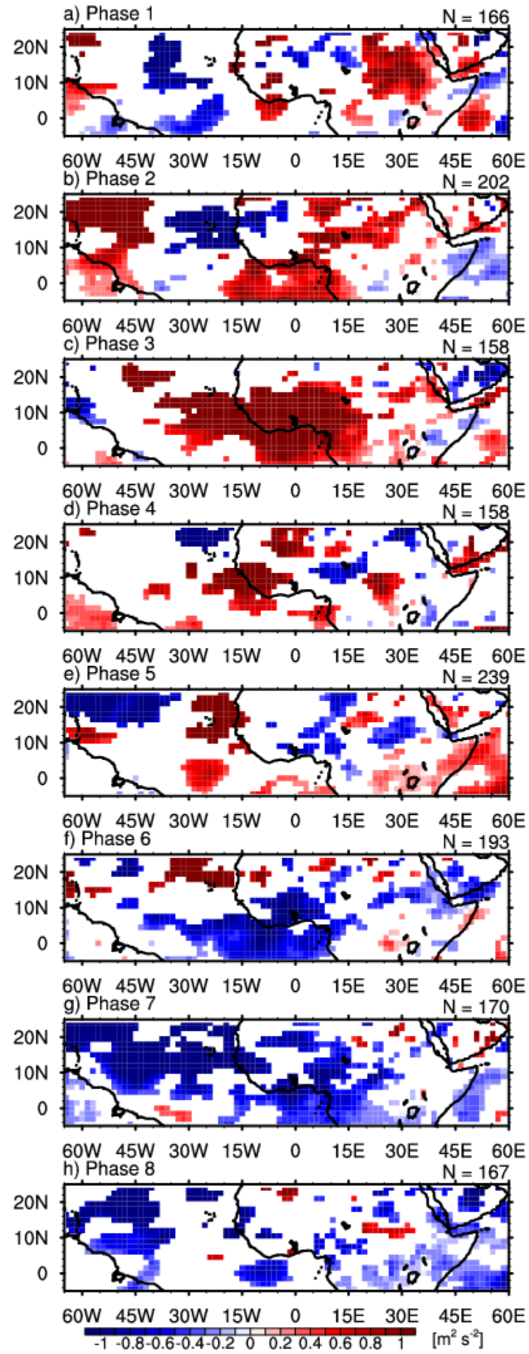

Fig. B. June-September (1990-2009) 2-10 day filtered EKE analysis at 700 hPa for each MJO phase using the VPM indices. Anomalies statistically significantly different than zero at the 90% level shaded.

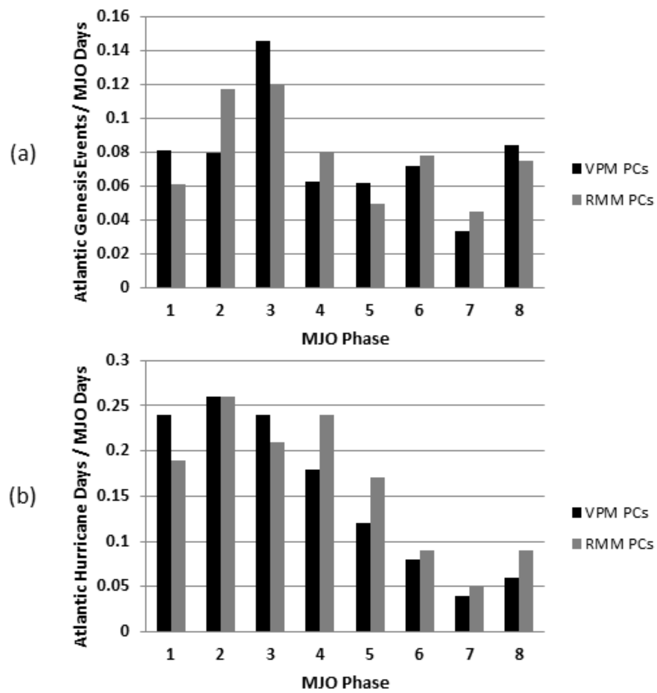

Fig. C. (a) Normalized Atlantic genesis events and (b) normalized Atlantic hurricane days (HDs) for each MJO phase for the VPM PCs (black) and the RMM PCs (grey) during the JJAS (1989-2009) season. Both (a) and (b) are normalized by the number of MJO days for each particular MJO Phase.

References

Agudelo, P. A., C. D. Hoyos, J. A. Curry, and P. J. Webster, 2010: Probabilistic discrimination between large-scale environments of intensifying and decaying African easterly waves. *Climate Dyn.*, **36**, 1379-1401.

Aiyyer, A., and C. D. Thorncroft, 2011: Interannual-to-multidecadal variability of vertical shear and tropical cyclone activity. *J. Climate*, **24**, 2949-2962.

Alaka, G. J., and E. D. Maloney, 2012: The influence of the MJO on upstream precursors to African easterly waves. *J. Climate*, *early online release*.

Ambrizzi, T., B. J. Hoskins, and H. H. Hsu, 1995: Rossby wave propagation and teleconnections patterns in the Austral Winter. *J. Atmos. Sci.*, **52**, 3661-3672,

Andrews, D. G., J. R. Holton, and C. B. Leovy, 1987: *Middle Atmosphere Dynamics*, 489 pp., Academic, San Diego, Calif.

Annamalai, H., and J. M. Slingo, 2001: Active/break cycles: Diagnosis of the intraseasonal variability of the Asian summer monsoon. *Climate Dyn.*, **18**, 85–102.

Avila, L.A. and R.J. Pasch, 1992: Atlantic tropical systems of 1991. *Mon. Wea. Rev.*, **120**, 2688-2696.

Berry, G., and C.D. Thorncroft, 2005: Case study of an intense African easterly wave. *Mon. Wea. Rev.*, **133,** 752–766.

——, C.D. Thorncroft and T. Hewson, 2007: African easterly waves during 2004—analysis using objective techniques. *Mon. Wea. Rev.*, **135**, 1251-1267.

Bessafi, M., and M. Wheeler, 2006: Modulation of south Indian Ocean tropical cyclones by the Madden-Julian Oscillation and convectively coupled equatorial waves. *Mon. Wea. Rev.*, **134**, 638-656.

Braun, S. A., 2010: Reevaluating the role of the Saharan air layer in Atlantic tropical cyclogenesis and evolution. *Mon. Wea. Rev.*, **138**, 2007-2037.

Briegel, L. M., and W. M. Frank, 1997: Large-scale influences on tropical cyclogenesis in the western North Pacific. *Mon. Wea. Rev*., **125**, 1397–1413.

Berry, G., and C.D. Thorncroft, 2005: Case study of an intense African easterly wave. *Mon. Wea. Rev.*, **133**, 752–766.

Carlson, T. N., 1969a: Synoptic histories of three African disturbances that developed into Atlantic hurricanes. *Mon. Wea. Rev*., **97**, 256–276.

——, 1969b: Some remarks on African disturbances and their progress over the tropical Atlantic. *Mon. Wea. Rev*., **97**, 716–726.

Chauvin, F., R. Roehrig, and J.-P. Lafore, 2010: Intraseasonal variability of the Saharan heat low and its link with midlatitudes. *J. Climate*, **23**, 2544-2561.

Chiao, S., and G. S. Jenkins, 2010: Numerical investigations on the formation of Tropical Storm Debby during NAMMA-06. *Wea. Forecasting*, **25,** 866-884.

Couvreux, F., F. Guichard, O. Bock, B. Campistron, J.-P Lafore, and J.-L Redelsperger, 2010: Synoptic variability of the monsoon flux over West Africa prior to the onset. *Quart. J. Roy. Meteor. Soc.*, **136**, 159-173.

Dee, D. P., and coauthors, 2011: The ERA-Interim reanalysis: configuration and performance of the data assimilation system. *Quart. J. Roy. Meteor. Soc.*, **137**, 553-597, doi:10.1002/qj.828.

Dias J., and O. Pauluis, 2009: Convectively coupled waves propagating along an equatorial ITCZ. *J. Atmos. Sci.*, **66**, 2237-2255.

Diedhiou, A., S. Janicot, S. Viltard, and H. Laurent, 1999: Easterly wave regimes and associated convection over West Africa and the tropical Atlantic: Results from NCEP/NCAR and ECMWF reanalyses. *Climate Dyn.*, **15**, 795–822.

Dunkerton, T. J., and F. X. Crum, 1995: Eastward propagating ;2- to 15-day equatorial convection and its relation to the tropical intraseasonal oscillation. *J. Geophys. Res.*, **100,** 25 781–25 790.

Duvel, J. P., 1989: Convection over tropical Africa and the Atlantic ocean during northern summer. Part I: Interannual and diurnal variations. *Mon. Wea. Rev.*, **117,** 2782–2799.

——, 1990: Convection over tropical Africa and the Atlantic Ocean during northern summer. Part II: Modulation by easterly waves. *Mon. Wea. Rev.*, **118**, 1855–1868.

Ferguson, J., B. Khouider, and M. Namazi, 2009: Two-way interactions between equatorially-trapped waves and the barotropic flow. *Chin. Ann. Math.*, **30**, 539-568.

Fink, A. H., and A. Reiner, 2003: Spatio-temporal variability of the relation between African Easterly waves and West African squall lines in 1998 and 1999. *J. Geophys. Res.*, **108**, 4332.

Frank, N. L., 1970: Atlantic tropical systems of 1969. *Mon. Wea. Rev.*, **98**, 307–314.

——, and P.E. Roundy, 2006: The role of tropical waves in tropical cyclogenesis. *Mon. Wea. Rev.*, **134**, 2397-2417.

Gill, A. E., 1980: Some simple solutions for heat-induced tropical circulation. *Quart. J. Roy. Meteor. Soc.*, **106**, 447–462.

Goldenberg, S. B., and L. J. Shapiro, 1996: Physical mechanisms for the association of El Niño and West African rainfall with Atlantic major hurricane activity. *J. Climate*, **9**, 1169-1187.

Gray, W. M., 1968: Global view of the origin of tropical disturbances and storms. *Mon. Wea. Rev.*, **96**, 669-700.

——, and R. W. Jacobson Jr., 1977: Diurnal variation of deep cumulus convection. *Mon. Wea. Rev.*, **105**, 1171-1188.

——, 1988: Environmental influences on tropical cyclones. *Aust. Meteor. Mag.*, **36**, 127–139.

——, 1998: The formation of tropical cyclones. *Meteor. Atmos. Phys.*, **67**, 37–69.

Griffin, K., 2012: Large-scale influences on the genesis of TC Karl (2010). *Masters Thesis,* University at Albany, Albany NY.

Grodsky, S.A., J.A. Carton, and S. Nigam, 2003: Near surface westerly wind jet in the Atlantic ITCZ. *Geophys. Res. Lett.*, **30**, 2009, doi:10.1029/2003GL017867.

——, 1984: Atlantic seasonal hurricane frequency. Part I: El Niño and 30 mb Quasi-Biennial Oscillation influences. *Mon. Wea. Rev.*, **112**, 1649-1668.

Gruber, A., 1974: The wavenumber-frequency spectra of satellite-measured brightness in the tropics. *J. Atmos. Sci.*, **31**, 1675-1680.

Hall, N. M. J., G. N. Kiladis, and C. D. Thorncroft, 2006: Three dimensional structure of African easterly waves. Part II: Dynamical modes. *J. Atmos. Sci.*, **63**, 2231–2245.

Hill, C. M., and Y-L. Lin, 2003: Initiation of a mesoscale convective complex over the Ethiopian highlands preceding the genesis of Hurricane Alberto (2000): A precursor to tropical cyclogenesis. *Geophys. Res. Lett.*, **30**, 1232, doi:10.1029/2002GL016655.

Hodges, K. I., and C. D. Thorncroft, 1997: Distribution and statistics of African mesoscale convective weather systems based on the ISCCP Meteosat imagery. *Mon. Wea. Rev.*, **125,** 2821–2837.

——, C.D. Thorncroft and K.R. Tyle, 2010: Analysis of African easterly wave structures and their role influencing tropical cyclogenesis. *Mon. Wea. Rev.*, **138**, 1399- 1419.

Hopsch, S.B, Thorncroft, C.D., Hodges, K., and A. Aiyyer, 2007: West African storm tracks and their relationship to Atlantic tropical cyclones. *J. Climate*, **20**, 2468-2483.

——,——, and K.R. Tyle, 2010: Analysis of African easterly wave structures and their role influencing tropical cyclogenesis. *Mon. Wea. Rev.*, **138**, 1399- 1419.

Hsieh, J.-H., and K. H. Cook, 2005: Generation of African easterly wave disturbances: Relationship to the African easterly jet. *Mon. Wea. Rev.*, **133**, 1311–1327.

——, and ——, 2008: On the instability of the African easterly jet and the generation of African waves: Reversals of the potential vorticity gradient. *J. Atmos. Sci.*, **65**, 2130-2151.

Huffman, G. J., and Coauthors, 2007: The TRMM Multisatellite Precipitation Analysis (TMPA): Quasi-global, multiyear, combined-sensor precipitation estimates at fine scales. *J. Hydrometeor.*, **8,** 38–55.

Janicot, S., and B. Sultan, 2001: Intraseasonal modulation of convection in the West African monsoon. *Geophys. Res. Lett.*, **28**, 523–526.

——, F. Mounier, N. M. Hall, S. Leroux, B, Sultan, and G. N. Kiladis, 2009: Dynamics of the West African Monsoon. Part IV: Analysis of 25—90-day variability of convection and the role of the Indian Monsoon. *J. Climate*, **22**, 1541-1565.

——, ——, S. Gervois, B. Sultan, and G. N. Kiladis, 2010: The dynamics of the West African Monsoon. Part V: The detection and role of the dominant modes of convectively coupled equatorial Rossby waves. *J. Climate*, **23**, 4005-4024.

Janowiak, J., P. A. Arkin, and M. Morrissey, 1994: An examination of the diurnal cycle in oceanic tropical rainfall using satellite and in situ data. *Mon. Wea. Rev.,* **122,** 2296–2311.

——, R. J. Joyce, and Y. Yarosh, 2001: A real-time global half-hourly pixel-resolution infrared dataset and its applications. *Bull. Amer. Meteor. Soc*, **82,** 205–217

Kikuchi, K., and B. Wang, 2010: Spatiotemporal wavelet transform and the multiscale behavior of the Madden–Julian oscillation. *J. Climate*, **23**, 3814–3834.

Kiladis, G. N., C. D. Thorncroft, and N. M. J. Hall, 2006: Three dimensional structure and dynamics of African easterly waves. Part I: Observations. *J. Atmos. Sci.,* **63,** 2212–2230.

——, M.C. Wheeler, P.T. Haertel, K. H. Straub, and P. E. Roundy, 2009: Convectively coupled equatorial waves. *Rev. Geophys.*, **47**, RG2003, doi:10.1029/2008RG000266.

Klotzbach, P. J., and W. M Gray, 2008: Multidecadal variability in North Atlantic tropical cyclone activity. *J. Climate*, **21**, 3929-3935.

——, 2010: On the Madden-Julian Oscillation-Atlantic hurricane relationship. *J. Climate*, **23**, 282-293.

Knapp, K. R., M. C. Kruk, D. H. Levinson, H. J. Diamond, and C. J. Neumann, 2010:

The international best track archive for climate stewardship (IBTrACS). *Bull. of Am. Mete. Soc.*, **91**, 363-376.

Knutson, T. R.,——, and J. E. Kutzbach, 1986: Global-scale intraseasonal oscillations of outgoing longwave radiation and 250-mb zonal wind during Northern Hemisphere summer. *Mon. Wea. Rev.,* **114**, 605–623

——, and K. M. Weickmann, 1987: 30–60 day atmospheric circulations: Composite lifecycles of convection and circulation anomalies. *Mon. Wea. Rev.,* **115**, 1407–1436.

Kwon, H. J., and M. Mak, 1990: A study of the structural transformation of the African easterly waves. *J. Atmos. Sci.*, **47**, 277-292.

Lafore, J.-P., and M. W. Moncrieff, 1989: a numerical investigation of the organization and interactions of the convective and stratiform regions of tropical squall lines. *J. Atmos. Sci.*, **46**, 521-544.

Laing, A. G., R.E. Carbone, V. Levizzani, and J. D. Tuttle, 2008: The propagation and diurnal cycles of deep convection in northern tropical Africa. *Quart. J. Roy. Meteor. Soc.*, **134,** 93–109.

——, ——, ——, 2011: Cycles and propagation of deep convection over equatorial Africa. *Mon. Wea. Rev.*, **139**, 2832-2853.

Landsea, C.W., Bell, G.D., Gray, W.M., and S. B. Goldenberg, 1998: The extremely active 1995 Atlantic hurricane season: Environmental conditions and verification of seasonal forecasts. *Mon. Wea. Rev.,* **126,** 1174–1193.

Lavender, S.L., and A.J. Matthews, 2009: Response of the West African Monsoon to the Madden–Julian Oscillation. *J. Climate,* **15**, 4097–4116.

Lavaysse, C., C. Flamant, S. Janicot, D. J. Parker, J.-P. Lafore, B. Sultan, and J. Pelon, 2009: Seasonal evolution of the West African heat low: A climatological perspective. *Climate Dyn.*, **33**, 313-330, doi:10.1007/s00382-009-0553-4.

——, ——, ——, and P. Knippertz, 2010a: Links between African easterly waves, midlatitude circulation, and intraseasonal pulsations of the West African heat low. *Quart. J. Roy. Meteor. Soc.*, **136**, 141-158, doi:10.1002/qj.555.

——, ——, ——, 2010b: Regional-scale convection patterns during strong and weak phases of the Saharan heat low. *Atmos. Sci. Lett.*, **136**, 141-158, doi:10.1002/asl.284.

Lee, C.-S., R. Edson, and W. M. Gray, 1989: Some large-scale characteristics associated with tropical cyclone development in the north Indian Ocean during FGGE. *Mon. Wea. Rev*., **117**, 407–426.

Leroux, S., and N. M. Hall, 2009: On the relationship between African easterly waves and the African easterly jet. *J. Atmos. Sci.*, **66**, 2303–2316.

——, ——, and G. N. Kiladis, 2010: A climatological study of transient–mean-flow interactions over West Africa. *Quart. J. Roy. Meteor. Soc.*, **136**, 397–410.

——, ——, ——, 2011: Intermittent African easterly wave activity in a dry atmospheric model: Influence of the extratropics. *J. Climate*, **24**, 5378-5396.

Liebmann, B., and C. A. Smith, 1996: Description of a complete (interpolated) outgoing long-wave radiation dataset. *Bull. Amer. Meteor. Soc.*, **77,** 1275–1277.

——, G. N. Kiladis, L. M. V. Carvalho, C. Jones, C. S. Vera, I. Bladé, D. Allured, 2009: Origin of convectively coupled Kelvin waves over South America. *J. Climate*, **22**, 300-315.

Lin, J. –L., and Coauthors, 2006: Tropical intraseasonal variability in 14 IPCC AR4 climate models. Part I: Convective signals. *J. Climate*, **19**, 2665–2690.

Lin, H., G. Brunet, and J. Derome, 2007: Intraseasonal variability in a dry atmospheric model. *J. Atmos. Sci.*, **64**, 2422-2441.

Lindzen, R. S., 1967: Planetary waves on beta-planes. *Mon. Wea. Rev.*, **95,** 441–451.

——, and T. Matsuno, 1968: On the nature of large scale wave disturbances in the equatorial lower stratosphere, *J. Meteorol. Soc. Jpn.*, **46**, 215–221.

MacRitchie, K., and P. E. Roundy, 2012: Potential vorticity accumulation following atmospheric Kelvin waves in the active convective region of the MJO. *J. Atmos. Sci.*, **69**, 908–914.

Madden, R. A., and P. R. Julian, 1972: Description of global-scale circulation cells in the Tropics with a 40–50 day period. *J. Atmos. Sci.*, **29**, 1109–1123.

——, ——,1994: Observations of the 40–50-day tropical oscillation—A review. *Mon. Wea. Rev.*, **122**, 814–837.

Maloney, E. D., and D. L. Hartmann, 2000b: Modulation of hurricane activity in the Gulf of Mexico by the Madden–Julian oscillation. *Science*, **287**, 2002–2004.

——, and J. Shaman, 2008: Intraseasonal Variability of the West African Monsoon and Atlantic ITCZ. *J. Climate*, **12**, 2898-2918.

Matsuno, T., 1966: Quasi-geostrophic motions in the equatorial area. *J. Meteorol. Soc. Jpn.*, **44**, 25-43.

Matthews, A. J., 2004: Intraseasonal variability over tropical Africa during northern summer. *J. Climate*, **17**, 2427–2440.

McGarry, M. M., and R. J. Reed, 1978: Diurnal variations in convective activity and precipitation during phases II and III of GATE. *Mon. Wea. Rev.*, **106,** 101–113.

Mekonnen, A., C.D. Thorncroft and A.R. Aiyyer, 2006: Analysis of convection and its association with African easterly waves. *J. Climate*, **19**, 5405-5421.

——, C.D. Thorncroft, A.R. Aiyyer, G.N. Kiladis, 2008: Convectively coupled Kelvin waves over tropical Africa during the boreal summer: structure and variability. *J. Climate*, **21**, 6649-6667.

Mo, K. C., 2000: The association between intraseasonal oscillations and tropical storms in the Atlantic basin. *Mon. Wea. Rev.*, **128**, 4097–4107.

Mohr, K.I., J.S. Famiglietti and E.J. Zipser, 1999: The contribution to tropical rainfall with respect to convective system type, size, and intensity estimated from the 85-GHz ice-scattering signature. *J. Appl. Meteorol.*, **38**, 596–606.

——, 2004: Interannual, monthly, and regional variability in the wet season diurnal cycle of precipitation in sub-Saharan Africa. *J. Climate,* **17**, 2441–2453.

Mounier, F., and S. Janicot, 2004: Evidence of two independent modes of convection at Intraseasonal timescale in the West African summer monsoon. *Geophys. Res. Lett.,* **31**, L16116, doi:10.1029/2004GL020665.

——, 2005: La variabilite´ intra-saisonnie`re de la mousson de l'Afrique de l'Ouest et Centrale. Ph.D. thesis, Ecole Polytechnique, 270 pp.

——, G. N. Kiladis, and S. Janicot, 2007: Analysis of the dominant mode of convectively coupled Kelvin waves in the West African monsoon. *J. Climate*, **20**, 1487–1503.

——, ——, and G. N. Kiladis, 2008: The West African monsoon dynamics. Part III: The quasi biweekly zonal dipole. *J. Climate,* **21**, 1911–1928.

Murakami, T., L.-X. Chen, A. Xie, and M. L. Shresha, 1986: Eastward propagation of

30–60-day perturbations as revealed from outgoing longwave radiation data. *J. Atmos. Sci.*, **43**, 961–971.

Nguyen, H. and J. P. Duvel, 2008: Synoptic Wave Perturbations and Convective Systems over Equatorial Africa. *J. Climate*, **23**, 6372-6388.

——, C. D. Thorncroft, and C. Zhang, 2011: Guinean coastal rainfall of the West African Monsoon. *Quart. J. Roy. Meteor. Soc.*, **137**, 1828–1840.

Nieto Ferreira, R., and W. H. Schubert, 1997: Barotropic aspects of ITCZ breakdown. *J. Atmos. Sci.*, **54,** 261–285.

Nolan, D. S., and M. G. McGauley, 2011: Tropical cyclogenesis in wind shear: climatological relationships and physical process. *Cyclones: Formation, Triggers, and Control*, submitted.

Payne, S. W., and M. M. McGarry, 1977: The relationship of satellite inferred convective activity to easterly waves over West Africa and the adjacent ocean during phase III of GATE. *Mon. Wea. Rev.*, **105**, 414–420.

Pires, P. J-L. Redelsperger, J-P. Lafore, 1997: Equatorial atmospheric waves and their association to convection. *Mon. Rev. Rev.*, **125**, 1167-1184.

Pohl, B., Janicot, S., Fontaine, B., and R. Marteau, 2009: Implication of the Madden–Julian Oscillation in the 40-day variability of the West African Monsoon. *J. Climate*, **13**, 3769–3785.

Pu, B., and K. H. Cook, 2010: Dynamics of the West African westerly jet. *J. Climate*, **23**, 6263-6276.

Reed, J. R., D. C. Norquist, and E. E. Recker, 1977: The structure and properties of African wave disturbances as observed during phase III of GATE. *Mon. Wea.*

Rev., **105**, 317-333.

Rennick, M. A., 1976: The generation of African waves. *J. Atmos. Sci.*, **33**, 1955-1969.

Rotunno, R., J. B. Klemp, and M. L. Weisman, 1988: A theory for strong, long-lived squall lines. *J. Atmos. Sci.*, **45**, 463-485.

Roundy, P.E., and W.M. Frank, 2004: Applications of a multiple linear regression model to the analysis of relationships between eastward- and westward-moving intraseasonal modes. *J. Atmos. Sci.*, **24**, 3041-3048.

——, 2008: Analysis of Convectively Coupled Kelvin Waves in the Indian Ocean MJO. *J. Atmos. Sci.*, **65**, 1342-1359.

——, C. J. Schreck III, and M. A. Janiga, 2009: Contributions of convectively coupled equatorial Rossby waves and Kelvin waves to the Real-Time Multivariate MJO Indices. *Mon. Wea. Review*, **137**, 469-478.

——, K. MacRitchie, J. Asuma, and T. Melino, 2010: Modulation of global atmospheric circulation by combined activity in the Madden-Julian Oscillation and the El Niño-Southern Oscillation during boreal winter. *J. Climate*, **23**, 3094-3119.

——, 2012a: Observed structure of convectively coupled waves as a function of equivalent depth: Kelvin waves and the Madden-Julian Oscillation. *J. Atmos. Sci.*, **69**, 2097-2106.

——, 2012b: The spectrum of convectively coupled Kelvin waves and the Madden-Julian Oscillation in regions of low-level easterly and westerly background flow. *J. Atmos. Sci.*, **69**, 2107-2111.

——, 2012c: Tracking and prediction of large-scale organized tropical convection by spectrally focused two-step space-time EOF analysis. *Quart. J. Roy. Meteor. Soc.*,

138, 919-931.

Schreck, C. J. III, and J. Molinari, 2011: Tropical cyclogenesis associated with Kelvin waves and the Madden-Julian Oscillation. *Mon. Wea. Rev.*, **139**, 2723-2734.

——, ——, and K. I. Mohr, 2011: Attributing tropical cyclogenesis to equatorial waves in the western North Pacific. *J. Atmos. Sci.*, **68**, 195–209.

Simmons, A. J., 1977: A note on the instability of the African easterly jet. *J. Atmos. Sci.*, **34**, 1670–1674.

——, S. Uppala, D. Dee, and S. Kobayashi, 2007: ERA Interim: New ECMWF reanalysis products from 1989 onwards. ECMWF Newsletter, No. 110, ECMWF, Reading, United Kingdom, 25–35.

Sippel, J. A., S. A. Braun, and C. L. Shie, 2011: Environmental influences on the strength of Tropical Storm Debby (2006). *J. Atmos. Sci.*, **early online release**.

Sobel, A. H. and D. Kim, 2013: The MJO-Kelvin wave transition. *Geophys. Res. Lett*., (in press).

Straub, K. H., and G. N. Kiladis, 2002: Observations of a convectively coupled Kelvin waves in the eastern Pacific ITCZ. *J. Atmos. Sci.*, **59,** 30–53.

——, and ——, 2003a: Extratropical forcing of convectively coupled Kelvin waves during austral winter. *J. Atmos. Sci.*, **60**, 526–543.

——, and ——, 2003b: Interactions between the boreal summer intraseasonal oscillation and higher frequency tropical wave activity. *Mon. Wea. Rev.*, **131**, 945–960.

——, and ——, 2003c: The Observed Structure of Convectively Coupled Kelvin Waves: Comparison with Simple Models of Coupled Wave Instability. *J. Atmos. Sci.*, **60**, 1655-1668.

——, ——, and P. E. Ciesielski, 2006: The role of equatorial waves in the onset of the South China Sea summer monsoon and the demise of El Niño during 1998. *Dyn. Atmos. Oceans*, **42**, 216–238.

Sultan, B., S. Janicot, and A. Diedhiou, 2003: The West African monsoon dynamics. Part I: Documentation of intraseasonal variability. *J. Climate*, **16**, 3389–3406.

Takayabu, Y. N., and M. Murakami, 1991: The structure of super cloud clusters observed in 1–20 June 1986 and their relationship to easterly waves. *J. Meteor. Soc. Japan,* **69,** 105–125.

——, 1994: Large-scale cloud disturbances associated with equatorial waves. Part I: Spectral features of the cloud disturbances. *J. Meteor. Soc. Japan,* **72,** 433–448.

The NCAR Command Language (Version 6.0.0) [Software]. (2012). Boulder, Colorado: UCAR/NCAR/CISL/VETS. http://dx.doi.org/10.5065/D6WD3XH5.

Thompson, R. M., Jr., S. W. Payne, E. E. Recker, and R. J. Reed, 1979: Structure and properties of synoptic-scale wave disturbances in the Intertropical Convergence Zone of the eastern Atlantic. *J. Atmos. Sci.,* **36**, 53–72.

Thorncroft, C. D., and B. J. Hoskins, 1994a: An idealized study of African easterly waves. Part I: A linear view. *Quart. J. Roy. Meteor. Soc.*, **120**, 953–982.

——, and ——, 1994b: An idealized study of African easterly waves. Part II: A non linear view. *Quart. J. Roy. Meteor. Soc.,* **120**, 983–1015.

——, and M. Blackburn, 1999: Maintenance of the African easterly jet. *Quart. J. Roy. Meteor. Soc.*, **125**, 763–786.

——, and K. Hodges, 2001: African easterly wave variability and its relationship to Atlantic tropical cyclone activity. *J. Climate*, **14**, 1166–1179.

——, D.J. Parker, r. Burton, M. Diop, J.H. Ayers, H. Barjat, R. Dumelow, D.R. Kindred, N.M. Price, C.M. Taylor, and A.M. Tompkins, 2003: The JET2000 experiment: Aircraft observations of the African easterly jet and African easterly Waves. *Bull. Amer. Meteorol. Soc.*, **84**, 337–351.

——, N. M. Hall, and G. K. Kiladis, 2008: Three-dimensional structure and dynamics of African easterly waves. Part III: genesis. *J. Atmos. Sci.*, **65**, 3596-3607.

Tuleya, R. E., and Y. Kurihara, 1981: A numerical study of the effects of environmental flow on tropical storm genesis. *Mon. Wea. Rev.*, **109**, 2487-2506.

Tulich, S. N., and G. N. Kiladis, 2012: Squall lines and convectively coupled gravity waves in the tropics: Why do most cloud systems propagate westward? *J. Atmos. Sci.*, **69**, 2012.

Ventrice, M. J., C. D. Thorncroft, and P. E. Roundy, 2011: The Madden Julian's Oscillation influence on African easterly waves and downstream tropical cyclogenesis. *Mon. Wea. Rev.*, **139**, 2704-2722.

——, ——, and M. A. Janiga, 2012a: Atlantic tropical cyclogenesis: A three-way interaction between an African easterly wave, diurnally varying convection, and a convectively-coupled atmospheric Kelvin wave. *Mon. Wea. Rev.*, **140**, 1108-1124.

——, ——, and Carl. J. Schreck, 2012b: Impacts of convectively coupled Kelvin waves on environmental conditions associated with Atlantic tropical cyclogenesis, *Mon. Wea. Rev..*, **140**, 2198-2214.

——, M. C. Wheeler, H. H. Hendon, C. J. Schreck III, C. D. Thorncroft, and G. N. Kiladis, 2013: A modified multivariate Madden Julian Oscillation index using velocity potential. (in submission).

Vizy, E. K. and K. H. Cook, 2009a: Tropical Storm development from African easterly waves in the eastern Atlantic: a comparison of two successive waves using a regional model as part of NASA AMMA 2006. *J. Atmos. Sci.*, **66**, 3313-3334.

——, and ——, 2009b: A mechanism for African monsoon breaks: Mediterranean cold air surges. *J. Geophys. Res.*, **114**, D01104, doi:10.1029/2008UD010654.

Wang, B., and H. Rui, 1990: Dynamics of moist Kelvin-Rossby wave on an equatorial β-plane. *J. Atmos. Sci.*, **47**, 397-413.

Wang, H., and R. Fu, 2007: The influence of Amazon rainfall on the Atlantic ITCZ through convectively coupled Kelvin waves, *J. Climate*, **20**, 1188–1201.

Wheeler, M., and G. N. Kiladis, 1999: Convectively coupled equatorial waves: Analysis of clouds and temperature in the wavenumber– frequency domain. *J. Atmos. Sci.*, **6,** 374–399.

——, ——, and P. J. Webster, 2000: Large-scale dynamical fields associated with convectively coupled equatorial waves. *J. Atmos. Sci.*, **57**, 613–640.

——, and K. M. Weickmann, 2001: Real-time monitoring and prediction of modes of coherent synoptic to intraseasonal tropical variability. *Mon. Wea. Rev.*, **129**, 2677–2694.

——, and H. H. Hendon, 2004: An all-season real-time multivariate MJO index: Development of an index for monitoring and prediction. *Mon. Wea. Rev.*, **132**, 1917–1932.

Yanase W, *M.* Satoh, H. Yamada, *K.* Yasunaga, and Q. Moteki, 2010: Continual influences of tropical waves on the genesis and rapid intensification of Typhoon Durian (2006). *Geophys. Res. Lett.*, **37**. DOI: 10.1029/2010gl042516.

Yang, G., and J. Slingo, 2001: The diurnal cycle in the tropics. *Mon. Wea. Rev.*, **129**, 784-801.

Zangvil, A., 1975: Temporal and spatial behavior of large-scale disturbances in tropical cloudiness deduced from satellite brightness data. *Mon. Wea. Rev.*, **103**, 904-920.

Zawislak, J., and E. J. Zipser, 2010: Observations of 7 African easterly waves in the east Atlantic during 2006. *J. Atmos. Sci.*, **67**, 26-43.

Zhang, C., 2005: Madden-Julian oscillation. Rev. Geophys., **43**, RG2003, doi:10.1029/2004RG000158

Zipser, E.J. and C. Gautier, 1978: Mesoscale events within a GATE tropical depression. *Mon. Wea. Rev.*, **106**, 789-805.

——, C.H. Twohy, S.C. Tsay, N.C. Hsu, G.M. Heymsfield, K. L. Thornhill, S. Tanelli, R. Ross, T.N. Krishnamurti, Q. Ji, G. Jenkins, S. Ismail, R. Ferrare, G. Chen, E.V. Browell, B. Anderson, R. Hood, H. M. Goodman, A. Heymsfield, J. Halverson, J. P. Dunion, M. Douglas and R. Cifelli, 2010: The Saharan air layer and the fate of African easterly waves—NASA's AMMA field study of tropical cyclogenesis. *Bull. Meteo. Soc.*, **90**, 1137-1156.